

Alma Mater Studiorum – Università di Bologna

DOTTORATO DI RICERCA IN
Meccanica e Scienze Avanzate dell'Ingegneria (DIMSAI)

Ciclo XXX

Settore Concorsuale: 09/C2 – Fisica Tecnica e Ingegneria Nucleare

Settore Scientifico Disciplinare: ING-IND/18 – Fisica dei Reattori Nucleari

MONTE CARLO MODELLING AND EXPERIMENTAL
MEASUREMENT METHODOLOGIES TO SUPPORT DECOMMISSIONING
PLANS OF BIOMEDICAL CYCLOTRONS

Presentata da: Sara Vichi

Coordinatore Dottorato
Prof. Marco Carricato

Supervisore
Prof. Domiziano Mostacci

Co-supervisore
Dott. Mario Marengo

Esame Finale Anno 2018

Contents

ABSTRACT.....	III
INTRODUCTION.....	1
CHAPTER 1 DECOMMISSIONING OF PARTICLE ACCELERATORS.....	5
1.1 INTRODUCTION	5
1.2 RADIOACTIVITY INDUCED IN PROTON ACCELERATORS.....	8
1.3 RADIATION PROTECTION ASPECTS IN DECOMMISSIONING OF PARTICLE ACCELERATORS.....	9
1.3.1 <i>International and National Regulations</i>	10
1.3.2 <i>Clearance levels</i>	13
1.4 DECONTAMINATION AND DISMANTLING STRATEGIES.....	22
CHAPTER 2 THE MONTE CARLO FLUKA CODE.....	24
2.1 MONTE CARLO METHODS.....	24
2.2 THE FLUKA CODE.....	27
2.2.1 <i>FLUKA</i>	27
2.2.2 <i>Flair</i>	29
CHAPTER 3 MONTE CARLO MODELS	31
3.1 THE GE PETTRACE CYCLOTRON FACILITY OF THE SANT'ORSOLA-MALPIGHI HOSPITAL IN BOLOGNA	32
3.1.1 <i>Geometry</i>	34
3.1.2 <i>Physics</i>	39
3.1.3 <i>Source</i>	41
3.1.4 <i>Scoring</i>	50
3.2 THE IBA C18/9 PET CYCLOTRON FACILITY.....	52
3.2.1 <i>Geometry</i>	56
3.2.2 <i>Source term, neutron emission from target</i>	61
CHAPTER 4 RADIATION DETECTORS USED IN EXPERIMENTAL MEASUREMENTS	66
4.1 NEUTRON DETECTION	66
4.1.1 <i>Neutron dosimetry with rem-counter</i>	67
4.1.2 <i>Neutron dosimetry with CR39</i>	69
4.1.3 <i>Neutron spectrometry with bubble detectors</i>	70
4.1.4 <i>BDS bubble detector spectrometer, basic features</i>	74
4.2 GAMMA SPECTROMETRY WITH SEMICONDUCTOR DETECTORS	76
4.2.1 <i>CAMBERRA HPGe detectors</i>	78

4.2.2	<i>Kromek GR1</i>	80
CHAPTER 5 EXPERIMENTAL MEASUREMENTS		81
5.1	ASSESSMENT OF THE NEUTRON DOSE FIELD AROUND THE PETTRACE OF S.ORSOLA-MALPIGHI HOSPITAL IN BOLOGNA	81
5.2	NEUTRON SPECTROMETRY INSIDE INSELSPIITAL CYCLOTRON BUNKER OF BERN WITH BUBBLE DETECTORS	83
5.2.1	<i>Unfolding procedure</i>	87
5.3	NON-DESTRUCTIVE ACTIVATION ASSESSMENT	90
5.3.1	<i>Monte Carlo model of the detector</i>	92
5.3.2	<i>Experimental validation of the model</i>	93
5.3.3	<i>Efficiency calibration</i>	93
5.3.4	<i>Experimental validation of the model</i>	93
5.3.5	<i>Efficiency calibration</i>	95
5.4	BUNKER CORE DRILLING ACTIVATION ASSESSMENT USING AN HPGE DETECTOR.....	96
CHAPTER 6 RESULTS.....		100
6.1	ASSESSMENT OF THE NEUTRON DOSE FIELD AROUND THE PETTRACE OF S.ORSOLA-MALPIGHI HOSPITAL IN BOLOGNA	100
6.2	ASSESSMENT OF THE NEUTRON SPECTRUM INSIDE THE BUNKER OF CYCLONE 18/9 IN BERN WITH BUBBLE DETECTORS	104
6.2.1	<i>Neutron spectrum generated irradiating Target 1</i>	105
6.2.2	<i>Neutron spectrum generated irradiating Target 2</i>	108
6.2.3	<i>Neutron spectrum generated irradiating Target 5</i>	110
6.2.4	<i>Neutron spectrum generated irradiating Target 6</i>	112
6.3	BUNKER WALLS ACTIVATION ASSESSMENT	115
6.3.1	<i>Non-destructive activation assessment using a portable CZT detectors in Bologna</i>	116
6.3.2	<i>IBA CICLONE18/9 Bunker activation assessment via core drilling</i>	120
6.4	PREDICTION OF INDUCED RADIOACTIVITY USING A MONTE CARLO APPROACH	124
6.4.1	<i>Prediction of residual induced radioactivity in the bunker wall of S.Orsola-Malpighi hospital (Bologna)</i>	124
6.4.2	<i>Prediction of residual induced radioactivity in the bunker wall of Insepsital (Bern)</i>	129
CHAPTER 7 CONCLUSIONS.....		135
REFERENCES		143

Abstract

Applications of particle accelerators in the biomedical field are grown significantly in the last two decades, and are still growing, especially for cancer diagnosis and treatment. During their operational lifetime accelerators and their surrounding structures are activated by primary and secondary particles; in the long run this represent a decommissioning issue. Only in recent years attention on the generation of radioactive waste and on the radiological hazards associated with decommissioning start to be significant. Regulations today require that decommissioning must be considered as part of the design and planning phase of an accelerator facility. Nevertheless there are no specific international standards or guideline documents, and cases of accelerator decommissioning have been described only sporadically in technical literature.

This work is focused on PET cyclotron facilities activation assessment. When considering the dismantling of these facilities a considerable amount of low level radioactive waste has to be characterized and disposed of. Secondary neutrons, generated during the routinely production of ^{18}F through the $^{18}\text{O}(p,n)^{18}\text{F}$ reaction, are mainly responsible for activation. Prediction of induced radioactivity is a challenging task since the activity produced varies considerably, depending on the type of accelerator, on its use and on the specific structure of the bunker: for this reason, each facility require its specific decommissioning strategy.

This work is aimed at developing a Monte Carlo approach to a preliminary assessment of activation, to define an *ad hoc* decommissioning strategy and to identify possible countermeasures to be taken during the construction phase of the facility.

In this work two main cases studies were analysed: The GE PETtrace facility of the Sant'Orsola-Malpighi Hospital (Bologna) and the IBA CYCLONE 18/9 facility of Inselspital (Bern). The Monte Carlo code FLUKA was used to model accurately the two facilities for activation assessment. The models include all the major components of the cyclotrons and of the cyclotron bunkers that are expected to interact with the particles. Activity was scored at different positions and depths of the two cyclotron bunkers.

Different kinds of experimental measurements were performed in the two facilities to evaluate MC models reliability in terms of neutron field and neutron activation.

To this aim an assessment of the neutron dose field was performed inside the bunker of the S.Orsola-Malpighi Hospital in Bologna, using a rem-counter and CR39

dosimeters, whereas in Inselspital Bern neutron spectrometry measurements with bubble detectors were conducted.

Two different kinds of measurements for activation assessment were conducted as well: a non-destructive in situ measurement methodology using a portable CZT detector was developed and used to measure induced activation in the S.Orsola-Malpighi hospital, while in the Inselspital bunker core drilling were performed and the concrete samples measured in HPGe spectrometry. All the experimental measurements were compared with Monte Carlo simulations to evaluate consistency of the results.

Once the level of accuracy of MC results was assessed, the prediction of residual activation at different positions and depths, and for different life expectancies of the cyclotron was assessed in the two cases studied.

FLUKA simulations provided an excellent agreement, within uncertainties, with the experimental measurements in term of the neutron radiation dose field.

Concerning activation assessment results, it was not expected a full correspondence between measured and calculated activity concentrations. It is well known that activation studies are influenced by many sources of variability, ranging from uncertainties in the basic cross section data to incomplete knowledge of the composition of materials; our results are in most cases within a factor of 3, and this is completely in line with predictions of activations published in other studies. Discrepancies are mainly due to the fact that concrete activation is strongly dependent on trace element concentration, and the latter is heterogeneous and generally unknown.

These results demonstrate that FLUKA can be used satisfactorily to assess the order of magnitude of the residual activation. The accuracy of results proved to be adequate for the purposes of this work.

The main long lived radionuclides founded in concrete were ^{152}Eu , ^{154}Eu , ^{134}Cs , ^{54}Mn , ^{46}Sc , ^{57}Co , ^{65}Zn and ^{60}Co . The highest activity concentration was founded in the first 30 cm of the walls closest to targets. As expected the walls of the bunker most activated are the nearest to targets and for both facilities nuclides with the highest activity concentrations were ^{60}Co and ^{152}Eu .

The activity concentrations found in the S.Orsola-Malpighi hospital were up to 1.4 Bq/g and 0.9 Bq/g respectively for ^{152}Eu and ^{60}Co . While in the Inselspital bunker were up to 0.2 Bq/g and 0.8 Bq/g respectively for ^{152}Eu and ^{60}Co .

The total activity concentration estimated after 20 years of cyclotron operating life was up to 4.10 Bq/g and up to 3.22 Bq/g respectively in Bologna and in Bern, exceeding in both cases the radiological exemption limit of 1 Bq/g.

Concluding, Monte Carlo simulation proved to be a very powerful and feasible tool in the planning of new biomedical cyclotron installations and in the definition of an optimized decommissioning strategy.

We proved also that there are experimental methodologies, commonly available or that can be implemented with limited investment, that make possible to integrate and confirm provisional estimates.

The availability of an experimentally validated Monte Carlo model makes it possible to revise the traditional approach to activation assessment.

Introduction

The use of accelerators in the medical field has grown significantly in the last two decades. Today thousands of cyclotrons can be found all over the world, even in small countries. The estimated life expectancy, as well as the reasons for shutting down accelerators can be different. For instance, accelerators facilities can be shut down due to financial or political issues, evolution in market strategy, technological improvements, changes in institution goals or simply due to aging of the equipment.

To protect all kind of biological targets, PET cyclotrons, as any other type of accelerators, are housed in thick-walled concrete buildings. During the operational life of the facility, the concrete walls of the cyclotron vault, as well as several components of the structure of the accelerator itself, are activated, mainly by secondary neutrons interacting with metals and rare earth's present in the equipment, in concrete or in the reinforcement bars. Other activation mechanisms give rise to activation of the metal parts of the accelerators themselves.

When considering the dismantling of such accelerators, considerable amounts of low level solid radioactive waste have to be taken into account. Furthermore during their life cycle cyclotrons normally undergo upgrade and maintenance generating amounts of radioactive waste that should be carefully managed.

To decrease future dismantling costs, which might easily be greater than the cost of purchase, the amount of radioactive waste has to be evaluated in advance to define an optimum decommissioning strategy and to identify any critical issues and possible countermeasures to be taken during the construction phase of the facility.

Only in recent years public administrators, facility managers, scientists and regulatory agencies as well started to pay the due attention to the generation of radioactive waste and on the costs and radiological hazards associated with decommissioning of accelerator facilities.

Regulations today require that decommissioning be considered as part of the design and planning of an accelerator facility starting from the early phases. Nevertheless there is limited specific international guidance, and cases of accelerator decommissioning have been only sporadically described in the scientific literature.

International guidance for site planning and installation, as well as for radiation protection assessment, is given in a number of international reports; these typically suggest analytical calculation methods to overcome radiation protection issues, but in approximate or idealized geometry set ups. However, no detailed "hands on" indications for the decommissioning of these types of accelerators have been published to date and there is a lack of references on specific procedures to follow during facility

dismantling. Furthermore, in most part of the cases each specific issue is considered separately, without paying proper attention to the inevitable interconnection between them: for example, an accurate choice of the materials to be used in the shielding is necessary in the planning, to meet the dose limits, as well as in the decommissioning since these material will become, in time, a radioactive waste to be managed.

In the last 20 years, the number of cyclotrons dedicate to the production of PET radionuclides increased by a factor of about 10, making these systems the most diffused positive particles accelerators in the world; this growth tendency has probably somewhat slowed down, but it is not yet finished.

This was the basis to decide to start a structured, scientifically oriented work focused on the assessment of activation around PET cyclotrons and on the management of consequent problems as regards the end of the operational life of a facility.

Prediction of induced radioactivity nevertheless is a challenging task not only because physical phenomena involved are very complex, but also because type and level of activation depends on several factors: the type of accelerator, the beam energy and intensity, the workload of the accelerator, the geometry of the bunker housing the accelerator, the composition of materials, their location with respect to the target, etc... These aspects make us understand that each facility needs a specific decommissioning strategy.

The analytical formulation of physical problems involved in activation assessment of a cyclotron bunker is therefore not possible without strong approximations that can affect significantly the accuracy of the results.

The purpose of this thesis work is therefore to propose an approach to activation assessment of a cyclotron bunker exploiting the potential Monte Carlo methods. Monte Carlo simulations allow to reproduce more accurately, compared to analytical methods, the real geometry of a bunker and to obtain more reliable results in case of complex geometry conditions. Nevertheless the accuracy of Monte Carlo results must always be supported by comparison with experimental measurements.

In this work two main cases studies were analysed: The GE PETtrace facility of the Sant'Orsola-Malpighi Hospital (Bologna) and the IBA CYCLONE 18/9 facility of Inselspital (Bern). The well-known Monte Carlo code FLUKA was used to quantify the induced radioactivity present in the two cases studies and to predict future residual activation.

The Monte Carlo code FLUKA was used to realize a very detailed and accurate model of both the cyclotrons and the facilities, with the study of activation as the primary goal; it has to be noted however that the models I realized are complete and detailed at a level that they will be usable in the future also of other studies, like in the field of optimization of production reactions, or for other aspects of radiation protection.

In parallel different kind of experimental measurements were conducted to assess simulated results accuracy. We proved that there are experimental methodologies, commonly available or that can be implemented with limited investment, that make possible to integrate and confirm provisional estimates.

Concluding, aim of this work is to define a methodology for the preliminary assessment of activation levels of a cyclotron bunker via Monte Carlo simulations and, in parallel, to conduct different kind of experimental measurements to support results reliability. This methodology is intended to become the basis for an optimal design of the facility in terms of residual activation during the construction phase of a new cyclotron site and for the definition of *ad hoc* decommissioning strategies.

This thesis, which is structured in six chapters, is divided in three different parts: introduction, material & methods and results. In detail:

The first chapter provides an overview regarding particle accelerator decommissioning. After a general introduction on the state of the art, the main radiation protection problems in the decommissioning of biomedical cyclotrons are discussed with reference to international regulations. A short review of the physics underlying the main mechanisms of induced radioactivity is also presented.

In the second chapter a brief introduction on the mathematical basis of the Monte Carlo Method is provided. Then the Monte Carlo FLUKA code is presented as well as its graphical interface Flair.

In the third chapter the two main case studies analysed in this work are presented: the GE PETtrace facility of the Sant'Orsola-Malpighi Hospital (Bologna) and the IBA CYCLONE 18/9 facility of Inselspital (Bern). In both cases, first the cyclotron, then the cyclotron bunker and more in general the facility is described. Then the Monte Carlo model implemented is presented focusing on the geometrical model, on the definition of materials and on the source terms. Details on the physical and transport parameters, on the scored results and on their subsequent analysis is also given.

In the fourth chapter devices used in experimental measurements to assess Monte Carlo results accuracy are presented. For each device first a general description of the operating principle is reported, secondly specific features regarding the devices used are discussed. Two main groups of devices are described:

- devices used in neutron detection, like rem-counters and CR39 for neutron dosimetry and bubble detectors for neutron spectrometry;
- Semiconductor detectors for gamma spectrometry, in particular HPGe detectors and portable CZT detectors.

A variety of experimental measurements were performed in the two facilities to evaluate more possible options depending on the case studied. All the experimental measurements were compared with Monte Carlo simulations to check the models implemented in terms of source term accuracy and in terms of neutron activation. To this aim an assessment of the neutron dose field was performed inside the bunker of the S.Orsola-Malpighi Hospital in Bologna, whereas in Inselspital Bern neutron spectrometry measurements with bubble detectors were performed. Then two different kinds of measurements for activation assessment were conducted: a non-destructive in

situ measurement methodology using a portable CZT detector was developed and used to measure induced activation in the S.Orsola-Malpighi hospital, while in Inselspital bunker core drilling were performed and concrete sample measured in HPGe spectrometry. All the experimental measurements are described in the fifth chapter.

In the sixth chapter results of experimental measurements are reported and compared with corresponding results obtained with FLUKA. The accuracy of MC models implemented in terms of neutrons fluence and residual activation is then discussed. Finally the potentiality of Monte Carlo approach in activation assessment is pointed out.

In the seventh chapter the conclusions of the work presented in this thesis are discussed.

Chapter 1

Decommissioning of particle accelerators

This chapter provides an overview regarding particle accelerator decommissioning. After a general introduction on the state of the art, the main radiation protection problems in the decommissioning of biomedical cyclotrons are discussed with reference to international regulations. A short review of the physics underlying the main mechanisms of induced radioactivity is also presented.

1.1 Introduction

Thousands of accelerators are in operation all over the world, ranging from big research institutions with multi GeV machines to small installations in low income countries. Accelerators have a wide variety of applications; some of the most common applications include:

- Medical applications, such as diagnosis and treatment of cancer.
- Radioisotope production.
- Mineral and oil prospection, using neutrons produced with small accelerators.
- Charged particle beams for processing semiconductor chips.
- Intense sources of X-rays for sterilization of medical devices equipment and food products.
- Security controls of containers in harbors.
- Charged particle beams for materials sciences and applications analysis, such as modification of material properties, neutron activation analysis and processing semiconductor chips.
- Fundamental and applied physics research.
- Radiocarbon Archaeological dating and research dating

According to IAEA statistics over 15 000 units are in use around the world in IAEA Member States. More than 97% of these accelerators are used for dedicated medical or commercial applications, while only a few hundred are used in scientific research.

The increasing demand for radioisotopes for medical application in the last decade has led to an increasing need for the availability of a large number of cyclotrons exclusively dedicated to the production of radioisotopes, distributed over the country even in small facilities. In 2006 IAEA published an update of the document called “Directory of Cyclotrons Used for Radionuclide Production in Member States” reporting the complete list of cyclotrons installed in all the member states, including technical, utilization and administrative information: at that time 262 operating cyclotrons were installed, in the 39 member states (IAEA, 2006). In the recent years this number has progressively increased. Large concentrations of cyclotrons for radionuclide production are located in the United States of America, Japan and Germany. Although the USA is one of the countries with the highest number of cyclotrons, the number of machines installed in the EU for medical radionuclide production is even higher. In Italy at present there are 36 PET cyclotrons (Figure 1.1). Most of these cyclotrons have been in use for 10-15 years, it is therefore expected that



Figure 1.1 PET cyclotron facilities in Italy

in the coming years some events of decommissioning or partial decommissioning for the replacement of some components, will take place.

The number of institutions that distribute radiopharmaceuticals and [^{18}F]FDG, in particular, is large. Among them, 75% of the cyclotrons are used to produce ^{18}F -FDG, either for internal use or for distribution. This is certainly an underestimation as the commercial suppliers are under-represented in the IAEA survey. The number of types of cyclotrons available commercially is also quite large and increasing. The energies range from a few MeV for PET isotope production only, to a few hundreds MeV for proton therapy. The beam currents range upwards from 40 μA to over 1 mA (IAEA,

2006). These operating conditions are very different if compared with accelerator for research purpose usually characterized by low current and high energy, for this reason these type of accelerators are considerably different in terms of residual activation and decommissioning issues.

For biological protection any kind of accelerator is housed in a thick-walled concrete building. During the operation, the accelerator itself and the surrounding structure become activated through the impact of primary and secondary particles. In the long run, this will represent a decommissioning issue. The amount of radioactivity induced and the level of decommissioning challenges are strongly dependent on the type of accelerator, its operating history and the field of application.

In the early years of constructing and operating accelerators the radiological hazards were not even recognised and did not receive the appropriate attention. Only in recent years the attention on the generation of radioactive waste and on radiological hazards associated with decommissioning started to be significant. Regulations today require that decommissioning is considered as part of the design and planning phase of an accelerator facility. During the planning phase of a new facility it has to be assured that decommissioning forms part of the lifecycle of accelerators. Funding for decommissioning should be made available from the start of operation of accelerator facilities throughout the life of the facilities. Critical issues that could be experienced during decommissioning should be preventively identified so that solutions can be found in time (Moritz, 2001).

Accelerator decommissioning and the disposal of activated materials pose a special challenge also because even very low levels of induced radioactivity must be assessed and managed. When considering the dismantling of accelerators, considerable amounts of low level solid radioactive waste have to be taken into account (European Commission, 1999).

Nevertheless there are no specific international standards or guideline documents and cases of accelerator decommissioning have been described only sporadically in technical literature. Some documents include accelerators as a small part of a much broader scope (IAEA, 2003). Most Countries have a national regulatory framework relevant to the nuclear industry, however this does not usually extend to cover specific facilities such as accelerators.

To date the question of how to deal with the quantities of radioactive waste generated during the operation and decommissioning of accelerators has not been answered satisfactorily and the current focus is rather on installation of new facilities. There is a lack of references on specific procedures to follow during the decommissioning of particle accelerators. Although a number of guideline documents have been published with the radiological protection requirements during the operation of accelerators, the decommissioning of these facilities has not been addressed sufficiently: a univocal guideline, fully accepted by the scientific community, has not been published yet. As a matter of fact, even though the number of cyclotrons installed in the world is continuously increasing, only a few instances of decommissioning have been conducted over the world. In literature there is a lack of data about practical experiences of decommissioning of particle accelerators, particularly cyclotrons, most of the data refers only to research accelerators (European Commission, 1999; IAEA, 2004;

Opelka, et al., 1979; Calandrino, et al., 2006; Birattari, et al., 1989; Carroll, 2002; Carroll, et al., 2001). Even if these data can be a valuable source of information, direct application in the planning of decommissioning strategy is not advisable due to the differences in the layout of the site, in the workload and technology of the different accelerators. The need to address the decommissioning of accelerators has been recognised by IAEA and the writing of a reference text is currently ongoing.

In the following subchapter, first the production mechanism of induced activity around a proton accelerator is described briefly, providing a short review of the basic principles involved in activation processes and listing the principal radioactive isotopes generated in accelerator environments and the surrounding structures. Then the Radiation protection aspects connected with decommissioning are presented. Finally some aspect connected with decontamination and dismantling strategies are pointed discussed.

1.2 Radioactivity induced in proton accelerators

During the interaction between a high-energy hadron and a nucleus, neutrons, protons and other nuclear fragments may be emitted, converting the nucleus to that of a different isotope and probably of a different element, with high probability of being radioactive. If secondary particles emitted have sufficient energy, they undergo further interactions and cause additional activation creating a nuclear particle cascade. Many of the nuclei are produced in excited states and de-excite by emitting neutrons, charged particles or fragments in a so called “evaporation” process; alternatively they may de-excite by emitting gamma-ray. This cascade process continues until the energies of the particles decrease below the thresholds of the nuclear reaction involved.

The amount of radioactivity induced in accelerators facilities depend on many factors, namely: the probability of producing a particular isotope, in turn a function of the composition of the material involved; the primary beam losses; the spectrum of the secondaries produced; and the cross section of the reaction involved. The amount of a radioactive isotope at a certain time also depends on the isotope half-life, the irradiation geometry, the workload of the accelerator, the time the accelerator has been in operation, as well as on the cooling time since cyclotron operation stopped. For these reasons the estimation of induced radioactivity in an accelerator and its vault is very complex and difficult to perform with analytical methods.

Considering protons interactions, the reactions involved at intermediate energy (from a few MeV up to 50 MeV) are various, the most probable reactions are (p,n), (p,np), (p,2n), (p,a). These reactions have thresholds increasing in the same order. At still higher energies other more complex reactions take place. As the energy of the incident particle increases the variety of radionuclide that can be produced increases because more reaction thresholds are crossed (NCRP, 2005).

In particular, in biomedical PET cyclotrons (p,n) is the reaction exploited in the daily production of ^{18}F from ^{18}O , for this reason this reaction has a key role within this work and in general for what concerns residual induced activation in biomedical cyclotron

facilities. More precisely, secondary neutrons arising from this reaction are mainly responsible for the activation of the structural materials. Neutron fields are in general complicated to assess because neutrons are produced in a variety of reactions and span a wide energy range. Neutrons can react at any energy producing radioactive nuclides and they are not repelled by electrostatic charge of target nuclei being unaffected by the coulomb barrier. The most probable reaction at thermal energy is neutron capture, while with increasing energy the most probable reaction are (n,p), (n,np), (n,2p), (n,a). High-energy neutrons cause spallation reactions but are not of interest for this work. Because of the high capture cross section of some materials for thermal neutrons, those are the main cause of induced radioactivity. The (n, γ) capture reactions on trace amounts of stable Europium, Cobalt and Caesium, which are present in concrete in concentrations of a few parts per million, is the main cause of residual activation. The activity concentration of these radionuclides change as a function of accelerator operating time, geometry and composition of the bunker. In table 1.1 some of the main radionuclides commonly identified in solid materials irradiated around accelerators are reported (European Commission, 1999).

Table 1.1 Radionuclides commonly identified in solid materials irradiated around accelerators

<i>Irradiated Material</i>	<i>Radionuclides</i>
<i>Plastics and oils</i>	^7Be , ^{11}C
<i>Concrete and aluminium</i>	^7Be , ^{11}C , ^{22}Na , ^{24}Na , ^{32}P , ^{42}K , ^{45}Ca
<i>Iron and steel</i>	^7Be , ^{11}C , ^{22}Na , ^{24}Na , ^{32}P , ^{42}K , ^{45}Ca , ^{44}Sc , $^{44}\text{Sc}^m$, ^{46}Sc , ^{47}Sc , ^{48}Sc , ^{48}V , ^{51}Cr , ^{52}Mn , $^{52}\text{Mn}^m$, ^{54}Mn , ^{56}Mn , ^{57}Co , ^{58}Co , ^{60}Co , ^{57}Ni , ^{55}Fe , ^{59}Fe
<i>Copper</i>	^7Be , ^{11}C , ^{22}Na , ^{24}Na , ^{32}P , ^{42}K , ^{45}Ca , ^{44}Sc , $^{44}\text{Sc}^m$, ^{46}Sc , ^{47}Sc , ^{48}Sc , ^{48}V , ^{51}Cr , ^{52}Mn , $^{52}\text{Mn}^m$, ^{54}Mn , ^{56}Mn , ^{57}Co , ^{58}Co , ^{60}Co , ^{57}Ni , ^{55}Fe , ^{59}Fe , ^{61}Cu , ^{64}Cu , ^{63}Zn , ^{65}Zn

1.3 Radiation Protection aspects in decommissioning of particle accelerators

Radiation protection (RP) aspects in the use of particle accelerators can be summarized in three point considering the working life of the accelerator itself:

- RP in Site planning
- RP in the routine use of the accelerator
- RP in the decommissioning of the facility

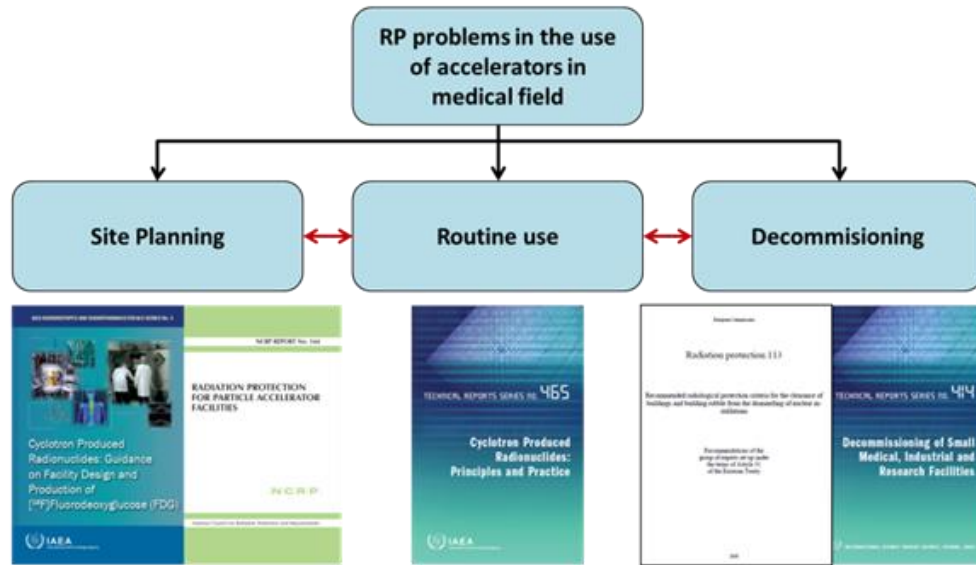


Figure 1.2 Radiation protection problems in the use of accelerators in the medical field (Infantino, 2015c).

Guidelines for site planning and installation, as well as for radiation protection assessment, are given in a number of international documents; however these well-established guidelines typically suggest analytical calculation methods to overcome RP issues. Moreover these guidelines refer to one problem at a time and do not consider interrelations between the various aspects. As an example, the choices in design in the shielding during the site planning influence the future activation of the components, and this involves a strong correlation with the decommissioning of the site.

1.3.1 International and National Regulations

Every radiation protection evaluation has to be performed according to the prescription of International and National regulation in terms of calculations, methodology applied and final result.

There is a well-established hierarchy in the available international regulations (figure 1.3).

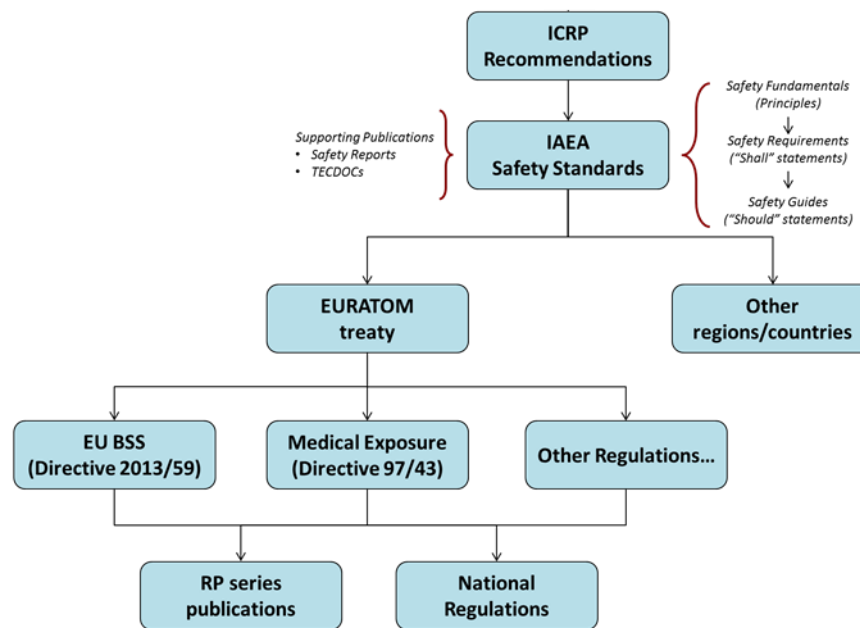


Figure 1.3 Hierarchy of the international regulations on radiation protection (Infantino, 2015c)

In view of avoiding political and economic influences an international commission of highly reputed experts in the field, the *International Commission on Radiological Protection* (ICRP), was established to publish periodical Reports that, thanks to their balance, scientific level and value, are considered the basis for any international and national regulation. The ICRP is an independent body: members of the Commission are not indicated by governments, the UN or other political or economic entities, but are expressed by the scientific community.

In the 1990 Recommendations the Commission gave the principles of protection for practices separately from intervention situations. The Commission continues to regard these principles as fundamental for the system of protection, and has now formulated a single set of principles that apply to planned, emergency, and existing exposure situations. In these Recommendations, the Commission also clarifies how the fundamental principles apply to radiation sources and to the individual, as well as how the source-related principles apply to all controllable situations. These principles are (ICRP, 2007):

- **The principle of justification.** “Any decision that alters the radiation exposure situation should do more good than harm”.
- **The principle of optimisation of protection.** “The likelihood of incurring exposures, the number of people exposed, and the magnitude of their individual doses should all be kept as low as reasonably achievable, taking into account economic and societal factors”.
- **The principle of application of dose limits.** “The total dose to any individual from regulated sources in planned exposure situations other than medical

exposure of patients should not exceed the appropriate limits recommended by the Commission”.

Two principles are source-related and apply to all exposure situations (justification and optimization) while one principle is individual-related and applies to planned exposure situations (application of dose limits).

The findings of the United Nations Scientific Committee on the Effects of Atomic Radiation (UNSCEAR) and the recommendations of ICRP, are taken into account in developing the Safety Standards of the International Atomic Energy Agency (IAEA).

The IAEA safety standards establish fundamental safety principles, requirements and measures to control the radiation exposure of people and the release of radioactive material to the environment, to restrict the likelihood of events that might lead to a loss of control over a nuclear reactor core, nuclear chain reaction, radioactive source or any other source of radiation, and to mitigate the consequences of such events if they were to occur. The standards apply to facilities and activities that give rise to radiation risks, including nuclear installations, the use of radiation and radioactive sources, the transport of radioactive material and the management of radioactive waste.

The IAEA safety standards reflect an international consensus on what constitutes a high level of safety for protecting people and the environment from harmful effects of ionizing radiation. They are issued in the IAEA Safety Standards Series, which are divided in three categories (IAEA, 2014):

- ***Safety Fundamentals***. Safety Fundamentals present the fundamental safety objective and principles of protection and safety, and provide the basis for the safety requirements;
- ***Safety Requirements***. An integrated and consistent set of Safety Requirements establishes the requirements that must be met to ensure the protection of people and the environment, both now and in the future. The requirements are governed by the objective and principles of the Safety Fundamentals. If the requirements are not met, measures must be taken to reach or restore the required level of safety. The format and style of the requirements facilitate their use for the establishment, in a harmonized manner, of a national regulatory framework. Requirements, including numbered “overarching” requirements, are expressed as “shall” statements. Many requirements are not addressed to a specific party, the implication being that the appropriate parties are responsible for fulfilling them;
- ***Safety Guides***. Safety Guides provide recommendations and guidance on how to comply with the safety requirements, indicating an international consensus that it is necessary to take the measures recommended (or equivalent alternative measures). The Safety Guides present international good practices, and increasingly they reflect best practices, to help users striving to achieve high levels of safety. The recommendations provided in Safety Guides are expressed as “should” statements.

The principal users of safety standards in IAEA Member States are regulatory bodies and other relevant national authorities. The IAEA safety standards are also used by co-sponsoring organizations and by many organizations that design, construct and operate nuclear facilities, as well as organizations involved in the use of radiation and radioactive sources. The IAEA safety standards are applicable, as relevant, throughout the entire lifetime of all facilities and activities, existing and new, utilized for peaceful purposes and to protective actions to reduce existing radiation risks. They can be used by States as a reference for their national regulations in respect of facilities and activities (IAEA, 2014).

An important issue to remember is that even if the above regulations provide the limitations to respect for a correct radiation safety practice (from a practical point of view the principle of application of dose limits) no information are provided on how to achieve this goal. In other words a regulation providing the *Radiation Protection Officer* (RPO) or the *Qualified Expert* (QE or RPE) with the methodology to do the calculation and satisfy the limits mentioned has not been published yet at any level, national or international. Generally, these methodologies are reported in “*good practice technical guides*” published by accredited organizations such as the *National Council on Radiation Protection and Measurements* (NCRP). (Infantino, 2015c)

1.3.2 Clearance levels

Radiation Protection requirements in Member State of the European Union (EU) are established at a national level, whereby national legislation is bound by the Euratom Treaty to comply with the general EU standards: “The Basic Safety Standards for the Health Protection and the General Public and Workers against the Dangers of Ionizing Radiation” (BSS). One of the requirements in EU BSS, in agreement with IAEA Safety Standard, is that the disposal, recycling and reuse of material containing radioactive substances is subject to prior authorisation by national competent authorities. The authorities in particular may specify clearance levels below which such materials are no longer subjected to the requirements of the Standards. Clearance levels shall be established on the basis of the general criteria for exemption and take into account technical guidance provided by the Community.

The scheme of figure 1.4 illustrates the decision making process indicated by the BSS. The scope of the BSS is defined in terms of practices and only indirectly in terms of any radioactive material. All practice involving radioactivity requires justification, then it must be decided if the practice should be put under the gradual system of reporting (simpler cases) or authorization (more complex situations), as prescribed by the BSS, or the practice is simply considered exempt. A practice can be considered exempt if the associated risks are sufficiently low. Radionuclide quantities and activities concentrations determining the “non relevance” of the risk are called exemption values, and have been derived for the most relevant radionuclides and republished in an Annex to the BSS (Commission of the European communities, 1993). Practices involving radioactive substances below any one of such levels are exempt from the regulatory requirements. Once a practice is put within the regulatory system all the associated activities and material movements are regulated. Sources and practices already under regulatory control may be cleared from regulatory requirements if the regulatory authority considers that this is warranted.

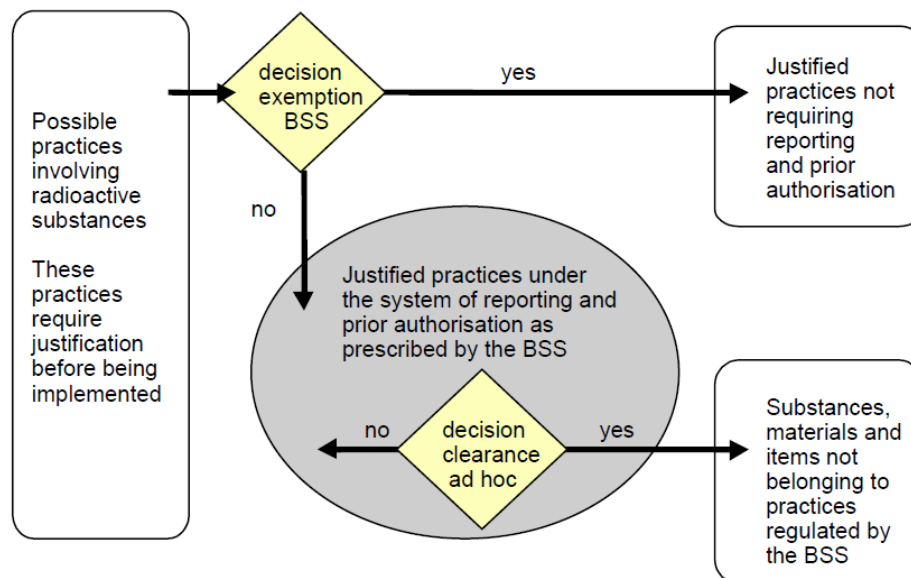


Figure 1.4 Schematic diagram illustrating the implementation of the European Union's Basic Safety Standards (European Commission, 2000)

National competent authorities may allow for a material arising from a practice to be released from the requirements of the BSS directive for disposal, reuse or recycling if the radioactivity content is below so-called “clearance levels”. The term clearance is used to describe the removal of control, and clearance levels are the recommended, nuclide specific, limits below which authorities could authorize clearance. Guidance for the dismantling of nuclear installations has been provided by a Group of Experts set up under the terms of Article 31 of the Euratom Treaty. The Working Party set up for this purpose has examined radiation exposures related to the recycling of steel,

copper and aluminium, in terms of nuclide specific mass activity concentration levels of these metals, and on terms of surface specific contamination levels for recycling or direct reuse. The technical guidance was published as “Recommended radiological protection criteria for the recycling of metals from dismantling of nuclear installations” (RP 89) (European Commission, 1998). A second technical guidance for the clearance of buildings and building rubble arising from the dismantling of nuclear installation was published in “Recommended radiological protection criteria for the clearance of buildings and building rubble from dismantling of nuclear installations” (RP 113) (European Commission, 2000). Aim of these recommendations is to propose radionuclide specific concentration limits below which construction materials, like concrete, bricks and others, could be released from regulatory control after dismantling.

The radiological protection criteria that must be met before the clearance of material can be authorised are laid down in Article 5 in conjunction with Annex I of the BSS. The recommendations RP 89 and RP 113 used these criteria to develop specific clearance levels for metallic items, equipment, scrap, building and building rubble.

The IAEA recommendation, laid down in Safety Series 89 (IAEA, 1988), refers to an individual dose of “some tens of microsieverts per year” ($\mu\text{Sv}/\text{y}$) as being trivial and therefore a basis for exemption. Furthermore to take in to account exposures from more than one exempt practice, “each exempt practice should utilize only a part of that criterion, and it may be reasonable for national authorities to apportion a fraction of that upper bound to each practice. This fractionation could lead to individual doses to the critical group of the order of $10 \mu\text{Sv}$ in a year from each exempt practice” (IAEA, 1988) In addition the IAEA recommends that for each practice a study of available options be made by regulating authorities in order to optimise radiation protection. If the study “indicates that the collective dose commitment resulting from one year of the unregulated practice will be less than about 1 manSv ... it may be concluded that the total detriment is low enough to permit exemption without a more detailed examination of other options”. The general international consensus on the basic criteria for exemption is reflected by their inclusion in both the IAEA BSS (IAEA, 1996) and Euratom BSS. Publication 60 of the International Commission of Radiological Protection (ICRP) (ICRP, 1990) also discusses the concept of exemption from regulatory control.

It is difficult to relate dose received by individuals to a specific practice, or to the level of radioactivity involved in a practice, especially in the definition of clearance criteria that must be evaluated according to a largely hypothetical “a priori” estimation. This problem was dealt by the working group considering a set of exposure scenarios that relates the activity content to an individual dose. The clearance levels proposed are derived radioactivity levels from the most critical scenario, which lead to calculated dose of either $10 \mu\text{Sv}/\text{y}$ or a skin dose of $50 \text{ mSv}/\text{y}$.

In the following the clearance levels given in RP 89 and RP 113 are reported. The nuclide specific clearance levels in table 1.2 are the lowest value for metal and metal scrap for which the only use after clearance is as input for the production of new metal. The mass specific clearance levels apply to the total activity per unit mass of the metal being released and are intended as an average over moderate amounts of metal. The

nuclide specific clearance levels in table 1.3 apply to metal components, equipment or tools for which a post-clearance use in the same or modified form is foreseen, i.e. direct reuse. The surface specific clearance levels apply to the total surface activity concentration and are intended as an average over moderate areas.

While clearance levels reported in table 1.4, 1.5 and 1.6 apply to buildings, rooms, sections of buildings and building structures in which practices requiring reporting or prior authorisation were carried out, and to building rubble resulting from the demolition of such structures. The radionuclides investigated are those with half-lives longer than 60 days, the list is not exhaustive and therefore it is possible that an unlisted radionuclide could be significant for clearance decisions. Regarding the act of clearance, three main groups of clearance levels for buildings are derived:

- Clearance for buildings for any purpose (reuse or demolition) (table 1.4);
- Clearance for buildings for demolition only (table 1.5);
- Clearance for building rubble (table 1.6).

The recommended clearance levels represent the total activity in the structure per unit surface area below which the clearance criteria will be satisfied.

In nearly all practical cases more than one radionuclide is involved. To determine if a mixture of radionuclides is below the clearance level a summation formula can be used:

$$\sum_{i=1}^N \frac{c_i}{c_{li}} < 1.0 \quad \text{Equation 1.1}$$

Where

c_i is the total activity on the structure per unit surface area of radionuclide i (Bq/cm²)

c_{li} is the clearance level of radionuclide i (Bq/cm²)

n is the number of radionuclides in the mixture

Table 1.2 Nuclide specific clearance levels for metal scrap recycling from RP 89 (European Commission, 1998)

Nuclide	Mass specific (Bq/g)	Surface specific (Bq/cm ²)	Nuclide	Mass specific (Bq/g)	Surface specific (Bq/cm ²)
H 3	1000	100000	Tm 171	1000	10000
C 14	100	1000	Ta 182	1	10
Na 22	1*	10	W 181	100	1000
S 35	1000	1000	W 185	1000	1000
Cl 36	10	100	Os 185	1	10
K 40	1	100	Ir 192	1	10
Ca 45	1000	100	Tl 204	1000	1000
Sc 46	1*	10	Pb 210	1*	1
Mn 53	10000	100000	Bi 207	1	10
Mn 54	1	10	Po 210	1	0.1
Fe 55	10000	10000	Ra 226	1	0.1
Co 56	1	10	Ra 228	1	1
Co 57	10	100	Th 228	1	0.1
Co 58	1	10	Th 229	1*	0.1
Co 60	1	10	Th 230	1*	0.1
Ni 59	10000	10000	Th 232	1*	0.1
Ni 63	10000	10000	Pa 231	1*	0.1
Zn 65	1	100	U 232	1	0.1
As 73	100	1000	U 233	1	1
Se 75	1	100	U 234	1	1
Sr 85	1	100	U 235	1	1
Sr 90	10	10	U 236	10	1
Y 91	10	100	U 238	1	1
Zr 93	10	100	Np 237	1	0.1
Zr 95	1	10	Pu 236	1	0.1
Nb 93m	1000	10000	Pu 238	1*	0.1
Nb 94	1	10	Pu 239	1*	0.1
Mo 93	100	1000	Pu 240	1*	0.1
Tc 97	1000	1000	Pu 241	10	10
Tc 97m	1000	1000	Pu 242	1*	0.1
Tc 99	100	1000	Pu 244	1*	0.1
Ru 106	1	10	Am 241	1*	0.1
Ag 108m	1	10	Am 242m	1	0.1
Ag 110m	1	10	Am 243	1*	0.1
Cd 109	10	100	Cm 242	10	1
Sn 113	1	100	Cm 243	1	0.1
Sb 124	1	10	Cm 244	1	0.1
Sb 125	10	100	Cm 245	1*	0.1
Te 123m	10	100	Cm 246	1*	0.1
Te 127m	100	100	Cm 247	1	0.1
I 125	1	100	Cm 248	1*	0.1
I 129	1	10	Bk 249	100	100
Cs 134	1*	10	Cf 248	10	1
Cs 135	10	1000	Cf 249	1	0.1
Cs 137	1	100	Cf 250	1	0.1
Ce 139	10	100	Cf 251	1	0.1
Ce 144	10	10	Cf 252	1	0.1
Pm 147	10000	1000	Cf 254	1	0.1
Sm 151	10000	1000	Es 254	10	1
Eu 152	1	10			
Eu 154	1	10			
Eu 155	10	1000			
Gd 153	10	100			
Tb 160	1	10			
Tm 170	100	1000			

Table 1.3 Nuclide specific levels for direct reuse of metal items (European Commission, 1998)

Nuclides	Surface specific (Bq/cm ²)	Nuclides	Surface specific (Bq/cm ²)
H 3	10000	Tm 171	10000
C 14	1000	Ta 182	10
Na 22	1	W 181	100
S 35	1000	W 185	1000
Cl 36	100	Os 185	10
K 40	10	Ir 192	10
Ca 45	100	Tl 204	100
Sc 46	10	Pb 210	1
Mn 53	10000	Bi 207	1
Mn 54	10	Po 210	0.1
Fe 55	1000	Ra 226	0.1
Co 56	1	Ra 228	1
Co 57	10	Th 228	0.1
Co 58	10	Th 229	0.1
Co 60	1	Th 230	0.1
Ni 59	10000	Th 232	0.1
Ni 63	1000	Pa 231	0.1
Zn 65	10	U 232	0.1
As 73	1000	U 233	1
Se 75	10	U 234	1
Sr 85	10	U 235	1
Sr 90	10	U 236	1
Y 91	100	U 238	1
Zr 93	100	Np 237	0.1
Zr 95	10	Pu 236	0.1
Nb 93m	1000	Pu 238	0.1
Nb 94	1	Pu 239	0.1
Mo 93	100	Pu 240	0.1
Tc 97	100	Pu 241	10
Tc 97m	1000	Pu 242	0.1
Tc 99	1000	Pu 244	0.1
Ru 106	10	Am 241	0.1
Ag 108m	1	Am 242m	0.1
Ag 110m	1	Am 243	0.1
Cd 109	100	Cm 242	1
Sn 113	10	Cm 243	0.1
Sb 124	10	Cm 244	0.1
Sb 125	10	Cm 245	0.1
Te 123m	100	Cm 246	0.1
Te 127m	100	Cm 247	0.1
I 125	100	Cm 248	0.1
I 129	10	Bk 249	100
Cs 134	1	Cf 248	1
Cs 135	100	Cf 249	0.1
Cs 137	10	Cf 250	0.1
Ce 139	10	Cf 251	0.1
Ce 144	10	Cf 252	0.1
Pm 147	1000	Cf 254	0.1
Sm 151	1000	Es 254	1
Eu 152	1		
Eu 154	1		
Eu 155	100		
Gd 153	10		
Tb 160	10		
Tm 170	1000		

Table 1.4 Radionuclide specific clearance levels for building reuse or demolition expressed as total activity in the structure per unit surface area (European Commission, 2000)

Radio nuclide	Most restrictive scenario	Clearance level (Bq/cm ²)	Rounded cl. level (Bq/cm ²)
H 3	water child	3.8E+3	10,000
C 14	β-skin	2.8E+3	1000
Na 22	external	4.4E-1	1
S 35	β-skin	2.6E+3	1000
Cl 36	vegetable	3.2E+1	100
K 40	external	5.6E+0	10
Ca 45	β-skin	1.1E+3	1000
Sc 46	external	1.3E+0	1
Mn 53	vegetable	2.3E+4	10,000
Mn 54	external	1.5E+0	1
Fe 55	inhalation	1.0E+4	10,000
Co 56	external	8.2E-1	1
Co 57	external	1.2E+1	10
Co 58	external	3.2E+0	10
Co 60	external	3.6E-1	1
Ni 59	inhalation	4.2E+4	100,000
Ni 63	inhalation	1.8E+4	10,000
Zn 65	external	2.3E+0	1
As 73	external	4.0E+2	1000
Se 75	external	5.2E+0	10
Sr 85	external	6.2E+0	10
Sr 90	vegetable	3.4E+1	100
Y 91	β-skin	4.1E+2	1000
Zr 93	inhalation	3.1E+2	1000
Zr 95	external	1.8E+0	1
Nb 93m	external	5.0E+2	1000
Nb 94	external	5.3E-1	1
Mo 93	external	7.5E+1	100
Tc 97	external	8.0E+1	100
Tc 97m	external	2.9E+2	100
Tc 99	vegetable	7.0E+1	100
Ru 106	external	5.6E+0	10
Ag 108m	external	5.1E-1	1
Ag 110m	external	4.8E-1	1
Cd 109	external	4.0E+1	100
Sn 113	external	7.2E+0	10
Sb 124	external	1.9E+0	1
Sb 125	external	2.1E+0	1
Te 123m	external	1.4E+1	10
Te 127m	external	1.3E+2	100
I 125	external	7.5E+1	100
I 129	water adult	7.5E+0	10
Cs 134	external	6.3E-1	1
Cs 135	β-skin	1.8E+3	1000
Cs 137	external	1.5E+0	1
Ce 139	external	1.2E+1	10
Ce 144	external	2.6E+1	10
Pm 147	β-skin	1.5E+3	1000
Sm 151	inhalation	3.6E+3	10,000
Eu 152	external	7.7E-1	1
Eu 154	external	6.9E-1	1
Eu 155	external	1.5E+1	10
Gd 153	external	1.2E+1	10
Tb 160	external	2.9E+0	1
Tm 170	external	3.7E+2	1000
Tm 171	external	1.5E+3	1000
Ta 182	external	1.7E+0	1
W 181	external	5.1E+1	100
W 185	β-skin	8.1E+2	1000
Os 185	external	3.3E+0	10
Ir 192	external	3.7E+0	10
Tl 204	β-skin	4.8E+2	1000
Pb 210	vegetable	1.4E+0	1
Bi 207	external	5.4E-1	1
Po 210	inhalation	4.2E+0	10
Ra 226	external	4.9E-1	1
Ra 228	inhalation	4.4E-1	1
Th 228	inhalation	2.7E-1	0.1
Th 229	inhalation	1.2E-1	0.1
Th 230	inhalation	3.3E-1	1
Th 232	inhalation	1.4E-1	0.1
Pa 231	inhalation	1.3E-2	0.1*
U 232	inhalation	1.7E-1	0.1
U 233	inhalation	1.2E+0	1
U 234	inhalation	1.4E+0	1
U 235	inhalation	1.3E+0	1
U 236	inhalation	1.5E+0	1
U 238	inhalation	1.6E+0	1
Np 237	inhalation	6.2E-1	1
Pu 236	inhalation	7.1E-1	1
Pu 238	inhalation	3.1E-1	1
Pu 239	inhalation	2.9E-1	0.1
Pu 240	inhalation	2.9E-1	0.1
Pu 241	inhalation	1.1E+1	10
Pu 242	inhalation	3.0E-1	1
Pu 244	inhalation	3.1E-1	1
Am 241	inhalation	3.4E-1	1
Am 242m	inhalation	3.2E-1	1
Am 243	inhalation	3.4E-1	1
Cm 242	inhalation	2.5E+0	1
Cm 243	inhalation	4.6E-1	1
Cm 244	inhalation	5.5E-1	1
Cm 245	inhalation	3.0E-1	0.1
Cm 246	inhalation	3.4E-1	1
Cm 247	inhalation	3.7E-1	1
Cm 248	inhalation	9.8E-2	0.1
Bk 249	inhalation	8.4E+1	100
Cf 248	inhalation	1.5E+0	1
Cf 249	inhalation	2.1E-1	0.1
Cf 250	inhalation	4.2E-1	1
Cf 251	inhalation	2.0E-1	0.1
Cf 252	inhalation	7.1E-1	1
Cf 254	inhalation	4.2E-1	1
Es 254	external	1.4E+0	1

Table 1.5 Radionuclide specific clearance levels for building demolition expressed as total activity in the structure per unit surface area (European Commission, 2000)

Radio nuclide	Most restrictive scenario	Clearance level (Bq/cm ²)	Rounded Cl. Level (Bq/cm ²)
H 3	water child	3.8E+3	10,000
C 14	water child	5.8E+3	10,000
Na 22	landfill	3.5E+0	10
S 35	ing. worker	2.0E+5	100,000
Cl 36	vegetable	3.2E+1	100
K 40	vegetable	2.4E+1	10
Ca 45	inhalation	6.4E+4	100,000
Sc 46	landfill	1.1E+1	10
Mn 53	vegetable	2.3E+4	10,000
Mn 54	landfill	1.2E+1	10
Fe 55	ing. child	2.4E+4	10,000
Co 56	landfill	6.1E+0	10
Co 57	landfill	1.3E+2	100
Co 58	landfill	2.6E+1	10
Co 60	landfill	2.9E+0	1
Ni 59	ing. child	8.9E+4	100,000
Ni 63	ing. child	3.7E+4	100,000
Zn 65	landfill	1.9E+1	10
As 73	landfill	2.1E+4	10,000
Se 75	landfill	4.9E+1	100
Sr 85	landfill	5.2E+1	100
Sr 90	vegetable	3.4E+1	100
Y 91	inhalation	5.4E+4	100,000
Zr 93	inhalation	2.5E+3	1000
Zr 95	landfill	1.5E+1	10
Nb 93m	ing. child	3.8E+4	100,000
Nb 94	landfill	4.3E+0	10
Mo 93	water adult	2.3E+3	1000
Tc 97	vegetable	6.9E+2	1000
Tc 97m	water child	5.2E+2	1000
Tc 99	vegetable	7.0E+1	100
Ru 106	landfill	4.5E+1	100
Ag 108m	landfill	4.2E+0	10
Ag 110m	landfill	3.9E+0	10
Cd 109	landfill	4.1E+3	10,000
Sn 113	landfill	6.7E+1	100
Sb 124	landfill	1.5E+1	10
Sb 125	landfill	1.8E+1	10
Te 123m	landfill	1.6E+2	100
Te 127m	landfill	3.3E+3	10,000
I 125	ing. worker	1.4E+4	10,000
I 129	water adult	7.5E+0	10
Cs 134	landfill	5.1E+0	10
Cs 135	vegetable	8.8E+3	10,000
Cs 137	landfill	1.2E+1	10
Ce 139	landfill	1.4E+2	100
Ce 144	landfill	2.4E+2	100
Pm 147	inhalation	2.4E+4	10,000
Sm 151	inhalation	2.9E+4	10,000
Eu 152	landfill	6.2E+0	10
Eu 154	landfill	5.7E+0	10
Eu 155	landfill	2.6E+2	100
Gd 153	landfill	2.9E+2	100

Radio nuclide	Most restrictive scenario	Clearance level (Bq/cm ²)	Rounded Cl. Level (Bq/cm ²)
Tb 160	landfill	2.3E+1	10
Tm 170	landfill	9.0E+3	10,000
Tm 171	landfill	5.8E+4	100,000
Ta 182	landfill	1.4E+1	10
W 181	landfill	1.7E+3	1000
W 185	ing. worker	3.9E+5	1000000
Os 185	landfill	2.9E+1	10
Ir 192	landfill	3.1E+1	100
Tl 204	vegetable	2.5E+3	1000
Pb 210	vegetable	1.4E+0	1
Bi 207	landfill	4.5E+0	10
Po 210	inhalation	7.4E+1	100
Ra 226	vegetable	9.4E-1	1
Ra 228	inhalation	3.8E+0	10
Th 228	inhalation	2.6E+0	1
Th 229	inhalation	9.4E-1	1
Th 230	inhalation	2.7E+0	1
Th 232	inhalation	1.2E+0	1
Pa 231	inhalation	1.1E-1	0.1
U 232	inhalation	1.4E+0	1
U 233	inhalation	9.7E+0	10
U 234	inhalation	1.1E+1	10
U 235	inhalation	1.0E+1	10
U 236	inhalation	1.2E+1	10
U 238	inhalation	1.3E+1	10
Np 237	inhalation	5.0E+0	10
Pu 236	inhalation	6.5E+0	10
Pu 238	inhalation	2.5E+0	1
Pu 239	inhalation	2.3E+0	1
Pu 240	inhalation	2.3E+0	1
Pu 241	inhalation	9.2E+1	100
Pu 242	inhalation	2.4E+0	1
Pu 244	inhalation	2.5E+0	1
Am 241	inhalation	2.8E+0	1
Am 242m	inhalation	2.6E+0	1
Am 243	inhalation	2.8E+0	1
Cm 242	inhalation	4.0E+1	100
Cm 243	inhalation	3.8E+0	10
Cm 244	inhalation	4.5E+0	10
Cm 245	inhalation	2.4E+0	1
Cm 246	inhalation	2.8E+0	1
Cm 247	inhalation	3.0E+0	1
Cm 248	inhalation	7.9E-1	1
Bk 249	inhalation	9.8E+2	1000
Cf 248	inhalation	1.7E+1	10
Cf 249	inhalation	1.7E+0	1
Cf 250	inhalation	3.5E+0	10
Cf 251	inhalation	1.6E+0	1
Cf 252	inhalation	6.6E+0	10
Cf 254	inhalation	1.4E+1	10
Es 254	landfill	1.2E+1	10

Table 1.6 Radionuclide specific clearance levels for building rubble expressed as total activity in the structure per unit surface area (European Commission, 2000)

Radio nuclide	Most restrictive scenario	Clearance level (Bq/g)	Rounded cl. level (Bq/g)
H 3	water child	6.2E+1	100
C 14	vegetable	1.0E+1	10
Na 22	landfill	1.0E-1	0.1
S 35	β-skin	1.0E+3	1000
Cl 36	vegetable	1.1E+0	1
K 40	vegetable	7.9E-1	1
Ca 45	β-skin	4.2E+2	1000
Sc 46	landfill	1.1E-1	0.1
Mn 53	vegetable	1.5E+3	1000
Mn 54	landfill	2.6E-1	0.1
Fe 55	ing. child	6.1E+2	1000
Co 56	landfill	6.2E-2	0.1
Co 57	landfill	2.7E+0	1
Co 58	landfill	2.3E-1	0.1
Co 60	landfill	8.9E-2	0.1
Ni 59	ing. child	2.9E+3	1000
Ni 63	ing. child	1.2E+3	1000
Zn 65	landfill	3.8E-1	1
As 73	landfill	2.1E+2	100
Se 75	landfill	6.7E-1	1
Sr 85	landfill	4.4E-1	1
Sr 90	vegetable	1.5E+0	1
Y 91	β-skin	1.6E+2	100
Zr 93	inhalation	8.2E+1	100
Zr 95	landfill	1.2E-1	0.1
Nb 93m	ing. child	1.2E+3	1000
Nb 94	landfill	1.4E-1	0.1
Mo 93	water adult	3.8E+1	100
Tc 97	vegetable	1.4E+1	10
Tc 97m	water child	8.6E+0	10
Tc 99	vegetable	1.4E+0	1
Ru 106	landfill	1.1E+0	1
Ag 108m	landfill	1.4E-1	0.1
Ag 110m	landfill	8.1E-2	0.1
Cd 109	landfill	1.0E+2	100
Sn 113	landfill	8.9E-1	1
Sb 124	β-skin	2.0E+2	100
Sb 125	landfill	5.4E-1	1
Te 123m	landfill	2.1E+0	1
Te 127m	landfill	4.3E+1	100
I 125	ing. worker	1.1E+2	100
I 129	water adult	1.2E-1	0.1
Cs 134	landfill	1.4E-1	0.1
Cs 135	ing. child	4.3E+2	1000
Cs 137	landfill	4.0E-1	1
Ce 139	landfill	2.1E+0	1
Ce 144	landfill	5.2E+0	10
Pm 147	β-skin	6.0E+2	1000
Sm 151	inhalation	9.5E+2	1000
Eu 152	landfill	2.0E-1	0.1
Eu 154	landfill	1.8E-1	0.1
Eu 155	landfill	8.1E+0	10
Gd 153	landfill	6.0E+0	10
Tb 160	landfill	2.1E-1	0.1
Tm 170	landfill	1.3E+2	100

Radio nuclide	Most restrictive scenario	Clearance level (Bq/g)	Rounded cl. level (Bq/g)
Tm 171	β-skin	1.5E+3	1000
Ta 182	landfill	1.8E-1	0.1
W 181	landfill	2.4E+1	10
W 185	β-skin	3.2E+2	1000
Os 185	landfill	3.3E-1	1
Ir 192	landfill	2.9E-1	0.1
Tl 204	vegetable	8.1E+1	100
Pb 210	ing. child	8.7E-2	0.1
Bi 207	landfill	1.5E-1	0.1
Po 210	inhalation	1.1E+0	1
Ra 226	ing. child	8.3E-2	0.1
Ra 228	inhalation	1.2E-1	0.1
Th 228	inhalation	7.3E-2	0.1
Th 229	inhalation	3.1E-2	0.1
Th 230	inhalation	8.8E-2	0.1
Th 232	inhalation	3.8E-2	0.1
Pa 231	inhalation	3.5E-3	0.1*
U 232	inhalation	4.5E-2	0.1
U 233	inhalation	3.2E-1	1
U 234	inhalation	3.6E-1	1
U 235	inhalation	3.4E-1	1
U 236	inhalation	3.9E-1	1
U 238	inhalation	4.3E-1	1
Np 237	inhalation	1.6E-1	0.1
Pu 236	inhalation	1.9E-1	0.1
Pu 238	inhalation	8.2E-2	0.1
Pu 239	inhalation	7.7E-2	0.1
Pu 240	inhalation	7.7E-2	0.1
Pu 241	inhalation	3.0E+0	1
Pu 242	inhalation	8.0E-2	0.1
Pu 244	inhalation	8.2E-2	0.1
Am 241	inhalation	9.1E-2	0.1
Am 242m	inhalation	8.5E-2	0.1
Am 243	inhalation	9.1E-2	0.1
Cm 242	inhalation	6.7E-1	1
Cm 243	inhalation	1.2E-1	0.1
Cm 244	inhalation	1.5E-1	0.1
Cm 245	inhalation	8.0E-2	0.1
Cm 246	inhalation	9.1E-2	0.1
Cm 247	inhalation	9.9E-2	0.1
Cm 248	inhalation	2.6E-2	0.1*
Bk 249	inhalation	2.2E+1	10
Cf 248	inhalation	4.0E-1	1
Cf 249	inhalation	5.5E-2	0.1
Cf 250	inhalation	1.1E-1	0.1
Cf 251	inhalation	5.4E-2	0.1
Cf 252	inhalation	1.9E-1	0.1
Cf 254	inhalation	1.1E-1	0.1
Es 254	landfill	2.5E-1	0.1

1.4 Decontamination and dismantling strategies

Clearly quantifying the extent and the order of magnitude of induced activation is the key factor in order to identify possible countermeasures to be taken during the construction phase of accelerators.

Some of the main aspects that should be taken into consideration and that could have a major impact during decommissioning are:

- Choice of materials. For example the selection of metals such as the use of aluminium instead of copper in magnet coils would reduce the production of ^{60}Co .
- Physical layout of the accelerator components. If there is a possibility to change the layout components and equipment should not be placed near locations where a large fraction of the accelerated beam interacts. This will shorten the operation life of electronic equipment and may result in the unnecessary generation of radioactive waste.
- Method of assembly. If the concrete shielding consists of individual removable blocks it will be much easier to remove each block and separate of waste during dismantling. Some accelerator facilities use a combination of removable blocks and massive walls.
- Care in operations and maintenance of equipment. Beam tuning will have a definite effect upon the amount of unwanted beam losses resulting in the activation of equipment and shielding, (creation of so-called hot spots). There should be a constant strive to higher efficiency in the extraction of the beam from the accelerator and transport to the target with minimum losses.

These kind of consideration during the design phase can decrease dismantling costs, minimize unavoidable activation areas, and maximize potential for reuse.

Large amounts of only slightly radioactive items originating from the operation of accelerators could result in high cost associated with the management of radioactive waste. In some cases, after an adequate evaluation, recycling of the mostly metallic radioactive material from the accelerator environment is not only reasonable but also the most economic approach.

The reuse of already established facilities is also a recommended approach: there are some examples of accelerator facilities that were decommissioned and reused again. The ANSTO Camperdown Facility is a recent initiative where ANSTO and The University of Sydney are working together to reuse the building that housed the 30 MeV cyclotron to construct a new 18 MeV cyclotron and associated ancillary works. (Ellis, 2011). This approach can be used in the case of PET cyclotrons facilities: adopting a careful design of the vault, it is generally possible to replace an outdated cyclotron at the end of its life cycle with a new machine, reusing the same bunker.

As a general consideration, if possible unconditioned and conditioned recycling are to be preferred to the apparently more simple method of disposal as radioactive waste, not least of all due to economic consideration (European Commission, 1999).

In the European Commission Report 19151 (European Commission, 1999) some techniques to dismantle particle accelerators in such a way that the volume of nuclear waste is kept to a minimum are proposed. The choice of dismantling activities and the use of dismantling technique are to be selected after adequate consideration of the residual radioactivity induced in the materials. A good activation assessment of individual equipment and structure component is therefore the basis for the definition of an optimized decommissioning strategy. The selection of techniques used for dismantling is optimised from the point of view of radiation protection, secondary waste generation and cost-efficiency. The EC report proposed a wide range of techniques for dismantling shielding vaults, to allow a clean dismantling of concrete and to separate the activated structures with the least possible generation of dust:

- Sawing, wire-cutting, circular sawing, chain sawing
- Drilling, core drilling
- Cutting with special hydraulic pincers, operated manually on gripper arms
- Thermal exposure of reinforcing steels by means of electric resistance heating

The in-depth activation study of shielding structures is fundamental to identify and remove the activated part of roof, walls and floors from the rest of the structures. It is important to separate the radiological waste generated in accelerator facilities from other kinds of waste throughout the operational as well as decommissioning period, it is also important to separate long lived and short lived isotopes as far as possible. Monitoring the potential residual activation during the operational life of a particle accelerator represents a good practice to preventively estimate decommissioning. Characterization may often provide technical challenges, incorrect characterization or methodology applied might result in wrong classification of waste. It is very important to have a well-defined characterization plan agreed on by the regulator, the waste disposal operator and the accelerator operator. Normally characterization methodologies and plans for accelerator facility are not regulated by standard procedure as in the case of other nuclear facilities such as Nuclear Power Plants and Nuclear Fuel Cycle Facilities.

Monte Carlo simulations, supported by experimental measurements, represent the most accurate way to assess preventively the level of activation of cyclotron components and shielding, to identify the most problematic radionuclides produced and to perform an optimal design of the whole site including the planning of an ad-hoc strategy of decommissioning. The great advantage of this methodology compared to analytical methods, is the possibility to reproduce the real geometry of the bunker and to obtain reliable results in complex geometry conditions.

Chapter 2

The Monte Carlo FLUKA code

The present chapter presents an introduction to the Monte Carlo methods and to the role of random numbers used to calculate approximate solutions to mathematical or physical problems. In particular the Monte Carlo FLUKA code used in this work will be described with an overview of the physical models it uses, underlying those aspects important for the present work.

2.1 Monte Carlo Methods

The analytical solution through differential equations of physical problems involved in this work, e.g. particle transport and radiation interaction with matter, is very complex and strong approximations are usually needed for an analytical formulation of the problem. Monte Carlo methods represent a valid alternative to analytical methods.

The Monte Carlo method was invented by John von Neumann, Stanislaw Ulam and Nicholas Metropolis (who named the method), and independently by Enrico Fermi. Originally it was not a simulation method, but a method to solve a multidimensional integro-differential equation by building a stochastic process such that some parameters of the resulting distributions would satisfy that equation. This technique is based on generation of random numbers. The equation itself did not necessarily refer to a physical process, and if it did, that process was not necessarily stochastic.

It was soon realised, however, that when the method was applied to an equation describing a physical stochastic process, such as neutron diffusion, the model could be identified with the process itself. In these cases the method has become known as a simulation technique, since every step of the model corresponds to an identical step in the physical process simulated. Typical applications of MC methods are physical processes described by probabilities, for instance particle-transport processes considering that cross section are interaction probabilities per unit distance (Fassò, et

al., 2009). In this case for example the solution of transport equations via Monte Carlo methods is not approached trying to solve all the differential equations describing the problem, but rather by making a virtual experiment similar to the real process. Every single physical event of the cascade is simulated and the particle stories are tracked.

Theoretical and mathematical foundations of Monte Carlo are well documented in a variety of basic textbooks (Kalos, et al., 2008; Lux, et al., 1990; Carter, et al. 1975; Hammersley, et al., 1964; Spanier, et al., 1969; Dunn & Shultis, 2012). In the following just a brief mention about the mathematical basis of Monte Carlo Methods will be reported.

Considering a variable x , distributed according to a function $f(x)$, the mean or average of a function of the same variable $A(x)$ over an interval $[a,b]$ is:

$$\bar{A} = \frac{\int_a^b A(x)f(x)dx}{\int_a^b f(x)dx} \quad \text{Equation 2.1}$$

Introducing the normalized distribution $f'(x)$

$$f'(x) = \frac{f(x)}{\int_a^b f(x)dx} \quad \text{Equation 2.2}$$

$$\bar{A} = \int_a^b A(x)f'(x)dx \quad \text{Equation 2.3}$$

Considering more than one dimension, given n variables x,y,\dots , distributed according to the normalised functions $f'(x), g'(y), \dots$, the mean or average of a function of those variables $A(x,y,\dots)$ over an n -dimensional domain is given by:

$$\bar{A} = \int_x \int_y \dots \int A(x, y, \dots) f'(x)g'(y) \dots dx dy \dots \quad \text{Equation 2.4}$$

An n -dimensional integral is often impossible to calculate with traditional methods, but N values of A can be sampled with probability $f'g' \dots$ and the sum of a sampled values will be divided by N :

$$S_N = \frac{\sum_1^N A(x, y, z, \dots)}{N} \quad \text{Equation 2.5}$$

Since each term of the sum is distributed like A , in this case the integration is also a simulation.

The Central Limit theorem, that is the mathematical foundation of the Monte Carlo method, states that for large values of N , the distribution of averages S_N of N independent random variables identically distributed tends to a normal distribution with mean \bar{A} and variance σ_A^2/N :

$$\lim_{N \rightarrow \infty} S_N = \lim_{N \rightarrow \infty} \frac{\sum_1^N A(x, y, \dots) f'(x) g'(x) \dots}{N} = \bar{A} \quad \text{Equation 2.6}$$

$$\lim_{N \rightarrow \infty} P(S_N) = \frac{1}{\sqrt{(2\pi/N)\sigma_A}} e^{-\frac{(S_N - \bar{A})^2}{2\sigma_A^2/N}} \quad \text{Equation 2.7}$$

In words: “Given any observable A, that can be expressed as the result of a convolution of random processes, the average value of A can be obtained by sampling many values of A according to the probability distribution of the random process”.

The Monte Carlo method is an integration technique to solve multi-dimensional integrals by sampling from suitable stochastic distributions.

The accuracy of a MC estimator depends on the number of samples:

$$\sigma \propto \frac{1}{\sqrt{N}} \quad \text{Equation 2.8}$$

In an analogue Monte Carlo calculation, not only the mean of the contributions converges to the mean of the actual distribution, but also the variance and all moments of higher order:

$$\lim_{N \rightarrow \infty} \left[\frac{\sum_1^N (x - \bar{x})^n}{N} \right]^{1/n} = \sigma_n \quad \text{Equation 2.9}$$

Then, partial distributions, fluctuations and correlations are all faithfully reproduced: in this case there is a real simulation.

The distinctive feature of Monte Carlo is the use of random sampling techniques. The central problem of Monte Carlo Techniques is:

“Given a Probability Density Function (pdf) of the x variable, f(x), generate a sample of x’s distributed according to f(x), where x can be multi-dimensional”

In the real physical world, an experiment samples a large number of random outcomes of physical processes: these correspond, in a computer calculation, to pseudo-random numbers sampled from pdf distributions.

Pseudo-random numbers (PRN) are sequences that reproduce the uniform distribution, constructed from mathematical algorithms (PRN generators). PRN generators have a period, after which the sequence is identically repeated. It is very important that the length of the sequence be such that no repetition would happen in any calculation.

A typical Monte Carlo particle transport code works as follows: each particle is followed on its path through matter. At each step the occurrence and outcome of interactions are decided by random selection from the appropriate probability distributions. All the secondaries issued from the same primary are stored in a “stack” or “bank” and are transported before a new history is started.

In the following chapter the Monte Carlo FLUKA approach to transport physics will be presented.

2.2 The FLUKA code

2.2.1 FLUKA

In this work, the FLUKA code (Bohlen, et al., 2014; Ferrari, et al., 2005) was used. FLUKA is a general purpose tool for calculations of particle transport and interactions with matter, covering an extended range of applications spanning from proton and electron accelerator shielding to target design, calorimetry, activation, dosimetry, detector design, Accelerator Driven Systems, cosmic rays, neutrino physics, radiotherapy, radiobiology. It was developed and is maintained under an INFN-CERN agreement. Microscopic models are adopted whenever possible, consistency among all the reaction steps and/or reaction types is ensured, conservation laws are enforced at each step, and results are checked against experimental data at single interaction level. As a result, final predictions are obtained with a minimal set of free parameters fixed for all energy/target/projectile combinations. Therefore results in complex cases, as well as properties and scaling laws, arise naturally from the underlying physical models, predictivity is provided where no experimental data are directly available, and correlations within interactions and among shower components are preserved. The FLUKA physical models are described in several journal and conference papers (Fassò, et al., 2003; Ferrari, 2006; Battistoni, et al., 2007; Fassò, et al., 1995). FLUKA can simulate with high accuracy the interaction and propagation in matter of about 60 different particles, including photons and electrons from 1 keV to thousands of TeV, neutrinos, muons of any energy, hadrons of energies up to 20 TeV and all the corresponding antiparticles, neutrons down to thermal energies and heavy ions. The program can also transport polarised photons (e.g., synchrotron radiation) and optical photons. Time evolution and tracking of emitted radiation from unstable residual nuclei can be performed online. FLUKA can handle even very complex geometries, using an improved version of the well-known Combinatorial Geometry (CG) package. The FLUKA CG has been designed to track correctly also charged particles (even in the presence of magnetic or electric fields). Various visualization and debugging tools are also available. For most applications, no programming is required from the user. However, a number of user interface routines (in Fortran 77) are available for users with special requirements (FLUKA, 2010).

For many years FLUKA has been known as one of the main tools for designing shielding of proton accelerators in the multi-GeV energy range (its hadron event generator has been adopted by the majority of the existing high-energy transport codes, including those used for particle physics simulations). In recent years, however, FLUKA has gone through an important process of transformation which has converted it from a specialized to a multi-purpose program, not restricted to a limited family of particles or to a particular energy domain. If in its original high energy field FLUKA

has few competitors, this is not the case in the intermediate and in the low energy range, where several well established transport codes exist. However, FLUKA can compare favourably with most of them, thanks to some important assets. One of them is the adoption of modern physical models, especially in the description of nuclear interactions. Some of these models have even been updated and extended with original contributions. Other advantages are the special care devoted to low-energy electromagnetic effects and the accurate combined treatment of multiple scattering and magnetic fields near material boundaries, essential for a correct simulation of many synchrotron radiation problems (Fassò, et al., 1995). In recent years, FLUKA has been widely used in the medical field to study different kinds of applications (Battistoni, 2012; Mairani, et al., 2013; Sommerer, et al., 2009; Parodi, et al., 2007a; Parodi, et al., 2007b; Infantino, et al., 2011; Infantino, et al., 2015a).

FLUKA reads user input from an ASCII text file with extension “.inp”. The input consists of a variable number of “commands” (called also “options”), each consisting of one or more “lines” (called also “cards” for historical reasons). Each card contains one keyword (the name of the command), six floating point values called *WHATs* and one character string called *SDUM*. The typical structure of a FLUKA input file is the following (Ferrari, et al., 2005):

- Titles and comments for documentation purposes (optional, but recommended)
- Description of the problem geometry (solid bodies and surfaces, combined to partition space into regions), (mandatory)
- Definition of the materials (mandatory unless pre-defined materials are used)
- Material assignments (correspondence material–region, mandatory)
- Definition of the particle source (mandatory)
- Definition of the requested “detectors”. Each of these is a phase space domain (region of space, particle direction and energy) where the user wants to calculate the expectation value of a physical quantity such as dose, fluence, etc. Various kinds of detectors are available, corresponding to different quantities and different algorithms used in the estimation (“estimators”). Detectors are optional, but one at least is expected, at least in the production phase
- Definition of biasing schemes (optional)
- Definition of problem settings such as energy cut-offs, step size, physical effects not simulated by default, particles not to be transported, etc. (optional)
- Initialisation of the random number sequence (mandatory if an estimation of the statistical error is desired)
- Starting signal and number of requested histories (mandatory)

In addition, special commands are available in FLUKA for more advanced problems involving magnetic fields, time-dependent calculations, writing of history files (so called “collision tapes”), transport of optical photons, event-by-event scoring, calling

user-written routines, etc. Details on the cards, the setup and the parameters used in this work will be given in the following chapters contextually to their use.

For geometry definition FLUKA uses combinatorial geometry: starting from simple geometrical entities, called “bodies”, (such as planes, cylinders and parallelepipeds) it is possible to create more complex space regions, called “REGIONS”, using the Boolean operations union, subtraction and intersection; then a specific material is assigned to each region. Each region is not necessary simply connected, since it can be made of two or more non contiguous parts, but must be of homogenous material composition. All the regions are surrounded by an infinitely absorbing material named “blackhole” absorbing all the escaping particles.

FLUKA is a powerful tool for induced radioactivity studies, especially with regard to nuclide production, their decay and the transport of residual radiation. Particles cascades by prompt radiation and residual radiation are simulated in parallel based on microscopic models for nuclide production and a solution of the Bateman equations for activity build-up and radioactive decay (Battistoni, et al., 2011). FLUKA allows detailed calculations of the radionuclide inventory based on theoretical models for nuclear interactions and fragmentations. Their implementation in the code has reached unprecedented detail enabling the user to predict the production of individual radioactive isotopes with high accuracy. This achievement has been quantified in comprehensive benchmark studies (Brugger, et al., 2006; Brugger, et al. 2003; Brugger, et al. 2005a; Brugger, et al. 2005b).

For what concerns FLUKA physical models, several models are employed in FLUKA for the transport of the different groups of particles in different energy ranges. Isotope production by hadronic interactions, except low-energy neutron interactions, is described by well-tested models. They comprise a sophisticated Generalized Intranuclear Cascade model; the Glauber-Gribov approach together with the Dual Parton Model; various mechanisms implemented for evaporation, fragmentation, fission and de-excitation by gamma-emission. The transport of neutrons with energies below 20 MeV is performed by a multi-group algorithm based on evaluated cross section data (ENDF/B, JEF, JENDL, etc.) binned into 260 energy groups, 31 of which are in the thermal energy region. Particularly significant for water, soil and concrete simulations, low-energy neutron transport is also provided with a detailed kinematics of elastic scattering on hydrogen nuclei as well as transport of recoil protons.

Multi-fragmentation is not taken into account in FLUKA, which might pose limitations to the predictions of intermediate and small-mass isotopes from heavy elements. However, this should have only little influence on integral quantities such as total activity. (La Torre, 2014)

2.2.2 *Flair*

Flair (Vlachoudis, 2009) is an advanced user graphical interface for FLUKA, to enable the user to start and control FLUKA jobs completely from a GUI environment without the need for command-line interactions. It is an integrated development

environment (IDE) for FLUKA. It does not only provide means for the post processing of the output, but a big emphasis has been put on the creation and checking of error free input files. It contains a fully featured editor for editing the input files in a human readable way with syntax highlighting, without hiding the inner functionality of FLUKA from the users. It provides also means for building the executable, debugging the geometry, running the code, monitoring the status of one or many runs, inspecting the output files, post processing the binary files (data merging) and interfacing to plotting utilities like gnuplot and PovRay for high quality plots or photorealistic images. The program includes also a database of selected properties of all known nuclides and their known isotopic composition as well as a reference database of ~300 predefined materials together with their Sterheimer parameters (Vlachoudis, 2009). Flair is also provided with a built-in Geometry Editor that allows working on 2D cross sections of the geometry, the interactive visual editing of the geometry in 2D, debugging of bodies/regions in a graphical way and fast 3D rendering of the geometry.

Chapter 3

Monte Carlo Models

In the present chapter the two main cases studies analysed in this work will be presented: The GE PETtrace facility of the S.Orsola-Malpighi Hospital (Bologna) and the IBA CYCLONE 18/9 facility of Inselspital (Bern). In table 3.1 some of the main features of these facilities are reported.

Table 3.1 Main features of the two cases studies analysed in this work

	<i>PETtrace of S.Orsola-Malpighi</i>	<i>CYCLONE 18/9 of Inselspital</i>
<i>Energy</i>	16.5 MeV	18 MeV
<i>Acceleration plan</i>	Vertical	Horizontal
<i>Fluorine targets</i>	1	4
<i>N° of irradiation per day for ¹⁸F production</i>	1	3
<i>Typical irradiation conditions</i>	60 A for 100 min	70 for 90 min
<i>Workload in a year for the ¹⁸F production</i>	≈ 25000 μAh	≈ 59000 μAh
<i>First irradiation year</i>	2002	2012

In both cases, first the cyclotron, then the cyclotron bunker and more in general the facility will be described. The Monte Carlo model implemented will be presented focusing on the geometrical model, on the definition of materials and on the source terms. Details on the physical and transport parameters, on the scored results and on their subsequent analysis will be also given in the following subsections.

3.1 The GE PETtrace cyclotron Facility of the Sant'Orsola-Malpighi hospital in Bologna

The first case study was the 16 MeV PETtrace (GE Medical System) cyclotron (Figure 3.1, 3.2) installed in the S. Orsola-Malpighi University Hospital (Bologna, IT) and used for the routine production of PET radionuclides. The GE PETtrace is a compact cyclotron with vertical acceleration plane, capable of accelerating negative hydrogen H^- and deuterium D^- ions up to an energy of 16.5 and 8.4 MeV respectively. Maximum beam intensity of 100 μA and 60 μA can be achieved for hydrogen and deuterium ions respectively.

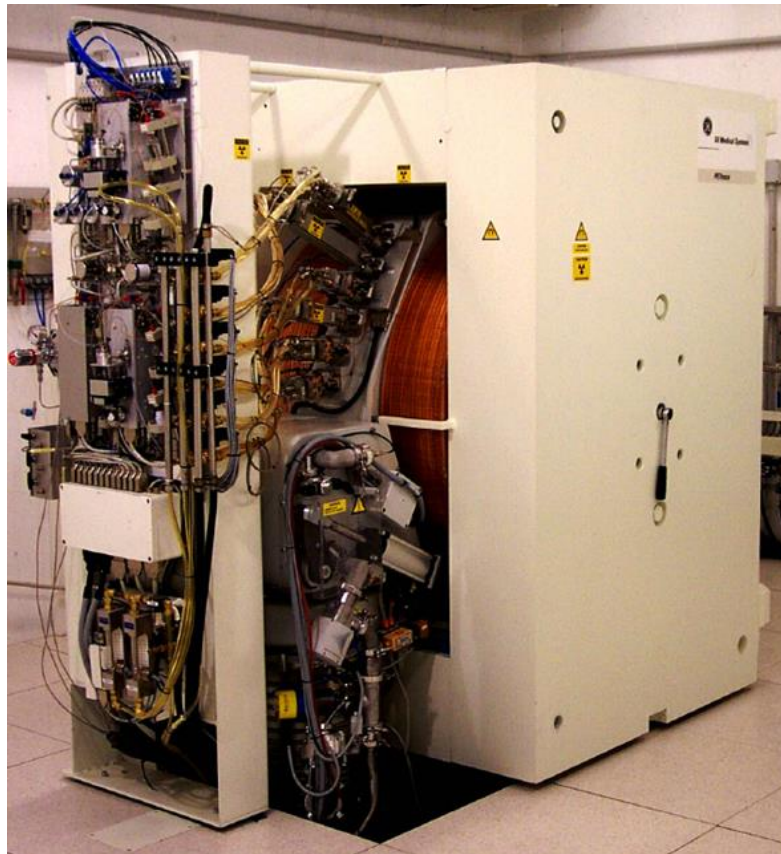


Figure 3.1 The GE PETtrace cyclotron installed at the S. Orsola-Malpighi Hospital.

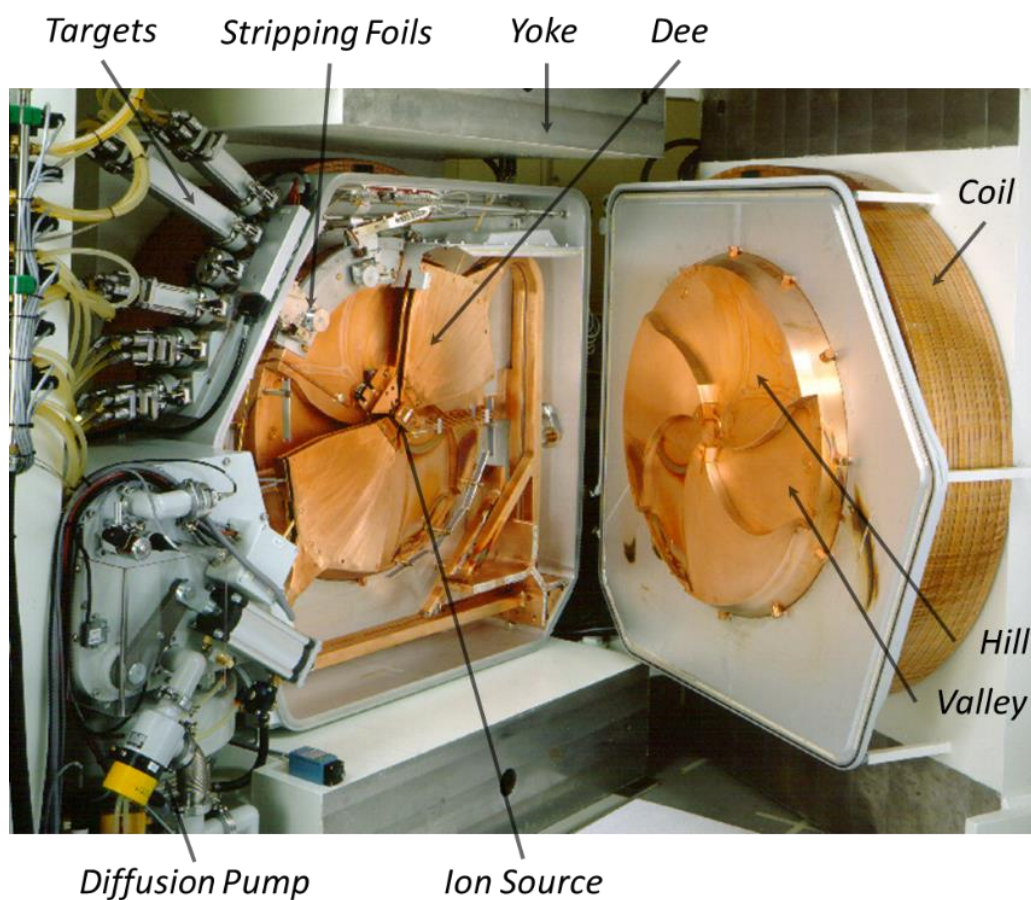


Figure 3.2 Overview of the vacuum chamber and the main components of the GE PETtrace cyclotron.

The beam of accelerated particles can be directed on one of the 6 output ports available (Figure 3.3). The cyclotron is equipped with several target assemblies for the routine production of the main radionuclides of interest for PET radiopharmaceuticals such as ^{11}C , ^{13}N , ^{18}F and $^{18}\text{F}_2$; in addition production of non-standard radionuclides, such as ^{64}Cu , ^{89}Zr , $^{99\text{m}}\text{Tc}$ and ^{68}Ga , is conducted for research purposes.

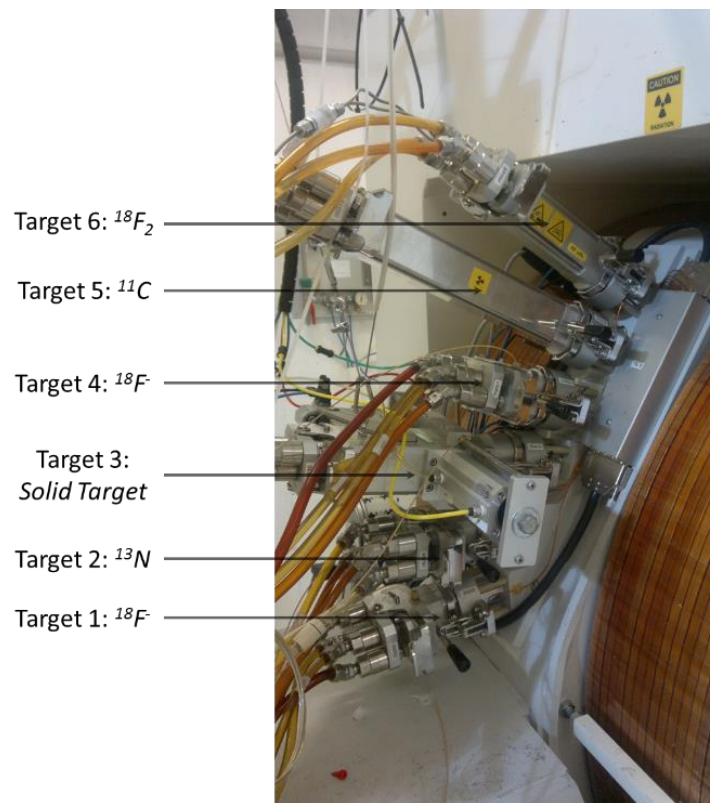


Figure 3.3 Targets currently mounted on the GE PETtrace cyclotron

The facility and the different cyclotron subsystems have been already described in a previous PhD Thesis (Infantino, 2015c), further details can be found in the accelerator manual (GE MEDICAL SYSTEMS, 2004).

A first MC model of the PETtrace cyclotron and of his bunker was already implemented in some previous works of our research group (GE MEDICAL SYSTEMS, 2004; Infantino, et al., 2011; Infantino, et al., 2014a) and in the PhD thesis already mentioned (Infantino, 2015c). Nevertheless the model was implemented for different purpose from the present work, the pre-existent model was further implemented modified and updated to suit better the analysis of activation of the components.

In the following a description of the model will be given, focusing on innovations introduced within this work.

3.1.1 Geometry

A detailed MC model of the GE PETtrace cyclotron was realized. The model includes the magnet and magnet poles (Iron), the vacuum chamber (Aluminium), an approximation of the coils (Copper), the cyclotron vault and the ducts through the vault walls. Data regarding the dimensions and features of the cyclotron and its components were taken from technical sheets and reference manuals of the vendor (GE MEDICAL SYSTEMS, 2004).

The cyclotron bunker was also modeled on the basis of the original construction drawings (Figure 3.4, 3.5). The inner dimensions of the bunker are: 650 cm by 535 cm with a height of 350 cm and with 200 cm thick concrete walls.

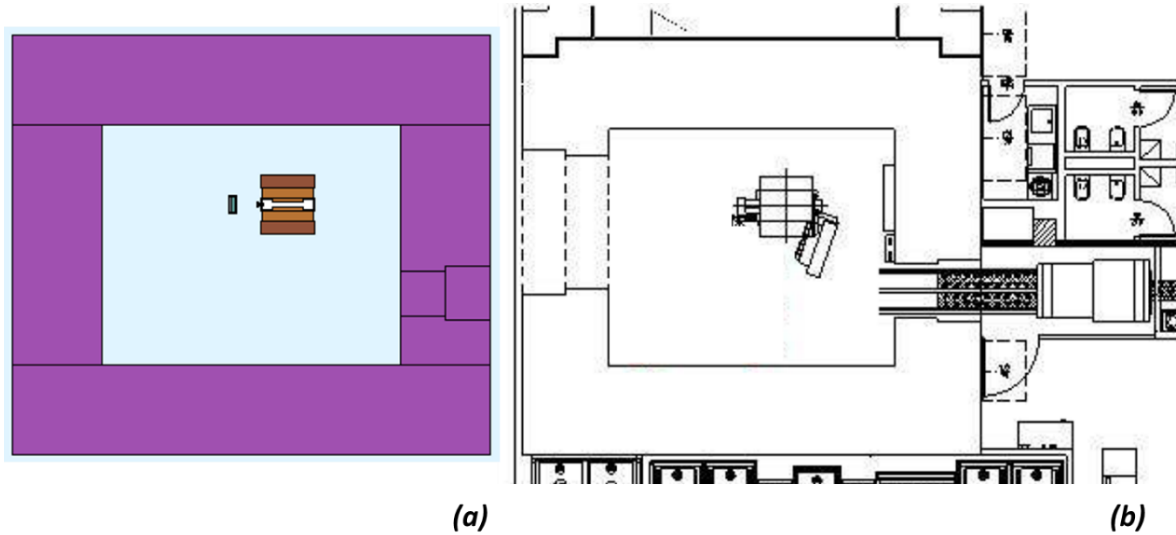


Figure 3.4 Comparison of the FLUKA MC model of the GE PETtrace cyclotron and the cyclotron vault (a) of "S. Orsola-Malpighi" Hospital with an original technical drawing (b).

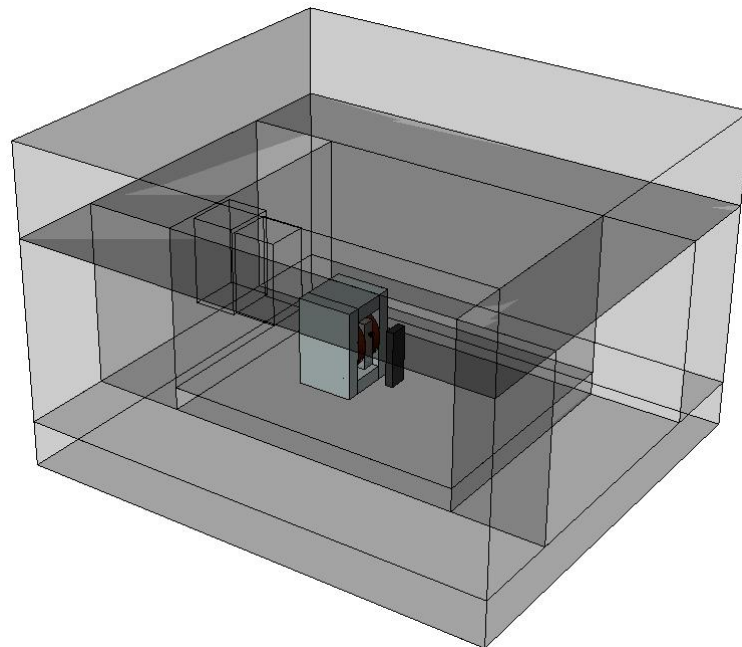


Figure 3.5 FLUKA Monte Carlo model of the cyclotron bunker of "S. Orsola -Malpighi" Hospital.

In this work the target system modelled was modified from the old GE assembly comprising a silver chamber to the new GE assembly comprising a niobium chamber that reduce target insert activation. The front of the target body (Aluminium), the 25 μm and 50 μm thick Havar™ foils (an alloy of cobalt (42.5%), chromium (20%), nickel (20%) and traces of manganese, molybdenum, iron and others) were also modeled. The upper and lower collimators were modeled as only one piece in graphite, 1 cm thick; the hole in the center is 1 cm in width by 0.8 cm in height (Figure 3.6).

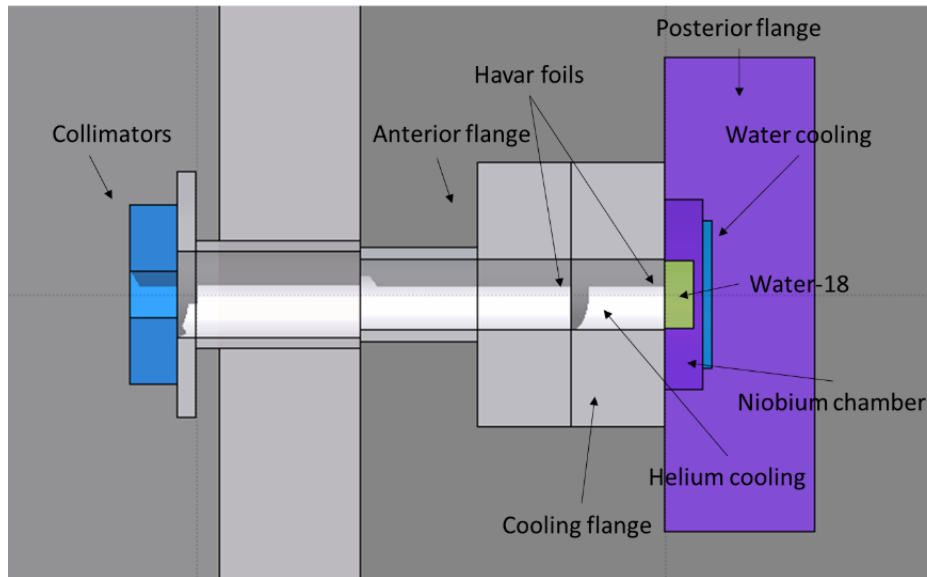


Figure 3.6 MC model of the GE niobium target assembly

An improvement in the modelling of all the major components of the cyclotron that are expected to interact and influence the neutrons fluence and spectrum was made. In particular a more accurate model of the target filling station panel (LTF) was implemented, the model includes a slab of 5 cm thick lead and 10 cm thick polyethylene, both enclosed in 1.5 cm thick structure of iron and was positioned in front of the cyclotron, close to the targets.

Also the internal structure of the cyclotron was improved, in particular the Dees structure, the ion source and the vacuum chamber were modeled more in details (figure 3.7).

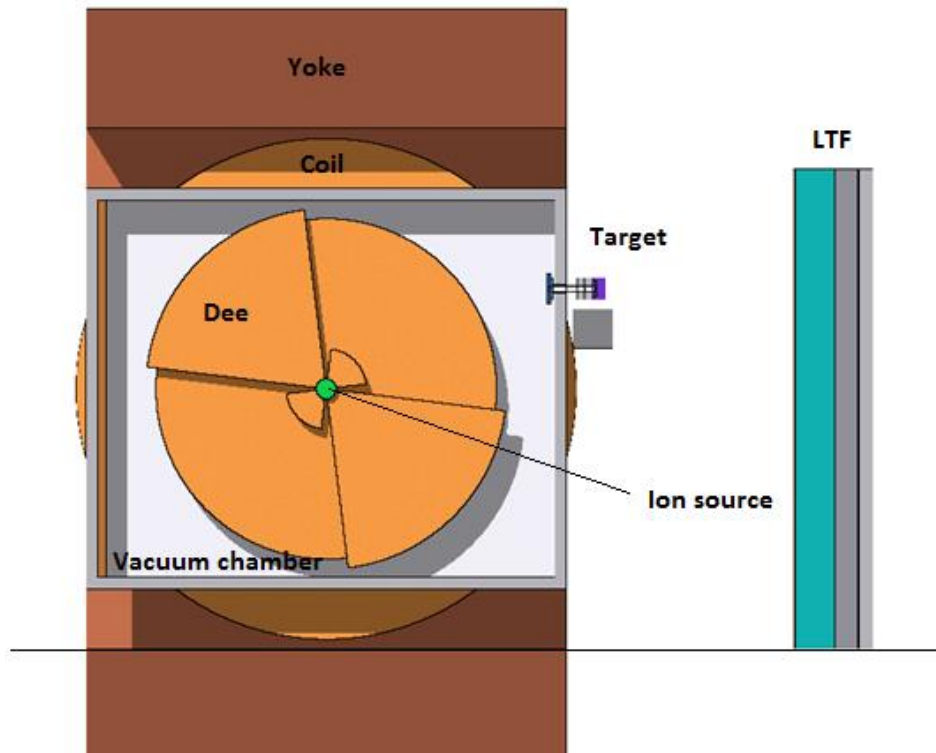


Figure 3.7 MC model of the internal structure of the Cyclotron and of the target filling station panel

The door of the bunker was also modeled as composed of a concrete structure enclosed in an external iron slab of 0.8 cm thick.

Reinforcement bars were accurately modelled based on the original construction drawings (figure 3.8, 3.9), their contribution in terms of activation is indeed very relevant.

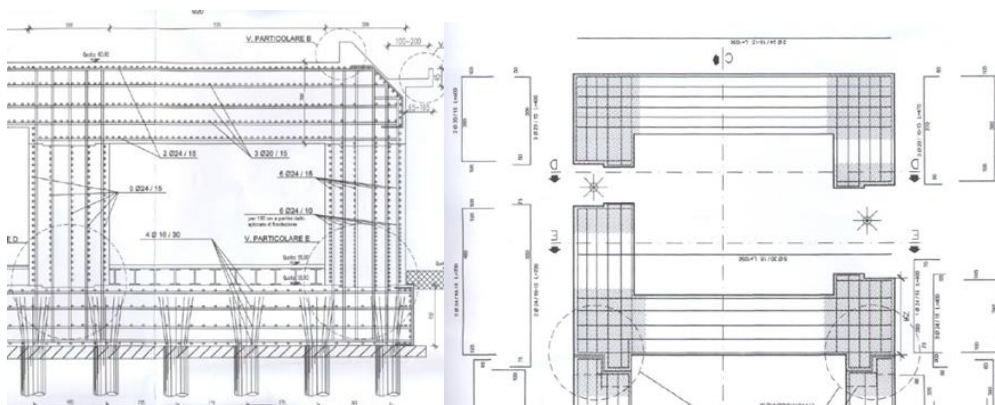


Figure 3.8 Reinforcement bars original construction drawings

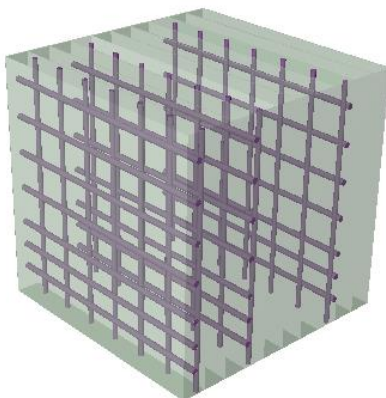


Figure 3.9 MC model of reinforcement bars inside concrete walls

Materials were assigned to each *REGION* of the input by a dedicated *ASSIGNMA* card: the assigned material was selected from the Flair material database or created when necessary. The [^{18}O]-water material, 98% enriched, was created within Flair using the dedicated *MATERIAL* and *COMPOUND* cards. When transport of low-energy neutrons ($E < 20$ MeV) is requested a correspondence is needed between each elemental “FLUKA material” and one of the “low-energy cross section materials” available in the FLUKA low-energy neutron library. Since the created element ^{18}O is not present in this library, the *LOW-MAT* card allows to assign the low-energy neutron cross section of Oxygen-16 to ^{18}O .

The density of concrete was well-known and equal to 2.35 g/cm^3 , whereas compositions of both concrete and reinforcement rods were unknown. The standard concrete Portland composition present in Flair does not include elements as caesium, cobalt and europium typically present in traces, however the amount of those elements, even if in small quantity, influences largely the resulting activation: for this reason they cannot be neglected in the simulation. Typical range values of concentration present in literature are reported in table 3.2 (EUROPEAN COMMISSION, 1999).

Table 3.2 Typical range values of cobalt, caesium and europium concentration in concrete

<i>ELEMENTS</i>	<i>Concentration in ppm</i>
<i>Co</i>	3.0 – 90.0
<i>Cs</i>	0.4 -1.0
<i>Eu</i>	0.3 – 1.8

The composition used in this work for concrete modelling was a combination of literature data and the standard concrete Portland present in FLUKA (table 3.3).

Table 3.3 Concrete composition used for the S. 'Orsola cyclotron bunker modeling

<i>ELEMENTS</i>	<i>Mass Fraction</i>	<i>ELEMENTS</i>	<i>Mass Fraction</i>
<i>Si</i>	0.24	<i>Ba</i>	0.00025
<i>Ca</i>	0.037	<i>Ni</i>	3.1E-5
<i>Al</i>	0.018	<i>Co</i>	6.6E-6
<i>Fe</i>	0.016	<i>Nb</i>	2.3E-6
<i>K</i>	0.0038	<i>Eu</i>	1.8E-6
<i>Mg</i>	0.0035	<i>Cs</i>	1.2E-6
<i>Na</i>	0.0013	<i>O</i>	0.667
<i>Mn</i>	0.0011	<i>H</i>	0.01
<i>Ti</i>	0.00095	<i>C</i>	0.001

For the reinforcement rods, instead, the composition used was a combination of steel SS316LN present in FLUKA adding impurities concentration values present in literature (Table 3.5) (EUROPEAN COMMISSION, 1999).

Table 3.5 reinforcement rods composition

<i>ELEMENTS</i>	<i>Mass Fraction</i>	<i>ELEMENTS</i>	<i>Mass Fraction</i>
<i>Cr</i>	1.85E-01	<i>Si</i>	1.00E-02
<i>Mn</i>	2.00E-02	<i>C</i>	3.00E-04
<i>Fe</i>	6.71E-01	<i>P</i>	4.50E-04
<i>Ni</i>	1.13E-01	<i>S</i>	3.00E-04
<i>Co</i>	1.00E-04		

3.1.2 Physics

In the previous works already mentioned (Infantino, 2015; Infantino, et al. 2011; Infantino, et al. 2014b) the production of ^{18}F by the $^{18}\text{O}(p,n)^{18}\text{F}$ reaction was studied to find the set of physical and transport parameters to optimize the results with minimum cpu-time usage. A 16.5 MeV pencil beam interacting with a target of a water solution (1.3 g) 98% enriched in ^{18}O , was modelled and used to perform a sensitivity analysis to find the optimal combination of default, physics and transport parameters. Three different sets of defaults were compared: NEW-DEFA, HADROTHER and PRECISIO.

In all three default chosen the low-energy neutron transport down to thermal energies is enabled.

The assessment of the saturation yield, of ^{18}F was performed using the *RESNUCLEI* card to score the activity produced at EOB. Results were compared with the recommended saturation activity for 1 μA (A_2) provided in the IAEA database for medical radioisotopes production: for 16.5 MeV protons A_2 turns out to be 13.078 GBq/ μA (IAEA, 2001a).

For each simulation two *PHYSICS* cards were used to enable coalescence mechanisms and the new FLUKA evaporation model, with heavy fragment evaporation

(Ferrari, et al., 2011); for some simulations, *PART-THR* card was used to overwrite the default particle transport threshold for one or more types of particles.

Actually, considering the production cross section of the $^{18}\text{O}(p,n)^{18}\text{F}$ reaction (figure 3.10) retrieved from the IAEA charged-particle cross section database for medical radioisotope production (IAEA, 2001a), it is possible to see how a large part of the area under the curve is lost when protons are not transported below 10 MeV.

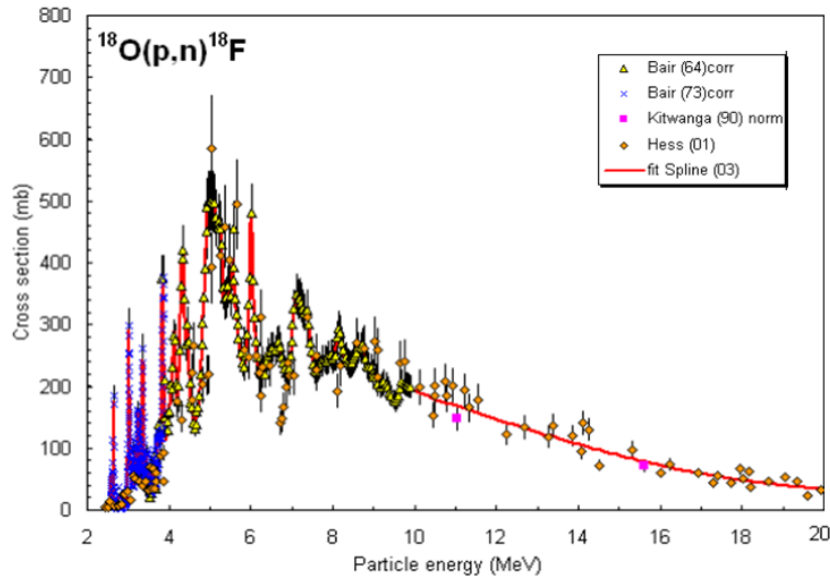


Figure 3.10 - Cross section of the $^{18}\text{O}(p,n)^{18}\text{F}$ reaction (IAEA, 2011a).

Simulations were performed on a core™ i7 laptop with four physical cores and hyper-thread enabled.

Results of the sensitivity analysis performed on defaults, physical and transport parameters are summarized in Table 3.6 (Infantino, 2015c).

Table 3.6 - Validation of the physics and transport parameters in the energy range of medical applications: assessment of the saturation yield of ^{18}F . (Infantino, 2015c)

DEFAULTS	NEW-DEFA	NEW-DEFA	NEW-DEFA	HADROTHER	HADROTHER	PRECISIO	PRECISIO
TRANSPORT	PART-THR: as default (10 MeV)	PART-THR: 0.1 MeV	PART-THR: 1 MeV for protons	PART-THR: as default (0.1 MeV)	PART-THR: 10 MeV	PART-THR: as default (0.1 MeV)	PART-THR: 10 MeV
Simulation Time [h]	1.05	5.04	3.12	25.17	3.43	25.48	2.26
$Y_{\text{sat}}^{18\text{F}}$ [GBq/μA]	6.521 \pm 0.006	13.166 \pm 0.009	13.161 \pm 0.009	13.169 \pm 0.010	6.508 \pm 0.005	13.200 \pm 0.010	6.486 \pm 0.006
A_2/Y_{FLUKA}	2.01 \pm 0.20	0.99 \pm 0.10	0.99 \pm 0.10	0.99 \pm 0.10	2.01 \pm 0.20	0.99 \pm 0.10	2.02 \pm 0.20

From Table 3.6, *NEW-DEFA* default and a proton transport threshold set at 1 MeV proved to be the best combination giving a good agreement with the IAEA recommended value in the shortest simulation time (Infantino, et al., 2015a).

3.1.3 Source

Because of the relatively rather low neutron production rate, simulating protons as primary particles for assessment of wall activation is quite inefficient to obtain low uncertainty results. The use, as source term, of secondary neutrons as primary particles is a more efficient approach allowing to decrease of about three order of magnitude the number of primaries needed to obtain the same uncertainty results.

Therefore the kinematic proprieties of emitted secondary neutrons from the target were determined in a separate and simplified simulation, the neutron spectrum obtained was then used directly as the source term for activation assessment.

For this purpose the 16.5 MeV proton pencil beam and only the materials interacting with it, as Havar foils, Helium chamber and water-18 chamber were modelled (Figure 3.11).

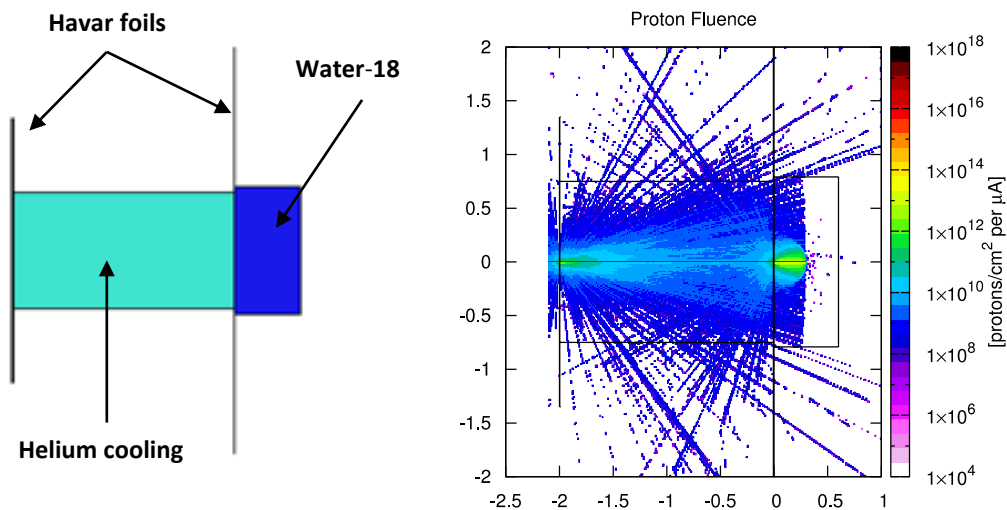


Figure 3.11 MC model of Havar foils, Helium cooling, Water-18 and proton fluence [protons/cm²per primary proton]

The neutron flux and the energy spectrum released were determined on a sphere surrounding the target using USRBIN and USRBDX cards.

The attenuation of the proton beam through the different materials was also scored using different USRTRACK cards (figure 3.12). Values obtained with FLUKA were compared with SRIM, a collection of software package that allow the calculation of many parameters regarding the transport of ions in matter. The estimated average kinetic energy of primary protons at the entry of water-18 chamber is equal to 15.28 ± 0.01 MeV, compatible, within the errors, with SRIM value of 15.29 ± 0.01 MeV. The

mean range of 17.37 MeV protons (point-like beam) in water-18 target estimated with FLUKA is 0.27 ± 0.01 cm, consistent with SRIM value of 0.27 ± 0.01 cm.

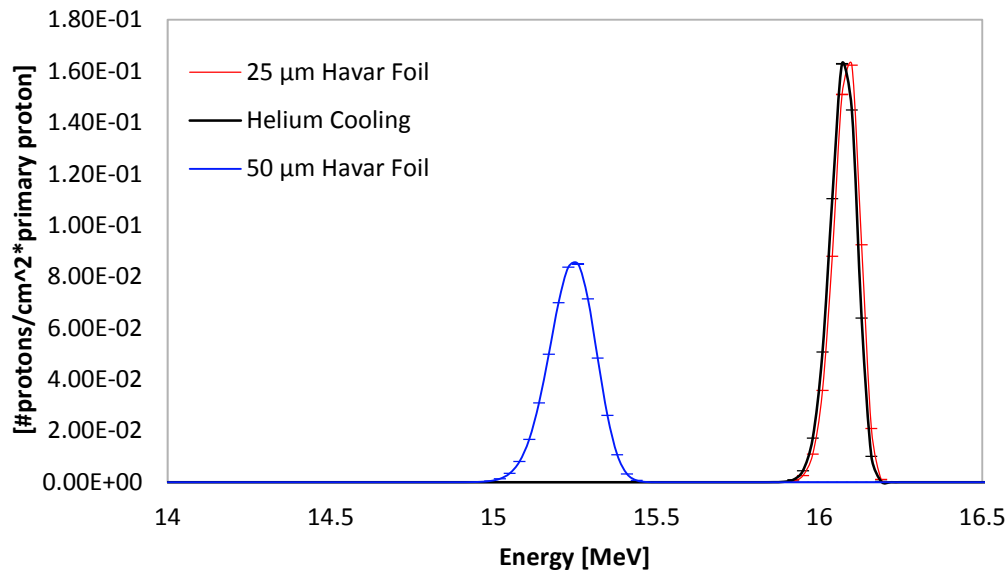


Figure 3.12 Proton beam attenuation

The average neutron spectrum of the neutrons emitted is shown in figure 3.13. The neutron kinetic energy shows a peak around 2.4 MeV with a large tail towards lower values down to 1 keV. The neutron polar angle distribution is shown in figure 3.14: as we can see neutron emission from target can be considered almost isotropic.

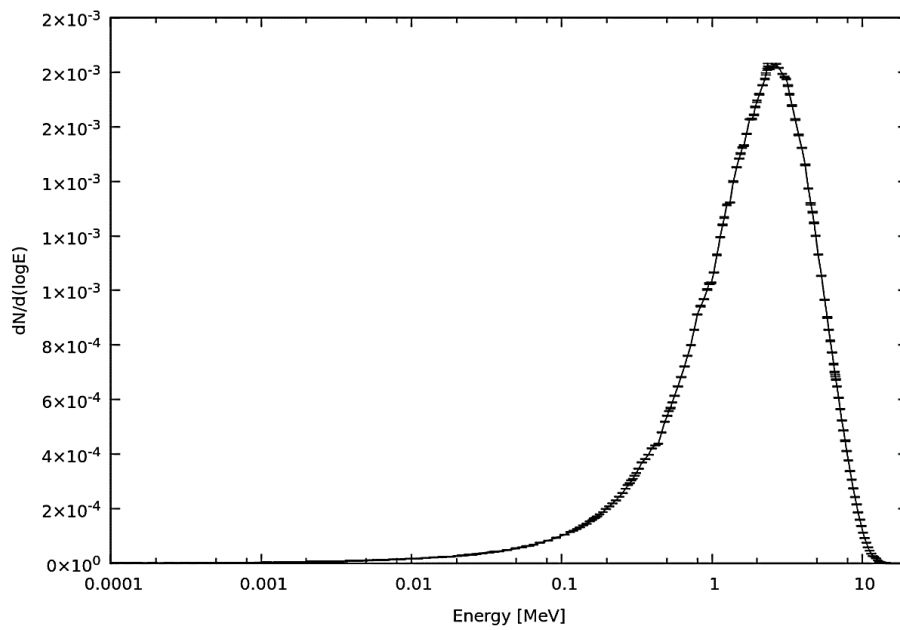


Figure 3.13 Neutron energy spectrum generated by the $^{18}\text{O}(p,n)^{18}\text{F}$ reaction

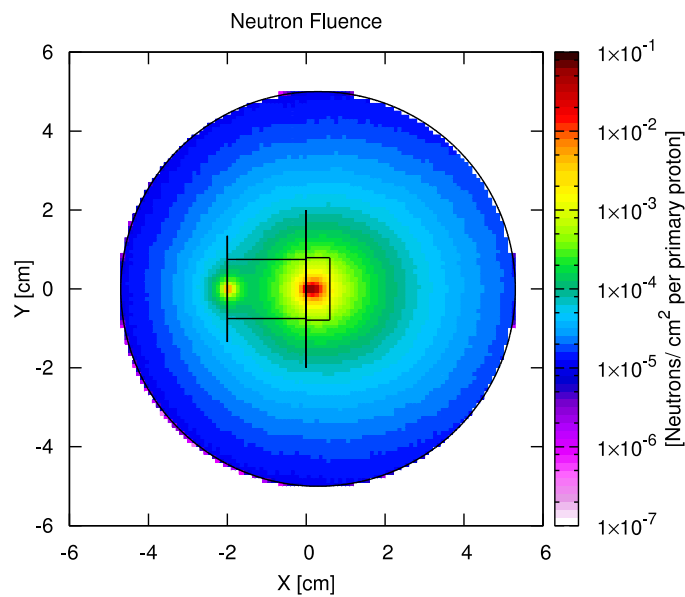


Figure 3.14 Neutron fluence expressed in neutrons/cm² per primary proton

Figure 3.15 shows how the energy spectrum of neutrons varies with the polar angle range: the forward neutrons (in red), exhibit a harder spectrum than those emitted by the sides (in green) and the backward neutrons (in blue).

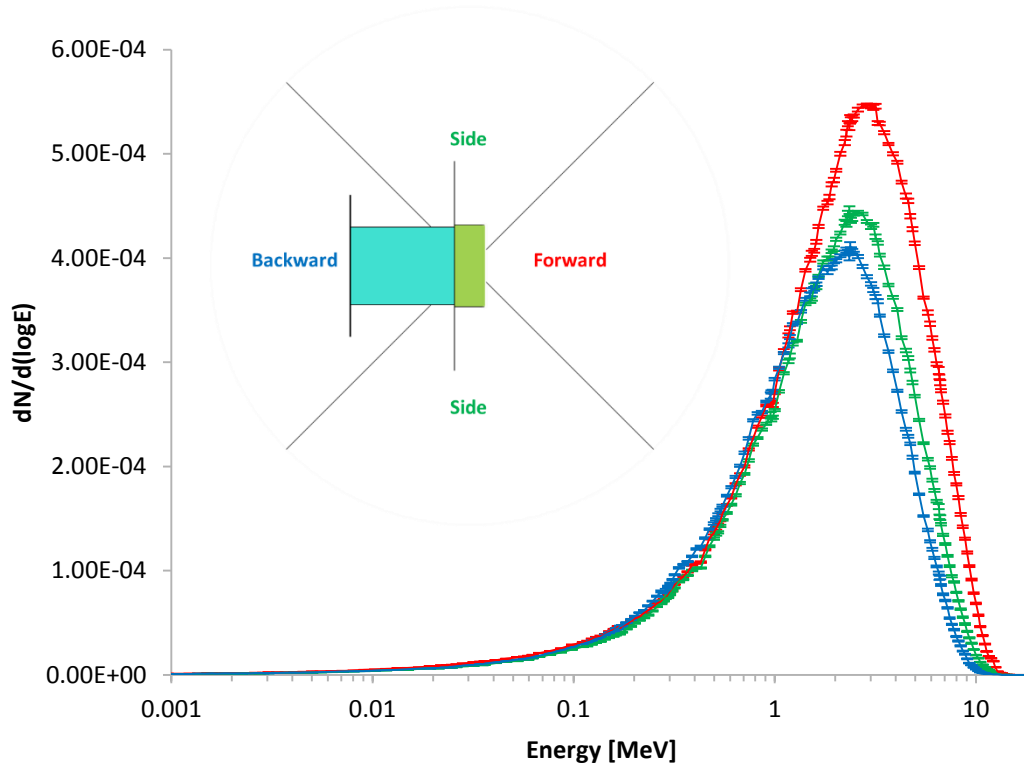


Figure 3.15 Comparison of neutron energy spectra obtained for different emitting directions

In the present work the neutron spectrum was modeled as independent from the emitting direction and equal to the average spectrum in all directions. The neutron multiplicity estimated, defined as the integrated number of neutrons produced by one proton, is equal to $3.99 \cdot 10^{-3} \pm 0.08 \cdot 10^{-3}$ [**#neutrons/primary proton**]. From this value the number of neutrons generated for proton current unit can be estimated:

$$n_p \left[\frac{\#protons}{\mu A} \right] = \frac{1 \cdot 10^{-6} [\mu A]}{1.602 \cdot 10^{-19} [C]} = 6.25 \cdot 10^{12} \quad \text{Equation 3.1}$$

$$\begin{aligned} n_n \left[\frac{\#neutrons}{\mu A} \right] &= 6.25 \cdot 10^{12} \left[\frac{\#protons}{\mu A} \right] * 3.99 \cdot 10^{-3} \left[\frac{\#neutrons}{proton} \right] \\ &= 2.49 \cdot 10^{10} \end{aligned} \quad \text{Equation 3.2}$$

In all simulations for bunker activation assessment, neutrons were generate as primary particles according to the kinetic determined.

In FLUKA the definition of non-standard sources (distributed, non monoenergetic mixture of particles or other complex source) should be treated by

means of a user-written external subroutine. A number of user routine templates are available and can be modified by the user to fulfil non-standard tasks. The user routine related to source generation is *source.f*. Flair can be used to edit, compile and link user routines to build a user-specific FLUKA executable. This subroutine is used to sample primary particle properties from different types of distributions, in the present case to read it from a file (Ferrari, et al., 2011).

A text file was created with the neutron spectral distribution obtained in the previous simulation and the *source.f* user routine was modified to model a point and isotropic source positioned inside the target and having the spectral distribution determined. In the following a list of the main steps to perform the energetic sampling is reported (figure 3.15):

- the histogram from spectrum text file is read;
- the corresponding cumulative distribution $SUMM(N)$ is calculated;
- the distribution is normalized and loaded in an array named $CUM(I)$;
- a uniform pseudo-random number $C \in [0,1)$ is generated;
- the I^{th} interval is found such that $CUM(I-1) \leq C \leq CUM(I)$;
- The energy value is selected sampling a random value E such that $ERGMAX(I) \leq E \leq ERGmin(I)$, where $ERGMAX(I)$ and $ERGmin(I)$ are respectively the maximum and minimum energies corresponding to I^{th} interval.

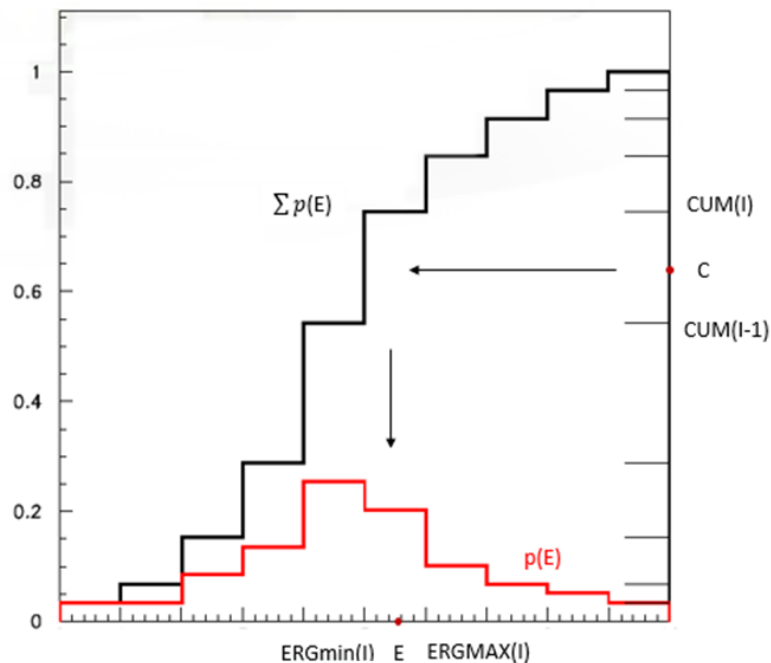


Figure 3.15 Graphical explanation of the main steps present in *source.f* user routine to perform the energetic sampling

The source.f routine is compiled using a FORTRAN compiler and an executable file is created. This executable is called during simulation by the SOURCE card; the OPEN card is also necessary to provide the file from which the distribution is taken.

Some tests were performed to assess the consistence between results obtained using the subroutine developed and protons as primary particles.

An activation assessment in simplified geometry was performed considering a concrete sphere surrounding the target (figure 3.16, 3.17). The RESNUCLEI card was used to evaluate activation after 1 hour irradiation at 1 μ A. All the simulations were performed on an i7-4790 computer (8 cores). In simulations with protons as primary particles the 16.5 MeV proton pencil beam was simulated as source term and the materials interacting with it, as Havar foils, Helium chamber and water-18 chamber were also modelled. The number of primary particles simulated was 1.00×10^{10} protons, corresponding to 3.99×10^7 neutrons, the simulation time was 40 hours. In simulations with neutron as primary particles the external routine was used to simulate a neutron isotropic point source in vacuum. The number of primary particles simulated was 1.00×10^9 neutrons, the simulation time was 45 min. In table 3.7 results are reported.

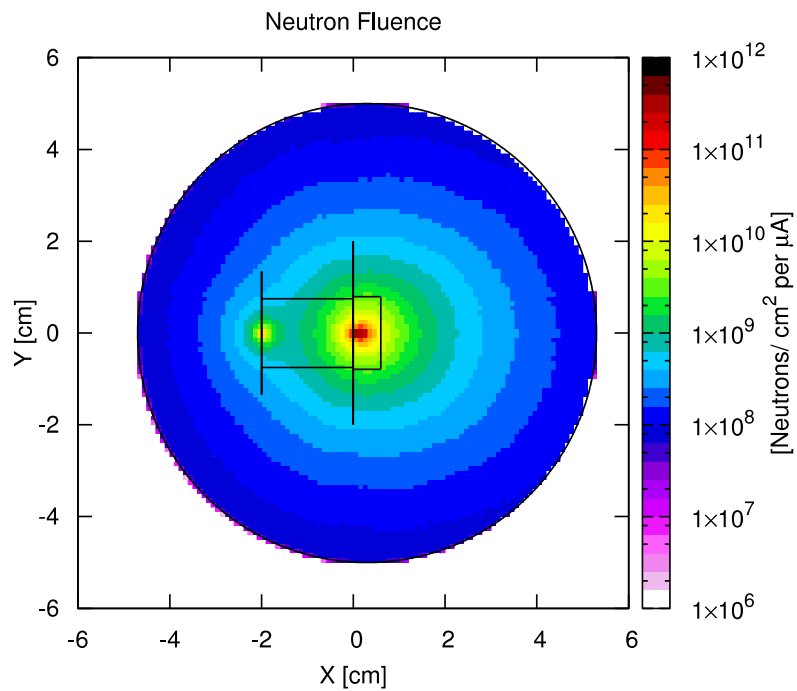


Figure 3.16 Neutron fluence simulating proton as primary particle

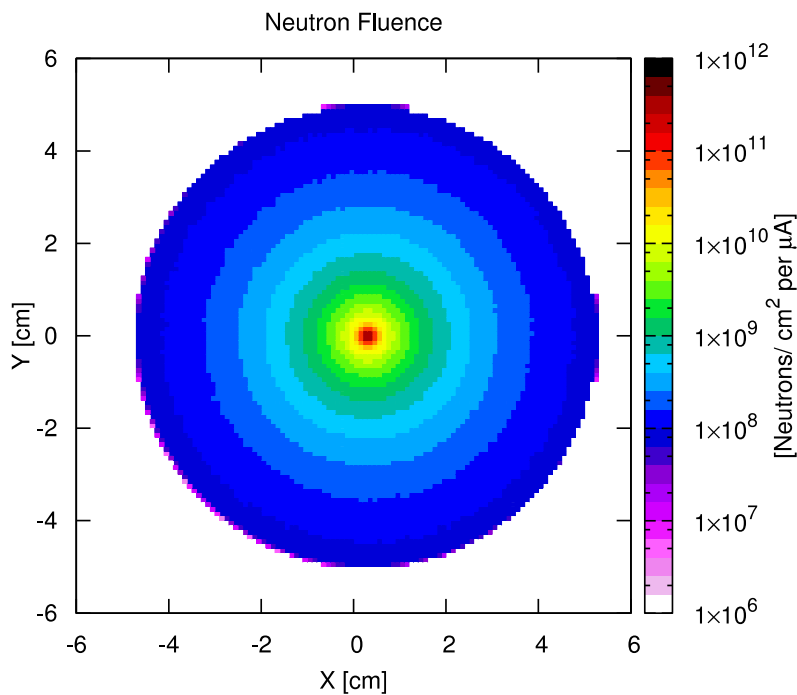


Figure 3.17 Neutron fluence simulating neutron as primary particle via the external user routine source.f

Table 3.7 Comparison of activation assessment using protons and neutrons as primary particles

Nuclide	Protons as primary particles		Neutrons as primary particles		Variance
	Bq	Uncertainty (%)	Bq	Uncertainty (%)	
²⁸ Al	2.97E+07	0.3	2.97E+07	0.1	0.1%
³⁹ Ar	7.11E-01	0.6	7.05E-01	0.1	0.7%
⁴¹ Ca	2.09E-03	0.7	2.10E-03	0.1	0.4%
³¹ Si	3.84E+05	0.7	3.85E+05	0.1	0.4%
²⁴ Na	1.13E+05	1.0	1.13E+05	0.2	0.4%
²⁷ Mg	1.44E+06	1.3	1.45E+06	0.3	0.8%
⁵⁶ Mn	5.33E+05	1.8	5.28E+05	0.4	0.8%
²⁹ Al	6.95E+05	1.9	7.05E+05	0.3	1.6%

As can be seen results obtained are consistent within uncertainties. It must also be considered that using protons as primary particles, $2.50 \cdot 10^{11}$ primaries and simulation time of 41 days are needed to produce results with the same uncertainty obtained simulating $1.00 \cdot 10^9$ neutrons.

Another test was performed considering the cyclotron bunker geometry. A first simulation was performed with $6.00 \cdot 10^9$ protons as primary particles corresponding to $2.39 \cdot 10^7$ neutrons (simulation time 1 day and 8 hours). A second simulation was then performed using the external source with $4.00 \cdot 10^9$ neutrons as primary particles, corresponding to $1.00 \cdot 10^{12}$ protons (simulation time 1 day and 1 hours). The average neutron spectrum inside the bunker and in five positions reported in figure 3.18 was scored using the USRTRAK cards and the results of the two different simulations compared (figure 3.19, 3.20, 3.21, 3.22, 3.23, 3.24).

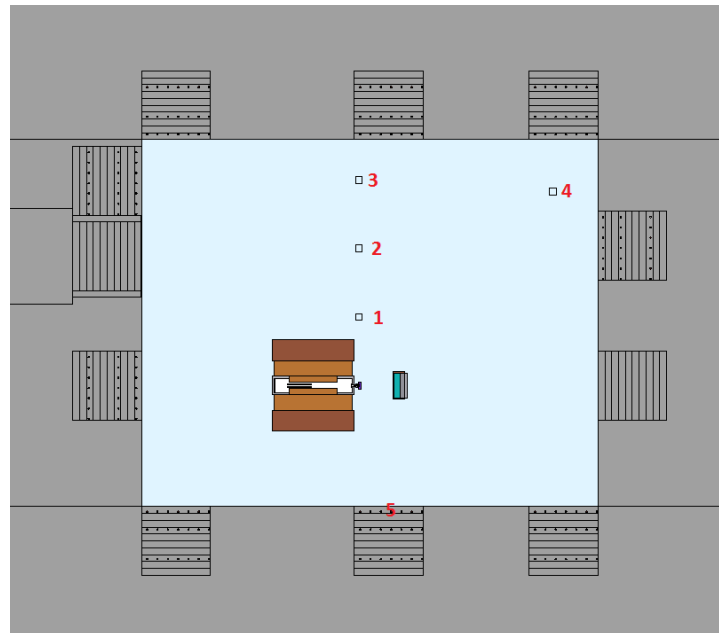


Figure 3.18 MC model of cyclotron bunker with the five positions of interest

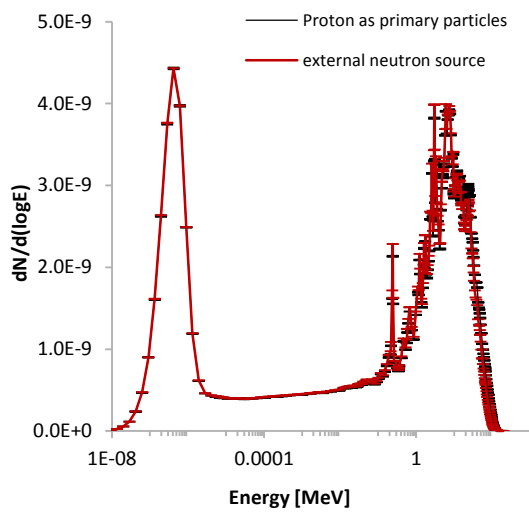


Figure 3.19 Average neutron spectra in air

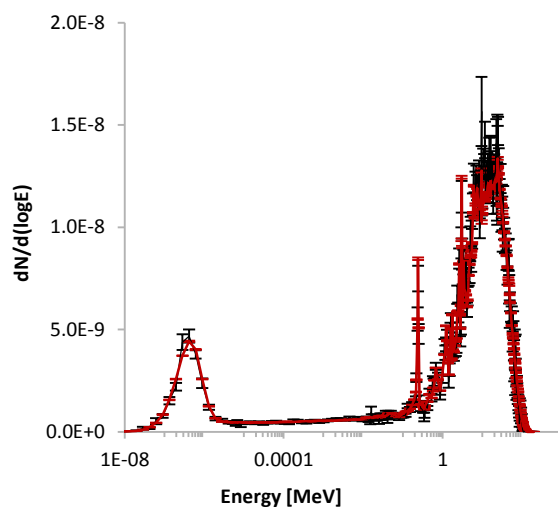


Figure 3.20 Neutron spectra at position 1

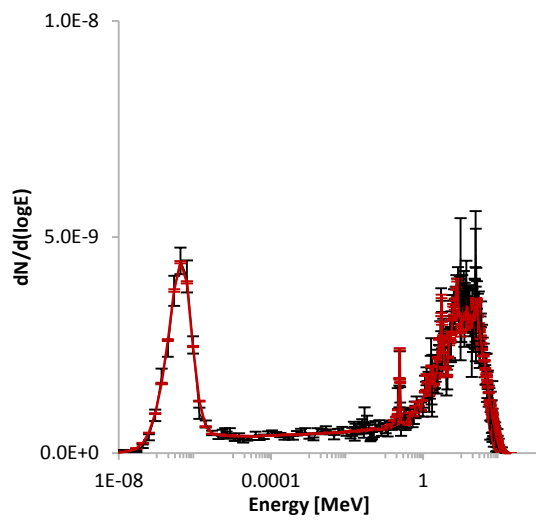


Figure 3.21 Neutron spectra at position 2

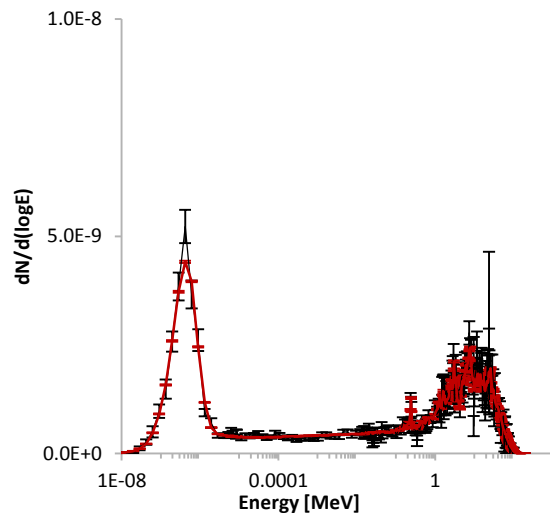


Figure 3.22 Neutron spectra at position 3

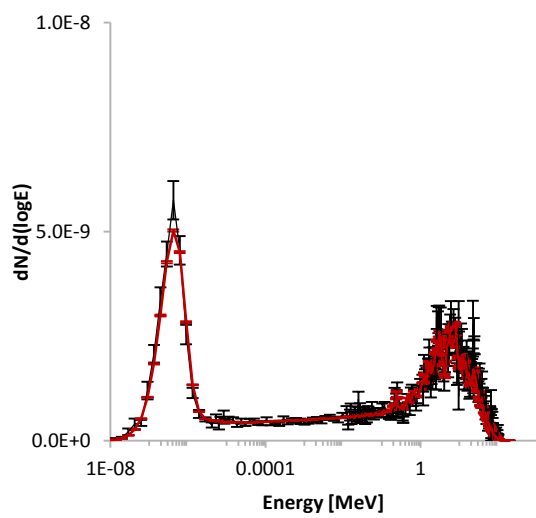


Figure 3.23 Neutron spectra at position 4

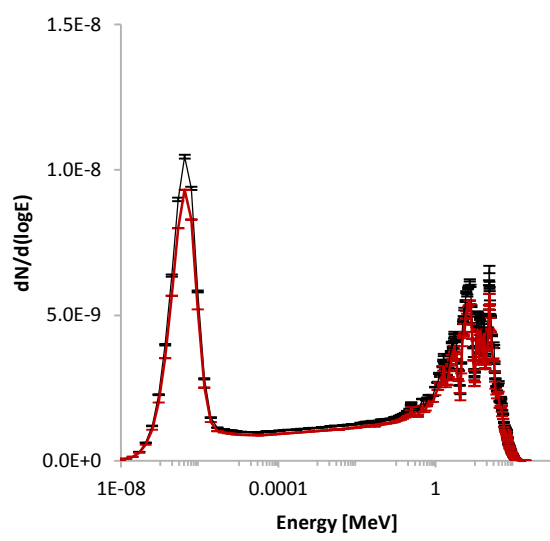


Figure 3.24 Neutron spectra at position 5

Spectra obtained with neutrons as primary particles using the external user routine are consistent with those obtained with protons as primary particles. The advantage in terms of CPU times is very significant especially considering simulation for activation assessment studies. Just to have an idea, to obtain in our simulations results in terms of activity concentration with an uncertainty on average lower than 10%, the number of neutrons as primary particles simulated must be higher than $2 \cdot 10^9$ whereas the number of protons as primary particles simulated must be higher than $5 \cdot 10^{11}$, the simulation time estimated was respectively about 17 hours using the neutron source and more than 4000 days simulating protons as primary particles.

Therefore in all activation assessment simulations the subroutine implemented was used to simulate an isotropic point source of neutrons positioned inside the target (figure 3.25). Since the self-absorption and interaction of neutrons with Havar foils, Helium chamber and water-18 were already considered in the previous simulation, materials of these regions were replaced with vacuum.

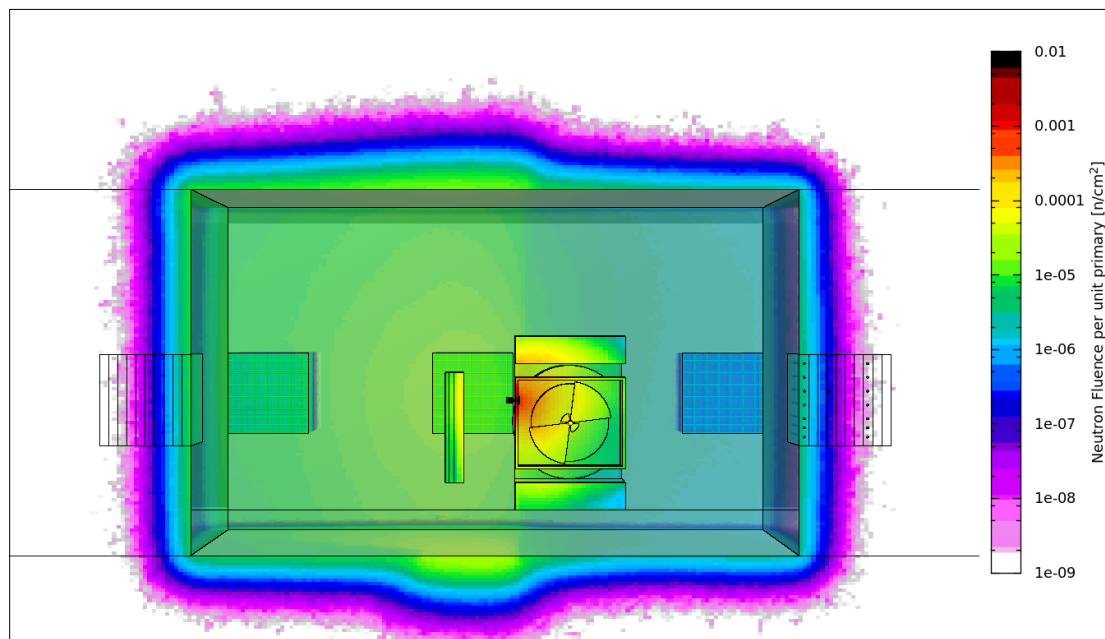


Figure 3.25 Neutron Fluence inside the cyclotron bunker

3.1.4 Scoring

The activation of the cyclotron vault walls and of the reinforcement rods was assessed using several RESNUCLEI cards; activity was scored at different positions, depth and for different life expectancy of the cyclotron.

Since RESNUCLEI scores nuclei on a region basis, bunker walls were modeled as the sum of rectangular slabs (100x100x10 cm) to evaluate the in-depth activation profile and to score the distribution of activity concentration for each nuclide inside the walls.

Results were expressed for each radionuclide in numbers of residual nuclei per cubic centimeter per primary particles, neutrons in this case. The estimations of residual activity after different life expectancy of the cyclotron was done off-line by an external spreadsheet that will be described in the following.

The activity concentration per current unit at the EOB was estimated from the number of nuclei for each radionuclide N_r , as

$$A \left[\frac{Bq}{g \mu A} \right] = N_r \left[\frac{\#nuclei}{cm^3 * primary\ neutron} \right] * \frac{1}{\rho} \left[\frac{cm^3}{g} \right] * n_n \left[\frac{\#neutrons}{\mu A} \right] * \frac{\ln(2)}{T_{1/2r}} \quad \text{Equation 3.3}$$

Where ρ is the material density, $T_{1/2r}$ is the radionuclide half life and n_n is the number of neutron generated for unit current. Then the saturation activity was calculated as

$$A_{sat} \left[\frac{Bq}{g \mu A} \right] = \frac{A}{1 - e^{-\frac{\ln 2 t}{T_{1/2}}}} \quad \text{Equation 3.4}$$

The estimation of residual activation after a certain lapse of time of normal production of ^{18}F was made considering typical daily irradiation of 60 μA with an irradiation time of 100 minutes excluding Saturday and Sunday.

The activity induced in materials as a function of time during the irradiation was calculated by the following equation

$$A(t) = A_{sat}(1 - e^{-\lambda t}) \quad \text{for} \quad 0 < t < t_{irr} \quad \text{Equation 3.5}$$

After irradiation ($t > t_{irr}$) the specific activity as a function of the cooling time $t_c = t - t_{irr}$ was calculated as

$$A(t) = A_{sat}(1 - e^{-\lambda t_{irr}}) * e^{-\lambda t_c} \quad \text{for} \quad t > t_{irr} \quad \text{Equation 3.6}$$

A typical activation profile as a function of time is reported in figure 3.26 and it was obtained by summing the residual activity produced day by day.

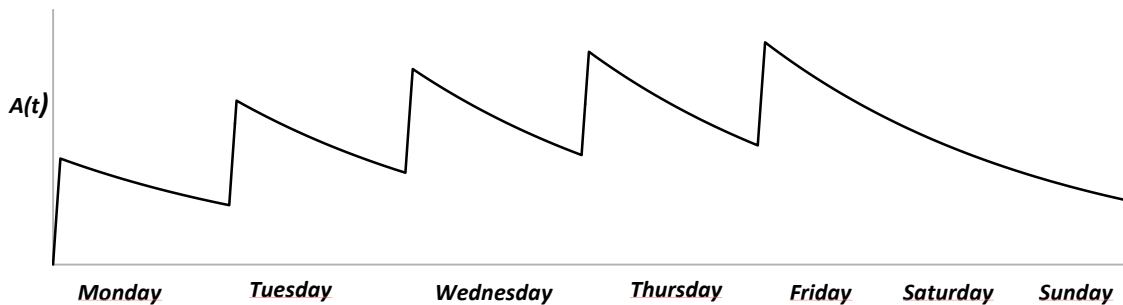


Figure 3.26 Typical activation profile as a function of time in a week

3.2 The IBA C18/9 PET Cyclotron Facility

In 2007 the University and the University hospital of Bern, Inselspital, with the support of some private investors started the SWAN (SWiss hAdroN) project. The result of this collaboration was the establishment of a multi-disciplinary clinical and research centre for radioisotope production and patient care. The construction of the "SWAN Haus", equipped with a 18 MeV cyclotron for PET radioisotopes production, ended in June 2011 and the whole facility was fully operational at the end of 2012. The facility is situated on the campus of the Inselspital and has been conceived to fulfil two main goals: produce PET radio tracers for Inselspital and for other healthcare institutions, and conduct cutting-edge multidisciplinary scientific activities (Braccini, 2013; Braccini, et al. 2010; Braccini, et al. 2007);.

The cyclotron installed in the facility was the IBA Cyclone 18/9 HC (Figure 3.28), a fixed-energy cyclotron with an horizontal acceleration plane, capable of accelerating negative hydrogen H^- and deuterium D^- ions up to an energy of 18 and 9 MeV respectively. Maximum beam intensities are 150 μA and 40 μA respectively for hydrogen and deuterium ions in single or dual beam mode.



Figure 3.28 IBA CYCLONE 18/9

The cyclotron includes eight independent exit ports, one of which connected with a 6 m long external transport beam line terminated in a second bunker mainly for research purpose (figure 3.29).

One port is connected with a solid target station for the production of non-standard radionuclides, four ports are connected with fluorine liquid targets and are used for the routine production of PET radionuclides.



Figure 3.29 CYCLONE 18/9 bunker

Therefore, the building design comprises two separated vaults, a vaults for the cyclotron (4.00 m (width) x 4.75 m (length) x 3.00 m (height)) connected by a gap on a 1.8 m thick wall with a second vaults (4.00 m (width) x 5.40 m (length) x 3.00 m (height)) for the external transport beam line (figure 3.30). For gamma and neutron shielding the two vaults are enclosed in 2.2 m thick concrete walls. The two vaults are connected via underground pipes to a physics laboratory situated on the same floor and to a dedicated radiochemistry and radiopharmacy laboratory situated on the floor above the cyclotron. Radioisotopes produced in any of the targets can be transferred to any of the hot cells located in the upper floor by means of shielded capillaries.

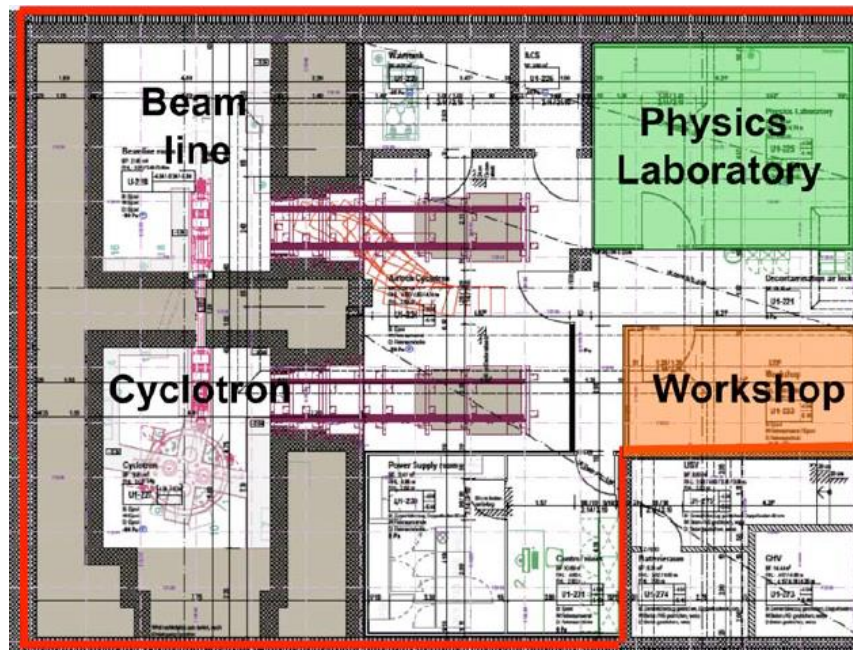


Figure 3.30 Planimetry of Insilpital Cyclotron bunker

In the following, details of the different cyclotron subsystems will be given (Figure 3.31); further information can be found in the accelerator manual (IBA Molecular, 2007).

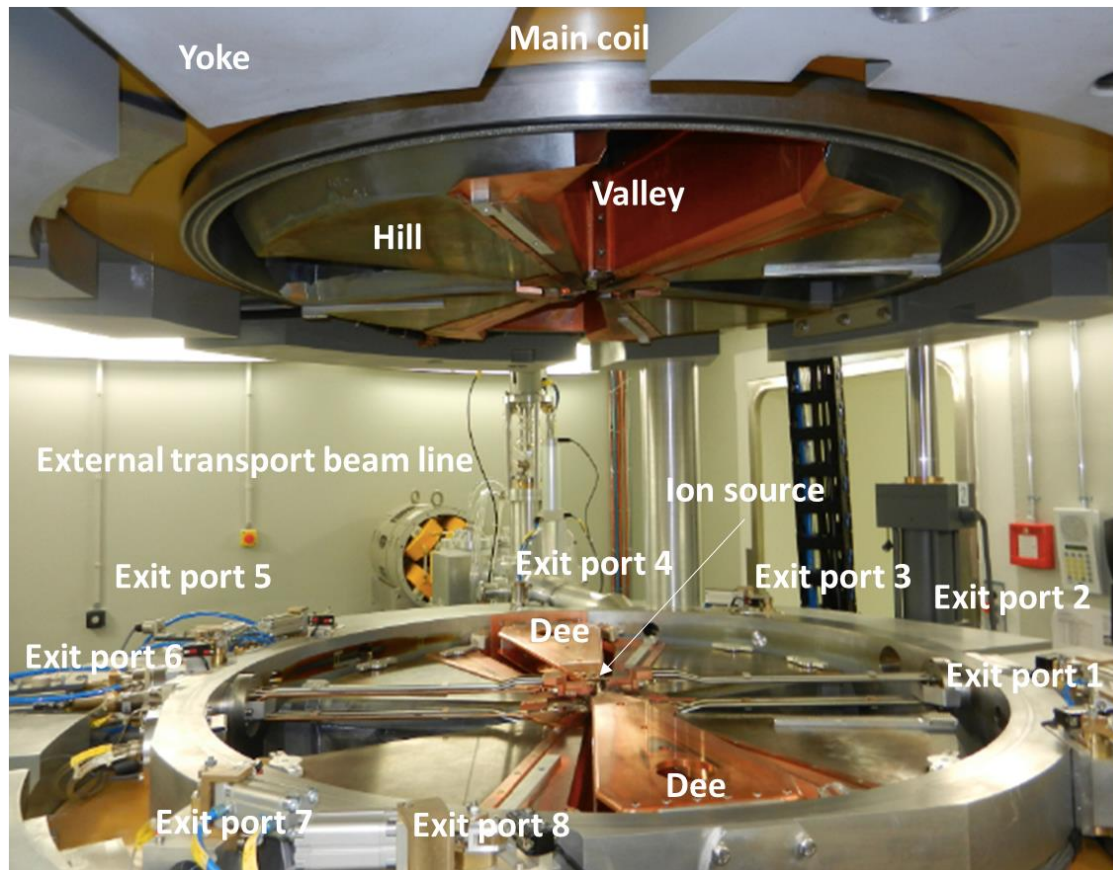


Figure 3.31 Overview of the vacuum chamber and the main components of the IBA CYCLONE 18/9.

The entire structure of Cyclone 18/9 HC has a diameter of 2 m and is 2.2 m height. The bearing structure of the cyclotron yoke is made of steel, the cyclotron uses a resistive magnet energized by two coils. The coils are made of hollow copper conductor, and are water cooled. The power requirement for the magnet is less than 15 kW. to maintain an isochronous field for the protons, a pair of wedge shaped steel pole pieces ("flaps") are automatically inserted into position between sectors on opposite sides of the cyclotron in both the upper and lower halves of the magnet. When switching to a deuteron beam, the poles are automatically retracted. The field is 1.9 Tesla (hill) and 0,35 Tesla (valley). The extraction radius is 0.48 m. The acceleration plane being horizontal, access to the median plane is achieved by lifting the top part of the cyclotron yoke on two hydraulic jacks included in the system. Yoke lifting is not required to access the targets or for target window maintenance.

The radio frequency (RF) system provides the electric field that pulls the ions from the ion sources and accelerates these ions across accelerating gaps where they gain energy with each turn until they reach the extraction radius. The main component of the RF System are:

- RF resonant cavity within the cyclotron vacuum chamber
- RF cavity tuning mechanism
- RF final amplifier with high voltage supplies and RF vacuum tube
- RF low level rack.

The RF amplifier feeds power to the cyclotron cavity through a 50 Ohms Coaxial cable. The RF power is inductively coupled to the RF cavity where two electrodes (Dees) are supported on one side by vertical copper stems that resonate on a quarter wavelength mode. The 30° Dees are located in two opposite valleys.

Two cold cathode *Penning ion gauge* (PIG) source are located in the centre of the cyclotron, one producing Hydrogen (H⁻) ions and the other producing Deuteron (D⁻) ions. The sources are located in the two valleys that do not contain a dee.

The vacuum system to prevent neutral stripping of the negative ions on the residual gases of the vacuum chamber consists of the vacuum chamber assembly, made of pure aluminium, four oil diffusion pumps, a roughing pump, various valves, O-rings, and also all the instrumentation, controls and interlocks to maintain proper vacuum system operation.

The cyclotron vacuum is maintained by four oil diffusion pumps with water-cooled baffles. A forepump (40 m³/hr.) is used to rough the vacuum chamber to 5 x 10⁻² mbar. The pumps are located under the cyclotron, with enough clearance for maintenance access. The time needed to establish a vacuum condition of 5 x 10⁻⁵ mbar is half an hour and, after two hours, the pressure is less than 9 x 10⁻⁶ mbar after dry nitrogen venting of the cyclotron.

Beam intensity measurements are performed at four different places along the beam path and transmitted to the control system:

- On a beam probe located at the 10 cm radius: to measure internal beam.
- At the stripper foil: the stripped beam current is given by measuring the current of electrons stripped from the H⁻ or D⁻ beam. These electrons will end on the stripper foil support. This measurement is divided by 2 (two electrons stripped out of each H⁻ or D⁻), and is automatically transferred to the controller.
- On the target collimator: to optimize the beam position on target.
- On the target itself to stop irradiation when the preset current is reached.
- Interlocks in the control system will turn off the beam if the ratio of beam-on-target to stripped-beam becomes too low or if the target pressure is too high.

The targets are located in the horizontal mid-plane, all around the cyclotron yoke. The beam is extracted by a two-foil stripper carousel positioned in front of each target port. The stripper foils are $400 \mu\text{gr}/\text{m}^2$ carbon foils.

The target system installed is NirtaR Liquid Target large volume (figure 3.32), comprised of a Niobium (99.9 % purity) irradiation chamber to reduce target insert activation.

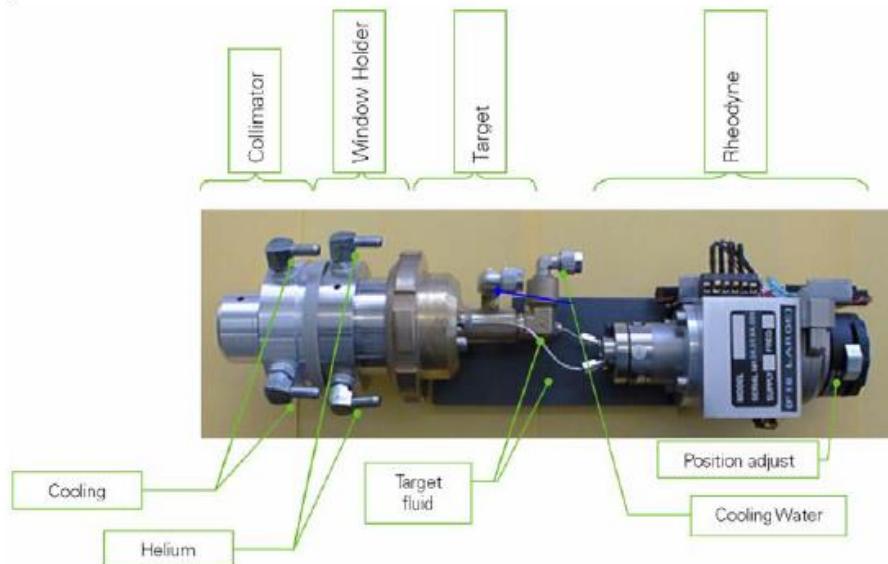


Figure 3.32 IBA Liquid target assembly (IBA Molecular, 2007)

The outer dimensions of target body are 85 mm length and 64 mm diameter, with an irradiation volume of 2.0 ml. The water cooled front collimator has a quick-connect flange that is directly inserted in the vacuum gate valve. The same helium cooled window design is used for all the targets. The helium gas is recirculated in a closed loop that includes a compressor and a heat exchanger. The bodies of the targets are water-cooled. A titanium foil ($12.5 \mu\text{m}$) is situated in the window between the vacuum and Helium chambers whereas Havar foil ($35 \mu\text{m}$) is situated in the window between Helium and irradiation chamber. (IBA Molecular, 2007)

3.2.1 Geometry

A detail MC model of the IBA C18/9 PET Cyclotron was realized to allow accurate transport of neutrons produced inside fluoride target by (p,n) reactions. The model includes all the major components of the cyclotron that are expected to interact with the particles generated (figure 3.34 and figure 3.35):

- the various component of the yoke (steel)
- the four poles (steel)
- an approximation of the coils (Copper)
- the vacuum chamber, the holes in the upper and lower yoke needed for vacuum pumping and to introduce the RF power into the RF cavities and the eight target exit ports

- four fluoride-18 target station
- the external beam line (Aluminium) with two quadrupoles (Copper)

Data regarding the dimensions and features of the cyclotron and its components were taken from technical sheets and reference manuals of the vendor.

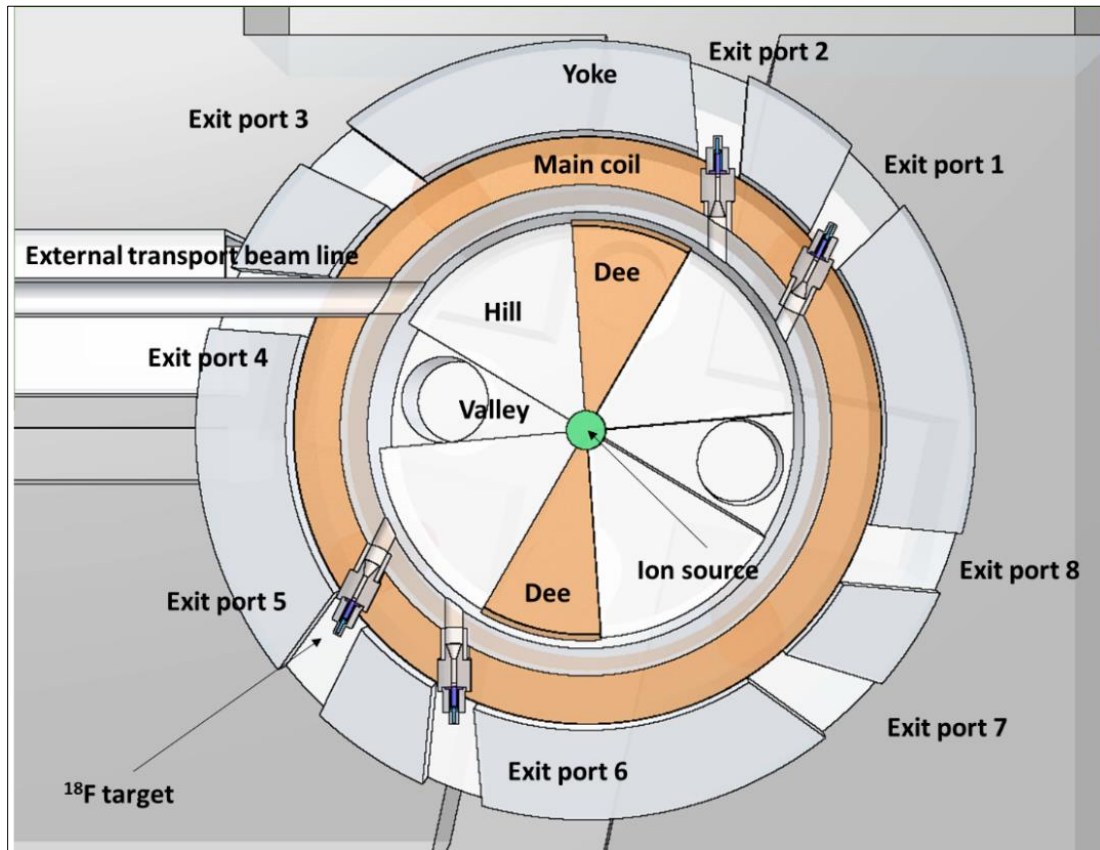


Figure 3.34 horizontal view of the IBA CYCLOPE 18/93D FLUKA model implemented in this work

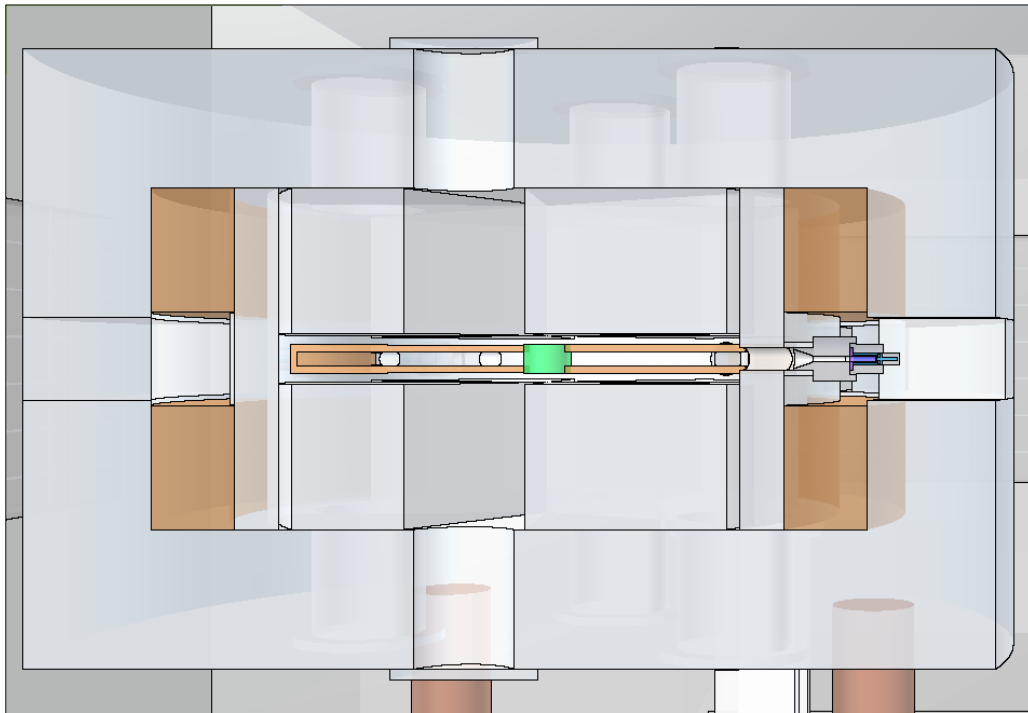


Figure 3.35 Vertical view of the IBA CYCLOPE 18/93D FLUKA model implemented in this work

A simplified model of the entire Liquid Target assembly was implemented with the following dimensions: 5 cm internal length, 1.2 cm diameter, 0.06 cm thick and including the aluminium structure, the niobium chamber, the water-cooling system, the helium-cooling system, the collimator, Titanium foil and Havar foil (figure 3.35).

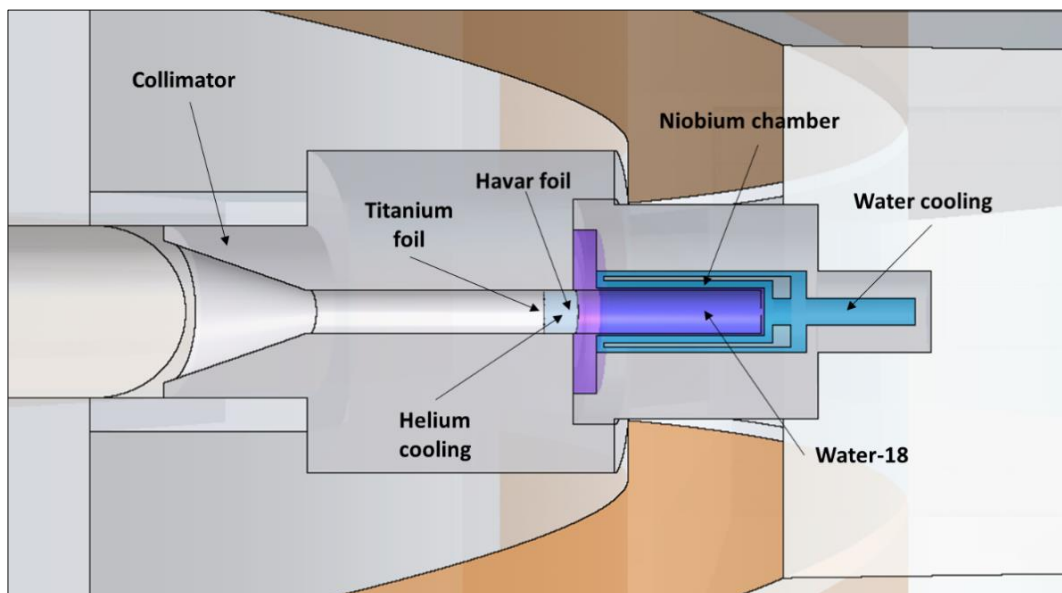


Figure 3.35 FLUKA model implemented in this work of IBA NirtaR Liquid Target large volume

A detailed MC model of the cyclotron vault was implemented on the basis of the bunker's original construction drawings; the model includes also the reinforcement rods (figure 3.36 and figure 3.37).

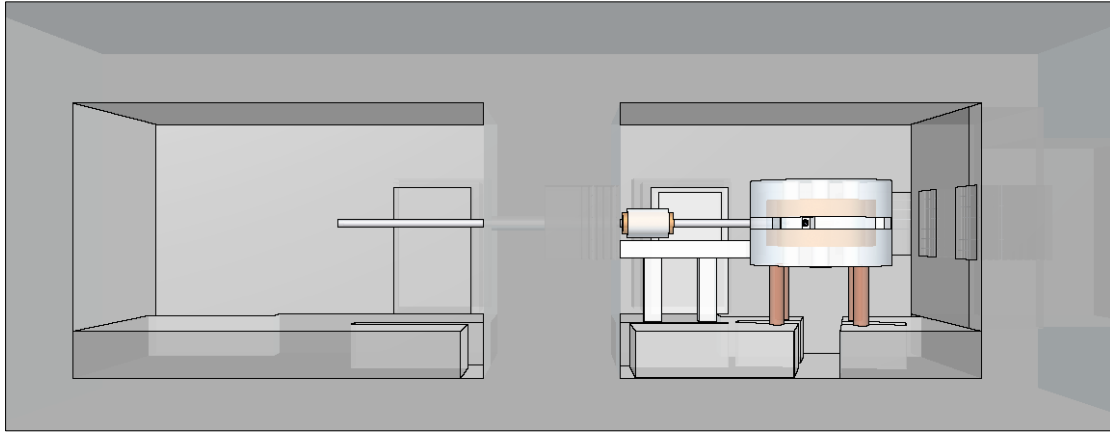


Figure 3.36 Vertical view of 3D MC model of cyclotron bunker

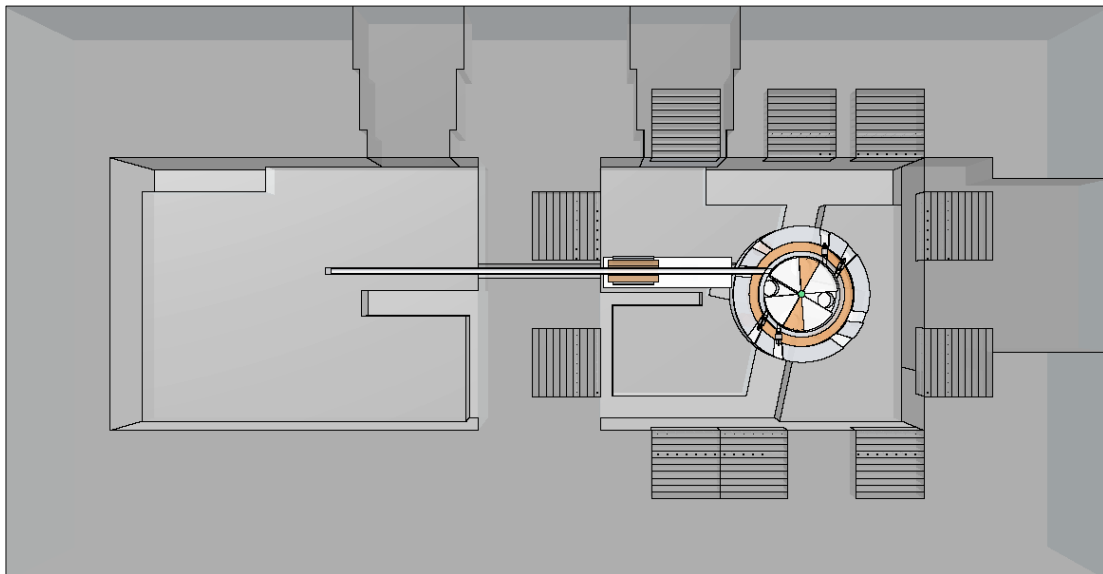


Figure 3.37 Horizontal view of 3D MC model of cyclotron bunker

During the construction phase of the Bunker a sample of concrete was taken from the walls and sent to EMPA *Material Science & Technology* laboratories (Dübendorf, Switzerland) for an XRF Analysis to determine concrete composition, 1.00 g of this sample was used for the XRF measurement, the potentially humidity were removed before the measurement drying the sample in 110 °C in air. The elements detected are listed in table 3.8.

Table 3.8 XRF detected element in concrete sample

<i>ELEMENTS</i>	<i>Mass-proportion in g/100g (%)</i>	<i>ELEMENTS</i>	<i>Mass-proportion in g/100g (%)</i>
<i>Na</i>	0.3	<i>Ca</i>	36
<i>Mg</i>	0.8	<i>Ti</i>	0.3
<i>Al</i>	3.6	<i>Mn</i>	0.05
<i>Si</i>	16	<i>Fe</i>	2.4
<i>P</i>	0.08	<i>Zn</i>	0.01
<i>S</i>	0.6	<i>Sr</i>	0.09
<i>Cl</i>	0.04	<i>Zr</i>	0.02
<i>K</i>	1.04		

The rest of the sample mass consists of 1st and 2nd period elements (from H to Ne), the quantification of which by XRF generally cannot be considered reliable in the case of inorganic solid matrices. The amounts of some elements as caesium, cobalt and europium appeared to be below the limit of detection, however the amount of those elements, as mentioned already said, influence largely the resulting activation. For this reason they cannot be neglected in the simulation, also in this case literature values reported in table 3.2 were used. The composition used in this work for concrete is a combination of all those information and standard concrete Portland present in Fluka (table 3.9). The average density of concrete was assumed to be 2.28 g/cm³ as reported in technical sheets.

Table 3.9 MC concrete composition

<i>ELEMENTS</i>	<i>Mass-proportion in g/100g (%)</i>	<i>ELEMENTS</i>	<i>Mass-proportion in g/100g (%)</i>
<i>Na</i>	0.3	<i>Zn</i>	0.01
<i>Mg</i>	0.8	<i>Sr</i>	0.09
<i>Al</i>	3.6	<i>Zr</i>	0.02
<i>Si</i>	16	<i>Ba</i>	0.025
<i>P</i>	0.08	<i>Ni</i>	3.1E-3
<i>S</i>	0.6	<i>Co</i>	1.9E-4
<i>Cl</i>	0.04	<i>Nb</i>	2.3E-4
<i>K</i>	1.04	<i>Eu</i>	6.6E-6
<i>Ca</i>	36	<i>Cs</i>	1.2E-4
<i>Ti</i>	0.3	<i>O</i>	37.5
<i>Mn</i>	0.05	<i>H</i>	1
<i>Fe</i>	2.4	<i>C</i>	0.1

No accurate informations regarding reinforcement rods composition were present, for this reason the composition used was the same of Table 3.5.

3.2.2 Source term, neutron emission from target

The physical input parameters used in the simulations are the same described in subsection 3.1.2. To simulate directly neutrons as primary particles the source.f user routine developed and described in subsections 3.1.3 was used.

The assessment of the neutron spectrum resulting from the (p,n) reaction in daily production of ^{18}F was performed simulating the 18 MeV pencil proton beam and all the materials interacting with it, as Titanium foil, Havar foil and water-18 volume (Figure 3.38 and figure 3.39). Neutrons fluence as a function of energy was scored on a sphere surrounding the target with the USRBDX card.

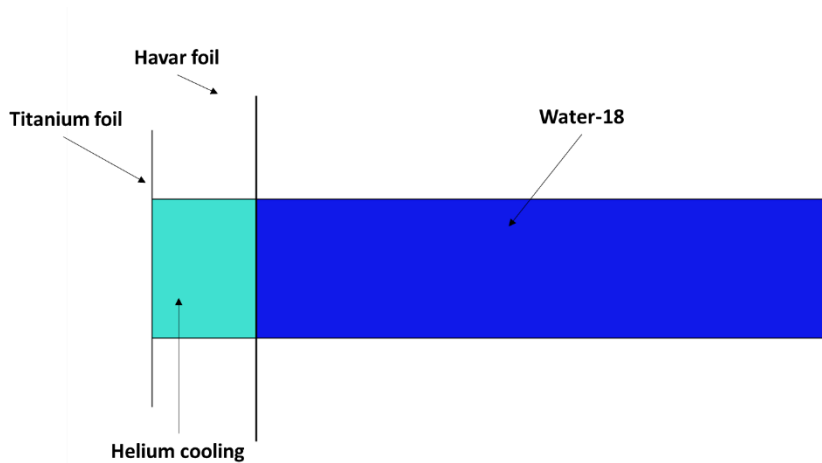


Figure 3.38 MC model of Titanium foil, Havar foil, Helium cooling and Water-18

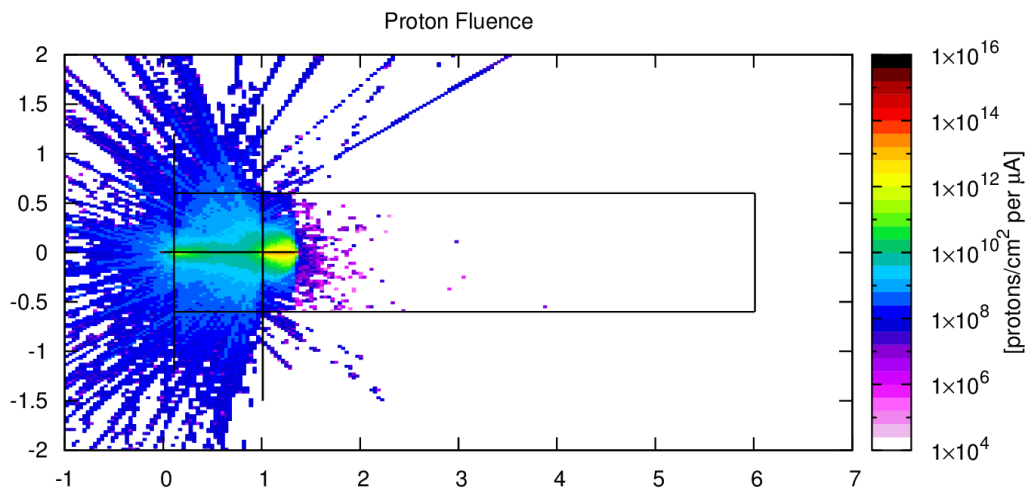


Figure 3.39 Proton fluence

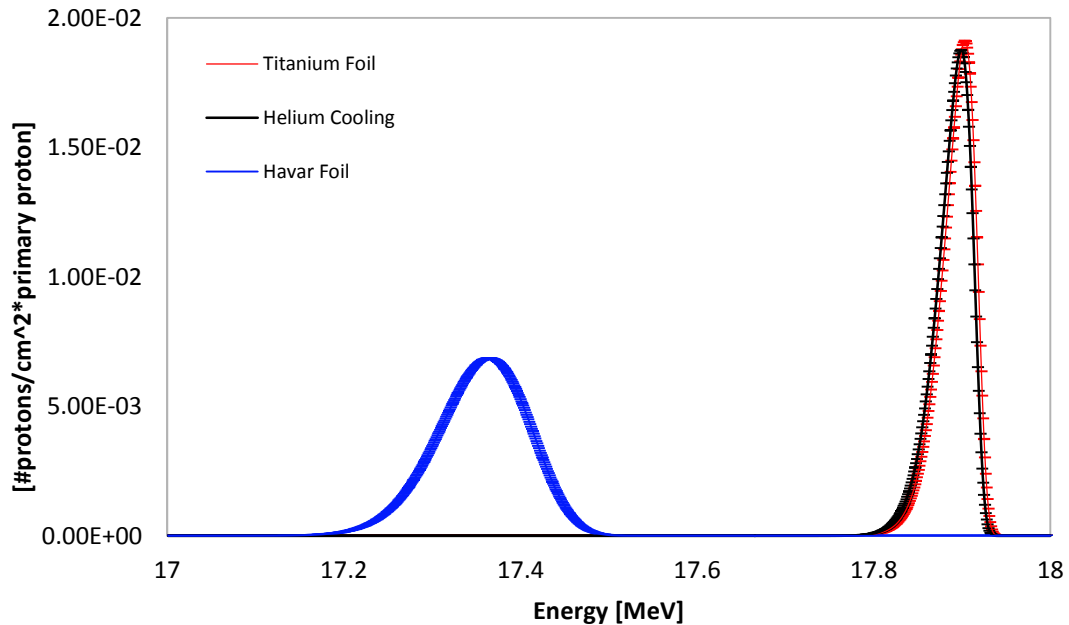


Figure 3.40 Proton beam attenuation

The attenuation of the proton beam through the different materials was also scored using different USRTRACK cards (figure 3.40). The average kinetic energy of primary protons at the entry of water-18 chamber is equal to 17.37 ± 0.01 MeV, compatible, within the errors, with SRIM value of 17.38 ± 0.01 MeV. The mean range of 17.37 MeV protons (point-like beam) in water-18 target estimated with FLUKA is 0.33 ± 0.01 cm, consistent with SRIM value of 0.32 ± 0.01 cm.

Even in this case the saturation yield of ^{18}F was estimated with FLUKA and compared with the recommended saturation activity for $1 \mu\text{A}$ (A_2) provided in the IAEA database for medical radioisotopes production: for 17.3 MeV protons A_2 equals 13.5 GBq/ μA (IAEA, 2001a). FLUKA estimated saturation yield result to be consistent with this value and equal to 13.77 ± 0.02 GBq/ μA .

The kinematic properties of the neutrons emitted are shown in figure 3.41. The neutron kinetic energy shows a peak around 2.8 MeV with a large tail towards lower values down to 1 keV. The neutron polar angle distribution is shown in figure 3.42. Figure 3.43 shows how the energy spectrum of neutrons varies with the direction of

emission. The neutron multiplicity is evaluated at $5.10 \cdot 10^{-3} \pm 0.01 \cdot 10^{-3}$ [#neutrons/primary proton].

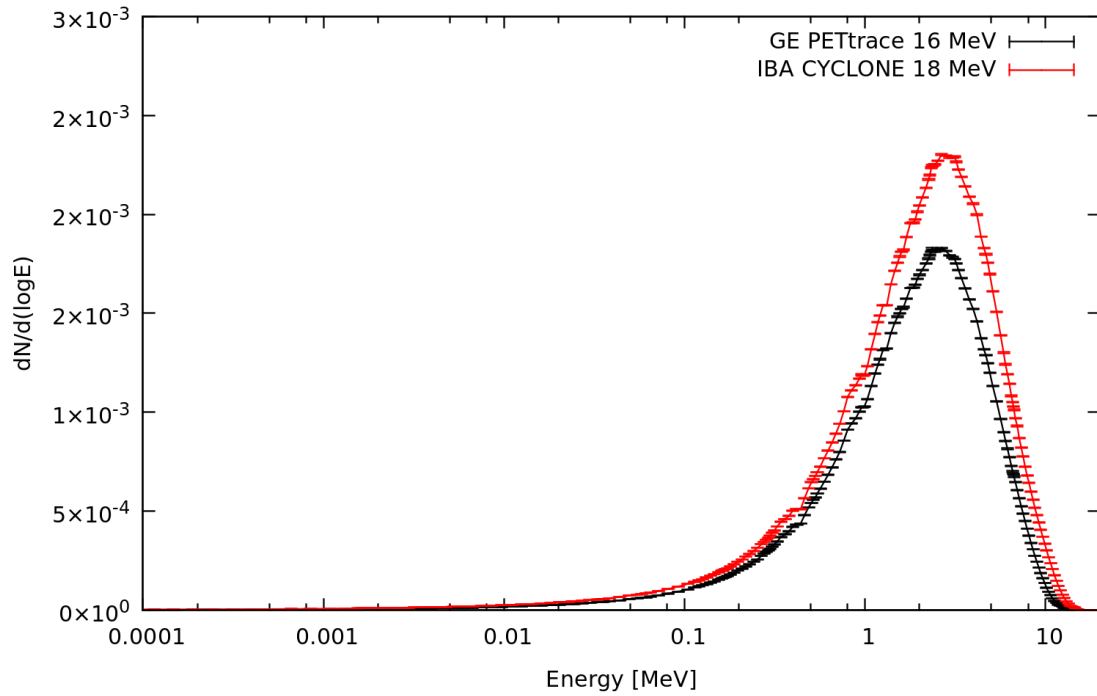


Figure 3.41 Comparison between neutron energy spectra generated by the $^{18}\text{O}(p,n)^{18}\text{F}$ reaction in PETtrace target (in black) and in CYCLONE target (in red)

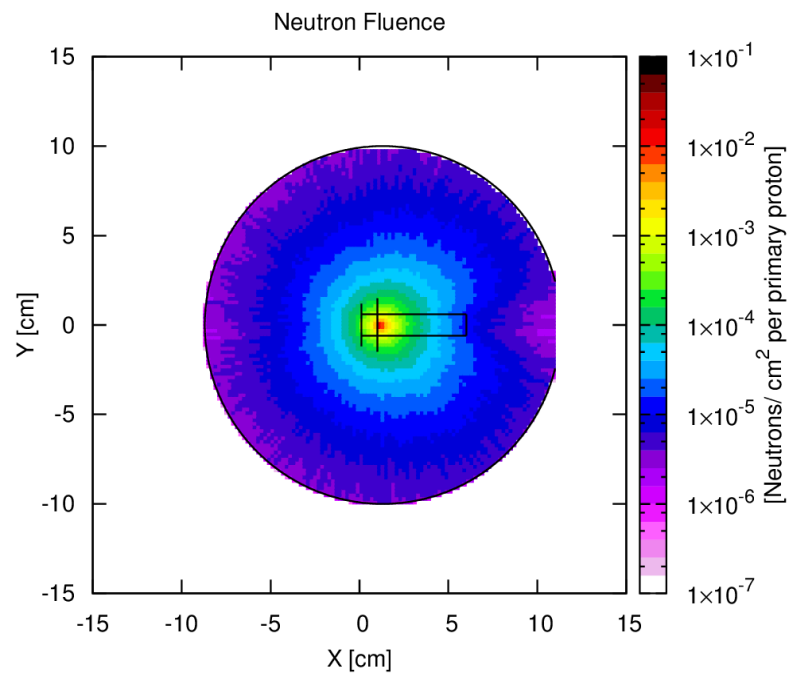


Figure 3.42 Neutron fluence

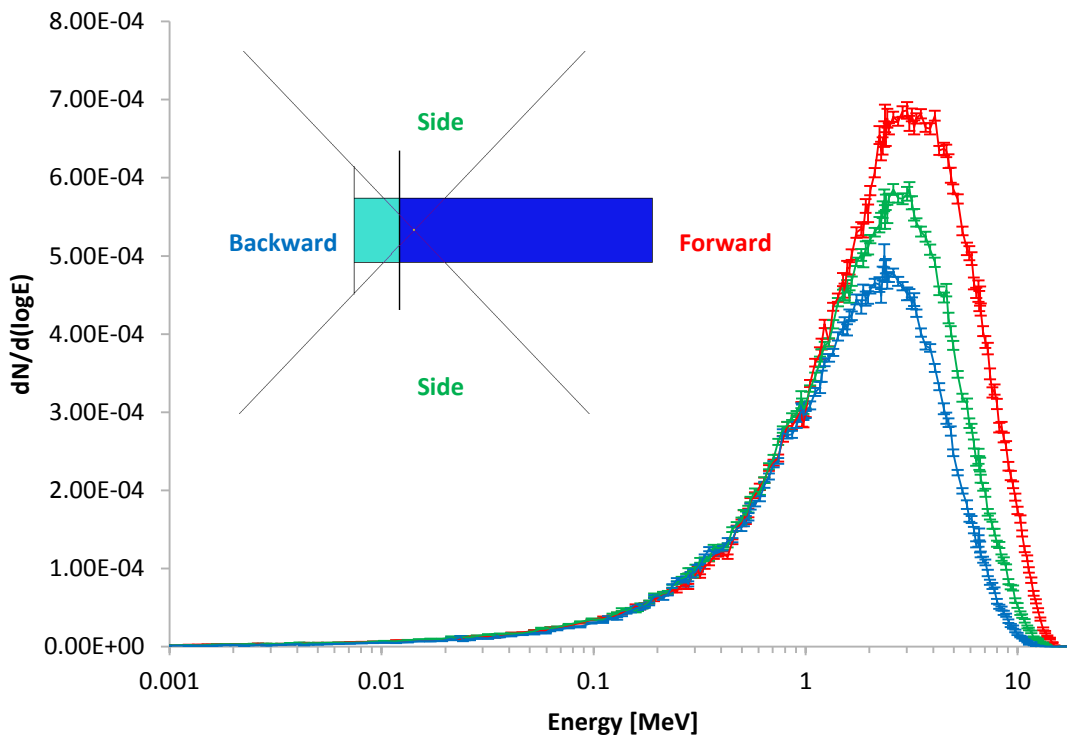


Figure 3.43 Comparison of neutron energy spectra obtained for different emitting directions

Also in this case the neutron spectrum was assumed as independent from the direction and equal to the average spectrum over all directions. The subroutine thus implemented was used to simulate four isotropic point neutron sources positioned inside the four fluorine targets (figure 3.44). The activation of the cyclotron vault walls and of the reinforcement rods was assessed using several RESNUCLEI cards; activity was scored at different positions, depth and for different life expectancy of the cyclotron using the same spreadsheet described in subsection 4.1.4 and considering 3 daily irradiations of 70 μ A and 90 minutes alternating the four liquid target.

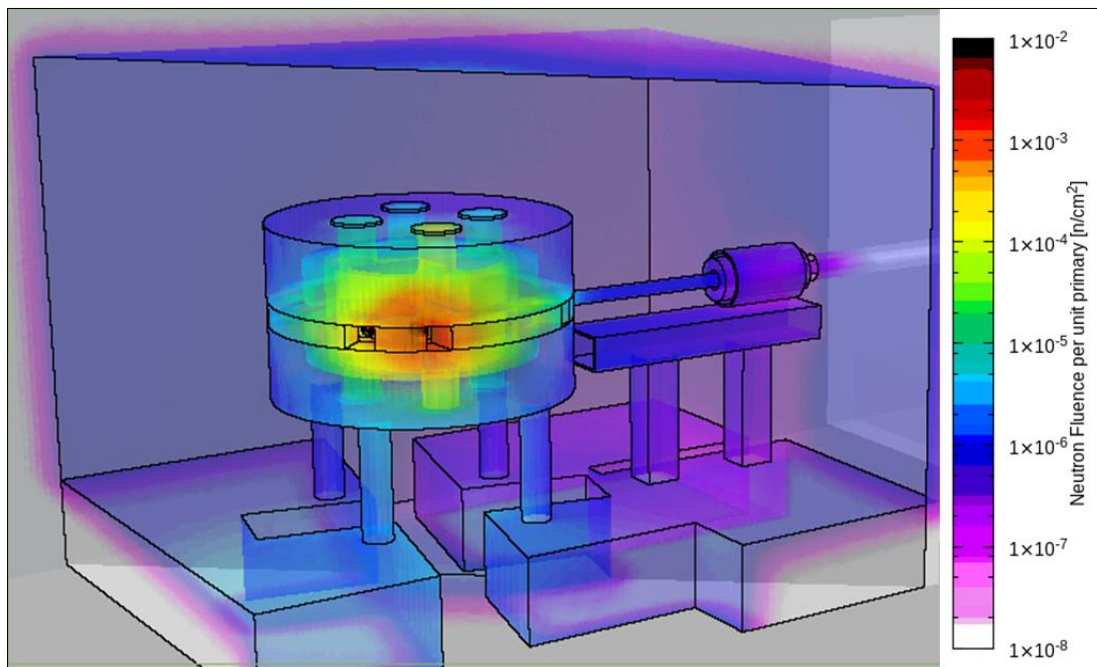


Figure 3.44 Neutron fluence inside the cyclotron bunker

Chapter 4

Radiation detectors used in experimental measurements

In this chapter devices used to assess Monte Carlo results accuracy through comparison with experimental measurements will be presented. For each device first a general description of the operating principle will be reported, secondly specific features specific to the device used will be described.

4.1 Neutron detection

Neutrons are generally not detected directly but through nuclear reactions that result in prompt energetic charged particles or through activation products. Because the cross section for neutron interactions in most materials is a strong function of neutron energy, rather different techniques have been developed for neutron detection in different energy regions. Every type of neutron detector involves the presence of an appropriate material designed to produce the conversion of neutrons to directly detectable charged particles or radioactive nuclei via different reactions depending on the neutron interaction cross section of detector material (Knoll, 1989; Stabin, 2007). Possible reactions exploited in neutron detection are reported below:

- (n, α) reactions, for example this reaction can be exploited for low energy neutron detection via gas filled detector as BF_3 proportional counter;
- (n,p) reaction, ^3He is also a widely used detection medium for neutron in gas filled detector exploiting the reaction $^3\text{He}(n,p)^3\text{H}$;
- (n,fission) reaction, thermal neutrons can be captured by fissile material and the fission fragment detected.
- Neutron activation, detecting radioactive nuclei produced via neutron activation it is possible to estimate neutron fluence.

In the following neutron detection methods used in this work will be described. The complexity of neutron detection physics, together with potentially high costs of neutron detection devices, has led to choose for this work relatively cheap and easy to use devices, easily available even to small facilities to define a methodology applicable in as many cases as possible.

4.1.1 Neutron dosimetry with rem-counter

Neutron rem meters are routinely used for direct in-field measurement of neutron dose equivalent. Those kind of detectors are usually composed of a thermal neutron proportional counter surrounded by a cylindrical or spherical moderator. Fast neutrons interacting with the moderator are slowed down to thermal energies by elastic scattering and detected by the gas proportional detector. Standard thermal neutron proportional counters filled with BF_3 or ^3He gas fillings.

In this work two different type of rem-counter were used depending on detectors availability of the facility: for measurements in the S.Orsola-Malpighi Hospital of Bologna a FH 40 G-L10 Thermo Scientific survey meter with a FHT-725 probe was used, while for measurements in Inselspital Hospital of Bern a Bhertold UMo LB 123 with an LB 6411 probed was used.

The FH 40 G-L10 (Thermo Scientific, 2013) is a multipurpose radiation detection instrument, with an internal proportional counter provided with different external detectors. In this work the device was used for neutron dose measurements associated with the neutron rem-counter probe FHT-725 provided with a BF_3 proportional-counter and a PE-moderator (figure 4.1).



Figure 4.1 FH 40 G-L10 Thermo Scientific survey meter with a FHT-725 probe (Thermo Scientific, 2013)

The basis of the detection process is the $^{10}\text{B}(n,\alpha)^7\text{Li}$ reaction, alpha particles and recoil nuclei ^7Li produced after neutron capture travel in opposite directions ionizing the gas. In figure 4.2 the cross section for this reaction is reported (Nuclear Data Service, 2017).

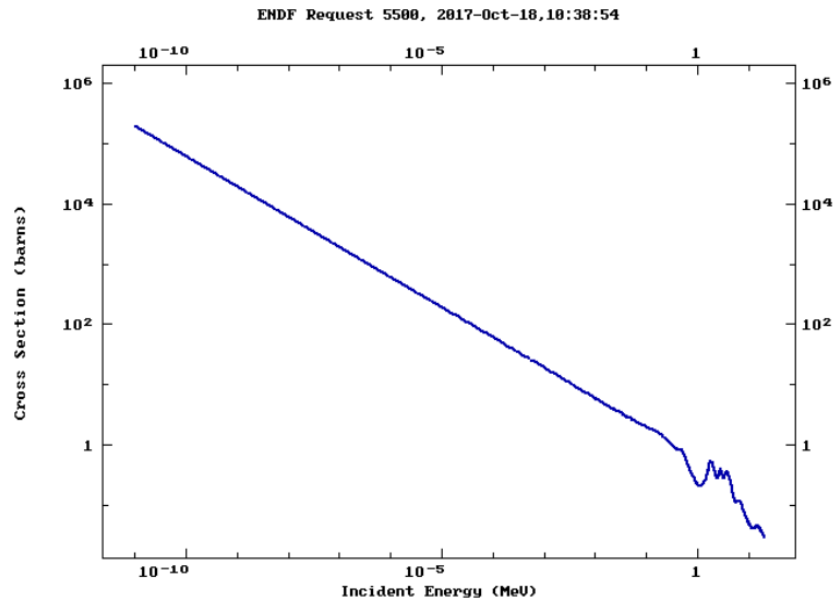


Figure 4.2 Cross section of the $^{10}\text{B}(n,\alpha)^7\text{Li}$ reaction (Nuclear Data Service, 2017)

As we can see the cross section is significantly higher for slow neutrons and decreases with increasing neutron energy according to the well-known $1/v$ dependence. Since bare BF_3 detectors are almost exclusively sensitive to slow neutrons, to detect fast neutrons the BF_3 tube must be surrounded by the moderator.

Berthold UMo LB 123 (Berthold Technologies, 2017a) is a universal monitor provided with a variety of different detectors enabling the measurement of alpha/beta-emitters, beta/gamma-emitters and neutrons. The detector used in this work for neutron dose rate monitoring was the moderator detector LB 6411 (Berthold Technologies, 2017b), provided with a He_3 proportional-counter and a polyethylene moderator (figure 4.3).



Figure 4.3 Berthold UMo LB 123 with LB 6411 detector probe (Berthold Technologies, 2017b)

The reaction exploited for neutron detection is ${}^3\text{He}(n,p){}^3\text{H}$, in figure 4.4 the cross section for this reaction is reported (Nuclear Data Service, 2017).

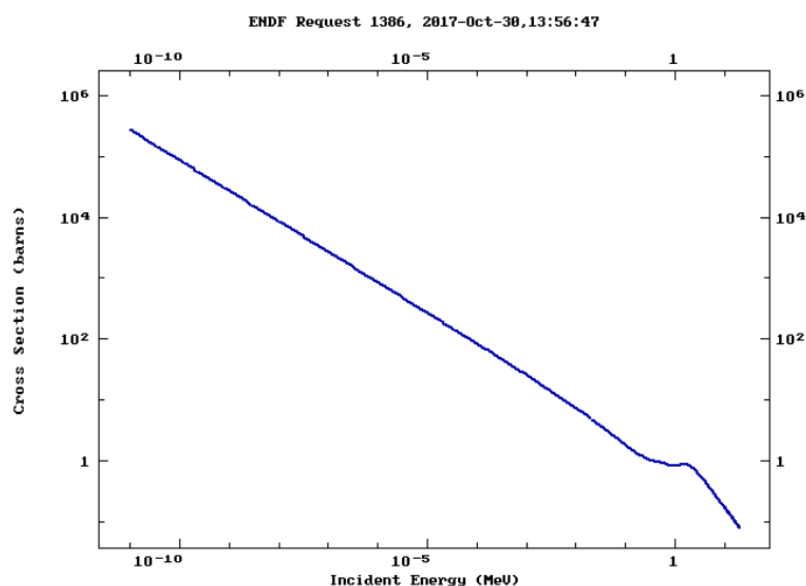


Figure 4.4 Cross section of the ${}^3\text{He}(n,p){}^3\text{H}$ reaction (Nuclear Data Service, 2017)

Both detectors were calibrated in ambient dose equivalent rate $H^*(10)$ based on ICRP 74 (ICRP, 1996). In table 4.1 the main features of the detectors are reported.

Table 4.1 Main features of the detectors used for the measurement of the neutron ambient dose equivalent.

	<i>FHT-752</i>	<i>LB 6411</i>
Measured quantity	$H^*(10)$	$H^*(10)$ (ICRP)
Energy range	0.025 eV – 20 MeV	0.025 keV – 20 MeV
Measuring range	1 nSv/h – 0.4 Sv/h	100 nSv/h – 100 mSv/h
Response	Neutron: $0.5 \text{ s}^{-1}/(\mu\text{Sv/h})$ for Cf-252 Gamma: $<10^{-5}$ at 1Sv/h for Cs-137	Neutron: 0.79 cps per $\mu\text{Sv/h}$ (Cf-252) Gamma: $<40 \mu\text{Sv/h}$ in 10 mSv/h (Cs-137)

4.1.2 Neutron dosimetry with CR39

CR39 is a polycarbonate plastic nuclear track detector comprising poly-allyl diglycol carbonate (PADC) widely used for personal neutron dosimetry. This kind of detectors are able to register charged particles by the radiation induced damage caused along their interaction path. Neutrons do not cause any ionization directly in the detectors but the recoil of detector nuclei under neutron impact leads to the production of charged particles that cause ionization, and consequently, etchable tracks. Following irradiation, the damaged regions are developed and amplified using a well reported technique known as chemical etching. After adequate calibration, to relate the track density to the neutron dose equivalent, dose assessment can be obtained from counting the number of tracks (Castillo, 2013; Hankins, 1986). All CR39 dosimeters used in this

work (figure 4.5) were provided by the Italian National Agency for New Technologies, Energy and Sustainable Economic Development (ENEA), detector specifications are reported in table 4.2 (ENEA, 2003).



Figure 4.5 CR39 dosimeters provided by ENEA (ENEA, 2003)

Table 4.2 Main features of CR39 dosimeters used for the measurement of the neutron ambient dose equivalent.

<i>CR39</i>	
Measured quantity	H*(10), Hp(10)
Energy range	200 keV – 14 MeV
Measuring range	0.1 – 20 mSv
Response	Energy dependence: $\pm 50\%$ Angular dependence: $\pm 15\%$

4.1.3 Neutron spectrometry with bubble detectors

Neutron energy spectrum characterisation is of great importance for activation studies and radiation protection evaluation on a cyclotron bunker. Some of the most well-known methods for measuring neutron fluence as a function of neutron energy are threshold methods. Most of these methods are based on neutron-induced activation, the observation of a radioactive product resulting from an endoergic neutron-induced nuclear reactions ($Q < 0$) indicates that the neutron energy must exceed the threshold for the reaction. Activation foils technique is an example: irradiating an appropriate set of target foils the energy spectrum may be determined by comparing measurements of several different neutron-induced activities with different threshold energies. Another type of threshold method is based on superheated bubble detectors, this method is less accurate compared to activation foils technique but it is also less expensive and easier to use, for example unfolding procedures are easier to perform and there is no need for an HPGe detector to measure foil activation, therefore it can be purchased even by small facilities. The detection process in these systems is characterized by a threshold

energy, related to the critical radius for bubble formation, which depend on the composition of the liquid used and on its temperature and pressure (Brooks, et al. 2002)

In this work measurements of the neutron spectrum were conducted using Bubble Detector Spectrometers (BDS), manufactured by BTI Bubble Technology Industries to assess neutron spectra generated during irradiation.

4.1.3.1 Basic principles and detection physics of bubble detectors

The bubble detector spectrometers are a major tool in neutron detection approved by the International Commission on Radiation Units and Measurements (ICRU, 1977) and by the organisation for Standardisation (ISO, 1998-2001)). These kind of detectors, also named “Superheated emulsions”, consist of uniform dispersions of over-expanded halocarbon and/or hydrocarbon droplets suspended in a compliant material.

A fluid is superheated or over-expanded when it is in a metastable state in liquid form but at temperature and pressure values corresponding to the vapour region in the phase diagram. A liquid may be kept in steady-state superheated conditions by fractionating it into droplets and dispersing the latter in an immiscible fluid via an emulsification process. To achieve a steady-state the drops must be perfectly smooth and free of nucleating impurities or heterogeneous nucleation sites. The emulsification process is rather complex, magnetic stirrers, ultrasound fractionation, or coaxial flow proprietary techniques are usually employed. Number, size and composition of the droplets can be varied in the formulation of the detectors to permit a wide range of applications. For example halocarbon with a moderate degree of superheat can be used for neutron detection since they are only nucleate by energetic heavy ions, instead halocarbons with an elevate degree of superheat can be used in the detection of sparsely ionising radiation, such as photons and electrons. One of the most important advantage of superheated emulsions is their ability to detect neutrons and discriminate sparsely ionising radiations.

The basic operating principle of superheated emulsions is the same as in bubble chambers, long used in high energy particle physics: charged particles liberated by radiation interaction nucleate the phase transition of the superheated liquid and generate detectable bubbles. In the specific case of neutrons detection bubble formation is induced by highly ionising charged particles generated in neutron interactions.

The thermal fluid dynamics problem of radiation-induced vaporisation in a metastable liquid is extremely complex and has not yet been solved in general form. But in the absence of a detailed theory semi-empirical models have been developed. These suggest the following explanation for the detection process: when a charged particle slows down crossing a liquid its kinetic energy is transferred as heat, creating trails of sub-microscopic vapour cavities inside the droplets. When these cavities exceed a critical size they keep growing until the whole droplet evaporates, on the contrary sub-critical cavities collapse back to the liquid phase under the action of external pressure and surface tension. The energy and the critical size that are necessary for bubble nucleation depend on the composition and degree of superheating of the emulsion. The mathematical formulation of the critical radius R_c can be derived from the condition of mechanical equilibrium between surface tension (σ) and pressure difference through the walls of the cavity

$$R_c = \frac{2\sigma}{p_l - p_v} \quad \text{Equation 4.1}$$

Where p_l and p_v are respectively the pressure in the liquid and vapour phase.

The energy W_0 required in the radiation-induced nucleation can be calculated with the following expression

$$W_0 = \frac{16\pi\sigma^3}{3(p_l - p_v)^2} \cdot \left(1 + \frac{2\Delta H}{(p_l - p_v)} - 3 \frac{T}{\sigma} \cdot \frac{d\sigma}{dT} \right) \quad \text{Equation 4.2}$$

Where all the symbols have been previously defined, except for ΔH and T , the vaporisation heat of the fluid and the temperature of the fluid respectively. The first factor represents the work required for the isothermal spontaneous nucleation of a critical size bubble in equilibrium with its surrounding (homogeneous nucleation), the second factor represent the additional work required when the liquid is not superheated enough to undergo homogeneous nucleation, and the vaporisation is heterogeneously initiated by an ionising particle. (D'Errico and Alberts, 1994; Apfel, 1992; Apfel, 1989; D'Errico, 2001; D'Errico, et al., 1997)

The response of those detector change depending on the emulsions and on the neutrons energy. The higher the degree of superheat of the liquid, defined as the difference between their operating temperature and the boiling temperature, the lower the minimum energy that neutrons, or rather secondary charged particles, must impart to the drops in order to nucleate their evaporation. For this reason, the emulsions present thresholds at specific energies followed by a fairly flat response at higher energies (Figure 4.6).

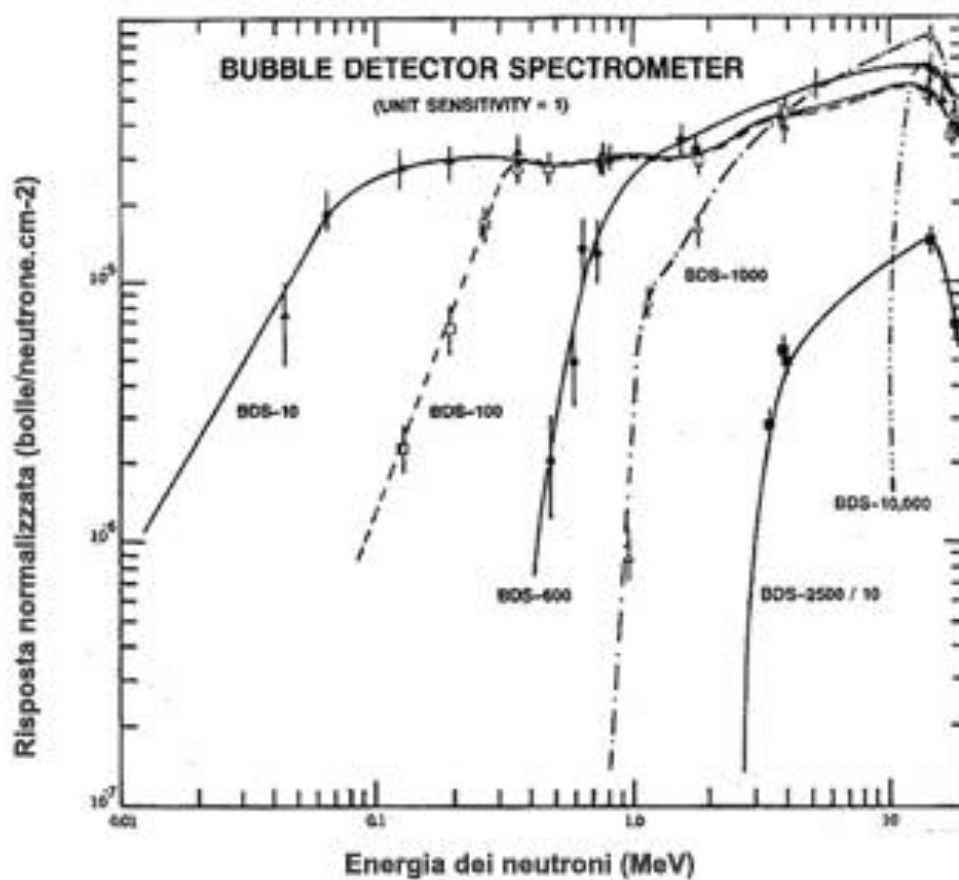


Figure 4.6 BDS Normalized Response Versus Neutron Energy (BTI Bubble Thecnology Industries, 2012a)

This kind of detectors are unfortunately very sensitive to operating temperature and the operator must be very careful to perform measurements at the calibration temperature (Figure 4.7). (Apfel, 1979; Apfel and Roy, 1984; BTI Bubble Thecnology Industries, 2012a; D'Errico, 1999)

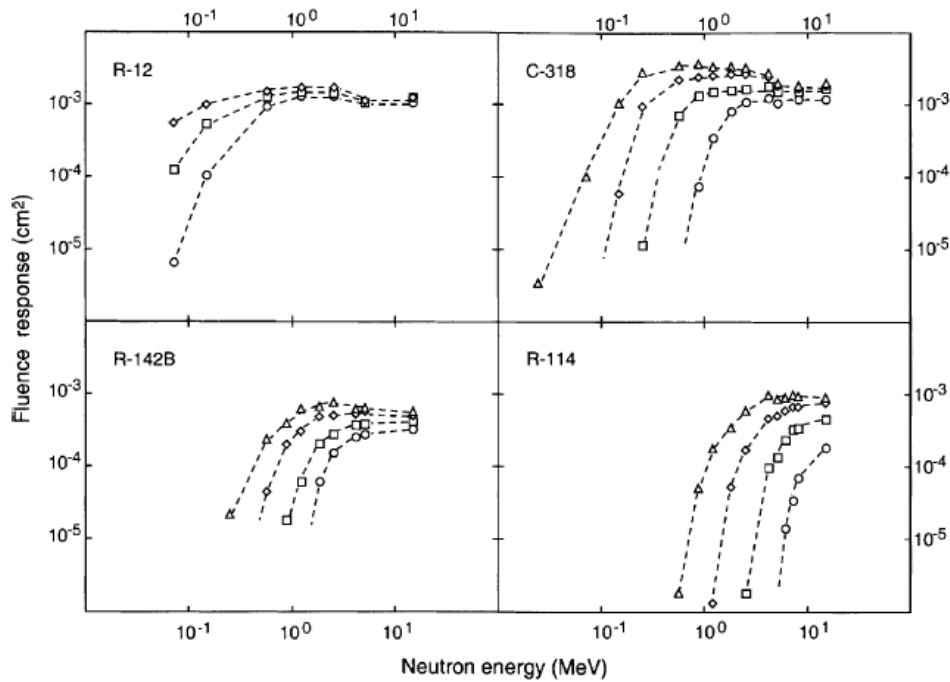


Figure 4.7 Fluence responses of superheated emulsions of dichlorofluoromethane (R-12), monochlorodifluoroethane (R-142B), octafluorocyclobutane (C-318) and dichlorotetrafluoroethane (R-114) measured as a function of neutron energy at 25 (○), 30 (□), 35 (◇), and 40 (△) °C. (D'Errico, 1999)

4.1.4 BDS bubble detector spectrometer, basic features

In this work three set of six Bubble Detector Spectrometers (BDS, manufactured by BTI Bubble Technology Industries) with six different energy threshold (10, 100, 600, 1000, 2500, 10000 keV) were used. Each detector is made of a vial (1.6 cm diameter, 8 cm length) containing a clear polymer where tiny droplets of superheated liquid are dispersed. As mentioned above the interaction between neutrons and polymer nuclei

induce droplet vaporization forming a visible gas bubble trapped in the polymer (figure 5.8).



Figure 4.8 Bubble dosimeter before and after neutron irradiation

The number of droplets provides a direct measurement of the tissue-equivalent neutron dose: a specific calibration certificate is provided by the manufacturer containing the average sensitivity (Bubbles/mrem or Bubbles/ μ Sv) at 20°C of each detector (table 4.3). The detectors were calibrated using an Am-Be source (strength = 1.13 n/s, fluence weighted average energy = 4.15 MeV) at 20°C.

Table 4.3 Bubble dosimeter spectrometer sensitivity (BTI Bubble Thecnology, 2012b)

<i>Detector Type</i>	<i>Detector Number</i>	<i>Average Sensitivity @20°C Bubbles/mrem</i>
BDS10	11178432	0.97
BDS10	13022337	0.99
BDS10	13280360	0.98
BDS100	15061335	1.0
BDS100	15268150	1.0
BDS100	15268206	1.0
BDS600	13018127	0.97
BDS600	15245403	0.99
BDS600	15245442	0.98
BDS1000	16067247	1.0
BDS1000	16323126	1.1
BDS1000	16323160	1.0
BDS2500	16175104	1.2
BDS2500	16175116	1.2
BDS2500	16175143	1.1
BDS10000	16176332	0.46
BDS10000	16176339	0.45
BDS10000	16176358	0.45

In table 4.4 average cross sections (bubble/neutrons*cm²) of BDS over various energy range provided by the manufacturer are reported.

Table 4.4 Average cross sections of BDS over Various Energy Ranges (BTI Bubble Thecnology Industries, 2012a)

<i>Energy Range (MeV)</i>	<i>Average cross section [bubble/n*cm²]</i>					
	<i>0.01-0.1</i>	<i>0.1-0.6</i>	<i>0.6-1.0</i>	<i>1.0-2.5</i>	<i>2.5-10</i>	<i>10-20</i>
BDS10	5.00E-06	2.50E-05	2.92E-05	2.97E-05	4.15E-05	4.78E-05
BDS100	-	2.27E-05	3.14E-05	3.23E-05	4.47E-05	5.09E-05
BDS600	-	-	1.60E-05	3.27E-05	4.75E-05	5.45E-05
BDS1000	-	-	-	1.32E-05	3.50E-05	5.90E-05
BDS2500	-	-	-	-	2.99E-05	8.70E-05
BDS10000	-	-	-	-	-	4.35E-05

Combining those information with detectors raw data and using unfolding procedures it is possible to evaluate the neutron fluence (neutrons/cm²) as a function of energy. After each exposure, the spectrometers can be re-used through recompression in a pressure chamber.

4.2 Gamma spectrometry with semiconductor detectors

Gamma-ray spectrometers are standard instruments used in a wide variety of scientific and industrial applications. Gamma-ray spectrometers are used to quantify both the energy of gamma rays and their relative intensities allowing the identification and the quantification of radionuclides by the analysis of gamma-ray energy spectra.

Detection process is based on the absorption by the detector of the energy of incident gamma rays and the conversion of this energy into an electronic signal. There are a large number of possible interaction mechanisms between photons and detector materials but the most relevant for detection are photoelectric interaction, Compton scattering and pair production.

The most common spectrometry devices currently in use are scintillation detectors and semiconductor detectors. Scintillation detectors comprise a scintillation crystal arranged above a photo-multiplier tube that converts light into the electrical signal measured. The most common crystal material used is sodium iodide doped with a trace of thallium NaI(Tl) (Knoll, 1989).

Nevertheless a step forward in gamma spectroscopy was achieved with high-density semiconductor detectors, in particular with the advent of Germanium detectors in the 1960' (Tavendale, et al. 1963).

The operating principle of semiconductor detector is based on their typical electronic band structure of energy states. When a photon interacts in the crystal, bound

electrons are excited to the conduction band by the primary electron from the interaction. These secondary electrons, if sufficiently energetic, can create additional secondary electrons. Through this cascading process, the energy of the primary electron is expended in the production of many electron-hole pairs that are then free to be collected at the electrodes of the device. The signal created is then amplified, shaped, digitized and stored. In figure 4.9 a typical electronic system of a semiconductor-detector spectrometer is drawn schematically. The system consist of a detector bias supply, preamplifier, amplifier, analogic-to-digital converter, a data storage device, a pulse generator if desired and a computer (Debertin et al., 1988).

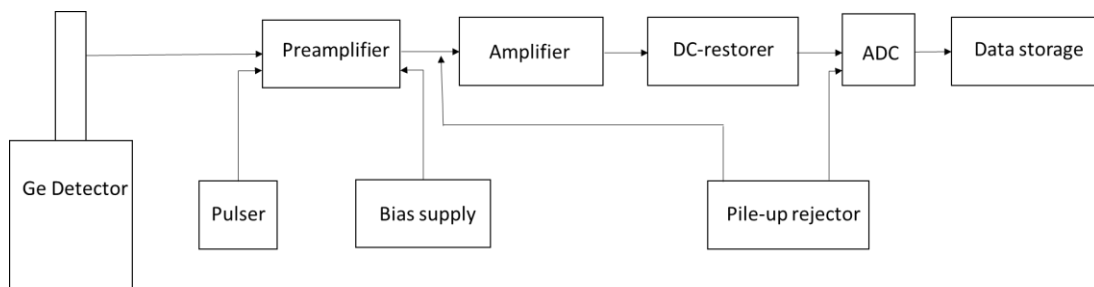


Figure 4.9 Schematic of electronics system for a semiconductor detector

Germanium is a semiconductor having a relatively low band-gap generating one electron-hole pair on average for every 3 eV deposited, this implies that for 1 MeV deposited the total number of charge carriers produced is of the order of 330000. Considering that typically in NaI(Tl) an energy loss of 1 MeV will generate about 38000 photons and assuming the quantum-efficiency of photon-multipliers is 25% so the number of charge-carriers detected from 1 MeV energy deposit is 8000. Considering the same amount of energy deposited, in HPGe the signal generated is 40 times higher than in NaI(Tl) consequently the statistical signal variance is significantly smaller. This results in an energy resolution @1332 keV typically comprise between 0.1% and 0.2% FWHM for HPGe detectors and of about 5% FWHM for NaI(Tl) detectors.

The high energy resolution of semiconductor detectors has been the basis for rapid progress in a wide fields of applications. The main disadvantages of this kind of detectors is their need to be cooled cryogenically requiring expensive and bulky equipment. This fact limits significantly their versatility and making them very expensive and available mostly in specifically dedicated areas for laboratory measurement. For this reason there is a growing interest in developing semiconductor detector with high Z materials able to operate at room temperature and providing at the same time good energy resolution. To this aim CdZnTe (CZT) detectors seems the most promising solution. This kind of semiconductor detector has a larger band gap than germanium allowing room temperature operation. Furthermore the higher atomic numbers of these materials, and hence larger absorption coefficients, make 2 mm of cadmium telluride crystal equivalent to 10 mm of germanium in terms of gamma-ray

absorption. Nevertheless a number of factors limit their use: material with a satisfactory crystalline perfection is not easily available; the charge carrier motilities in these materials are considerably lower than those for germanium, especially because of hole trapping, this means that only small detectors can be made with these crystals; the energy needed to create each charge carrier is higher than in germanium detectors and consequently the energy resolution achievable is lower. (Marengo, 2002)

In table 4.5 some of the main features of the detectors cited are reported.

Table 4.5 Gamma spectrometers main features

	<i>Bandgap (eV) 300 K</i>	<i>Energy per e-h pair (eV)</i>	<i>Atomic number</i>	<i>Maximal volume (cm³)</i>	<i>Energy resolution @662 keV (keV)</i>	<i>Commercial price of the whole spectrometry system (euro)</i>
HPGe	0.67	2.96	32	100	1.1	~ 70000
CZT	1.57	4.64	49.1	3.4	10.8	~ 10000
NaI(Tl)	-	-		>100	46.5	~ 30000

In the following subsections detectors used for spectrometry measurements within this work will be described.

4.2.1 CAMBERRA HPGe detectors

HPGe detectors are semiconductor diodes having a P-I-N structures in which the intrinsic (I) region is sensitive to ionizing radiation. Under reverse bias, an electric field extends across the intrinsic or depleted region. When photons interact with the material within the depleted volume of a detector, charged carriers are produced and are swept by the electric field to the P and N electrodes.

The detector used in this work in particular is a coaxial detector composed of a cylinder germanium crystal 55 mm diameter 53 mm length (Figure 4.10, 4.11).



Figure 4.10 HPGe detector of the S.Orsola-Malpighi Hospital

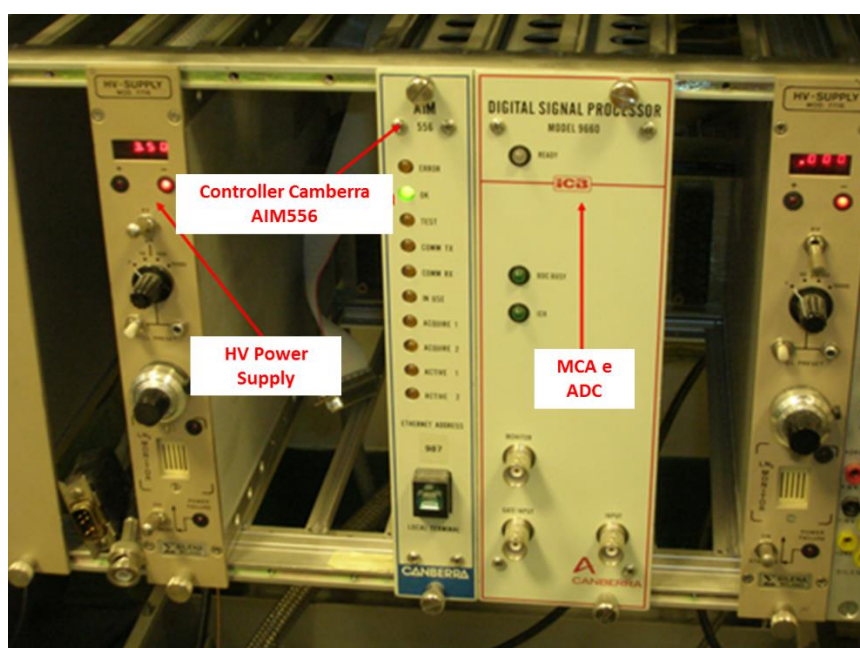


Figure 4.11 Power supply, Digital Signal Processor and Controller Canberra

The detector has 30% relative efficiency (measured at 25 cm source-detector distance, relative to a 3''x 3'' NaI(Tl) detector) and a resolution of 1.8 keV at 1332 keV. The spectrometry system is periodically calibrated in the 59-1836 keV range by means of a multi-radionuclide certified reference solution, obtained from an accredited Standardization Laboratory (Areva CERCA LEA, Pierrelatte Cedex, France). The calibration process is performed according to the IEC 61452 standard.

4.2.2 Kromek GR1

The Kromek GR1 is a high-performance portable gamma-ray spectrometer composed of a 1 cm³ CdZnTe crystal. The device, with built-in preamplifier, shaping amplifier, baseline restorer, pulse height digitizer and HV supply, is completely self-contained in 25 x 25 x 63 mm (figure 4.12).



Figure 4.12 Kromek GR1

The digitized pulse heights of detected gamma-ray signals are sent to a PC via a USB port. The unit is powered entirely from the USB so no external supply is needed. The main features of the detector are reported in table 4.6.

Table 4.6 Kromek GR1 specifications

Kromek GR1	
Detector	10mm x 10mm x 10mm CZT coplanar-grid detector
Energy range	30 keV – 3.0 MeV
Energy resolution	2.0 – 2.5% FWHM @662 keV
Maximum throughput	30000 counts/s
Number of channels	4096 (12 bit)
Dimensions	25mm x 25mm x 63mm
weight	60 gram

The K-Spect software included with the kromek GR1 spectrometer provides the spectrum acquisition, display and storage functions.

Chapter 5

Experimental measurements

In the present chapter experimental measurements performed in this work will be described, including those made at the S.Orsola-Malpighi Hospital of Bologna, and in Inselspital of Bern to validate a variety of case to case possibilities. Basically, two kind of experimental measurements were performed:

- a) Monte Carlo simulations were checked in terms of source term accuracy, to evaluate if the neutron flux modelled with Fluka is an accurate estimation of the real neutron radiation field inside the bunker. To this aim measurements were conducted in the Bologna hospital to assess neutron dose field inside the bunker during irradiation, while in Inselspital Bern neutron spectrometry measurements with bubble detectors were performed;
- b) Results of Monte Carlo simulations in terms of neutron activation were assessed comparing the residual activity estimated with Fluka with the experimentally measured activity present inside the bunker walls. To this aim non-destructive in situ measurements using a portable CZT detector were performed in the S.Orsola-Malpighi hospital, while core drilling was performed in the Inselspital bunker and concrete sample measured in HPGe spectrometry.

All the experimental measurements were compared with Monte Carlo simulations modelled to reproduce as close as possible the real irradiation conditions and this made possible the overall check of consistence of the results.

In the following a detailed description of the experimental work performed is given.

5.1 Assessment of the neutron dose field around the PETtrace of S.Orsola-Malpighi Hospital in Bologna

Measurements of neutron ambient dose equivalent $H^*(10)$ were taken inside the bunker, around the PETtrace, in the S.Orsola-Malpighi Hospital to validate the MC model in terms of neutron dose. The experimental setup adopted refers to a previous work conducted by our group and published by Gallerani, et al. (Gallerani, et al. 2008).

In that work measurements were conducted in 12 points located along 8 directions at the same height as the target used for the production of ^{18}F (Figure 5.1): a set of 3 dosimeters for fast neutrons (CR-39) and 3 for thermal neutrons (GR-200 and GR-207) was used at each measurement point to improve measurement statistics; all dosimeters were provided by the Italian National Agency for New Technologies, Energy and Sustainable Economic Development (ENEA).

For the new series of measurements conducted in the present work were performed using both active and passive dosimeters were used:

- The FH 40 G-L10 survey meter (Thermo Scientific) with its neutron rem-counter probe FHT-752 described in chapter 4.1.1.
- The set of 12 CR39, supplied by ENEA described in chapter 4.1.2.

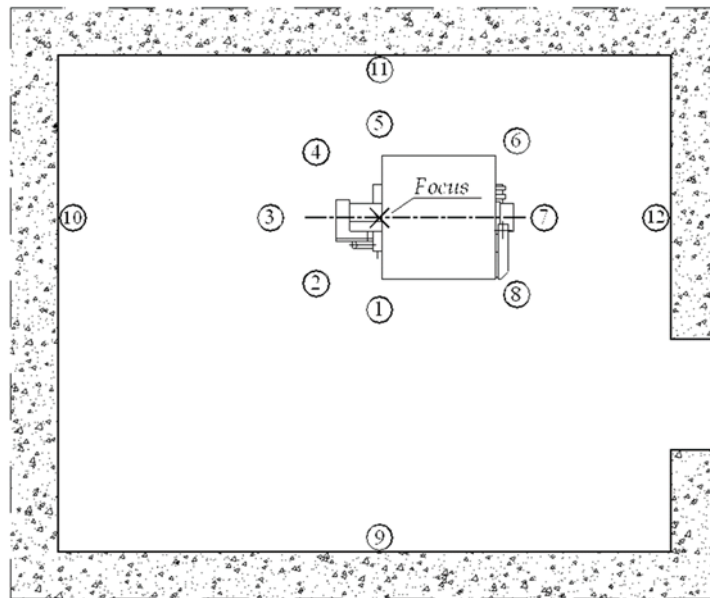


Figure 5.1 Experimental setup used in the measurement campaign: numbers indicate the position of the dosimeters (Gallerani, et al., 2008).

To obtain dose rates in the measurement range of the detectors and to limit the effects of dead time, irradiation tests were conducted with an integrated current between 0.005 and 0.05 μAh ; the uncertainty in the integrated charge, of the order of 5%, was essentially that of the ammeter used for the calibration of the current measuring board. Data obtained using the neutron rem-counter were then corrected for the experimentally determined dead-time of the instrument. While the position of the neutron probe was varied according to the experimental setup of figure 5.1, the CR39 dosimeters were left in the same locations for the whole measurement campaign. Results were normalized to the total charge accumulated on the target in each irradiation test, expressed in μAh and compared with Monte Carlo simulations of neutron dose field performed in the same conditions of irradiation. Two different

neutron transport thresholds were used in different simulations: in the first case, the predefined transport threshold of the NEW-DEFA default was used, being 10^{-14} GeV; in the second case a transport cut-off of 200 keV was set to reproduce the features of the CR39 dosimeters. The evaporation of heavy fragments and the coalescence mechanisms were also activated. Finally, radiation decay was activated in “analogue mode”, meaning that the radiation decay is calculated analytically but at fixed times. An irradiation profile of 1 h irradiation time and 1 μ A extracted proton current was set and used for all the simulations. (Infantino, A. et al., 2016)

The USRBIN score was used to assess the dose equivalent distribution in a regular spatial structure (binning detector) independent of geometry. In particular, a Cartesian mesh XYZ over the whole bunker (10 cm pitch in all directions) was used. The card AUXSCORE was used to filter out the contribution of neutrons below a certain energy and to apply the fluence-to-dose conversion factors labelled “AMB74”, based on ICRP74 (ICRP, 1996) and data from Pelliccioni (Pelliccioni, 2000).

5.2 Neutron spectrometry inside Inselspital cyclotron bunker of Bern with bubble detectors

The measurements performed in Bern include the assessment of neutron spectrum inside the bunker during ^{18}F production. The three sets of six Bubble Detector Spectrometers described in chapter 4.1.3 were placed at the same height as targets used for the production of ^{18}F . In figures 5.2 and 5.3 experimental setup conditions are shown.

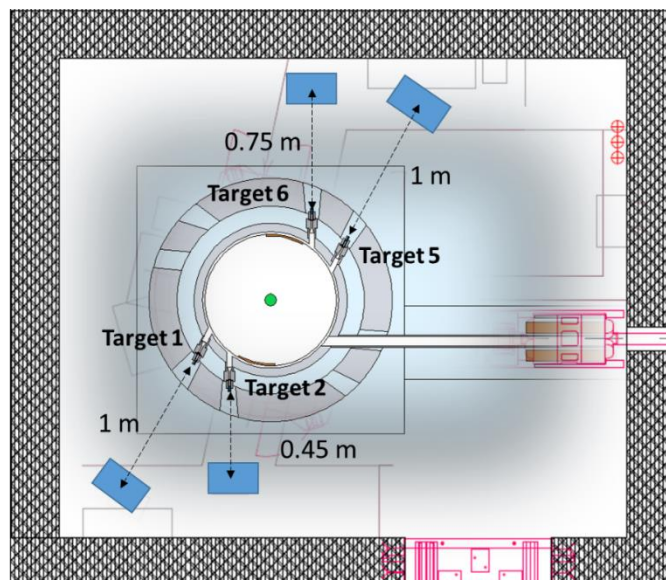


Figure 5.2 Bern facility bubble detectors experimental set-up

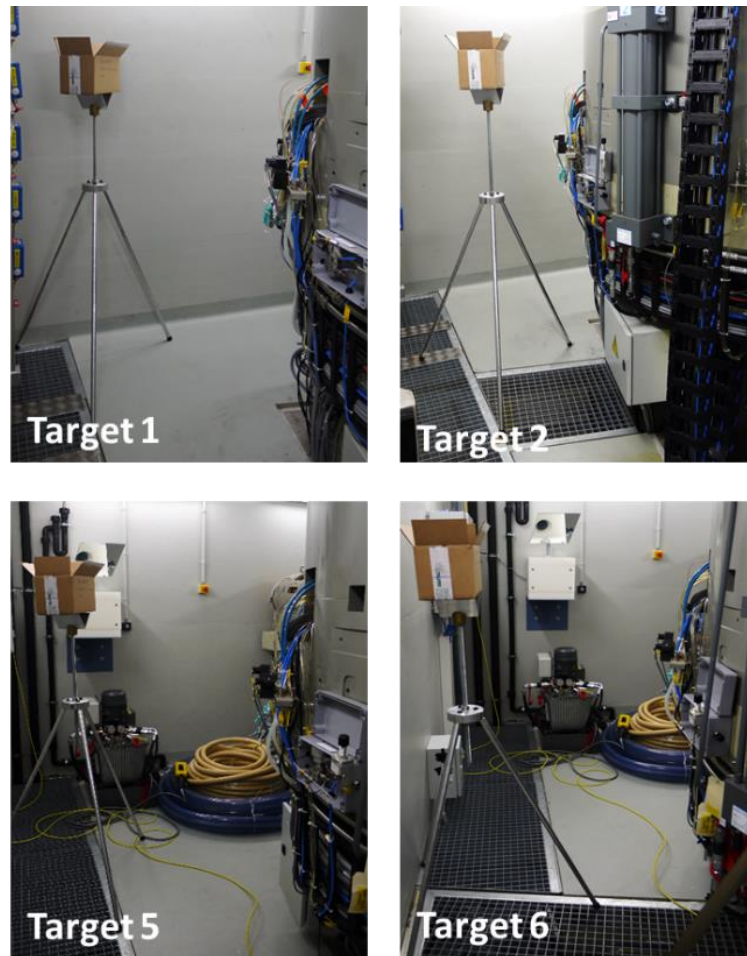


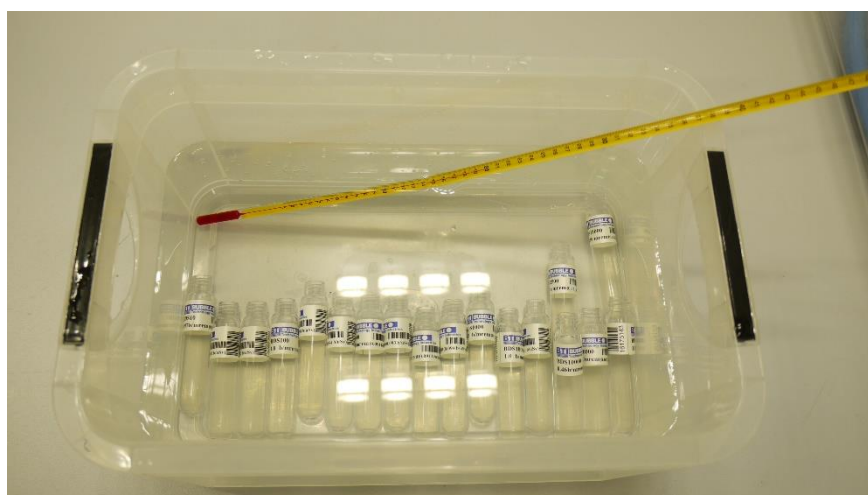
Figure 5.3 bubble detectors positioning around IBA CYCLONE 18/9

Since the manufacturer of bubble detectors recommend a reading of about 100 bubbles for optimal visual counting, a quick evaluation of the order of magnitude of neutron dose rate was preliminary assessed, in order to estimate the approximate integrated irradiation current necessary to yield about 100 bubbles, avoiding thus detectors saturation. This was made with a Berthold LB 123 UMo connected to the moderator detector LB641. The detector was placed at the entrance of the bunker at about 300 cm from Target 2 and a first trial irradiation was performed for 5 sec with a target current of $0.87 \mu\text{A}$ (integrated current $4.5 \mu\text{As}$). The neutron dose rate measured experimentally was $4.78 \mu\text{Sv/s}$. Considering approximately 1 mSv as the integrated dose on detectors corresponding to 100 bubbles, the integrated current on target estimated to obtain 1 mSv at measurement position (about 300 cm from target) was 182 μAs . Since all the measurement with bubble detectors were performed at a distance comprised between 45 and 100 cm, the integrated current estimated to reach an optimized number of bubble was comprised between 5 and 10 μAs . In table 5.1 specific irradiation conditions of each experiment are reported:

Table 5.1 Irradiation conditions

	<i>Target 1</i>	<i>Target 2</i>	<i>Target 5</i>	<i>Target 6</i>
Current on Target	0.75 μA	0.81 μA	0.82 μA	0.76 μA
Irradiation Time	7 sec	5 sec	10 sec	4 sec
Integrated Current	5.25 μAsec	5.25 μAsec	8.2 μAsec	3.04 μAsec
Distance of detectors from Target	1 m	0.45 m	1 m	0.75 cm

When not used, the dosimeters were stored in their original box inside a refrigerator (6°C) with bubble recompressed, before measurements they were equilibrate to 20°C letting them stand for a night exposed to suitable room air or for some hours in a temperature controlled water bath (figure 5.4).

*Figure 5.4 Bubble detectors in a controlled water bath of 20°C*

Since the bunker temperature was about 23°C the detectors that have been equilibrated to 20°C were placed in foam pipe insulation to ensure that the detector temperature remains at 20°C for the exposure time (figure 5.5).



Figure 5.5 Bubble detectors in foam pipe insulation

After each exposure the individual detectors were counted visually: each detector tube was placed in front of a uniform field of light and photographed with a camera (figure 5.6).

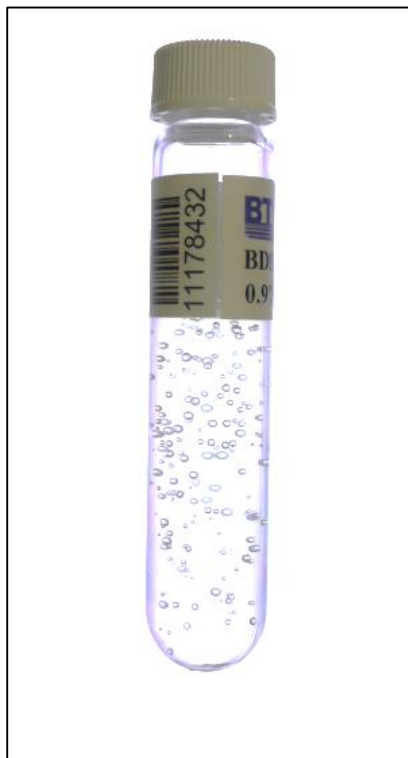


Figure 5.6 bubble detector after irradiation placed in front of a uniform field of light

Three digital pictures were taken, turning the detector at three different angles. Images were then transferred to a PC and the bubbles were counted interactively with the help of the cell counter plugin included in the ImageJ package. Also in this case, results were normalized to the total charge accumulated on the target in each irradiation test, expressed in μAh and compared with Monte Carlo simulations of neutron flux performed in the same conditions of irradiation. The USRTRACK score was used to assess the neutron spectra.

5.2.1 Unfolding procedure

Any kind of raw data obtained by different neutron spectrometry systems, such as activation foils, Bonner sphere and bubble detectors, must be processed through a deconvolution or unfolding procedure to obtain an estimation of the spectral distribution. The aim of these procedures is to solve the so called Fredholm-integral equation, that relates the differential neutron flux to the response function of the detection apparatus through the convolution integral (Seghour and Seghour, 2001):

$$N(E) = \int K(E, E')\Phi(E')dE' \quad \text{Equation 5.1}$$

In which $N(E)$ represents the data observed, $K(E, E')$ is the response function of the detection apparatus, and $\Phi(E')$ is the differential neutron flux at the neutron energy E . Unfolding the neutron spectrum from the data is complicated, and requires specialized techniques because the number of detector used (six in this case) is much less compared to the number of energy intervals in which the flux distribution is sought. Therefore, the system of equations represented by the discrete form of equation 5.1 becomes undetermined.

Over time, to perform a reliable unfolding as much as possible free from bias coming from the imposed computing system conditions, some dedicated codes have been developed such as BUNKI, LOHUI, GRAVEL, MAXED, BUMS, MITOM, FRUIT and BESPOKE (Danyluk, 2010, Bedogni et al., 2007, Tomas et al., 2004, Sweezy, Hertel and Veinot, 2002, Reginatto and Goldhagen, 1999, Matzke, 1994, Routti and Sandberg, 1985). These codes use different algorithms to unfold the spectrum from the response of single detectors (foil, sphere or bubble detector); some derive the final spectrum by perturbing an initial guess spectrum using mathematical or numerical methods; others model the initial spectrum using a set of physical parameters. In the codes, quality of the initial guess spectrum considered could affect the final solution.

In this work we started from the very basic “spectral stripping” supplied by the manufacturer. This method was then modified and an iterative procedure implemented.

The first step for neutron spectrum determination was bubble counting and the normalization of such values by dividing the number of bubbles (A_{ik}) by detector's specific sensitivity (S_{ik}) reported in table 5.3, where i is an index for the different detector thresholds and k is an index for the different detectors of the same threshold.

$$R_{ik} = \frac{A_{ik}}{S_{ik}} \quad \text{Equation 5.2}$$

Then the average values R_i for each of the six thresholds was calculated.

$$R_i = \frac{1}{N} \sum_{k=1}^N R_{ik} \quad \text{Equation 5.3}$$

Where N in our case is 3.

Detector response can be written as a function of neutron flux $\Phi(E)$ as follows

$$R_i = \int \sigma_i(E) \Phi(E) dE \quad \text{Equation 5.4}$$

Where R_i is the standard response of the i -th detector with a specific energy threshold and $\sigma_i(E)$ is the detector cross sections for neutrons (BTI Bubble Thecnology Industries, 2012).

The characterisation of the neutron flux density as a function of energy from the discrete sampling obtained with bubble detector measurements can be derived solving the following equation system

$$R_i \times f_i = \sum_{j=1}^N \sigma_i(E_j) \Phi(E_j), \quad i = 1, m \quad \text{Equation 5.5}$$

Where the continuous integral in Equation 6.4 has been rewritten in a discrete form over a set of N energy groups, m is the number of bubble detectors with different energy thresholds and f_i is a correction factors variable in the interval 0.7 - 1.3, introduced to take in to account a series of aspects specific to bubble detectors:

- The BDS algorithm assumes a somewhat non-natural “stepwise” trend of cross section values;
- only average cross sections of BDS are given for each energy “bin” (Table 4.1);
- detectors threshold and response are influenced by operational temperature that for technical reasons cannot be warm up to 20°C
- possible overlapping of two adjacent bins due to the combination of previous points.

However, the unfolded spectrum determined solving equation 5.5 in this simplistic way, will maintain the stepwise, non-continuous distribution deriving from the assumptions made on the cross sections.

Introducing some “a priori” knowledge into the model, can help to obtain a more realistic, continuous distribution. According to nuclear evaporation theory, that explains the physical phenomena of neutrons production at the lower energy range typical of biomedical cyclotrons, the energy distribution of neutrons can be described by a maxwellian distribution function of the form:

$$n(E)dE = const * E * e^{\left(-\frac{E}{\tau}\right)} \quad \text{Equation 5.6}$$

Where τ is a so-called nuclear temperature, has the dimensions of energy and represents the most probable energy of the neutrons emitted (Weisskopf, V., 1937, IAEA, 1988). However, in our measurements the influence of the target material in partially degrading the neutron spectra should be taken into account, as well as the variations in the response of the detector as a function of the temperature. The latter, in particular, shows as a modifier in the scale of Energy. To take into account these factors, the equations has been slightly modified as follows:

$$n(E)dE = A + const * (E + b) * e^{\left(-\frac{(E+b)}{\tau}\right)} \quad \text{Equation 5.7}$$

Where A is a scale factor and b is the energy modifier.

To improve the deconvolution, results obtained form Eq. 5.5 were then iteratively fitted according to a maxwellian function. All the parameters A , b , τ and the corrections factor f_i were determined using an iterative process to minimize the root mean square deviation between experimental values and theoretical maxwellian distribution. The initial guess maxwellian distribution can be evaluated analytically, with the adoption of proper values for the parameters in Eq. 5.7 (IAEA 1988), or be derived by other means, like a preliminary Monte Carlo simulation.

Given the availability of the Fluka results, the latter was the preferred approach in this work.

A first guess value of 1, corresponding to BTI unfolding procedure was used for the correction factors f_i of Eq. 5.5.

The uncertainties for the unfolded neutron fluence were calculated on the basis of the counts from each detector, according to the method supplied by the manufacturer (BTI Bubble Thecnology Industries, 2012). The counts in the detectors are expected to follow a Poisson distribution and have an uncertainty equal to the square root of the number of counts observed in the detector. Each bin in the unfolding spectrum may have contributions to its uncertainty that arise from uncertainties from all of the individual bubble counts. The determination of the uncertainty of each spectral bin is composed of several steps. First, the bubble counts are unfolded to make the spectrum, the counts for a single detector sensitivity are artificially incremented by one standard deviation, and then the unfolding is repeated to make an artificial spectrum; the

difference between these two unfolded spectra is calculated. For each bin this yields the uncertainty in the spectrum due to the count from one bubble detector. This can be repeated for all detector sensitivities. Because the counts are statistically independent, so are the spectral differences calculated. For this reasons the total contribution to each bin is the sum in quadrature of the spectral differences.

5.3 Non-destructive activation assessment

As long as an accelerator is operational, experimental measurements for material activation assessment are problematic mostly because of the impossibility of core drilling in some facilities. Concerning direct measurements inside the bunker, instead, critical issues are the limited access time, the high radioactive background due to activated material of the cyclotron itself and the presence of short-lived radionuclides with an activity concentration significantly higher than that of the long-lived radionuclides.

In this part of the work we developed a non-destructive in situ measurement methodology for a preliminary activation assessment of a cyclotron bunker, avoiding the need for expensive and “invasive” core drilling. The detector chosen for this purpose is the Kromek GR1 described in subsection 4.2.2. The reduced size, light weight and unnecessary of cooling of this detector, and its energy resolution (intermediate between those of NaI(Tl) and HPGe detectors), make this type of devices ideal for in-situ measurements. On the other hand, the critical aspect of this kind of measurements in non-standard geometry, is the efficiency calibration of the detector: the unavailability of a reference source in the complex geometry “in the field”, rules out an accurate experimental calibration.

Once again, Monte Carlo methods offer a solution for problems in complex, non-standard geometries and the efficiency calibration was performed developing an appropriate model (Zagni, et al. 2014).

Experimental measurements were conducted inside the Bunker of the GE PETtrace cyclotron installed at the S. Orsola-Malpighi Hospital in Bologna during cyclotron maintenance. The measurements setup is shown in Figure 5.7.

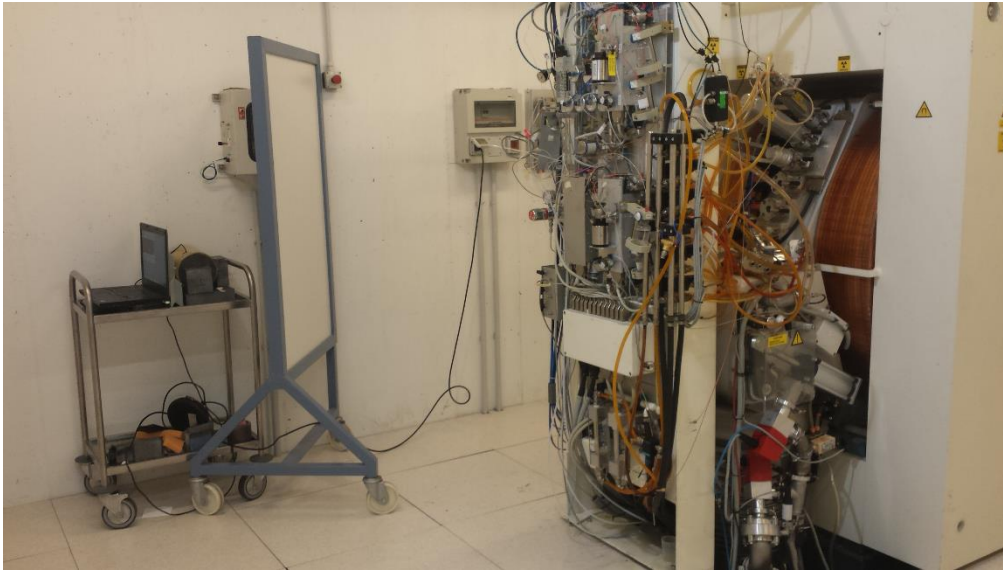


Figure 5.7 Experimental measurement setup

The detector was placed in contact with the bunker wall inside a 5 cm thick cylindrical lead shielding. To minimize the background due to the active components of the cyclotron, a mobile lead barrier, 5 cm thick, was placed between the cyclotron and the measurement position. Measurements were conducted inside the bunker in three different positions (figure 5.8), starting at different times from the end of bombardment and with different acquisition times. The spectra were visualized with the K-Spect software.

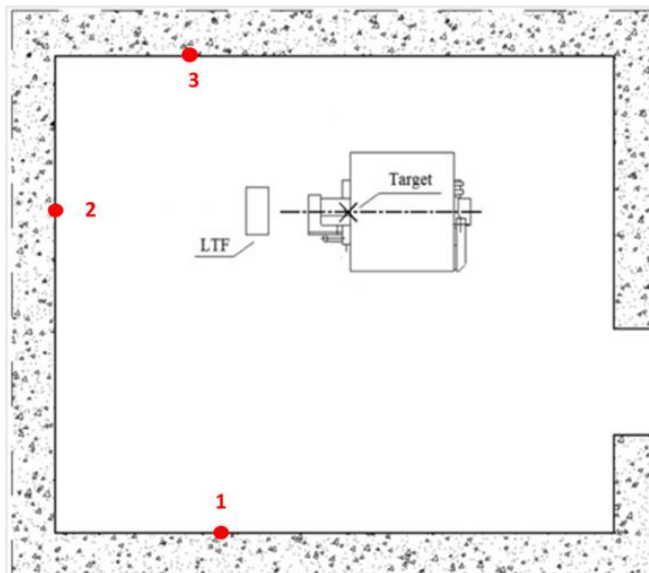


Figure 5.8 measurement positions

In Table 5.1 acquisitions specifications are reported

Table 5.1 Acquisitions specifications

Positions	Acquisition time	Average dead time	Time after last irradiation	Time after facility installation
1	15 h	0.03 %	130 h	14 years
2	21 h	0.02 %	73 h	14 years
3	24 h	0.04 %	130 h	14 years

5.3.1 Monte Carlo model of the detector

Geometry of the detector and particle physics were modelled using FLUKA. The set of default parameters chosen for this work is EM-CASCADE producing an accurate modelling of the phenomena related to the interaction of photons with matter, such as Compton scattering, photoelectric absorption, electron and positron scattering ionization, pair production and bremsstrahlung radiation (Fasso, A. et al. 2011). The energy thresholds for electron and photon production and transport was set at 1 keV. The detector was accurately modelled on the basis of the manufacturer’s specifications (Kromek Personal communications) using the FLUKA graphical interface Flair 2.2 (Vlachoudis, V., 2009) (Figure 5.9).

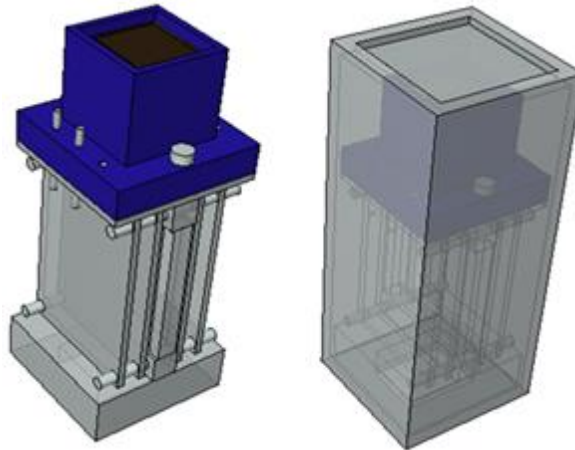


Figure 5.9 Kromek GRI MC model

The data supplied by the device producer were supplemented with information coming from a microCT scan of the detector. To score the photopeak efficiency the “DETECT” card was used, this card gives the energy deposited in one region by one primary particle and its descendants (Fasso, A. et al., 2011).

5.3.2 *Experimental validation of the model*

The MC model was validated simulating a set of certified standard sources available in our laboratories and comparing the simulated results with experimental measurements in terms of photopeak efficiency. The aim was to verify that the model was able to reproduce accurately the response of the detector in the 100 keV-2000 keV energy range and in different standard geometries.

The reference sources used, all manufactured by accredited Standardization Laboratories, are reported below:

- A multi-radionuclide point source (Areva CERCA LEA, Pierrelatte Cedex, France) containing ^{57}Co , ^{139}Ce , ^{51}Cr , ^{113}Sn , ^{85}Sr , ^{137}Cs , ^{88}Y , ^{60}Co .
- A multi-radionuclide solution in a 5 cm³ vial (Areva CERCA LEA, Pierrelatte Cedex, France) containing ^{57}Co , ^{137}Cs , ^{60}Co .
- A ^{133}Ba flood source (CEA-ORIS (DAMRI), Saclay, France), with an active diameter of 450 mm and 6 mm thickness.

The first two reference sources were placed 6 cm away from detector and the measurements were conducted inside a 5 cm thick lead shielding; a plastic sample holder was used to secure a reproducible acquisition geometry. For measurements with the flood source the detector was placed inside a 1.5 cm lead shielding, at a distance of 1.5 cm from the source.

5.3.3 *Efficiency calibration*

Once the FLUKA model was validated, it was used for efficiency calibration for wall activation assessment. The geometry model for efficiency calibration included the 5 cm lead shielding setup and the concrete walls.

The first step was the evaluation of the field of view (FOV) of the detector. Source dimensions were widened until the increase in source size no longer produced an increase in the detector response.

The bunker wall was therefore modelled as a concrete cylinder of appropriate dimensions as above, uniformly activated using photons as primary particles at different energies: 121 keV, 165 keV, 320 keV, 344 keV, 391 keV, 514 keV, 604 keV, 661 keV, 795 keV, 834 keV, 898 keV, 1173 keV, 1332 keV, 1368 keV, 1408 keV, 1810 keV, 1836 keV, 2113 keV, 2754 keV. High statistic simulations (10^9 primary particles) were run on a conventional intel i7 PC with different simulation times depending on the photon energy (typically <24h). The efficiency calibration curve was determined by Ordinary Least Square Regression (Debertin, K., et al., 1988).

5.3.4 *Experimental validation of the model*

The ratio between photopeak efficiencies obtained in simulations and in experimental measurements for point source, 5 cm³ vial and flood source acquisition geometries are reported in Table 5.2, 5.3, 5.4 respectively.

Table 5.2 Ratio between photopeak efficiency obtained in simulations and in experimental measurements for multi-radionuclide point source

Nuclide	Energy (keV)	Experimental measurements		FLUKA		FLUKA/Experimental
		Efficiency	Uncertainty (%)	Efficiency	Uncertainty (%)	
⁵⁷ Co	122	1.21E-03	1.6	1.21E-03	0.9	1.00±0.01
¹³⁹ Ce	166	1.11E-03	1.6	1.10E-03	1.0	0.99±0.02
⁵¹ Cr	320	3.94E-04	1.8	3.91E-04	1.6	0.99±0.03
¹¹³ Sn	392	2.56E-04	1.6	2.59E-04	2.2	1.01±0.04
⁸⁵ Sr	514	1.67E-04	1.7	1.57E-04	2.8	0.94±0.05
¹³⁷ Cs	662	9.89E-05	1.6	9.91E-05	3.2	1.00±0.05
⁸⁸ Y	898	5.50E-05	1.8	5.83E-05	4.6	1.06±0.09
⁶⁰ Co	1173	3.31E-05	1.8	3.36E-05	1.7	1.02±0.03
⁶⁰ Co	1332	2.92E-05	1.8	2.97E-05	5.8	1.02±0.11
⁸⁸ Y	1836	1.57E-05	2.2	1.59E-05	6.8	1.01±0.15

Table 5.3 Ratio between photopeak efficiency obtained in simulations and in experimental measurements for multi-radionuclide 5 cm³ Vial source

Nuclide	Energy (keV)	Experimental measurements		FLUKA		FLUKA/Experimental
		Efficiency	Uncertainty (%)	Efficiency	Uncertainty (%)	
⁵⁷ Co	122	7.67E-04	1.9	7.35E-04	1.2	0.96±0.02
¹³⁷ Cs	662	6.09E-05	1.6	6.33E-05	4.0	1.04±0.07
⁶⁰ Co	1173	2.42E-05	1.8	2.41E-05	2.0	1.00±0.04
⁶⁰ Co	1332	1.99E-05	1.9	2.03E-05	2.2	1.02±0.04

Table 5.4 Ratio between photopeak efficiency obtained in simulations and in experimental measurements for ¹¹³Ba flood source

Energy (keV)	Experimental measurements		FLUKA		FLUKA/Experimental
	Efficiency	Uncertainty (%)	Efficiency	Uncertainty (%)	
276	5,40E-05	4.1	5.63E-05	1.3	1.04±0.06
303	4,76E-05	4.0	4.95E-05	1.4	1.04±0.06
356	3,81E-05	1.6	3.80E-05	1.6	1.00±0.02
384	3,31E-05	1.7	3.32E-05	1.8	1.00±0.03

The results for all the reference sources tested are consistent within uncertainties, with 5% being the maximum discrepancy. The agreement between simulated and experimental results reflects a good modelling of both detector and particle physics.

5.3.5 Efficiency calibration

Modelling of the bunker wall measurement setup showed that the cylindrical volume of 30 cm of radius by 30 cm depth in front of the detector determined alone more than 99% of detector response. To define the efficiency calibration curve the source was therefore modelled as a concrete cylinder of 30 cm of radius and 30 cm depth, in keeping with this finding.

Photopeak efficiency calculated via Monte Carlo simulation for in-situ measurements are reported in Table 5.5.

Table 5.5 Photopeak efficiency for activation assessment

Energy (keV)	Efficiency	Uncertainty (%)
121	7.89E-06	1.1
165	8.11E-06	1.1
320	3.99E-06	1.6
344	3.57E-06	1.7
391	2.94E-06	1.8
514	2.04E-06	2.2
604	1.64E-06	2.5
661	1.44E-06	2.6
795	1.17E-06	3.0
834	1.07E-06	3.0
846	1.08E-06	3.0
898	1.01E-06	3.1
1173	7.46E-07	5.2
1332	6.52E-07	5.5
1368	5.91E-07	4.1
1408	5.67E-07	4.2
1810	4.43E-07	4.8
1836	4.33E-07	4.8
2113	3.42E-07	5.4
2754	2.63E-07	6.2

The efficiency curve for wall activation assessment was calculated (Figure 5.10).

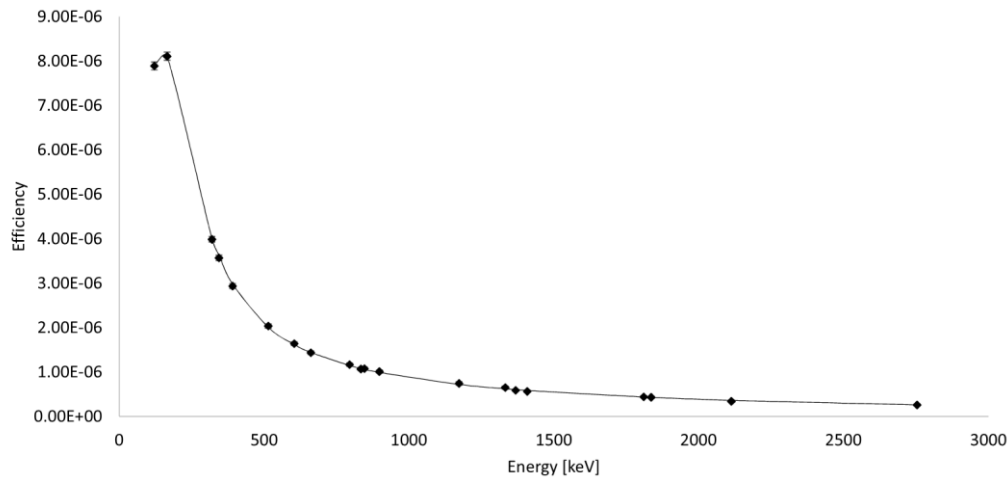


Figure 5.10 Efficiency calibration curve. Note that the error bar (see Table 5.5) are smaller than the size of the points.

A dual logarithmic polynomial efficiency curve was used. Up to 320 keV, the calibration curve calculated is

$$\ln(\varepsilon) = -41.218 + 11.837 \cdot \ln(E) - 1.187 \cdot [\ln(E)]^2 \quad \text{Equation 5.8}$$

Over 320 keV

$$\ln(\varepsilon) = 23.549 - 13.461 \cdot \ln(E) + 1.709 \cdot [\ln(E)]^2 - 0.079 \cdot [\ln(E)]^3 \quad \text{Equation 5.9}$$

where ε is the photopeak efficiency and E is the energy of interest.

Once the definition of efficiency calibration curve was determined, it was possible to evaluate activity concentrations quantitatively. (Vichi, S. et al., 2016)

5.4 Bunker core drilling activation assessment using an HPGe detector

During the maintenance of CYCLONE 18/9 in Bern it was possible to perform three core drilling on the bunker walls of the cyclotron (Figure 5.11).

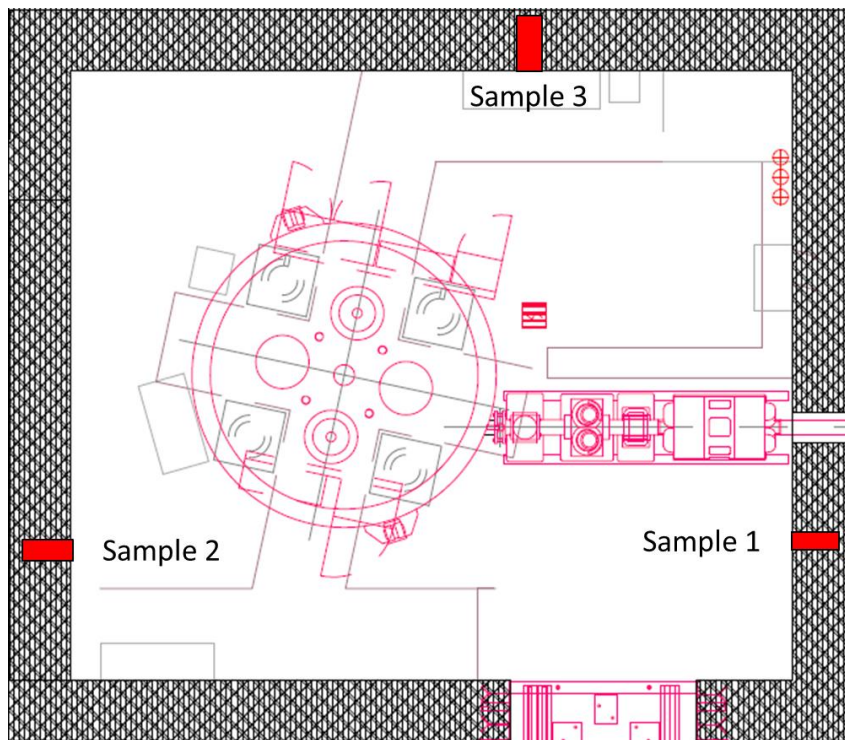


Figure 5.11 core drilling position inside the bunker



Figure 5.12 Core drilling



Figure 5.13 concrete sample

The concrete cores were 10 cm deep and 5 cm in diameter. Each core was then measured in gamma spectroscopy with the HPGe detector described in subsection 4.2.1 for activation assessment. Because the acquisition was in non-standard geometry it was not possible to perform an experimental efficiency calibration of the detector, for this reason the calibration of the detector was performed using the well-known and validated LabSOCS code, an optional package of the Genie 2000 suite (Bronson, 2003; Venkataraman, et al., 2005). This software performs mathematical efficiency calibration after the definition of sample geometry through a Geometry Composer present in Genie 2000. To this aim the concrete samples were modeled reproducing in each case the specific acquisition geometry (figure 5.14) and the correspondent efficiency curve evaluated (figure 5.15).



Figure 5.14 LabSOCS concrete sample geometry

Spectra were analyzed using the spectroscopy software Genie™ 2000 (Camberra, Meriden, USA), dedicated analysis sequences and nuclide libraries were created to this aim. The method implemented in the software accounts for propagation of the uncertainties in the calibration of the reference source (1-2% at 1 sigma level, depending on the peak in the mixture), in the tabulated yield (typically <1%), in the net peak area (<1% for calibration peaks) and in the interpolation of the efficiency values, the latter being evaluated from the covariance matrix of the fitting of the efficiency curve (typically <3%). The calibration uncertainty is founded to be about 4-5% at 1 sigma level.

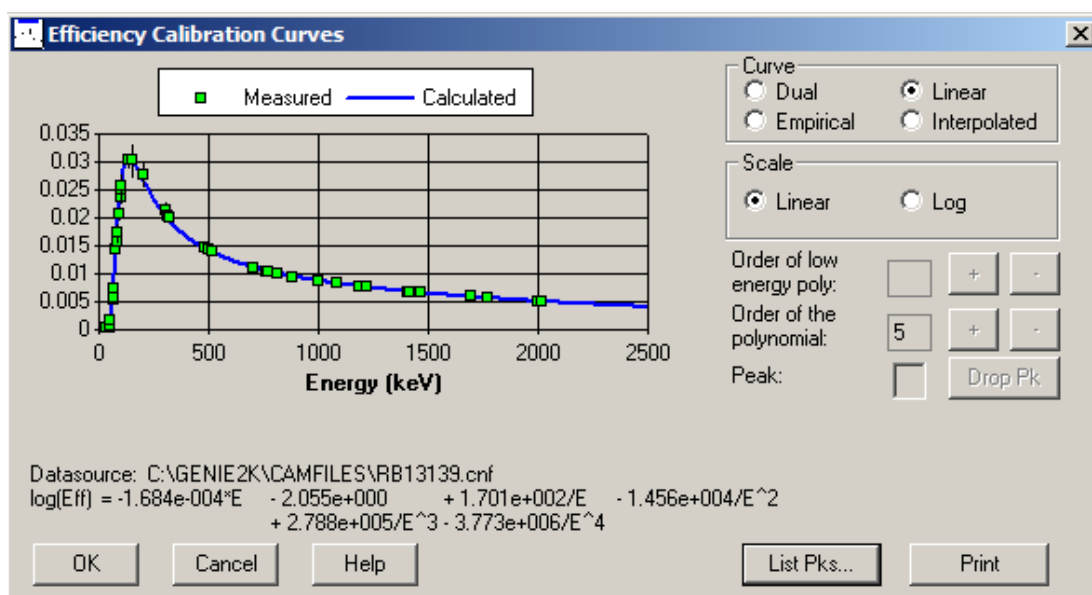


Figure 5.15 Efficiency calibration curve obtained with LabSOCS

Chapter 6

Results

In the present chapter the most significant results obtained in this work will be presented. First of all results of experimental measurements will be reported and compared with corresponding results obtained with FLUKA to evaluate the accuracy of the MC models implemented in terms of neutron fluence and residual activation. Once reliability of MC results was assessed the potentiality of a Monte Carlo approach in activation assessment will be pointed out.

6.1 Assessment of the neutron dose field around the PETtrace of S.Orsola-Malpighi Hospital in Bologna

Figure 6.1 shows the neutron ambient dose equivalent distribution assessed using FLUKA on the basis of the model described in chapter 3.1 and represented through a Cartesian mesh. For comparison with experimental measurements in positions 1-12 data were taken from the binning (5 cm x 5 cm x 5 cm) of the Cartesian mesh as calculated by FLUKA at the same coordinates as the real dosimeters.

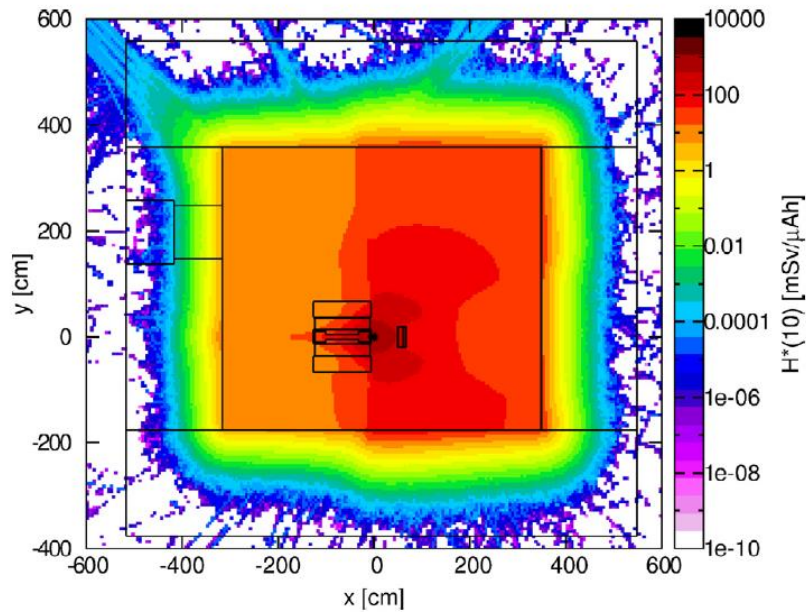


Figure 6.1 FLUKA assessment of the neutron ambient dose equivalent $H^(10)$ over the whole cyclotron vault with a Cartesian mesh*

The results of the experimental measurement performed in this work and of FLUKA MC simulations are reported in table 6.1. As stated before, data obtained using the neutron rem-counter were corrected for the dead time of the instrument. While the active detectors allowed the direct reading of the dose, passive dosimeters needed to be read, in our case, by an external laboratory. To compare different irradiations conditions, results were normalized to the total charge accumulated on the target in each irradiation test, expressed in $\mu\text{A}\cdot\text{h}$. In addition, results of the simulations were compared with previous measurements conducted by our group and published by Gallerani et al. (Gallerani, R. et al., 2008) and re-evaluated in the present work. To allow a more accurate comparison with MC simulations, data from Gallerani et al. were updated taking into account also some unpublished corrections concerning the normalization of the data to the integrated charge and the contribution of thermal neutrons.

Table 6.1 Comparison of neutron ambient dose equivalent $H^(10)$ obtained from Monte Carlo simulations and experimental measurements. Data from Gallerani et al. were re-evaluated and updated to take into account the contribution of thermal neutrons.*

Position	Gallerani et al. (updated)	Dose \pm uncertainty [mSv/ μ Ah]			
		FHT-752	CR39	FLUKA (cutoff 10^{-14} GeV)	FLUKA (cutoff 200 keV)
1	270 \pm 140	330 \pm 130	380 \pm 200	300 \pm 5	276 \pm 5
2	350 \pm 190	430 \pm 170	310 \pm 170	459 \pm 6	442 \pm 6
3	45 \pm 24	90 \pm 40	60 \pm 30	96 \pm 3	87.1 \pm 2.6
4	330 \pm 180	420 \pm 170	340 \pm 180	475 \pm 6	461 \pm 6
5	290 \pm 150	330 \pm 130	340 \pm 180	311 \pm 5	309 \pm 5
6	4.6 \pm 2.8	27 \pm 11	6 \pm 5	18.4 \pm 1.0	12.2 \pm 1.0
7	30 \pm 16	32 \pm 13	19 \pm 14	34.7 \pm 1.6	27.2 \pm 1.5
8	2.4 \pm 1.7	23 \pm 9	6 \pm 5	18.5 \pm 1.0	12.8 \pm 1.0
9	28 \pm 15	55 \pm 22	31 \pm 19	54.1 \pm 2.0	47.5 \pm 1.9
10	8 \pm 5	45 \pm 18	38 \pm 22	42.6 \pm 1.6	37.9 \pm 1.7
11	120 \pm 60	190 \pm 80	130 \pm 70	156 \pm 3	153 \pm 4
12	11 \pm 6	22 \pm 9	50 \pm 29	25.6 \pm 1.3	20.8 \pm 1.3

As shown in Table 6.1, the uncertainty associated with the CR39 dosimeters is quite high: as reported in the technical specifications of the manufacturer, the total uncertainty is a function of the dose measured, in the range 54-72%. This is substantially due to the significant dependence on the energy response of the detector in an intense and complex radiation field, such as the one inside the cyclotron vault during an irradiation; besides, the spectrum used for the calibration differed from the one inside the cyclotron vault during an irradiation; furthermore, the spectrum used for the calibration differed from the one the dosimeters were exposed to. On the other hand, the use of an electronic instrument like the rem-counter allows to improve the counting statistics thanks to the greater dimensions of the probe, compared with the CR39, even if the correct positioning might be affected by uncertainty. An assessment of the total uncertainty in the measurements acquired with the rem-meter was made by a quadratic propagation of the uncertainty on the calibration factor (5%), on the counting frequency (5%), on the correction for the dead time (10%), on the pressure of the BF₃ gas (15%), on the integrated charge (5%) on the energy (25%) and angular response (25%). The total uncertainty resulted of the order of 40%.

The ratios between FLUKA and the measurements obtained using the FHT-725, the CR39 and the data from the previous measurement campaign were calculated for each position.

The comparison of the different data sets are reported in Figure 6.2 and 6.3.

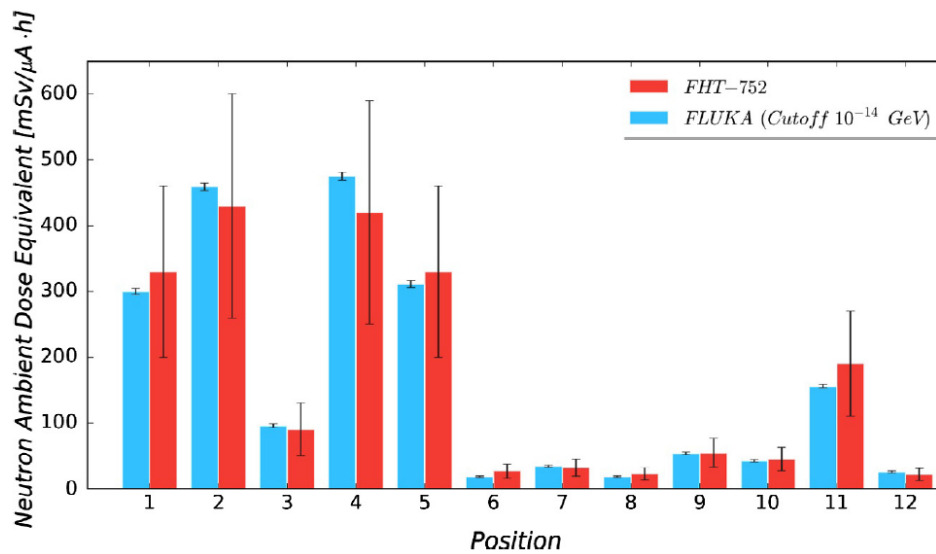


Figure 6.2 Comparison of the FLUKA simulation (neutron transport cutoff of 10^{-14} GeV) and the measurements performed using the neutron rem-counter in each position considered in this work.

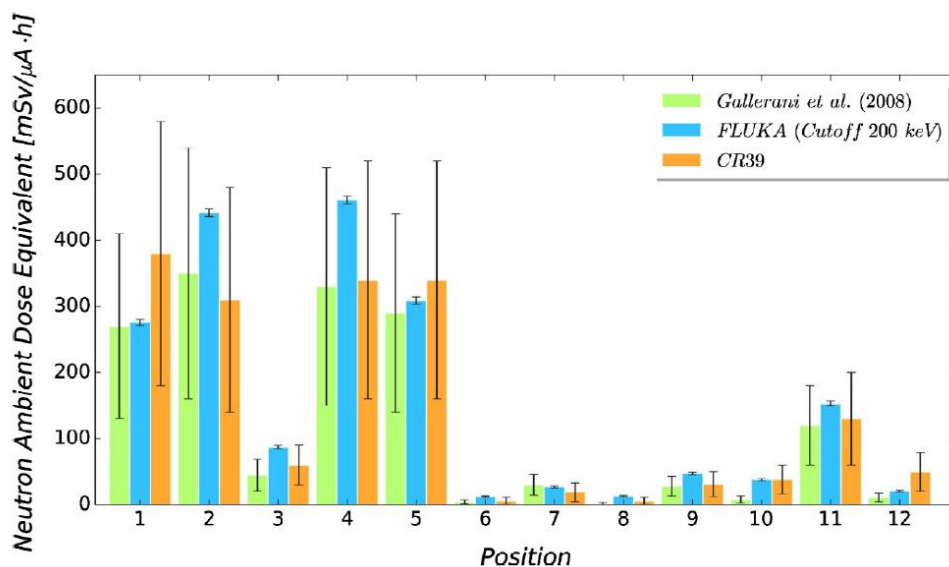


Figure 6.3 Comparison of the FLUKA simulation (neutron transport cutoff of 200 keV) and the measurements performed using the neutron rem-counter in each position considered in this work.

As can be seen in figure 6.2, the results of FLUKA simulations are in agreement with experimental rem-meter measurements, within uncertainties, for all the position. We consider this as a non-trivial achievement; even a quick search in the literature will show that agreement between MC simulations and experimental results within a factor of 2 is frequently the best result attainable. The possibility of performing repeated

measurements in the facility of Bologna and the extensive work dedicated to improve continuously the model of the cyclotron explains the quality of the results presented in this work. With regard to the contribution of fast neutrons only (figure 6.3), FLUKA simulations with a neutron transport threshold set at 200 keV are in agreement within uncertainties with the two available set of measurements made with CR39 detectors in 10 out of 12 measurement positions, the exceptions being positions 6 and 8.

It has to be noted that these positions are in the rear corners of the magnet of the cyclotron. The doses expected from fast neutrons in these positions are the lowest in our experimental setup, and are close to the minimum detectable dose of the CR39 dosimeters. Due to the strong angular dependency of the CR39 response, small misplacement and uncertain in the orientation may involve a significant influence in the results. The total neutron dose is modelled accurately as shown by the comparison between FLUKA total dose and the rem-counter measurements.

Considering data in table 6.1, it is important to note that the dimensions of the FHT-752 make this detector less prone, compared to small TLD or CR39 dosimeters, to small differences in the positioning of the device. It is also important to underline once again that CR39 dosimeters allow measuring only neutrons with an energy above 200 keV; taking into account the contribution from thermal neutrons the agreement between FLUKA and the experimental measurements would therefore improve. On the other hand, data from Gallerani et al., even if updated to take into account the contribution from thermal neutrons, suffer in our opinion from some inaccuracy in the positioning of the dosimeters in that first series of measurements inside the bunker at our installation; these most likely affect the comparison against FLUKA simulations. Considering all the factors listed above and small differences in the modelling of the cyclotron components, FLUKA simulation provided an excellent agreement with the experimental measurements and allowed an accurate estimation of the neutron radiation dose field. Furthermore, from the radiation protection point of view the slightly conservative estimates obtained from FLUKA simulation grant a safe approach in the design of shielding. (Infantino, A. et al., 2016)

6.2 Assessment of the neutron spectrum inside the bunker of CYCLONE 18/9 in Bern with bubble detectors

In the following subsection results of assessment of neutron spectra during the production of ^{18}F inside the bunker of Inselspital in Bern will be presented. For each experiment the response of bubble detectors is reported first; then results from the unfolding procedure will be presented in terms of neutron flux and compared with the corresponding results obtained using Fluka, and finally the maxwellian function obtained via the iterative procedure described in chapter 5.2.1 is reported.

6.2.1 Neutron spectrum generated irradiating Target 1

The responses of bubble detectors during irradiations of target 1 are shown in table 6.2: results before and after the iterative process described in chapter 5.2.1 are reported with the respective correction factors.

Table 6.2 Bubble detectors response obtained during irradiation of target 1

<i>Detector</i>	<i>Standard Response R_i</i>	<i>Uncertainty (%)</i>	<i>Correction factor f_i</i>	<i>$R_i \times f_i$</i>	<i>Uncertainty y (%)</i>
BDS10	21.06	3.2	0.72	15.20	3.2
BDS100	15.03	3.8	0.97	14.55	3.8
BDS600	12.29	4.2	0.70	8.60	4.2
BDS1000	4.76	6.5	0.96	4.60	6.5
BDS2500	3.34	7.4	0.95	3.16	7.4
BDS10000	0.28	40.8	1.30	0.36	40.8

In table 6.3 neutron fluence as a function of energy, estimated starting from bubble detectors row data through the unfolding procedure described in chapter 5.2.1, is reported and compared with FLUKA simulations results.

Table 6.3 Comparison between the neutron fluence measured experimentally and the correspondent neutron fluence estimated using Fluka during irradiation of target 1

<i>Energy Range</i>	<i>Fluence N_i</i>			
	<i>Bubble detectors</i>	<i>Uncertainty (%)</i>	<i>Fluka</i>	<i>Uncertainty (%)</i>
0.01-0.1	1.82E+05	104	8.55E+04	1.3
0.1-0.6	2.10E+05	31	2.74E+05	1.2
0.6-1.0	6.93E+04	47	7.35E+04	1.3
1.0-2.5	1.05E+05	27	1.33E+05	1.7
2.5-10	7.62E+04	35	8.38E+04	2.4
10-20	8.34E+03	31	2.00E+03	9.7

The uncertainties reported for the FLUKA simulations here are only the random deviations, as calculated by the code; non-random “systematic” errors are not included in the model. This explains the evident difference in the entity of these uncertainties compared to those of experimental measurements.

Figure 6.4 reports the same results in graphical form:

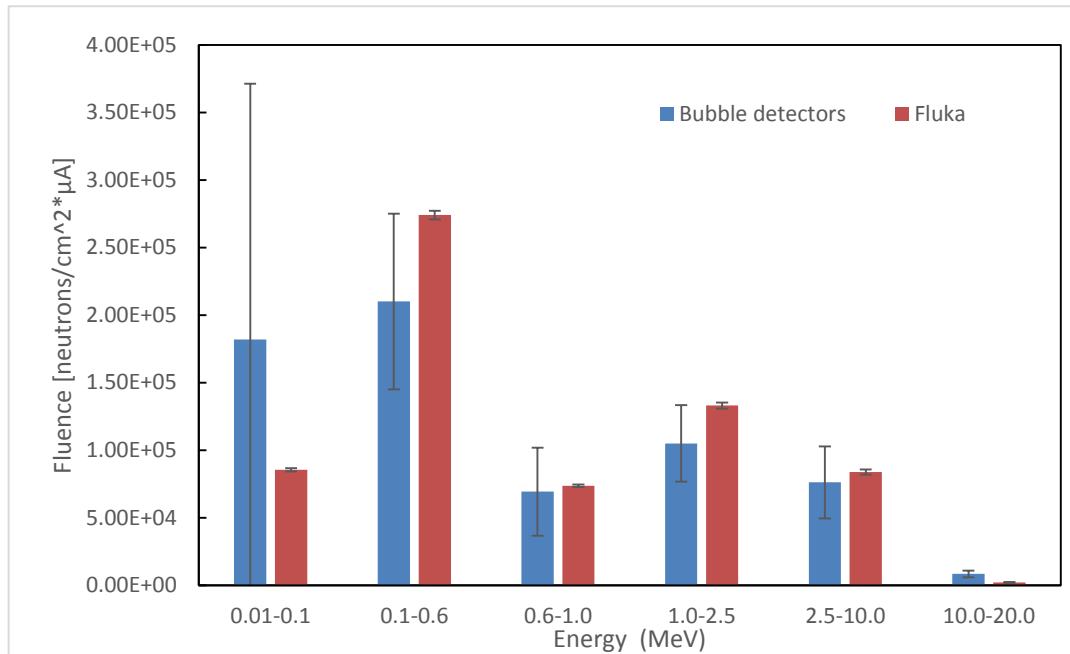


Figure 6.4 Comparison between neutron fluence measured with bubble detectors and the correspondent neutron fluence estimated using Fluka during irradiation of target 1

As can be seen, there is agreement between the results of the simulations with the experimental data, within the uncertainties. Clearly, spectra measurements with relatively inexpensive bubble detectors are not of high accuracy, but this reflects a situation that is inherent to many neutron spectrometry systems. It has also to be noticed that the unfolding procedure suffers from error accumulation, that leads to large errors in the lower energy region of the spectrum.

In equation 6.1 the maxwellian function that represents data in a more realistic form is reported and graphically compared with the correspondent neutron spectrum obtained with FLUKA (figure 6.5).

$$n(E)dE = 5.89 \cdot 10^{-4} + 9.86 \cdot 10^{+5} * (E + 2.17 \cdot 10^{-1}) * e^{\left(\frac{-(E+2.17 \cdot 10^{-1})}{2.17 \cdot 10^{-1}}\right)} \quad \text{Equation 6.1}$$

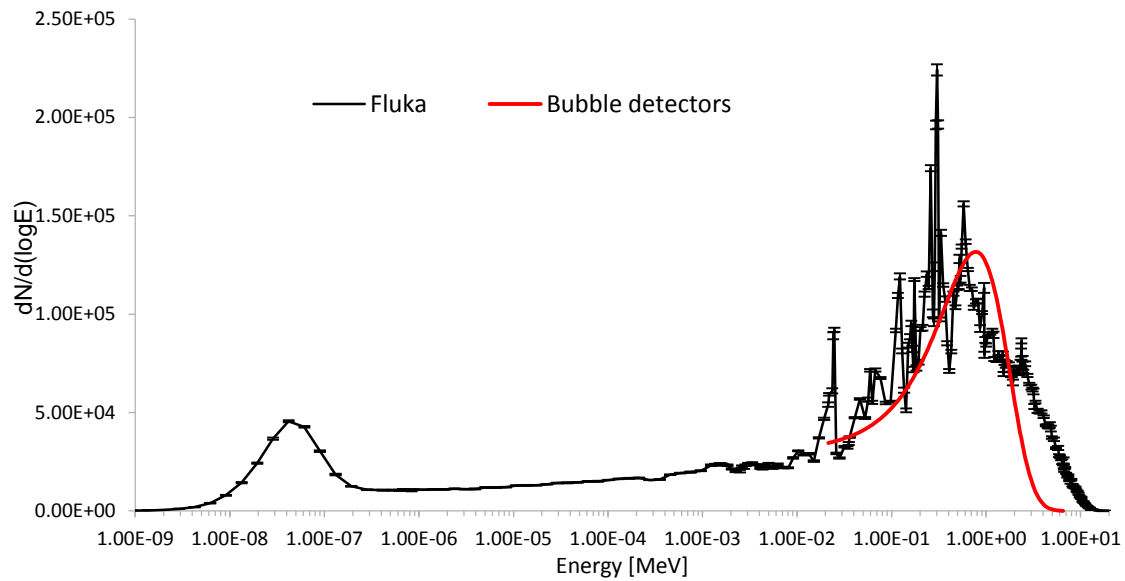


Figure 6.5 comparison of neutron spectra obtained using Fluka with the correspondent neutron spectrum obtained with bubble detectors during irradiation of target 1. Bubble detectors spectrum (equation 6.1) was obtained using the unfolding procedures described in chapter 5.2.1

As it can be seen there is a good agreement between FLUKA results and experimental measurements considering, as previously said, that bubble dosimeters measurements are not high precision measurements for different reasons ranging from temperature sensitiveness to uncertainty in visual counting and errors propagation in the unfolding procedure. In both cases neutron spectra shows a peak at around 1 MeV with a large tail towards lower values and with a maximum energy of about 10 MeV. The energy range of bubble dosimeters with the lowest threshold at 10 keV make these detectors completely insensitive to thermal neutrons; for this reason, as can be seen from figure 6.5, the spectrum derived from bubble detectors does not comprise the thermal region.

6.2.2 Neutron spectrum generated irradiating Target 2

The responses of bubble detectors during irradiations of target 2 are shown in table 6.4, results before and after the iterative process described in chapter 5.2.1 are reported.

Table 6.4 Bubble detectors response obtained during irradiation of target 2

<i>Detector</i>	<i>Standard Response R_i</i>	<i>Uncertainty (%)</i>	<i>Correction factor f_i</i>	<i>$R_i \times f_i$</i>	<i>Uncertainty (%)</i>
BDS10	37.2	2.3	0.8	31.4	2.3
BDS100	34.7	2.4	0.8	31.1	2.4
BDS600	30.6	2.6	0.7	21.4	2.6
BDS1000	15.2	3.5	0.7	11.9	3.5
BDS2500	11.5	3.8	0.7	8.7	3.8
BDS10000	0.8	22.9	2.1	1.7	22.9

In table 6.5 neutron fluence as a function of energy, estimated starting from bubble detectors row data through the unfolding procedure described in chapter 5.2.1 is reported and compared with FLUKA simulations results.

Table 6.5 Comparison between the neutron fluence measured experimentally and the correspondent neutron fluence estimated using Fluka during irradiation of target 2

<i>Energy Range</i>	<i>Fluence N_i</i>			
	<i>Bubble detectors</i>	<i>Uncertainty (%)</i>	<i>Fluka</i>	<i>Uncertainty (%)</i>
0.01-0.1	2.46E+05	149	1.33E+05	1.0
0.1-0.6	3.56E+05	39	4.90E+05	0.8
0.6-1.0	1.48E+05	98	1.43E+05	0.9
1.0-2.5	2.63E+05	31	2.74E+05	1.1
2.5-10	1.75E+05	15	1.83E+05	1.6
10-20	3.98E+04	15	4.35E+03	6.1

Figure 6.6 reports the same results in graphical form:

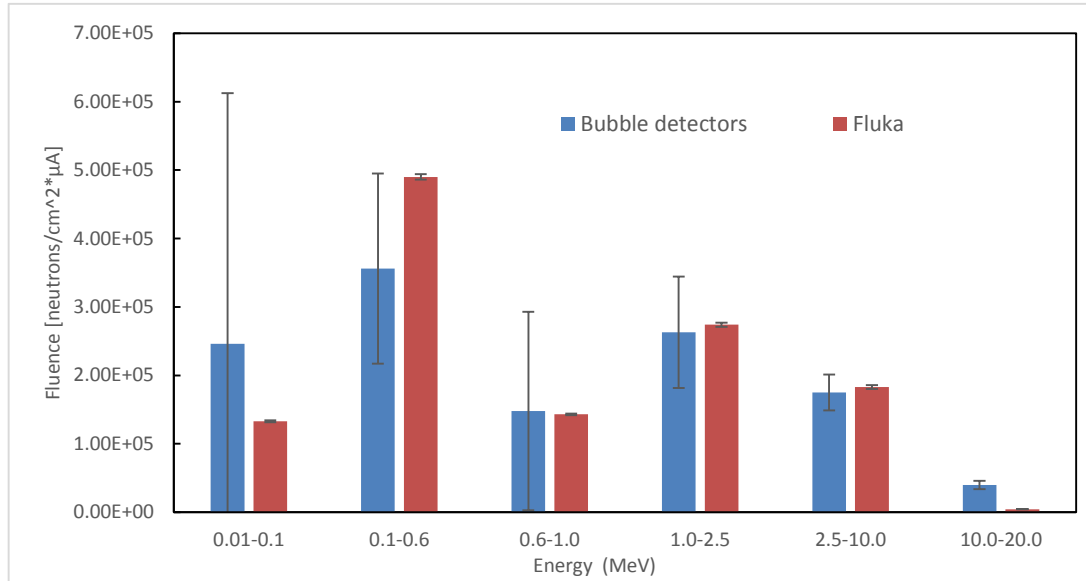


Figure 6.6 Comparison between neutron fluence measured with bubble detectors and the correspondent neutron fluence estimated using Fluka during irradiation of target 2

Also in this case the agreement between FLUKA and experimental results is within the uncertainties for all energy ranges, except for 10-20 MeV region. It has to be considered that in a 18 MeV proton accelerator, neutrons generated in the $^{18}\text{O}(p,n)^{18}\text{F}$ reaction with an energy comprised between 10 and 20 MeV are significantly less than neutrons with lower energies (as can be seen from figure 3.41). For this reason the number of bubbles generated in the same irradiation conditions and consequently the measurements accuracy was lower in 10-20 MeV region if compared with others energy ranges.

In equation 6.2 the maxwellian function which represent data in a more realistic form, obtained via the iterative procedure already mentioned is reported and compared graphically with the correspondent neutron spectrum obtained with FLUKA (figure 6.7).

$$n(E)dE = 4.51 \cdot 10^{-2} + 1.02 \cdot 10^{+6} * (E + 4.03 \cdot 10^{-1}) * e^{\left(\frac{-(E+4.03 \cdot 10^{-1})}{7.14 \cdot 10^{-1}}\right)}$$

Equation 6.2

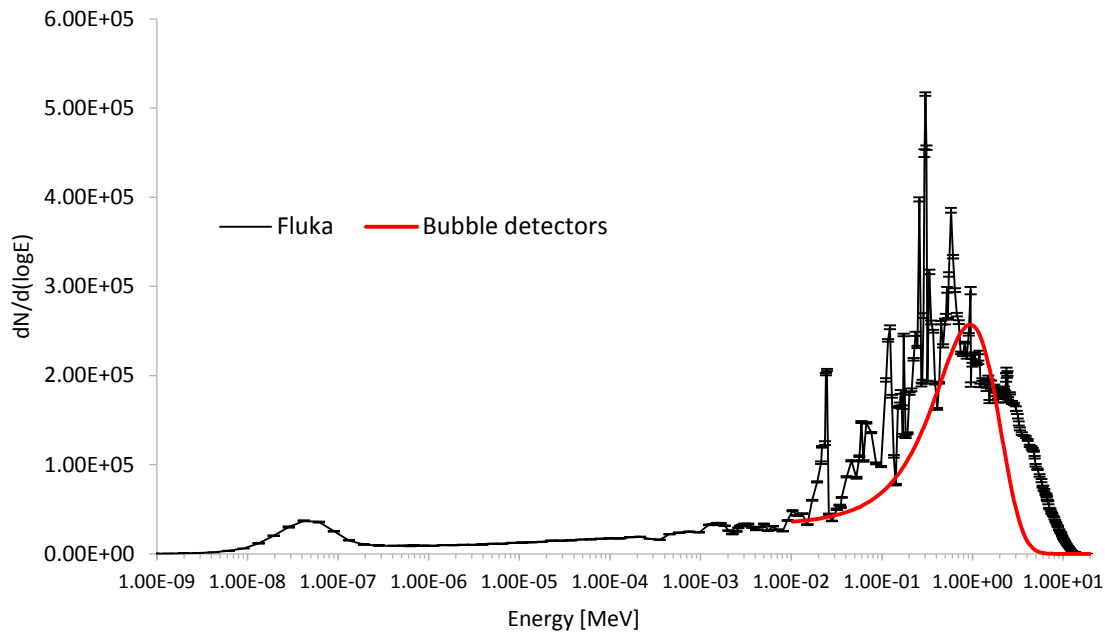


Figure 6.7 comparison of neutron spectra obtained using Fluka with the correspondent neutron spectrum obtained with bubble detectors during irradiation of target 2. Bubble detectors spectrum (equation 6.2) was obtained using the unfolding procedures described in chapter 5.2.1.

As can be seen, also in this case the agreement can be considered satisfactory, once again taking into account that the limited energy sampling of bubble detectors does not allow for accurate comparison with the detailed MC results. The neutron fluence is higher because the measurement positions was closer to the target, while the thermal neutron peak is lower because the measurements positions was further from the walls compared to set 1 of measurements.

6.2.3 Neutron spectrum generated irradiating Target 5

The responses of bubble detectors during irradiations of target 5 are shown in table 6.6, results before and after the iterative process described in chapter 5.2.1 are reported.

Table 6.6 Bubble detectors response obtained during irradiation of target 5

Detector	Standard Response R_i	Uncertainty (%)	Correction factor f_i	$R_i \times f_i$	Uncertainty (%)
BDS10	13.1	3.2	1.0	13.1	3.2
BDS100	9.9	3.7	1.3	12.5	3.7
BDS600	7.9	4.2	0.8	6.9	4.2
BDS1000	3.0	6.5	1.1	3.4	6.5
BDS2500	2.2	7.2	0.9	2.1	7.2
BDS10000	0.2	40.8	1.3	0.2	40.8

In table 6.7 neutron fluence as a function of energy, estimated from bubble detectors row data with the unfolding procedure described in chapter 5.2.1, is reported and compared with FLUKA simulations results.

Table 6.7 Comparison between the neutron fluence measured experimentally and the correspondent neutron fluence estimated using Fluka during irradiation of target 5

Energy Range	Fluence Ni			
	Bubble detectors	Uncertainty (%)	Fluka	Uncertainty (%)
0.01-0.1	1.35E+05	90.2	6.99E+04	1.2
0.1-0.6	2.12E+05	19.4	2.32E+05	1.4
0.6-1.0	6.28E+04	63.1	6.36E+04	1.5
1.0-2.5	9.45E+04	23.6	1.18E+05	2.1
2.5-10	5.44E+04	13.5	7.76E+04	1.6
10-20	5.34E+03	30.0	1.84E+03	2.9

Figure 6.8 reports the same results in graphical form:

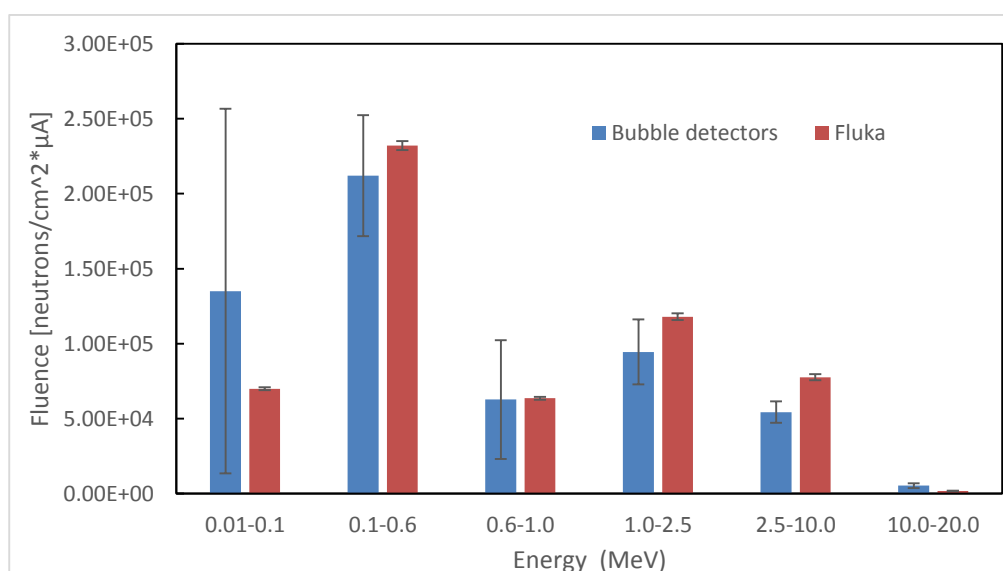


Figure 6.8 Comparison between neutron fluence measured with bubble detectors and the correspondent neutron fluence estimated using Fluka during irradiation of target 5

The results of FLUKA simulations are in agreement with experimental measurements within uncertainties, for all the energy range except in 2.5-10 MeV energy range and in 10-20 MeV energy range.

In equation 6.3 the maxwellian function representing data in a more realistic form, obtained with the iterative procedure already mentioned, is reported and compared graphically with the correspondent neutron spectrum obtained with FLUKA (figure 6.9).

$$n(E)dE = 4.51 \cdot 10^{-2} + 4.86 \cdot 10^{+5} * (E + 4.08) * e^{\left(-\frac{(E+4.08 \cdot 10^{-1})}{6.57 \cdot 10^{-1}}\right)} \quad \text{Equation 6.3}$$

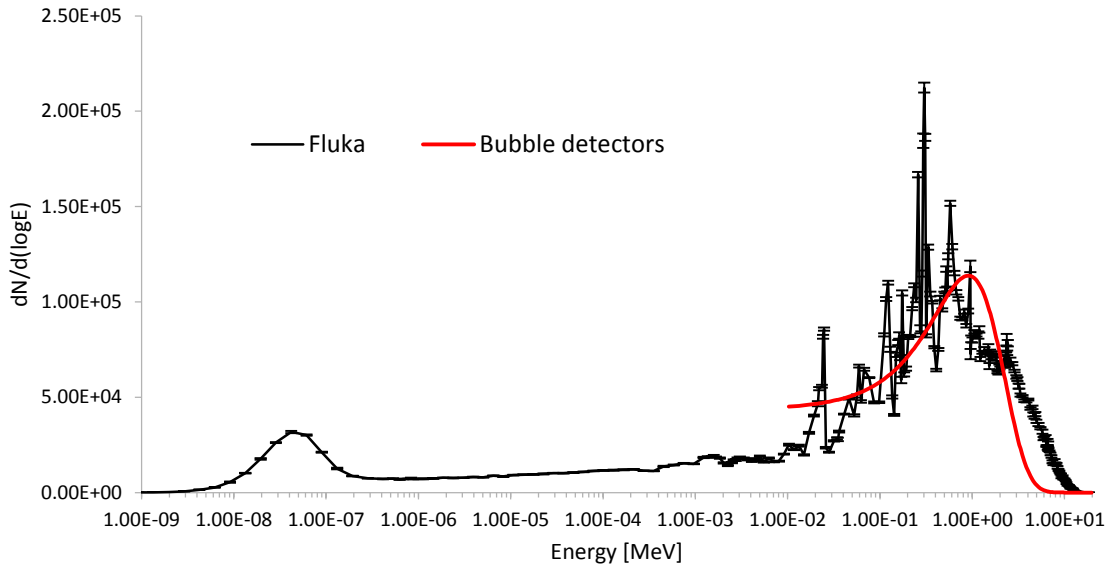


Figure 6.9 comparison of neutron spectra obtained using Fluka with the correspondent neutron spectrum obtained with bubble detectors during irradiation of target 5. Bubble detectors spectrum (equation 6.3) was obtained using the unfolding procedures described in chapter 5.2.1.

The spectrum obtained experimentally also in this case is consistent with the neutron spectrum estimated with FLUKA simulations and has, at least as can be measured with bubble detectors, the same trend of spectra determined in previous measurements.

6.2.4 Neutron spectrum generated irradiating Target 6

The responses of bubble detectors during irradiations of target 6 are shown in table 6.8, results before and after the iterative process described in chapter 5.2.1 are reported.

Table 6.8 Bubble detectors response obtained during irradiation of target 6

Detector	Standard Response R_i	Uncertainty (%)	Correction factor f_i	$R_i \times f_i$	Uncertainty (%)
BDS10	36.3	3.2	0.7	25.4	3.2
BDS100	25.9	3.8	0.9	24.7	3.8
BDS600	21.2	4.2	0.7	15.1	4.2
BDS1000	8.2	6.5	1.0	8.3	6.5
BDS2500	5.8	7.4	0.9	5.7	7.4
BDS10000	0.5	40.8	1.3	0.6	40.8

In table 6.9 neutron fluence as a function of energy is reported and compared with FLUKA simulations results.

Table 6.9 Comparison between the neutron fluence measured experimentally and the correspondent neutron fluence estimated using Fluka during irradiation of target 6

Energy Range	Fluence Ni			
	Bubble detectors	Uncertainty (%)	Fluka	Uncertainty (%)
0.01	2.17E+05	151.1	9.97E+04	0.7
0.1-0.6	3.77E+05	29.4	3.42E+05	0.5
0.6-1.0	1.01E+05	110.3	9.76E+04	0.8
1.0-2.5	1.74E+05	39.7	1.82E+05	1.2
2.5-10	1.48E+05	19.5	1.17E+05	2.2
10-20	1.44E+04	54.1	2.84E+03	8.6

Figure 6.10 reports the same results in graphical form:

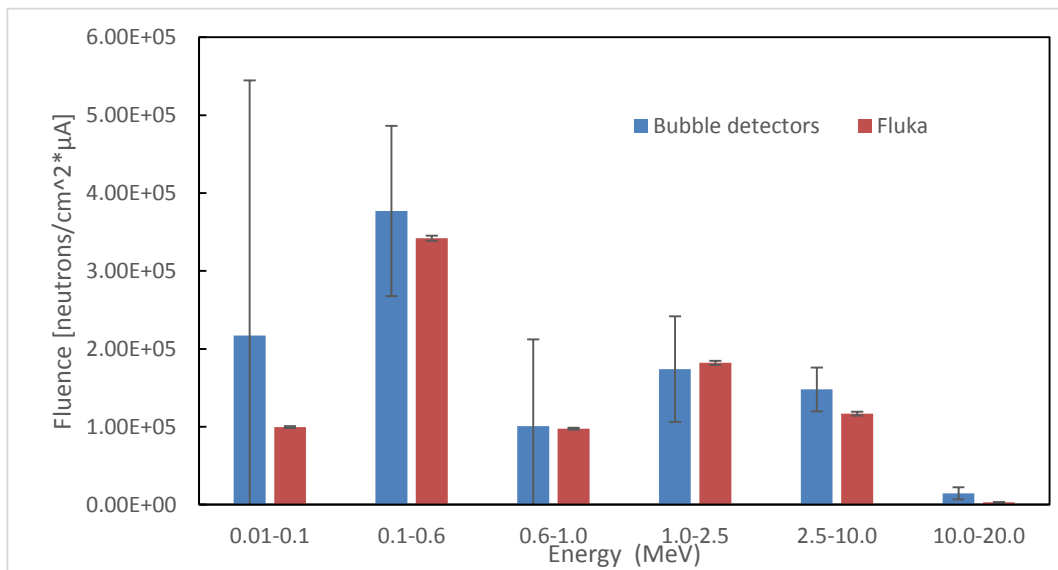


Figure 6.10 Comparison between neutron fluence measured with bubble detectors and the correspondent neutron fluence estimated using Fluka during irradiation of target 6

In this case, as can be seen from figure 6.10, the results of FLUKA simulations are in agreement with experimental measurements within uncertainties, for all the energy ranges.

In equation 6.4 the maxwellian function representing the data in a more realistic form, obtained via the iterative procedure already mentioned, is reported and compared graphically with the correspondent neutron spectrum obtained with FLUKA (figure 6.11).

$$n(E)dE = 4.51 \cdot 10^{-2} + 6.47 \cdot 10^{+5} * (E + 4.20 \cdot 10^{-1}) * e^{\left(\frac{(E+4.20 \cdot 10^{-1})}{7.06 \cdot 10^{-1}}\right)} \quad \text{Equation 6.4}$$

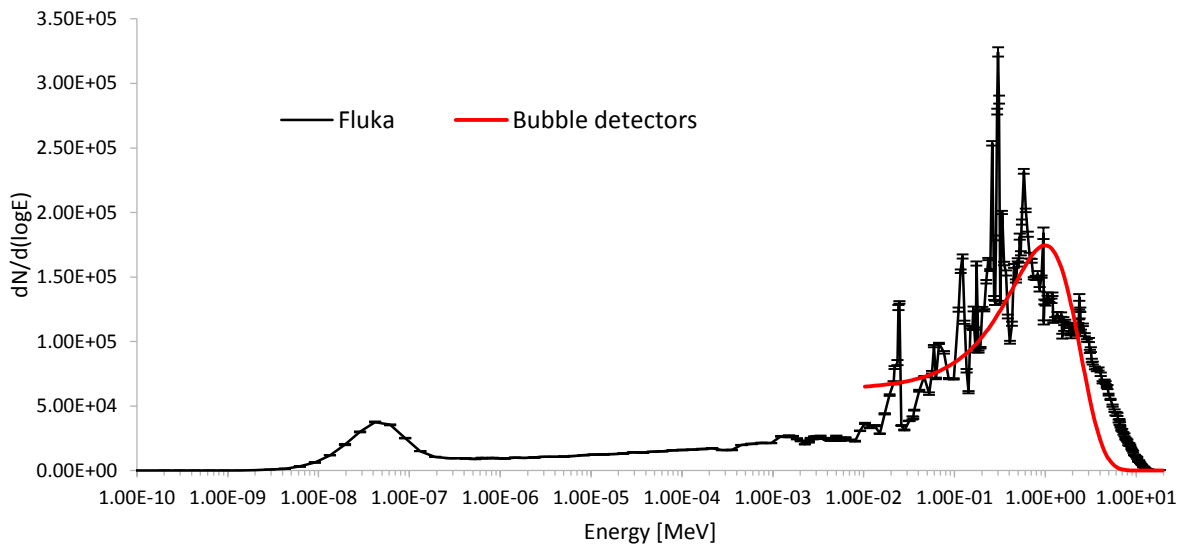


Figure 6.11 comparison of neutron spectra obtained using Fluka with the correspondent neutron spectrum obtained with bubble detectors during irradiation of target 6. Bubble detectors spectrum (equation 7.4) was obtained using the unfolding procedures described in chapter 5.2.1.

Also in this case the neutron spectrum obtained experimentally is consistent with the spectrum estimated with FLUKA and with spectra measured in previous measurements.

Considering the four measurements performed, FLUKA simulations are in agreement with experimental measurements. It has to be noted once again that bubble detectors measurements have high uncertainties due to different aspects:

- Fluence responses of superheated emulsions is very sensitive to operating temperature;
- The unfolding procedure suffer from error accumulation which leads to large errors in the lower energy region of the spectrum;
- Detector sensitivity is very high if compared with neutron fluxes normally present inside a bunker during the production of ^{18}F , for this reason dedicated irradiation must be performed with low integrated currents. This implies higher uncertainty in the integrated charge, which is essentially that of the ampere-meter used for the calibration of the current measuring board;
- Manual counting implies higher uncertainties compared to automatic counting with bubble detector reader.
- Limited number of energy bins in the practical, inexpensive bubble detectors system

Each one of those aspects may have a significant influence on the results. However this method guarantees an accuracy of the results adequate for the purposes of this work with low costs and quick measurements compared with other neutron detection methods.

Considering all the factors listed above and small differences in the modelling of the cyclotron components, FLUKA simulation provided a good agreement with the experimental measurements allowing for an accurate estimation of the neutron flux inside the bunker.

6.3 Bunker walls activation assessment

In this subsection results of experimental measurements for activation assessment of the two case studied were reported and compared with the corresponding results obtained with Fluka in order to assess the accuracy of Monte Carlo results in terms of residual activation. As a general consideration, the activation of trace elements (e.g. europium and caesium) and of particular metals in concrete and in reinforcement rods turns out to be mainly responsible for residual activation of the biological shielding. Long living radionuclide are mainly created by neutron capture with high cross sections and by some threshold reactions with lower yield. Because of the high ^{151}Eu cross section for thermal neutrons and of the long half life of ^{152}Eu this radionuclide is the most important in terms of residual activation, followed by ^{60}Co mainly present in reinforcement rods.

The main long lived radionuclides found in both cases are reported with the most probable production reactions in table 6.10. Physical data are derived from the ENDF/B-VI and JEF-2.2 neutron database and from IAEA Report EUR19151.

Table 6.10 Main long lived radionuclides founded in bunker walls

<i>Nuclide</i>	<i>Half life</i>	<i>Possible Reaction</i>	<i>Cross section</i>	<i>Abundance (%)</i>	<i>Activated material</i>
^{152}Eu	13.33 years	$^{151}\text{Eu}(n,\gamma)^{152}\text{Eu}$	9198 barn	48	concrete
^{154}Eu	8.8 years	$^{153}\text{Eu}(n,\gamma)^{154}\text{Eu}$	312 barn	52	concrete
^{134}Cs	2.06 years	$^{133}\text{Cs}(n,\gamma)^{134}\text{Cs}$ $^{134}\text{Ba}(n,p)^{134}\text{Cs}$	29 barn 9 mbarn at $E_n = 16$ MeV	100 2	concrete
^{54}Mn	312 days	$^{54}\text{Fe}(n,p)^{54}\text{Mn}$	590 mbarn at $E_n = 10$ MeV	6	Concrete and reinforcement rods
^{46}Sc	83 days	$^{45}\text{Sc}(n,\gamma)^{46}\text{Sc}$	27 barn	100	Concrete
^{60}Co	5.3 years	$^{59}\text{Co}(n,\gamma)^{60}\text{Co}$	37 barn	100	Concrete and reinforcement rods
^{59}Fe	44 days	$^{58}\text{Fe}(n,\gamma)^{59}\text{Fe}$	1.15 barn	0.3	Concrete and reinforcement rods
^{65}Zn	244 days	$^{64}\text{Zn}(n,\gamma)^{65}\text{Zn}$	0.78 barn	49	concrete
^{57}Co	272 days	$^{58}\text{Ni}(n,x)^{57}\text{Co}$	0.6 barn	68	Concrete and reinforcement rods

Before presenting results obtained in gamma spectrometry measurements and comparing them with corresponding FLUKA results, it is important to underline that this methodology does not intend to assess activation at high precision level. Concrete activation is in fact strongly dependent on trace element concentration that is heterogeneous and usually unknown, furthermore differences from real irradiation geometry can affect final results. The aim of this work is to define a methodology to have a preventive idea of the order of magnitude of the activation level depending on materials, positions, bunker design and type, workload, life expectancy of the cyclotron and to have an idea of the induced residual activity distribution inside the bunker. From this perspective Monte Carlo methods represent a very powerful tool if compared with analytical methods, especially during the design of a new facility.

6.3.1 Non-destructive activation assessment using a portable CZT detectors in Bologna

In this subsection results obtained in the experimental campaign conducted inside the PETtrace bunker of the S.Orsola-Malpighi hospital and described in chapter 5.3 will be presented.

In figure 6.13, 6.14, 6.15 spectra measured in the three positions of figure 6.12 are reported, while in table 6.11, 6.12, 6.13 activity concentrations of the main radionuclides detected experimentally are compared with correspondent activity concentrations estimated with FLUKA.

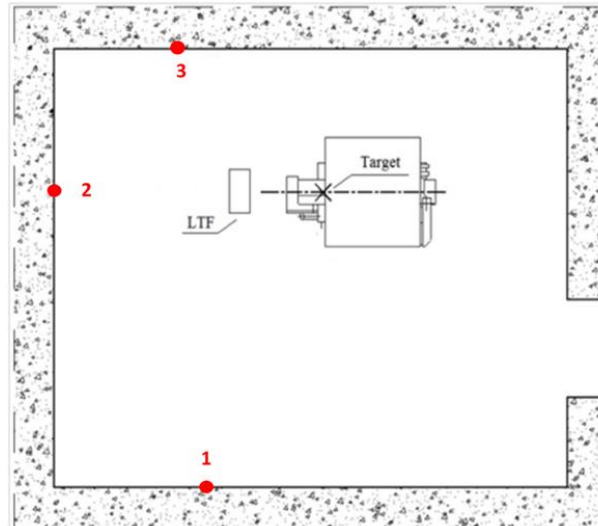


Figure 6.12 Measurements positions

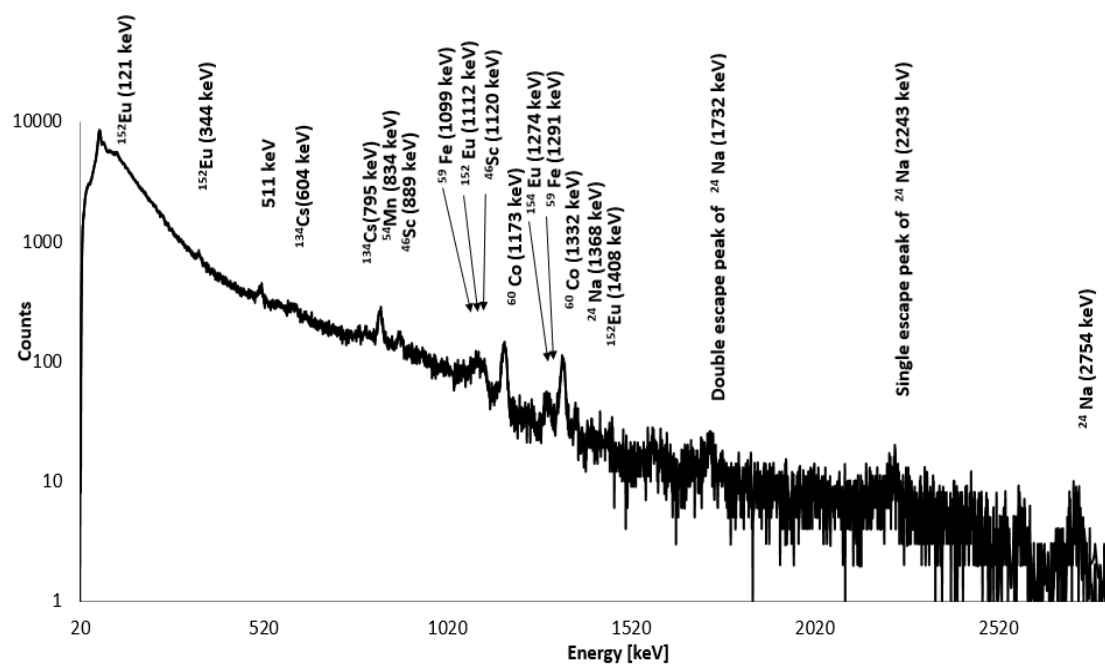


Figure 6.13 Gamma spectrum acquired at position 1

Table 6.11 Comparison between activity concentrations measured experimentally and the corresponding activity concentrations estimated with Fluka for position 1

Nuclide	Experimental		Fluka		FLUKA/ Experimental
	Activity concentration [Bq/g]	Uncertainty (%)	Activity concentration [Bq/g]	Uncertainty (%)	
¹⁵² Eu	1.20E-01	11	7.50E-01	6	6.25 ± 0.10
¹³⁴ Cs	6.00E-02	11	1.00E-02	42	0.16 ± 0.09
⁵⁴ Mn	2.50E-01	11	1.40E-01	2	0.56 ± 0.07
⁴⁶ Sc	3.70E-01	11	-	-	-
⁶⁰ Co	2.60E-01	12	2.10E-01	4	0.81 ± 0.13

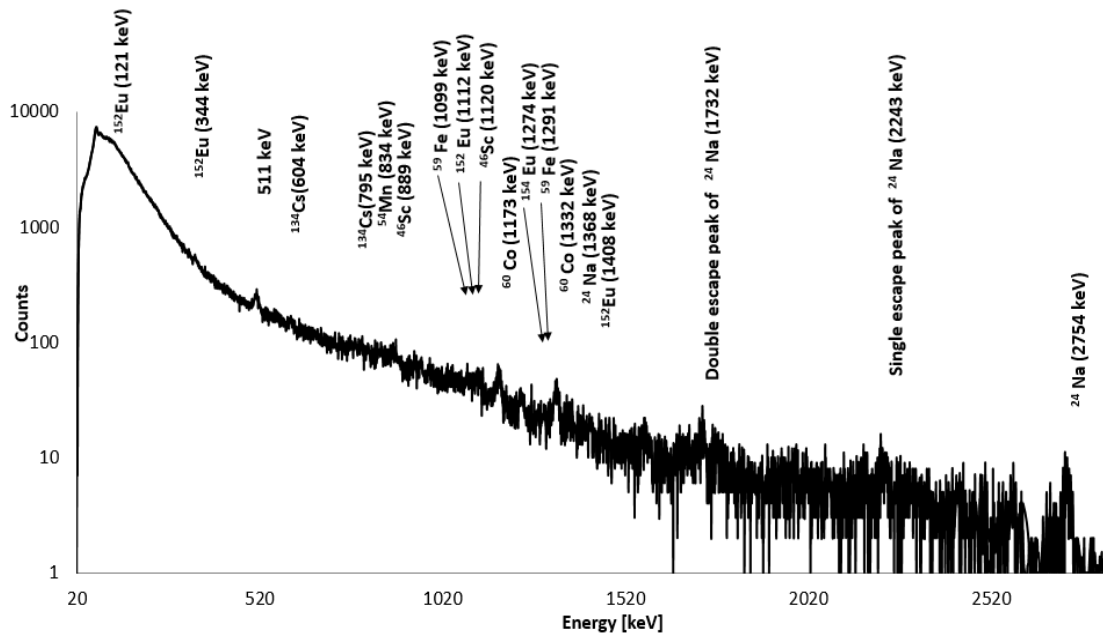


Figure 6.14 Gamma spectrum acquired at position 2

Table 6.12 Comparison between activity concentrations measured experimentally and the corresponding activity concentrations estimated with Fluka for position 2

Nuclide	Experimental		Fluka		FLUKA /Experimental
	Activity concentration [Bq/g]	Uncertainty (%)	Activity concentration [Bq/g]	Uncertainty (%)	
¹⁵² Eu	<4.00E-02*	10	8.00E-01	4	-
¹³⁴ Cs	<1.00E-02*	10	1.00E-02	26	-
⁵⁴ Mn	<1.00E-02*	10	1.00E-02	1	-
⁴⁶ Sc	<2.00E-02*	10	1.00E-02	-	-
⁶⁰ Co	4.00E-02	11	1.30E-01	16	3.25 ± 0.09

*Minimum Detectable activity of the detector (MDA)

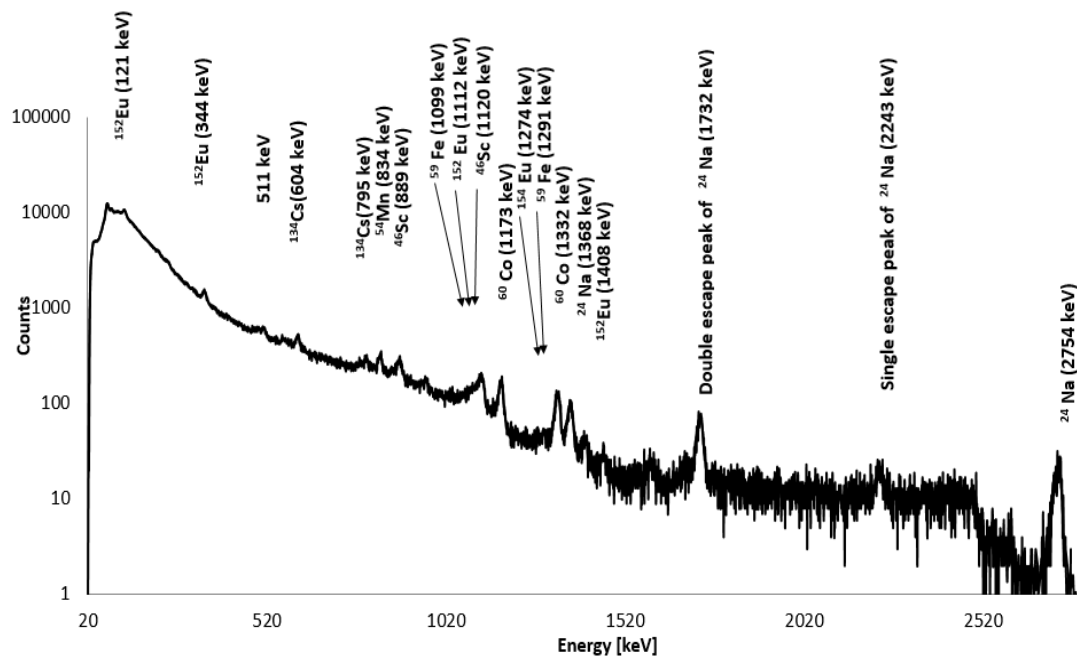


Figure 6.15 Gamma spectrum acquired at position 3

Table 6.13 Comparison between activity concentrations measured experimentally and the corresponding activity concentrations estimated with Fluka for position 3

Nuclide	Experimental		Fluka		FLUKA/ Experimental
	Activity concentration [Bq/g]	Uncertainty (%)	Activity concentration [Bq/g]	Uncertainty (%)	
¹⁵² Eu	3.60E-01	10.35	1.72E+00	4.02	4.78 ± 0.69
¹³⁴ Cs	7.00E-02	10.56	3.00E-02	25.99	0.43 ± 0.16
⁵⁴ Mn	8.00E-02	10.81	2.00E-01	1.13	2.50 ± 0.23
⁴⁶ Sc	1.30E-01	10.75	-	-	-
⁶⁰ Co	1.80E-01	11.47	4.80E-01	2.7	2.67 ± 0.38

Activity concentrations measured experimentally are not consistent within the uncertainty with FLUKA estimations, however considering the order of magnitude of activity concentrations and the related activation distributions in the three different positions, between FLUKA estimations and experimental measurements for the scope of this work there is sufficient level of agreement. Discrepancies in activation assessment are mainly due to the fact that, as already said, concrete activation is strongly dependent on trace element concentration that is heterogeneous and usually unknown. The literature values used in simulations could be quite different from the real trace element concentration. For example the absence of ^{46}Sc in simulated results is due to the absence of ^{45}Sc in the concrete composition modeled.

It has also to be considered that direct measurements inside the bunker are critical because of the high radioactive background due to activated material of the cyclotron itself and because of the presence of short-lived radionuclides with an activity concentration significantly higher than that of the long-lived radionuclides. This fact, coupled with the limited access time to perform measurements during cyclotron lifetime and the complexity of the acquisition geometry, limits the accuracy of this methodology if compared with measurements of concrete samples with HPGe detectors. However this methodology allows a direct measurement that can be taken periodically to monitor activation levels inside the bunker during cyclotron lifetime without the need of any destructive analysis. Furthermore, performing core drilling in bunker walls is expensive, requires time and is not always possible during the cyclotron lifetime.

6.3.2 IBA CICLONE18/9 Bunker activation assessment via core drilling

The three spectra obtained from the experimental measurement of concrete samples from Inselspital bunker walls (figure 6.16) and described in subsection 5.4, are reported in figure 6.17, 6.18, 6.19. In table 6.14, 6.15, 6.16 activity concentrations of the main radionuclides detected experimentally are compared with correspondent activity concentrations obtained with Fluka.

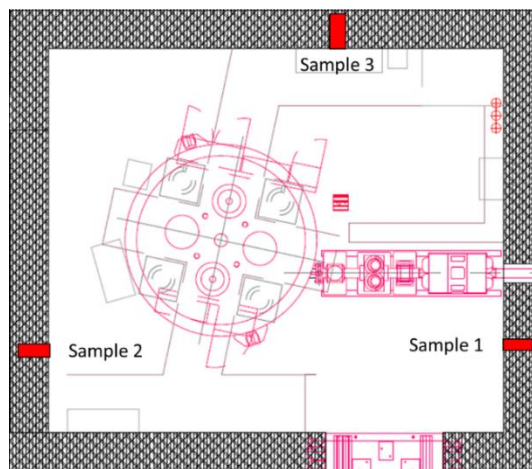


Figure 6.16 Core drilling positions

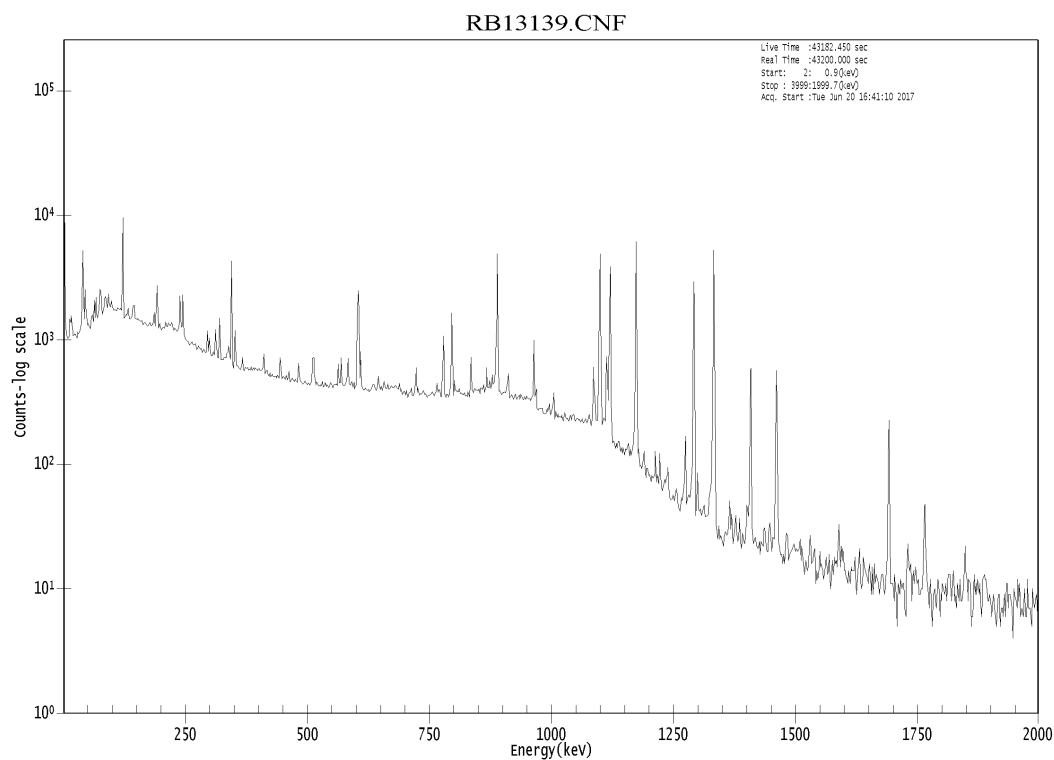


Figure 6.17 Gamma-ray spectrum of concrete sample 1

Table 6.14 Comparison between activity concentrations measured experimentally and the corresponding activity concentrations estimated with Fluka for sample 1

Nuclide	Experimental		Fluka		FLUKA/Experimental
	Activity concentration [Bq/g]	Uncertainty	Activity concentration [Bq/g]	Uncertainty	
⁴⁶ Sc	1.00E-01	2.93E-03	-	-	
⁵⁴ Mn	7.77E-03	8.23E-04	7.94E-03	1.54E-03	1.02 ± 0.31
⁵⁷ Co	1.15E-02	2.96E-03	-	-	
⁵⁹ Fe	2.24E-01	5.88E-03	2.54E-01	1.61E-02	1.13 ± 0.10
⁶⁰ Co	1.71E-01	4.90E-03	2.05E-01	7.48E-02	1.20 ± 0.47
⁶⁵ Zn	1.68E-02	9.08E-04	1.04E-01	2.50E-02	6.19 ± 1.82
¹³⁴ Cs	3.23E-02	8.49E-04	3.30E-02	1.41E-02	1.02 ± 0.46
¹⁵² Eu	1.03E-01	1.85E-03	1.01E-01	2.32E-02	0.98 ± 0.24
¹⁵⁴ Eu	1.26E-02	9.49E-04	1.25E-03	1.24E-03	0.10 ± 0.11

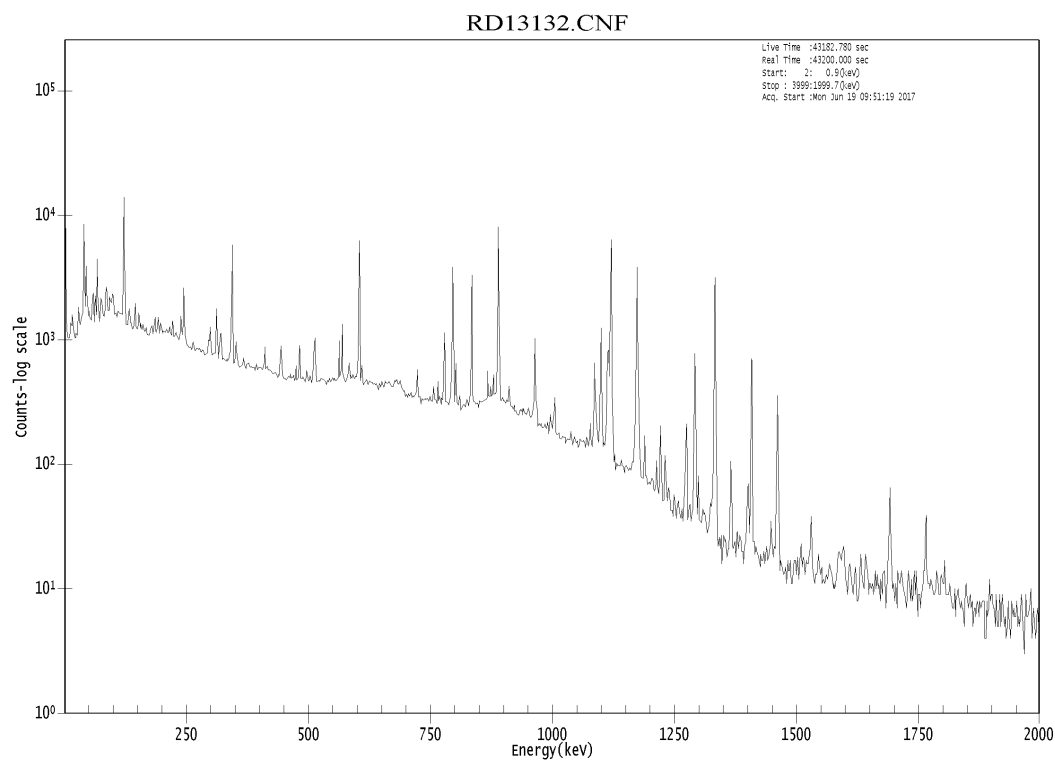


Figure 6.18 Gamma-ray spectrum of concrete sample 2

Table 6.15 Comparison between activity concentrations measured experimentally and the corresponding activity concentrations estimated with Fluka for sample 2

Nuclide	Experimental		Fluka		FLUKA/Experimental
	Activity concentration [Bq/g]	Uncertainty	Activity concentration [Bq/g]	Uncertainty	
⁴⁶ Sc	5.86E-01	1.70E-02	-	-	
⁵⁴ Mn	9.49E-02	4.21E-03	7.59E-02	2.22E-02	0.80 ± 0.27
⁵⁷ Co	7.23E-02	1.51E-02	-	-	
⁵⁹ Fe	1.97E-01	6.60E-03	3.68E-01	8.57E-02	1.87 ± 0.50
⁶⁰ Co	3.23E-01	9.23E-03	2.69E-01	5.75E-02	0.83 ± 0.20
⁶⁵ Zn	1.06E-01	4.55E-03	3.67E-01	4.60E-02	6.19 ± 1.82
¹³⁴ Cs	2.10E-01	4.13E-03	2.28E-01	3.60E-02	1.02 ± 0.46
¹⁵² Eu	5.24E-01	7.29E-03	2.17E-01	4.89E-02	0.41 ± 0.01
¹⁵⁴ Eu	6.43E-02	1.96E-03	1.82E-02	6.69E-03	0.28 ± 0.11

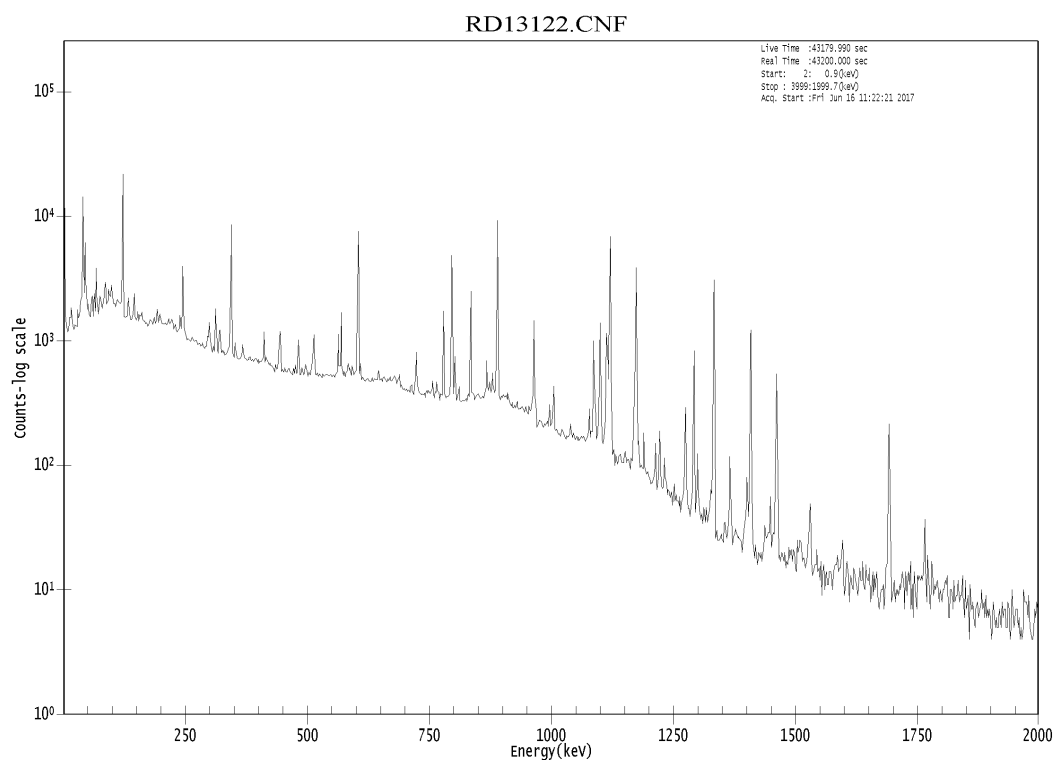


Figure 6.19 Gamma-ray spectrum of concrete sample 3

Table 6.16 Comparison between activity concentrations measured experimentally and the corresponding activity concentrations estimated with Fluka for sample 3

Nuclide	Experimental		Fluka		FLUKA/Experimental
	Activity concentration [Bq/g]	Uncertainty [Bq/g]	Activity concentration [Bq/g]	Uncertainty [Bq/g]	
⁴⁶ Sc	3.77E-01	1.10E-01	-	-	
⁵⁴ Mn	8.27E-02	3.73E-03	6.85E-02	2.68E-02	0.83 ± 0.36
⁵⁷ Co	3.92E-02	1.10E-02	-	-	
⁵⁹ Fe	1.20E-01	4.33E-03	1.00E-01	6.49E-02	0.83 ± 0.57
⁶⁰ Co	2.14E-01	6.17E-03	2.90E-01	5.26E-02	1.35 ± 0.28
⁶⁵ Zn	5.63E-02	2.65E-03	3.93E-01	5.68E-02	6.98 ± 1.34
¹³⁴ Cs	2.09E-01	4.06E-03	2.28E-01	5.10E-02	1.09 ± 0.26
¹⁵² Eu	4.06E-01	6.15E-03	1.89E-01	4.88E-02	0.47 ± 0.13
¹⁵⁴ Eu	5.30E-02	1.83E-03	1.82E-02	7.48E-03	0.34 ± 0.15

The most active sample was sample 2 with an activity concentration of about 0.5 Bq/g for ^{152}Eu and 0.3 Bq/g for ^{60}Co , followed by sample 3 with an activity concentration of 0.4 Bq/g and 0.2 Bq/g respectively for ^{152}Eu and ^{60}Co . These samples were extracted from positions closer to the targets compared to position 1. In position 1 activity concentrations of about 0.1 Bq/g and 0.2 Bq/g respectively for ^{152}Eu and ^{60}Co were measured. The higher activity concentration of ^{60}Co compared to ^{152}Eu in sample 1 is due to the presence of part of a steel bar in the sample, while samples 2 and 3 are only composed of concrete. As we can see from table 6.13 in the case of sample 1 the consistence between FLUKA and experimental measurements is within the uncertainty, except for ^{46}Sc and ^{57}Co . In sample 2 and 3 the consistence between measured and simulated results is rather good, within a factor of 3 except for ^{65}Zn . It has also to be considered that sample 2 and 3 have been damaged during extraction and only parts of the samples were measured.

6.4 Prediction of induced radioactivity using a Monte Carlo approach

Once the consistence between experimental and simulated result was assessed in some reference points and the accuracy of Monte Carlo results was checked, it was possible with the MC models developed to estimate preliminary the residual activity at different positions and depth and for different life expectancy of the cyclotron. In the following, to demonstrate the potentially of a Monte Carlo approach to activation assessment, some of the main significant results are reported.

6.4.1 Prediction of residual induced radioactivity in the bunker wall of S.Orsola-Malpighi hospital (Bologna)

The assessment of neutron fluence inside the bunker of Bologna during ^{18}F production is reported in figures 6.20 and 6.21. The knowledge of neutron fluence distribution inside the bunker has a key role during the planning of a new facility, first of all for shielding calculation and secondly for a preliminary assessment of activation, giving an idea for example of the bunker areas more exposed to neutrons flux, or of the in-depth attenuation of neutron fluence inside the bunker walls.

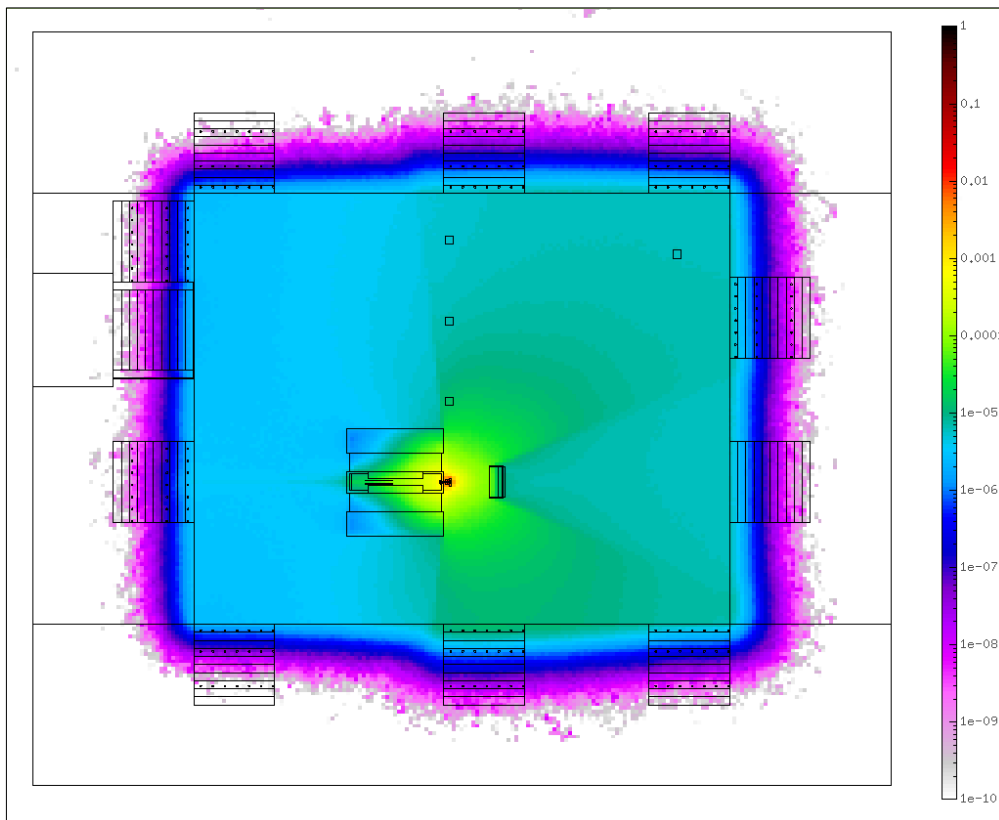


Figure 6.20 Fluka assessment of neutron fluence over the whole cyclotron bunker, expressed in neutron fluence per unit primary [n/cm^2]. Horizontal view.

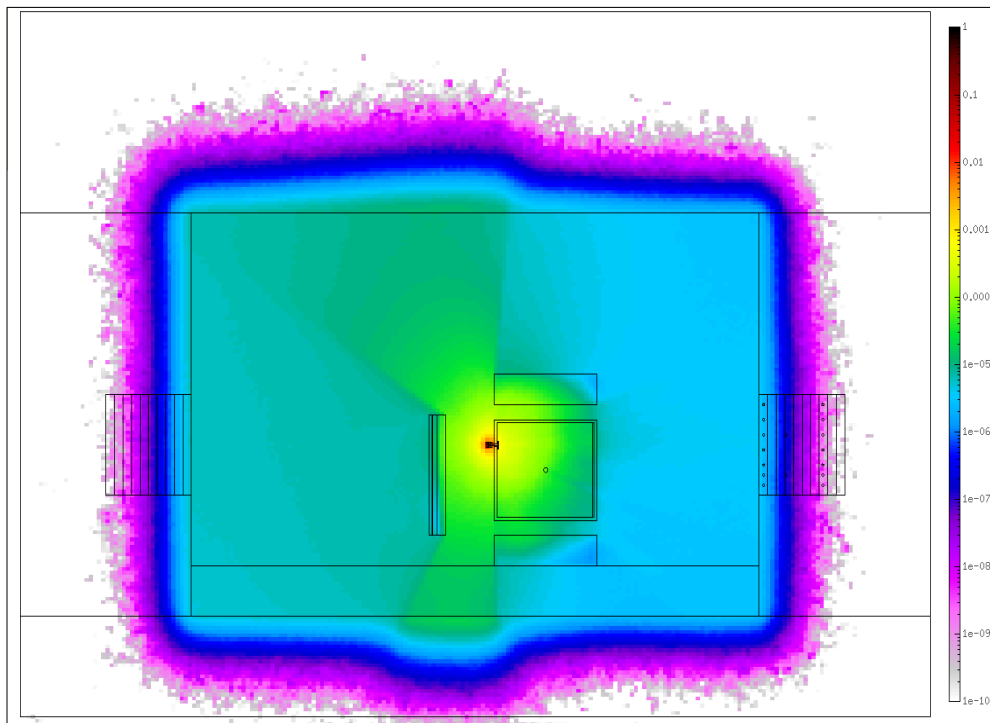


Figure 6.21 Fluka assessment of neutron fluence over the whole cyclotron bunker, expressed in neutron fluence per unit primary [n/cm^2]. Vertical view.

Figures 6.22, 6.23, 6.24 show an overview of a set of representative in-depth activation profiles for some of the main radionuclides detected in the three positions of figure 6.12

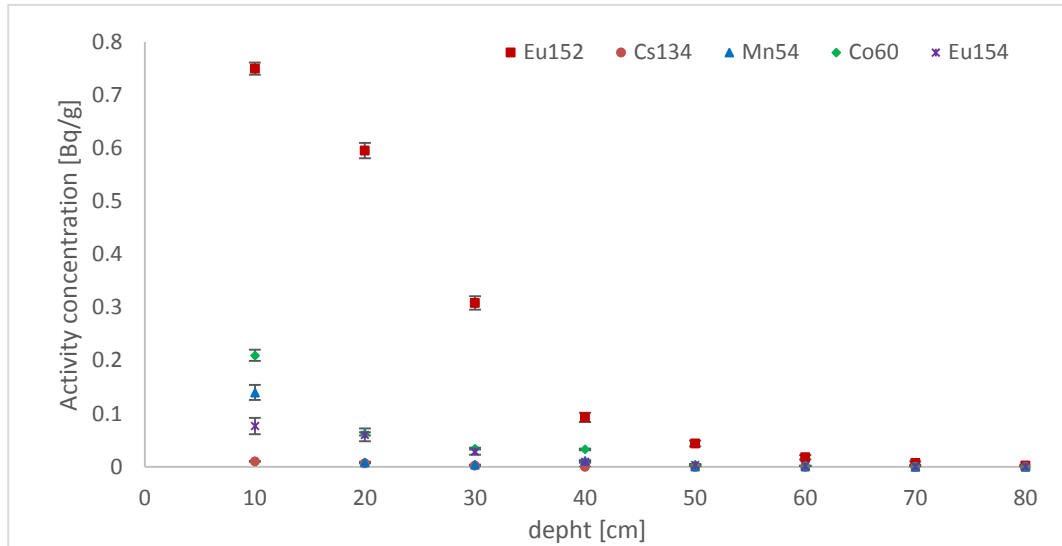


Figure 6.22 In-depth activation profile of some of the main radionuclides at position 1

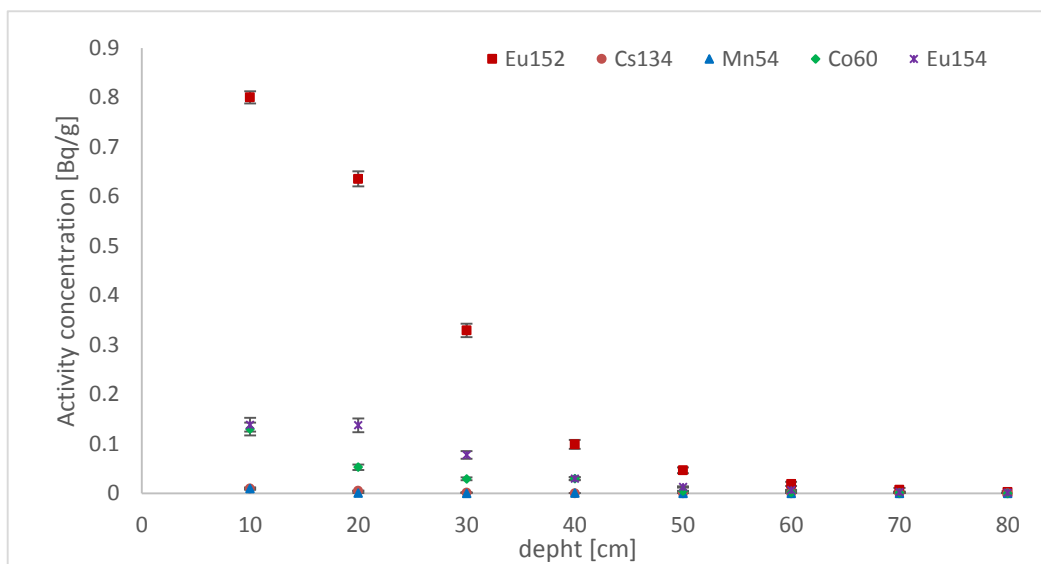


Figure 6.23 In-depth activation profile of some of the main radionuclides at position 2

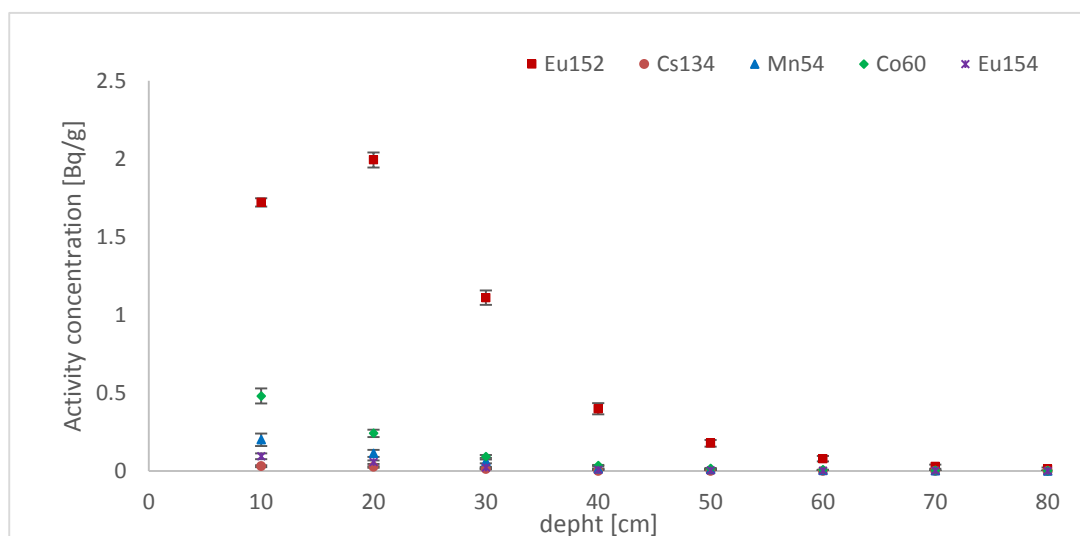


Figure 6.24 In-depth activation profile of some of the main radionuclides at position 3

The main nuclide present is ^{152}Eu followed by ^{60}Co . The specific activity of long-lived radionuclides reported at positions 1 and 2 is highest in the first 10 cm and decrease with increasing depth, while at position 3 the highest activity concentration for ^{152}Eu is at a depth of 20 cm, this means that at position 3 fast neutrons are slowed down inside the concrete and the thermal neutron component increases up to a depth of about 20 cm while at position 1 and 2, farther from the target, the thermal neutron component increases up to a depth of about 10 cm. In all the positions the activity concentration is almost negligible at depths larger than 60 cm. Summarizing only at position 3 ^{152}Eu has a specific activity higher than 1 Bq/g in the first 30 cm of concrete.

From figure 6.25 to figure 6.30 the activity concentrations in the first 10 cm inside the wall at different positions are reported.

The walls of the bunker are activated, as expected, most at position 7, the nearest position to targets and the most irradiated by neutrons. In that position an activity concentration of about 1.4 Bq/g and 0.9 Bq/g is expected respectively for ^{152}Eu and ^{60}Co . The larger is the distance from the targets increases, the smaller is the activation. The lowest activation is therefore present at the other end of the cyclotron vault, at positions 1, 8, 9 and 10. A second important factor, in addition to the distance, is the shielding of the neutrons by the machine itself. As can be noticed, for ^{60}Co and ^{54}Mn the position with the lowest activation is position 5, this is due to the fact that at position 5 the wall is only made of concrete bricks and reinforcement rods are not present.

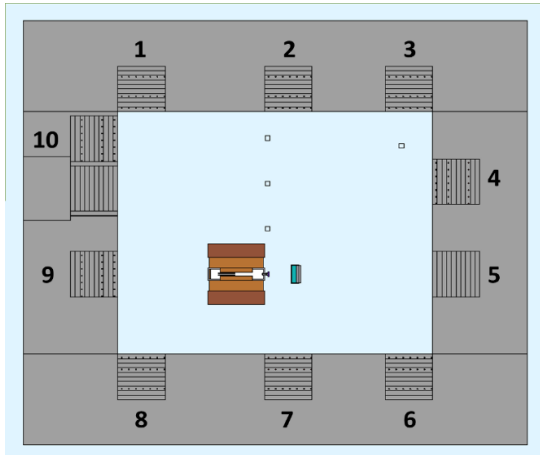


Figure 6.25 MC model of PETrace bunker where the positions in which activity concentration was estimated are indicated

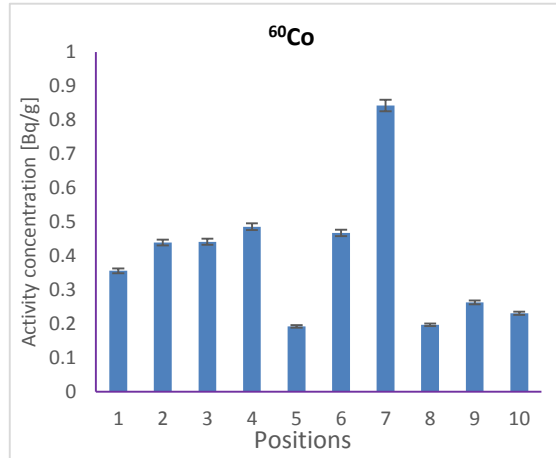


Figure 6.26 Activity concentration of ⁶⁰Co in first 10 cm inside the wall at different positions

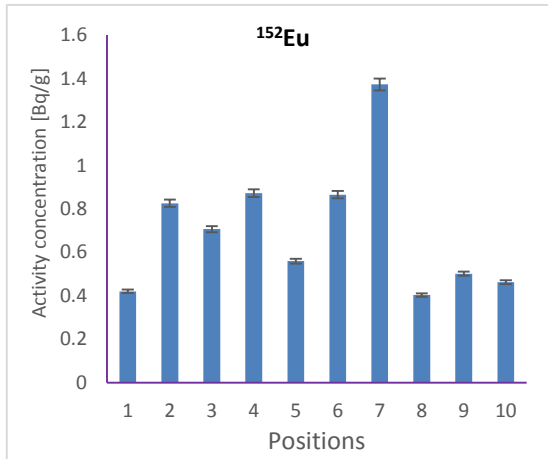


Figure 6.27 Activity concentration of ¹⁵²Eu in first 10 cm inside the wall at different positions

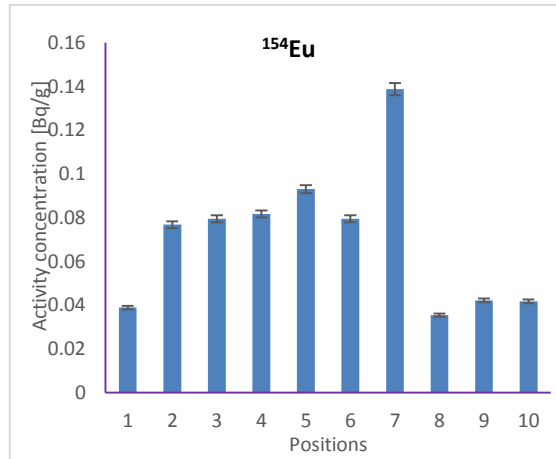


Figure 6.28 Activity concentration of ¹⁵⁴Eu in first 10 cm inside the wall at different positions

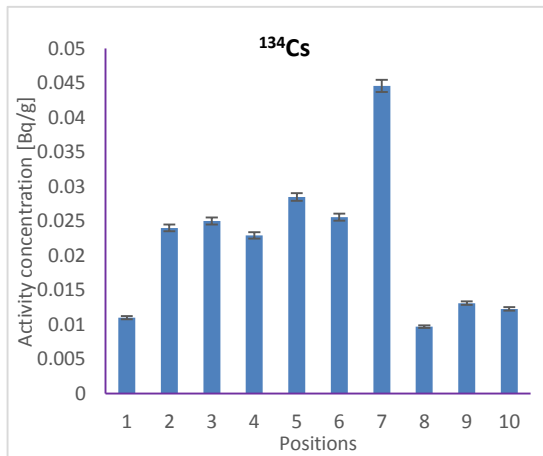


Figure 6.29 Activity concentration of ¹³⁴Cs in first 10 cm inside the wall at different positions

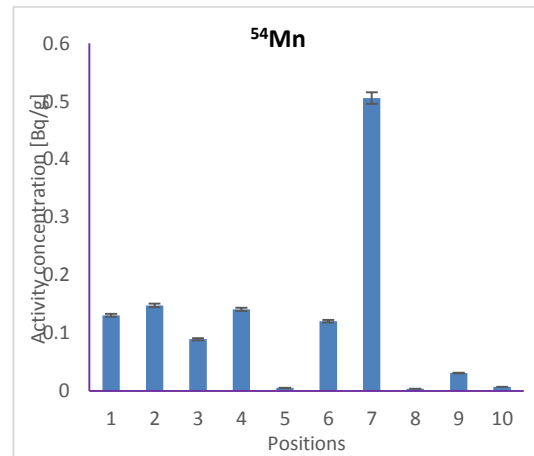


Figure 6.30 Activity concentration of ⁵⁴Mn in first 10 cm inside the wall at different positions

The prediction of activation induced was reported in table 6.17 for different life expectancies of the cyclotrons in the first 10 cm at position 7.

Table 6.17 Prediction of residual activity in the first 10 cm inside the wall of position 7 considering different life expectancy of the cyclotron

Nuclide	14 years		20 years		40 years	
	Activity concentration [Bq/g]	Uncertainty [Bq/g]	Activity concentration [Bq/g]	Uncertainty [Bq/g]	Activity concentration [Bq/g]	Uncertainty [Bq/g]
^{60}Co	8.43E-01	2.06E-02	9.30E-01	2.28E-02	9.97E-01	2.44E-02
^{134}Cs	4.46E-02	2.02E-03	4.49E-02	2.04E-03	4.50E-02	2.04E-03
^{152}Eu	1.96E+00	1.47E-02	2.46E+00	1.84E-02	3.34E+00	2.50E-02
^{154}Eu	1.39E-01	4.71E-03	1.64E-01	5.55E-03	1.97E-01	6.67E-03
^{54}Mn	5.06E-01	7.12E-03	5.06E-01	7.12E-03	5.06E-01	7.12E-03

6.4.2 Prediction of residual induced radioactivity in the bunker wall of Inselspital (Bern)

The assessment of neutron fluence inside the bunker of Bern during ^{18}F production with the four available different targets is reported in figure 6.31, 6.32, 6.33, 6.34.

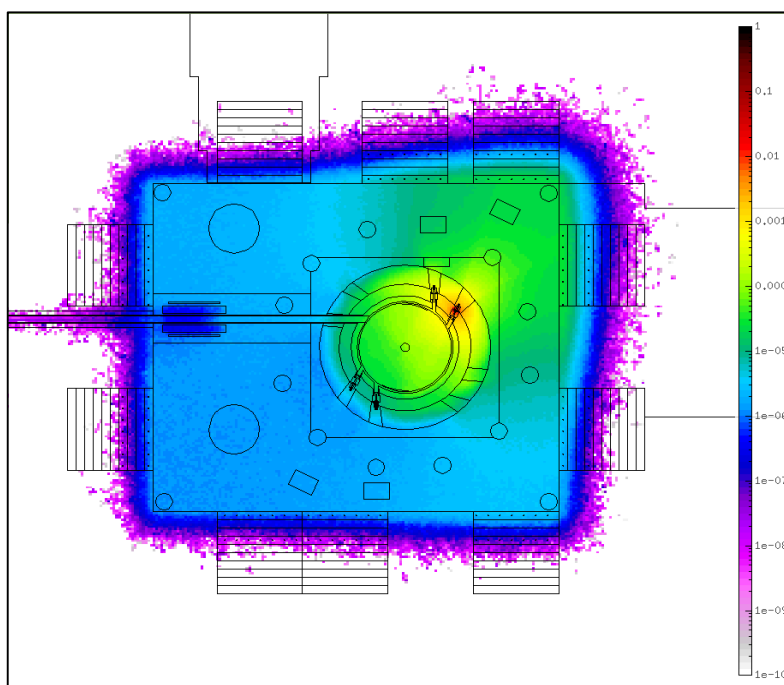


Figure 6.31 Fluka assessment of neutron fluence over the whole cyclotron bunker, expressed in neutron fluence per unit primary [n/cm^2], during target 1 irradiation.

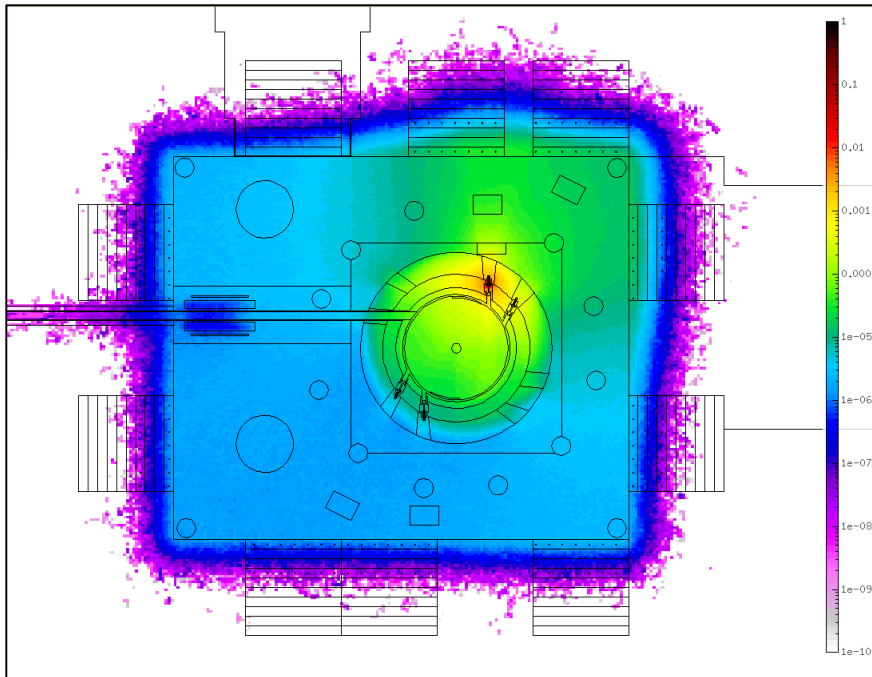


Figure 6.32 Fluka assessment of neutron fluence over the whole cyclotron bunker, expressed in neutron fluence per unit primary [n/cm^2], during target 2 irradiation.

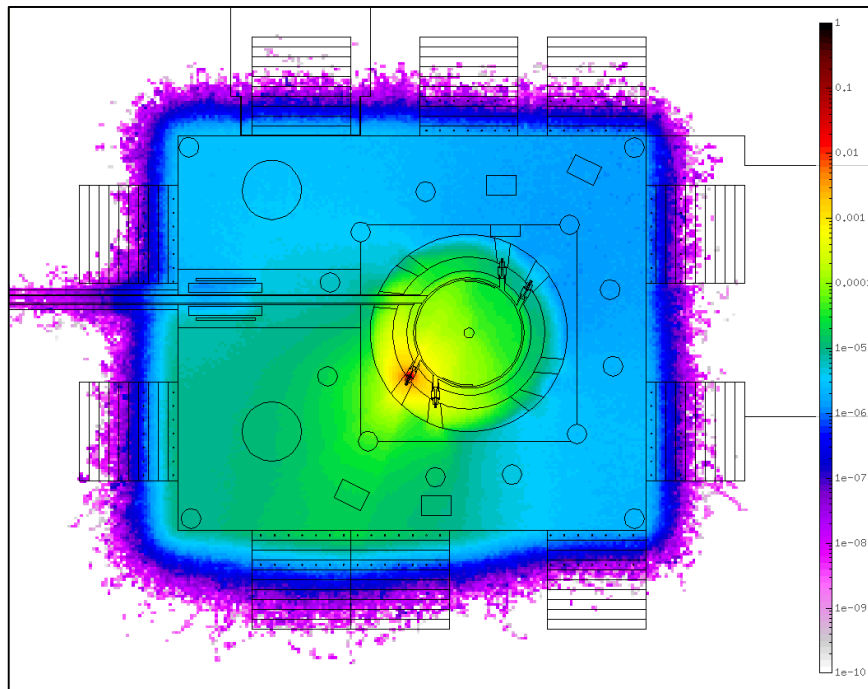


Figure 6.33 Fluka assessment of neutron fluence over the whole cyclotron bunker, expressed in neutron fluence per unit primary [n/cm^2], during target 5 irradiation.

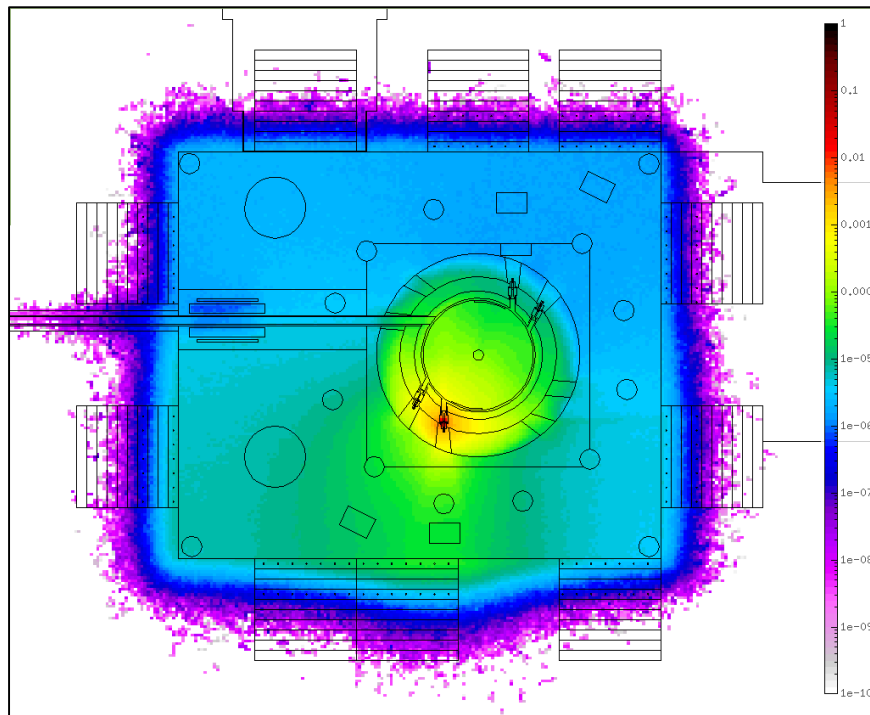


Figure 6.34 Fluka assessment of neutron fluence over the whole cyclotron bunker, expressed in neutron fluence per unit primary [n/cm^2], during target 6 irradiation.

Figures 6.35, 6.36, 6.36 show an overview of a set of representative in-depth activation profile for some of the main radionuclides detected in the three position of measurement of figure 6.16

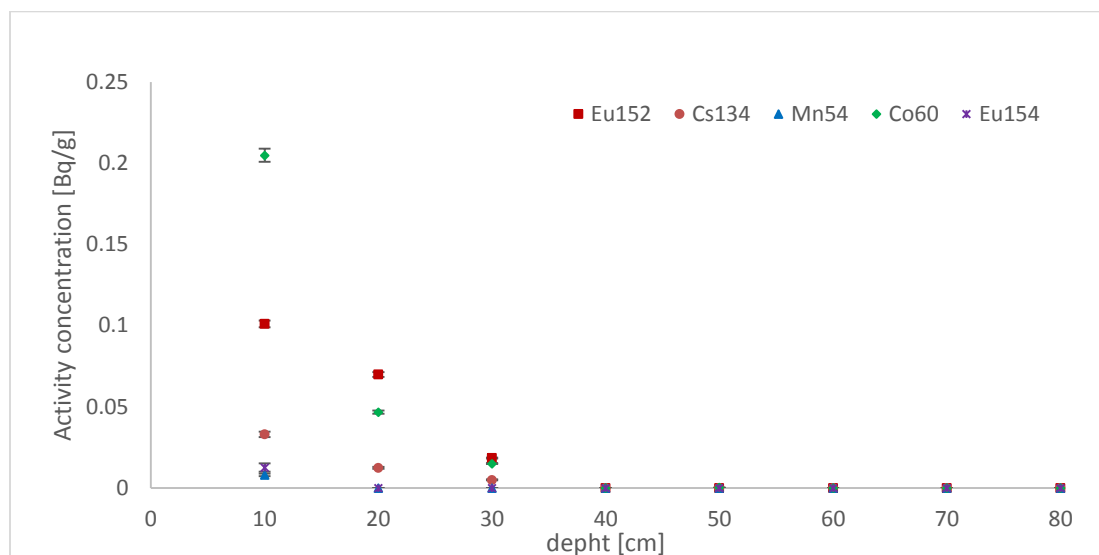


Figure 6.35 In-depth activation profile of some of the main radionuclides at position 1

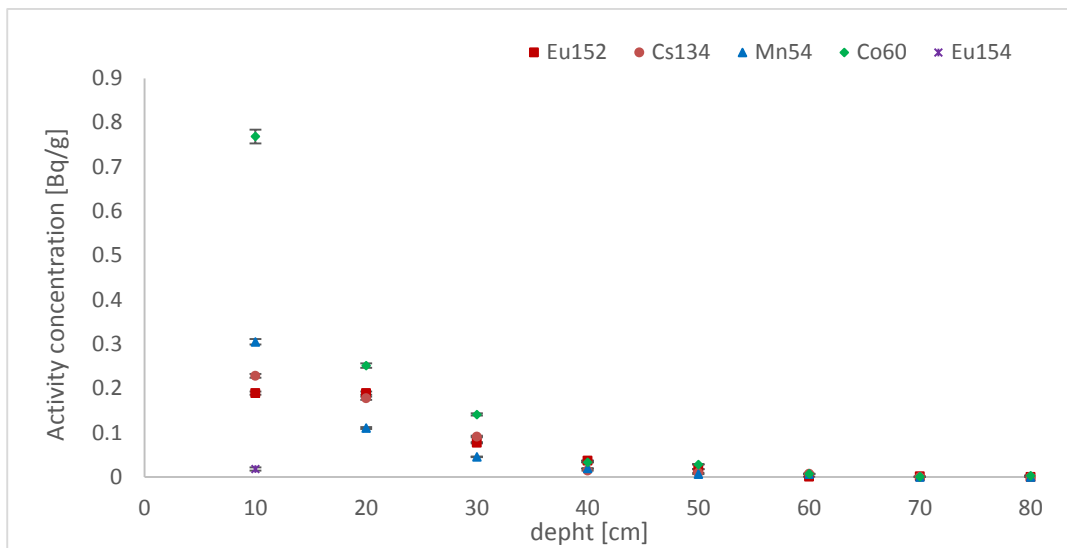


Figure 6.36 In-depth activation profile of some of the main radionuclides at position 2

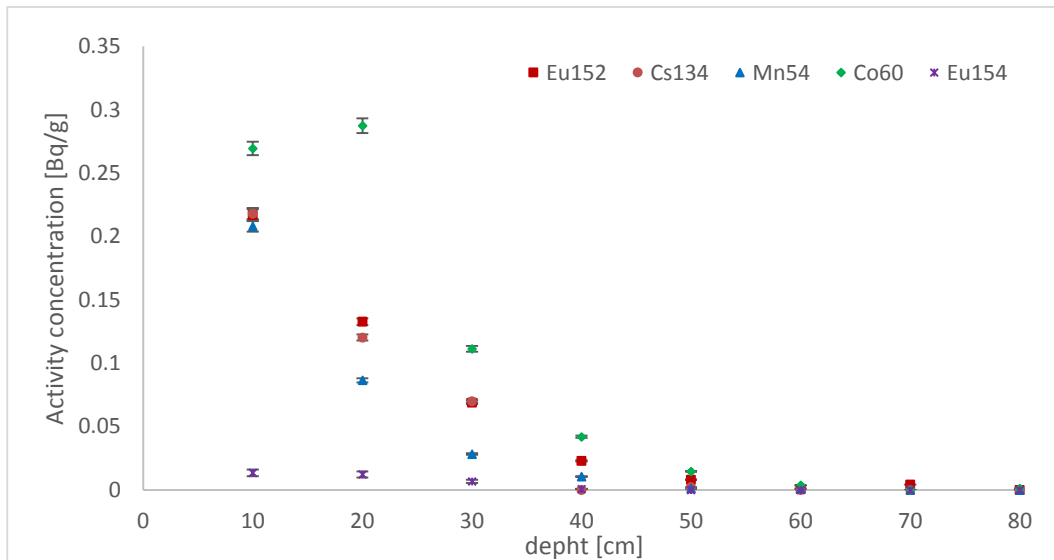


Figure 6.37 In-depth activation profile of some of the main radionuclides at position 3

The radionuclide with the highest activity concentration in this case is ^{60}Co , followed by ^{152}Eu . This is probably due to higher presence of reinforcement rods and to the different composition of the concrete with respect to the S.Orsola-Malpighi hospital bunker. Also in this case the specific activity of long-lived radionuclides reported at position 1 and 2 is highest in the first 10 cm and decreases with depth, while at position 3 the highest activity concentration for ^{60}Co is found at a depth of 20 cm. In all the positions the activity concentration is almost negligible at a depth larger than 60 cm.

Also in this case from figure 6.38 to figure 6.43 the activity concentration in the first 10 cm inside the wall at different positions is reported.

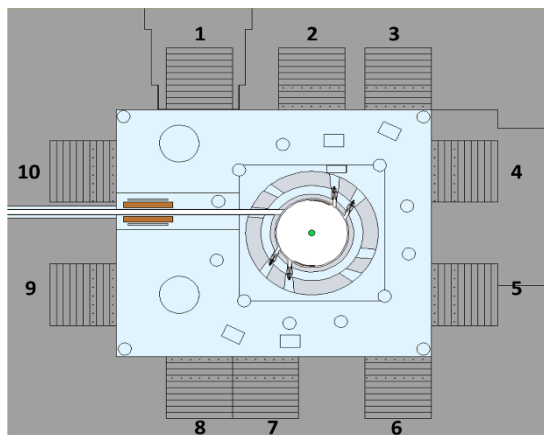


Figure 6.38 MC model of CYCLONE 18/9 bunker where the positions in which activity concentration was estimated are indicated

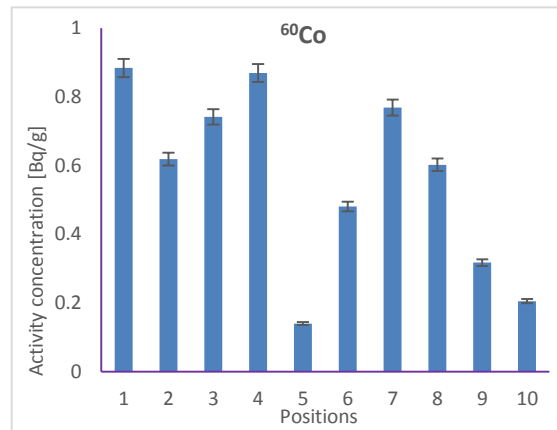


Figure 6.39 Activity concentration of ⁶⁰Co in first 10 cm inside the wall at different positions

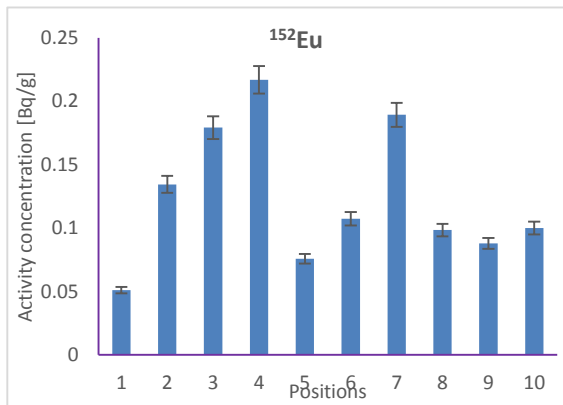


Figure 6.40 Activity concentration of ¹⁵²Eu in first 10 cm inside the wall at different positions

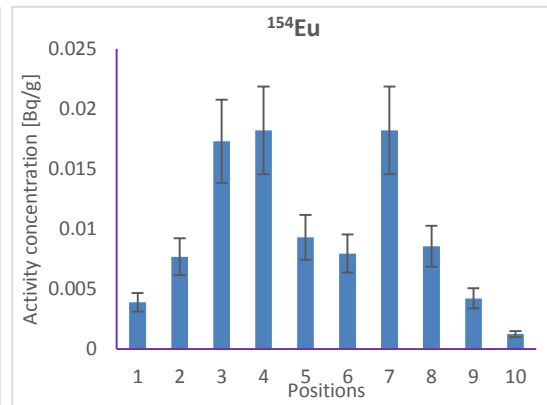


Figure 6.41 Activity concentration of ¹⁵⁴Eu in first 10 cm inside the wall at different positions

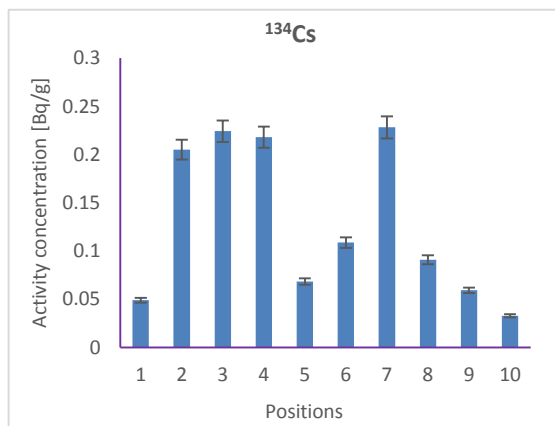


Figure 6.42 Activity concentration of ¹³⁴Cs in first 10 cm inside the wall at different positions

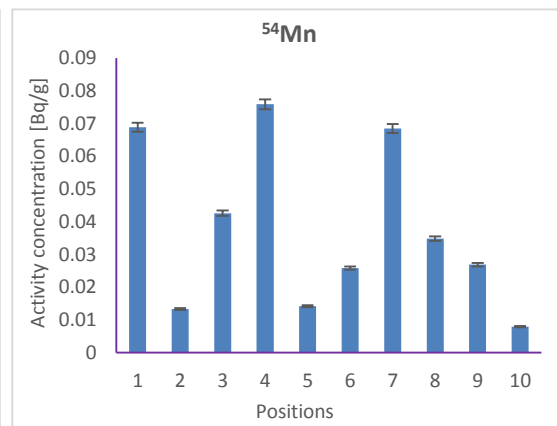


Figure 6.43 Activity concentration of ⁵⁴Mn in first 10 cm inside the wall at different positions

The walls of the bunker are most activated in positions 3, 4 and 7, as those are the positions nearest to the targets. In those positions an activity concentration of about 0.2 Bq/g and 0.8 Bq/g is expected respectively for ^{152}Eu and ^{60}Co . The lowest activation is present at positions 9, 10 and 5. As can be noticed for ^{60}Co and ^{54}Mn position 1 is the position with one of the highest activity concentration, this is due to the fact that position 1 corresponds to the bunkers door, where high concentration of steel is present.

In table 6.18 the prediction of induced activation for different life expectancies of the cyclotron in the first 10 cm at position 7 was reported.

Table 6.18 Prediction of residual activity in the first 10 cm inside the wall at position 7 considering different life expectancy of the cyclotron

Nuclide	14 years		20 years		40 years	
	Activity concentration [Bq/g]	Uncertainty [Bq/g]	Activity concentration [Bq/g]	Uncertainty [Bq/g]	Activity concentration [Bq/g]	Uncertainty [Bq/g]
^{60}Co	1.58E+00	3.02E-01	1.74E+00	3.33E-01	1.83E+00	3.58E-01
^{65}Zn	3.99E-01	6.08E-02	3.99E-01	6.08E-02	3.99E-01	6.08E-02
^{54}Mn	6.85E-02	1.92E-02	6.85E-02	1.92E-02	6.85E-02	1.92E-02
^{134}Cs	3.06E-01	6.84E-02	3.09E-01	6.89E-02	3.09E-01	6.90E-02
^{152}Eu	5.23E-01	1.35E-01	6.55E-01	1.69E-01	8.47E-01	2.43E-01
^{154}Eu	4.47E-02	1.84E-02	5.29E-02	2.17E-02	6.09E-02	2.68E-02

Chapter 7

Conclusions

This thesis presents a study on induced radioactivity inside PET Cyclotrons bunkers that I conducted with a Monte Carlo approach. During my PhD work I studied in detail two selected cases using both Monte Carlo techniques and experimental measurements. Aim of this work was to develop methodologies for the preliminary assessment of activation induced in a bunker, using the Monte Carlo code FLUKA accompanied by experimental measurements - mostly conducted with portable and relatively inexpensive equipment - to support the accuracy of tailored, site specific MC models.

The first case studied was the 16 MeV PETtrace (GE Medical System) cyclotron bunker installed in 2002 in the “S.Orsola-Malpighi” University Hospital in Bologna. A detailed MC model of the GE PETtrace cyclotron and of the bunker in which it is housed was realized using FLUKA. Since secondary neutrons, arising from the (p,n) reaction in the production of ^{18}F , are the main source of activation, an assessment of neutrons kinetic properties and angular distribution was performed via MC simulations. The average neutron spectrum emitted in the above mentioned reaction is characterized by a maxwellian shape with a peak around 2.4 MeV and with a large tail toward the low energies down to 1 keV. The neutron emission can be considered almost isotropic and the neutron multiplicity estimated is about $3.99\text{E-}03$ (#neutrons/primary proton). To assess the accuracy of the MC model developed in terms of neutron fluence, experimental measurements of neutron ambient dose equivalent $\text{H}^*(10)$ were conducted inside the bunker. Measurements were taken in 12 positions using a Thermo Scientific FH 40 G-L10 survey meter with the neutron rem-counter probe FHT-752 and a set of 12 CR39 dosimeters. Results of experimental measurements were then compared with MC simulations. FLUKA simulations were in excellent agreement with the experimental measurements, producing an accurate estimate of the neutron radiation dose field.

Gamma spectrometry measurements were performed on bunker walls in three different positions. A non-destructive in-situ measurement methodology was developed using a portable CZT detector, circumventing the need for expensive and

invasive core drilling. The detector used was a Kromek GR1. Critical aspects experienced in this kind of measurements were: the limited access time inside the bunker; the high radioactive background due to activated materials of the cyclotron itself and the efficiency calibration of the detector in non standard geometries. All these aspects can unfortunately largely influence the accuracy of final results. Activation products and residual radioactivity were calculated using FLUKA.

The results of the simulations were compared with the gamma spectrometry measurements. Discrepancies are mainly due to the fact that concrete activation is strongly dependent on trace element concentration, and the latter is heterogeneous and generally unknown. The main radionuclide detected were ^{152}Eu , ^{134}Cs , ^{54}Mn , ^{46}Sc and ^{60}Co . For ^{152}Eu the differences between measured and calculated activity concentrations are within a factor of 6, while for the other radionuclides in most cases they are within a factor of 3. Discrepancies in activation assessment are mainly due to the fact that concrete activation is strongly dependent on trace element concentration that is heterogeneous and usually unknown and the literature values used in simulations could be quite different compared to actual trace element concentration.

These results demonstrate that FLUKA can be used satisfactorily to assess the order of magnitude of the residual radioactivity, the accuracy of results increasing with better knowledge of the composition of the materials. On the other hand, the methodology developed allows direct measurements that can be performed periodically to monitor the order of magnitude of activation levels inside the bunker without the need for destructive analysis like core drilling. This methodology can be therefore very useful to assess in advance the level of activation of a cyclotron bunker in view of defining the optimum decommissioning plan.

The second case studied was the 18 MeV IBA CYCLONE 18/9 cyclotron bunker installed in 2012 in Insespital (Bern). Also in this case a detailed MC model of the IBA cyclotron and of the bunker was realized using FLUKA. Neutrons generated inside the target in the $^{18}\text{O}(p,n)^{18}\text{F}$ reaction were studied. The neutron spectrum shows a peak at around 2.8 MeV with a large tail towards lower values down to 1 keV. The neutron emission can be considered also in this case almost isotropic while the neutron multiplicity estimated is $5.10\text{E-}03$ (#neutrons/primary proton). In this case, experimental measurement of neutron spectra inside the bunker to assess the accuracy of the MC model developed in terms of neutron fluence, were performed using bubble detectors.

Three set of six Bubble Detector Spectrometer (BDS, manufactured by BTI Bubble Technology Industries) with six different energy threshold (10, 100, 600, 1000, 2500, 10000 keV) were used. Detectors were placed at the same height as targets used for the production of ^{18}F and four different measurements were performed using the four targets available. From raw data (number of bubbles per detector) it was possible to evaluate the neutron fluence (neutrons/cm²) as a function of energy using an unfolding procedures developed within this work.

It has to be considered that bubble detectors measurements have high uncertainties due to different aspects: the sensitiveness to operating temperature; error accumulation in the unfolding procedure that leads to large errors in the lower energy region of the spectrum; and possible errors connected with visual counting. Each one of these aspects may have a significant influence on the results. On the other hand, the critical issues mentioned are inherent in many neutron spectrometry systems. Furthermore this methods guarantees an accuracy of the results that is adequate for the purposes of this work, with low-cost and quick measurements if compared with other neutron detection methods.

Considering all the factors listed above FLUKA simulation was in good agreement with experimental measurements. Simulated and measured neutron spectra show the same trend and a peak around 1 MeV with a large tail towards lower values.

An assessment of residual activation was obtained in this case using a different approach. During the maintenance of CYCLONE 18/9 in Bern three core drilling were extracted from the bunker walls. Each concrete sample extracted was then measured in gamma spectrometry with an HPGe detector. A parallel activation calculation in the same irradiation conditions was performed with FLUKA. The results of the simulations were compared with the gamma spectrometry measurements. The main radionuclide detected were ^{152}Eu , ^{154}Eu , ^{134}Cs , ^{54}Mn , ^{46}Sc , ^{57}Co , ^{59}Fe , ^{65}Zn and ^{60}Co . In sample 1 the difference between measured and calculated activity concentrations were within the uncertainty, while for the other samples in most cases differences were within a factor of 3. The better consistence between experimental and simulated results in this case compared to the Bologna plant can be due to different reasons. First of all it has to be considered that, except for trace elements, the concrete composition was well known allowing a better level of accuracy in MC model. Furthermore Gamma spectrometry measurements of a core sample in a laboratory facility, with a well shielded HPGe detector guarantees a high level of accuracy. However, drilling cores during the operational life of a cyclotron is not always possible and can be quite expensive if compared with *in situ* measurement with a CZT detector, moreover an HPGe gamma-ray spectrometry system is not always available, particularly in small facilities. A good practise could be to perform a certain number of core drilling in strategic points of bunker walls during the building construction, before cyclotron installation, in order to reduce costs and to make samples extraction easier and less invasive: removable concrete samples could be inserted to fill the holes and to periodically extracted, measured on a gamma ray spectrometer and then reinserted.. In this way the activation of the bunker could be monitored periodically to assess activation during cyclotron life time.

Once the level of accuracy of MC results was assessed through comparison with different kind of experimental results, the prediction of residual activity at different positions and depths and for different life expectancies of the cyclotron was assessed in the two cases studied. Some of the main results were reported to prove the potentiality of a MC approach. The investigation can be widened depending the needs iof the specific case.

First the neutron flux assessment was reported, then an overview of a set of representative in depth activation profiles for some of the main radionuclides detected and the activation distribution inside the bunker were presented. Finally the prediction of residual activation for different life expectancies of the two cyclotrons were reported.

Considering the S.Orsola-Malpighi study, the most important radionuclide from a radiation protection point of view were ^{152}Eu and ^{60}Co . The highest specific activation was found at locations closest to the targets in the first 30 cm of the wall: up to 1.4 Bq/g for ^{152}Eu and up to 0.9 Bq/g for ^{60}Co . After the first 30 cm the activity concentrations decrease becoming almost zero at 60 cm depth. The total activity concentration estimated after 14 years of cyclotron operating life was up to 3.5 Bq/g in the location closest to target exceeding the radiological exemption limit of 1 Bq/g.

As expected the walls of the bunker most activated are the ones nearest to targets being the most irradiated by neutrons. The greater the distance from the targets, the lesser the activation; the shielding of the neutrons by the machine itself is also an extremely influential factor. It is important to notice how some irregularities in bunker geometry may affect final results. For example in the part of the wall made of concrete bricks, without the presence of reinforcement rods, activation product mainly present in steel, like ^{60}Co and ^{54}Mn , have a lower concentration. Considering that, it is possible to understand how reproducing a geometry as close as possible to the real case is important for the accuracy, and overall utility, of final results. In this perspective the potentiality of the Monte Carlo methods in the study of complex geometries is apparent.

Considering the Inselspital bunker study, the most important radionuclide from a radiation protection point of view are, as in the previous case, ^{152}Eu and ^{60}Co with activity concentrations of up to 0.2 Bq/g and 0,8 Bq/g respectively. The total activity concentration in positions closest to the target is estimated to reach 1.3 Bq/g, exceeding also in this case the radiological exemption limit of 1 Bq/g. To compare induced activation with the previous case, the activity concentration expected after 14 years of cyclotron operation as is high as 2.9 Bq/g. The radionuclide with the highest activity concentration in this case is ^{60}Co instead of ^{152}Eu , this is probably due to the highest concentration of steel in the first 10 cm of the wall. Once again it is important to underline from this results the importance of the accuracy in the reproduction of the real geometry, starting for, e.g., from the original construction drawing of the building. Also in this case the activity concentration decreases significantly after the first 30 cm of the wall and after 60 cm depth the induced activation is practically zero.

As expected the walls of the bunker most activated are the ones nearest to targets. In this case it is also important to notice that the residual activation distribution is more homogeneous than in the case of the Bologna facility. This is probably due to differences in geometry irradiation conditions compared to the latter: the walls of the bunker are closer to the targets and the cyclotron comprises four targets with a horizontal acceleration plan.

The prediction of future activation shows that, considering the half-life of the main radionuclides expected, estimation after 15 – 20 years of cyclotron operations offers a sufficiently approximated picture of the equilibrium situation. It can be noticed that in both cases the nuclides with the highest activity concentrations are ^{60}Co and ^{152}Eu .

This information should be the basis in the definition of a decommissioning strategy.

In the following the main steps characterizing an hypothetical strategy that could be adopted in the two cases analysed are reported:

❖ Planning

- Site characterization. First of all a characterization of the site is needed at the end of the operational life cycle of the facility. Having monitored periodically the residual activation with the methodology proposed in this work, the time needed for this operation can be drastically reduced. Furthermore, as mentioned, Monte Carlo simulations provide a predictive idea of the activity distribution inside the bunker helping to organize at best characterisation measurements.

Typically a waiting time of no less than 15-30 days for the decay of short lived isotopes is needed to start any measurements operation. For the bunker activation assessment, depending on the possibilities, one of the two measurements methodologies proposed in this work should be adopted. The best choice would be to combine both methodologies. The methodology developed for the non-destructive measurement using a portable CZT detectors can also be applied to the activation assessment of cyclotron and other components. The detector can be calibrated via Monte Carlo simulations using the model of the detector developed for wall measurements. New specific source terms can be implemented in the model depending on the component to be measured.

The combined use of Monte Carlo simulations and experimental measurements proposed in this work will allow a more accurate and faster mapping of activation during site characterization.

- Decommissioning Planning. Once the characterization phase has been completed, it is possible to proceed with planning the interventions. This can be structured as follows:
 - Dismantling of systems and components within the bunker. Many metal components will be activated; among these: elements of pipes and metal tubing; components of monitoring and security systems; electronic cards etc.; possible metallic frames of the lighting system; possible pedestals of raised floor, etc. The main long lived radionuclide expected in the metal components, as indicated by the results of the present work, are ^{60}Co and ^{54}Mn . This kind of waste, characterized by modest volumes and reduced

activities, can be sent for collection and disposal to authorized radioactive waste management plants.

- Cyclotron disassembling, which is expected to be carried out by the company supplying the cyclotron or by another specialized company. The in situ methodology of gamma ray spectrometry with CZT detector can be used in this phase, to identify the most activated items and guide safe operation.
- Measurements after dismounting: at the end of this operation, the site will be inspected in order to confirm removal of all radioactive sources and to evaluate the residual activation of the bunker walls. Once again, the methodology developed in this work will be of great relevance. Both in situ spectrometry and laboratory analysis of samples will help to have a final confirmation of the level of activation in the concrete, to evaluate the most activated zones and the relevant thickness, and finally to evaluate the total mass of concrete activated above clearance levels.
- On the basis of the prediction and measurements described of this work, two possible scenario can be expected:
 - Facility demolition. In the perspective of facility demolition for example, the selective removal of concrete separating the first 30 or 45 cm of the walls closest to targets from the rest of the building can be an optimized approach. This would lead to the generation of about 51 m³ low level radioactive waste in the case of S.Orsola-Malpighi facility (figure 7.1). While the low level radioactive waste expected for Inseispital facility are about 37 m³ (figure 7.2).

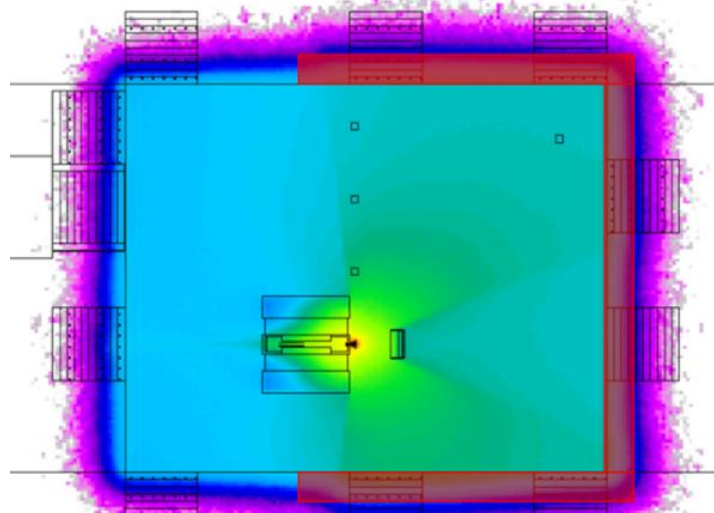


Figure 7.1 selective removal of concrete in the S.Orsola-Malpighi hospital. The part of the wall that should be selectively removed is underlined in red

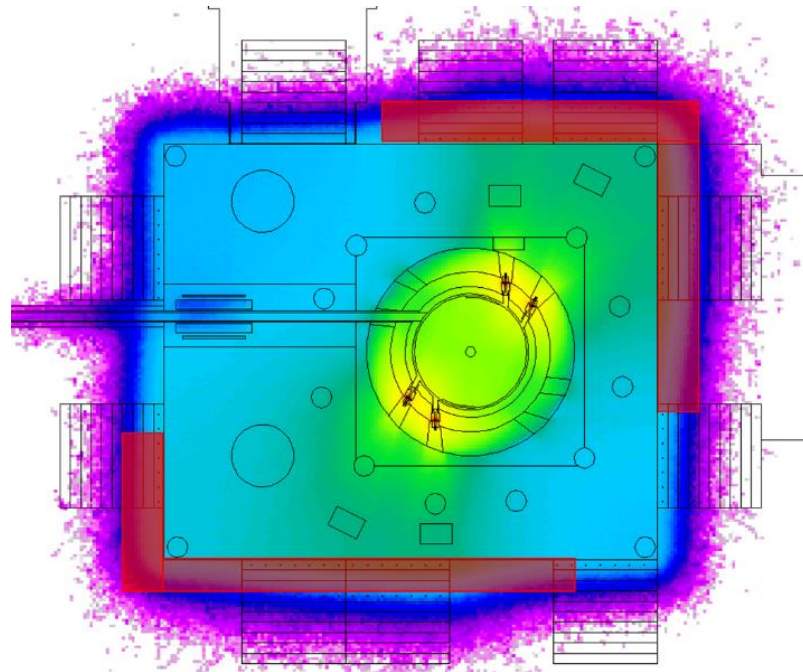


Figure 7.2 selective removal of concrete in Inespital. The part of the wall that should be selectively removed is underlined in red

Considering the current cost for management of radioactive waste in Italy, the cost for collection and storage of the amount of material deriving from a partial demolition in Bologna will be of the order of 600.000 – 800.000 Euro. This sort of evaluation is of fundamental relevance to proper decision making and selection of the options.

- Facility reuse. For example for the installation of a new accelerator or as a radioactive waste repository. In the perspective of a different reuse of the facility on the basis of this study a selective removal of the most activated part of the building can also in this case be evaluate.

Some consideration for the improvement in the design of a new facility in terms of residual activation, based on the results of this work, are reported below:

- The choice of materials that are supposed to interact with primary particles significantly influences secondary neutron production. The choice of these materials can be made in a way to limit neutron generation. An example can be the replacement of collimators in Tantalum with graphite. The 18 MeV threshold for the (p,n) reaction in Carbon guarantees indeed a lower total neutron yield for incident proton beams up to 25 MeV (European Commission, 1999). This consideration is important especially in the choice of collimators or parts of target holder materials.

- Results of this work show how the main causes of induced activation are traces of ^{151}Eu present in the sand and aggregate of concrete and the rather large amounts of ^{59}Co in reinforcement rods but also in concrete. Any measure aimed at decreasing the amount of these elements will result in a drastic reduction of residual activation.
- Considering that activity concentrations, on the basis of our results, are expected to exceed 1 Bq/g typically in the first 30 – 40 cm depth, another possible measure can be to minimize or totally remove the amount of iron bars in the superficial layer of concrete, placing the reinforcement bars at greater depths. Another aspect to consider can be the modular construction of shielding walls, planning a concrete shielding structure comprised of removable blocks in the first layer, in order to render much easier the removal of each block and the separation of waste during dismantling.
- An adequate local shielding around targets using moderator materials, like for example concrete blocks, paraffin, polyethylene, borated water etc., can also significantly reduce the neutron flux.

In conclusion Monte Carlo simulation is a very powerful and feasible tool in the planning of new biomedical cyclotron installations and in the definition of an optimized decommissioning strategy.

The availability of an experimentally validated Monte Carlo model makes it possible to revise the traditional approach to activation assessment. The results obtained show the importance of the definition of a well defined and systematic methodology that include companion experimental measurements to assess MC accuracy of results.

As shown in this work different kinds of experimental measurements can be chosen on the basis of case to case possibilities. We proved also that there are experimental methodologies, commonly available or that can be implemented with limited investment, that make possible to integrate and confirm provisional estimates.

The great advantage of Monte Carlo simulations compared to analytical methods is the possibility to reproduce more accurately the neutron source term of radiation and to obtain reliable results in the case of complex geometry conditions. The Build-up effect is taken into account more accurately than in analytical methods and without any assumption on the radiation field. Most important, Monte Carlo simulation allows a unified approach to radiation protection problems considering simultaneously the interconnections between different aspects, contrary to traditional analytical methods.

References

ANSI, 1999. *ANSI N42.14-1999. Calibration and Use of Germanium Spectrometers for the Measurement of Gamma-Ray Emission Rates of Radionuclides*. Washington: American National Standards Institute (ANSI).

Apfel, R.E., 1979. The superheated drop detector, *Nucl. Instrum. Meth.* 162, 603-608.

Apfel, R.E., 1992. Characterisation of new passive superheated drop (bubble) dosimeters, *Rad. Prot. Dosim.* 44, 343-346.

Apfel, R.E. and Roy, S.C., 1984. Investigations on the applicability of superheated drop detection in neutron dosimetry, *Nucl. Instrum. Meth.* 219, 582-587.

Apfel, R.E. and Lo, Y.-C. 1989. Practical neutron dosimetry with superheated drops, *Health Phys.* 56, 79-83.

Battistoni, G., 2012. *Medical Applications of FLUKA*. [Online] Available at: [http://ssfm.fisica.unimi.it/Didattica/Slides di Corsi file/Metodo Monte Carlo e applicazioni in Fisica Medica-parte 2.pdf](http://ssfm.fisica.unimi.it/Didattica/Slides%20di%20Corsi%20file/Metodo%20Monte%20Carlo%20e%20applicazioni%20in%20Fisica%20Medica-parte%202.pdf)

Battistoni, G. et al., 2007. *The FLUKA code: Description and benchmarking*. Fermilab 6--8 September 2006, AIP Publishing, p. 896.

Bedogni, R., Domingo, C., Esposito, A., Fernández, F., 2007. FRUIT: An operational tool for multisphere spectrometry in workplaces. *Nucl. Instrum. Meth. Phys. Res. A* 580, 1301-1309.

Berthold Technologies, 2017a. LB 123 UMo – universal monitor for radiation protection applications; 2017. Available at: <http://www.berthold-us.com/48-rad-products/dose-dose-rate-monitors/129-lb123-umo.html>

Berthold Technologies, 2017b. LB 6411 Neutron Probe; 2017. Available at: <http://www.berthold.com/en/neutron-probe-lb-6411.html>

Birattari, C., Cantone, M. C., Ferrari, A. & Silari, M., 1989. Residual Activity at the Milan AVF Cyclotron. *Nuclear Instruments and Methods in Physics Research B*, Volume 43, pp. 119-126.

- Bohlen, T. T. et al., 2014. The FLUKA Code: Developments and Challenges for High Energy and Medical Applications. *Nuclear Data Sheets*, Volume 120, pp. 211-214.
- Bronson, F. L., 2003. Validation of the accuracy of the LabSOCS software for mathematical efficiency calibration of Ge detectors for typical laboratory samples. *Journal of Radioanalytical and Nuclear Chemistry*, 255(1), pp. 137-141.
- Braccini, S., 2016. Particle Accelerators and Detectors for medical Diagnostics and Therapy. arXiv:1601.06820 [physics.med-ph].
- Braccini, S., Aebersold, D. M., Ereditato, A., Scampoli, P., von Bremen, K., 2010 SWAN: a combined centre for radioisotope production, proton therapy and research in Bern, Proceedings of the Workshop on Physics for Health in Europe, CERN, February 2010, p. 29.
- Braccini, S., 2007. A cyclotron laboratory for radioisotope production and research located in Bern: technical specifications, document of the SWAN Project.
- Bronson, F. L., 2003. Validation of the accuracy of the LabSOCS software for mathematical efficiency calibration of Ge detectors for typical laboratory samples. *Journal of Radioanalytical and Nuclear Chemistry*, 255(1), pp. 137-141.
- Brooks, F.D. & Klein H., 2002. Neutron spectrometry - historical review and present status. *Nuclear Instruments and Methods in Physics Research*. A 476 (2002) 1 - 11.
- Brugger, M., Donjoux, Y., Mitaroff, W. A., Roesler, S., 2003. Measurements and simulation of induced activity at the CERN-EU high-energy reference field facility. Proceedings of 6th International Meeting on Nuclear Applications of Accelerator Technology, San Diego, CA, USA, 1 – 5 Jun 2003, 391 – 398
- Brugger, M., Ferrari, A., Roesler, S. & Sala, P. R., 2007. *Calculation of radionuclide production cross sections with FLUKA and their application in the energy hadron collider studies*. Nice, France, s.n.
- Brugger, M., Ferrari, A., Roesler, S. & Ulrici, L., 2006. Validation of the FLUKA Monte Carlo code for predicting induced radioactivity at high-energy accelerators. *Nuclear Instruments and Methods in Physics Research A*, Volume 562, pp. 814-818.
- Brugger, M. et al., 2004. *Benchmark studies of induced radioactivity produced in LHC materials, part I: specific activities*. Madeira, Portugal, s.n.
- Brugger, M., Khater, H, Mayer, S., Prinz, A., Roesler, S., Ulrici, L., Vincke, H., 2005a. Benchmark studies of induced radioactivity produced in LHC materials, part I: specific activities, *Radiation Protection Dosimetry* 116 (1 – 4) 6 – 11.

Brugger, M., Khater, H, Mayer, S., Prinz, A., Roesler, S., Ulrici, L., Vincke, H., 2005b. Benchmark studies of induced radioactivity produced in LHC materials, part II: specific activities, *Radiation Protection Dosimetry* 116 (1 – 4) 6 – 11.

BTI Bubble Thecnology Industries, 2012a. BTI bubble detector spectrometer BDS™ For Low Resolution Neutron Spectroscopy MANUAL. March 8 2012.

BTI Bubble Thecnology Industries, 2012b. Calibration Certificate Bubble Dosimeter Spectrometer (BDS). 10 Apr 2012.

Calandrino, R. et al., 2006. Decomissioning procedures for an 11 MeV Self-Shielded Medical Cyclotron after 16 Years of Working Time. *Health Physics*, 90(6), pp. 588-596.

Carroll, L., 2002. *Decommissioning and Recommissioning Cyclotrons*. Turku, s.n.

Carroll, L., Ramsey, F., Armbruster, J. & Montenero, M., 2001. *Recycling and Recommissioning a Used Biomedical Cyclotron*. Denton, s.n.

Carter, L. L. and Cashwell, E. D., 1975. Particle-Transport Simulation with the Monte Carlo Method, ERDA Crit. Serv. Ser., Springfield, MA: National Technical Information Service.

Castillo, F., Espinosa, G., Golzarri, J.I., Osorio, D., Rangel, J., Reyes, P.G., Herrera, J.J.E., 2013. Fast neutron dosimetry using CR-39 track detectors with polyethylene as radiator.

Commission of the European communities, 1993. Principle and methods for establishing concentrations and quantities (Exemption values) below which reporting is not required in the European directive, radiation protection 65.

Danyluk, P., 2010. Measurement of neutron spectra in the AWE workplace using Bonner sphere spectrometer. *J. Radiol. Prot.* 30, 699-715

Debertin, K. & Helmer, R.G., 1988. *Gamma- and X-Ray spectrometry with semiconductor detectors*. North-Holland.

D'Errico, F., 1999. Fundamental Properties of superheated drop (Bubble) detectors. *Radiation protection dosimetry* Vol.84, Nos. 1-4, pp. 55-62 (1999) Nuclear Technology publishing

D'Errico, F. and Alberts, W.G, 1994. Superheated-drop (bubble) neutron detectors and their compliance with ICRP-60, *Rad. Prot. Dosim.* 54, 357-360.

Dunn, W. L. & Shultis, J. K., 2012. *Exploring Monte Carlo Methods*. s.l.:Elsevier.

Ellis, B., 2011. Safety Analysis Report of the ANSTO Camperdown Facility, ANSTO/T/TN/2011-1 .

ENEA, 2013. *DOSIMETRO A CORPO INTERO PER NEUTRONI VELOCI (nv)*. [Online] Available at: <http://www.irp.enea.it/it/servizi/documenti/a5-dosimetro-neutroni-veloci>

European Commission, 1998. Recommended radiological protection criteria for the recycling of metals from dismantling of nuclear installations. Radiation protection 89. Recommendations of the group of experts set up under the terms of Article 31 of the Euratom treaty.

European Commission, 1999. *Report EUR 19151. Evaluation of the Radiological and Economic Consequences of Decommissioning Particle Accelerators.*, Brussel: European Commission. Nuclear Safety and the Environment.

European Commission, 2000. Recommended radiological protection criteria for the clearance of buildings and building rubble from dismantling of nuclear installations. Radiation protection 113. Recommendations of the group of experts set up under the terms of Article 31 of the Euratom treaty.

Fassò, A., Ferrari, A., Ranft, J. & Sala, P. R., 1995. *FLUKA: Performances and applications in the intermediate energy range*. Arlington, s.n.

Fassò, A. et al., 2003. *The physics models of FLUKA: status and recent developments*. La Jolla, California, s.n.

Fassò, A., Ferrari, A. & Sala, P. R., 2009. Radiation Transport calculations and Simulations. *Radiation Protection Dosimetry*, 137(1-2), pp. 118-133.

Ferrari, A., 2006. *Introduction and Applications of FLUKA*. [Online] Available at: <http://ins00.psi.ch/mcworkshop/papers/Fluka-PSI.pdf>

Ferrari, A., Fasso, A., Ranft, J. & Sala, P. R., 2011. *FLUKA2011 Manual*. s.l.:s.n.

Ferrari, A., Sala, P. R., Fasso, A. & Ranft, J., 2005. *FLUKA: a multi-particle transport code*, s.l.: s.n.

FLUKA, 2010. *FLUKA*. [Online] Available at: <http://www.fluka.org>

Gallerani, R. et al., 2008. Neutron production in the operation of a 16.5 MeV PETrace cyclotron. *Progress in Nuclear Energy*, Volume 50, pp. 939-943.

GE MEDICAL SYSTEMS, 2004. *PETtrace REFERENCE MANUAL - Rev 3*. Uppsala: GE Medical Systems.

GR1 – Gamma ray spectrometer specifications. 2017. Available at: <https://www.kromek.com/index.php/products/applications/radiation-detection/gr1-gamma-ray-spectrometer> .

Hammersley, G. M. and Handscomb, D. C., 1964. Monte Carlo Methods, New York: Wiley.

Hankins, D.E., Homann, S. and Wesermark, j., 1986. Personnel neutron dosimetry using electrochemically etching CR-39 foils lawrence livermore national laboratory.

IAEA, 1988a. Safety Series No. 89. Principles for the exemption of radiation sources and practices from regulatory control. Vienna, 1988.

IAEA, 1988b. *Technical Reports Series No. 283. Radiological Safety Aspects of the Operation of Proton Accelerators* , Vienna: International Atomic Energy Agency.

IAEA, 1996. Safety Standards, Safety Series No. 115. International basic safety standards for protection against ionizing radiation and for safety of radiation sources. Vienna, 1996.

IAEA, 2001a. *Charged particle cross-section database for medical radioisotope production: diagnostic radioisotopes and monitor reactions. IAEA-TechDoc-1211*, Vienna: International Atomic Energy Agency.

IAEA, 2001b. *Technical Reports Series No. 403. Compendium of Neutron Spectra and Detector Response for Radiation Protection Purposes. Supplement to Technical Reports Series No. 318*, Vienna: International Atomic Energy Agency.

IAEA, 2003. Technical report series No 414. Decommissioning of small medical, industrial and research facilities, Vienna.

IAEA, 2004. *Status of the Decommissioning of Nuclear Facilities Around the World*, Vienna: International Atomic Energy Agency.

IAEA, 2006. *IAEA-DCRP/2006. Directory of Cyclotrons used for Radionuclide Production in Member States 2006 Update* . , Vienna: International Atomic Energy Agency.

IAEA, 2008. *Cyclotron Produced Radionuclides: Principles and Practice* Technical. *Technical Reports Series No. 465*, Vienna: International Atomic Energy Agency.

IAEA, 2009. *Cyclotron produced radio-nuclides: Physical Characteristics and production methods. IAEA Technical Report No. 468*, Vienna: International Atomic Energy Agency.

IAEA, 2011a. *Charged-particle cross section database for medical radioisotope production - Diagnostic radioisotopes and monitor reactions*. [Online] Available at: <https://www-nds.iaea.org/medical/>

IAEA, 2011b. *Cross section database for medical radioisotope production - Production of Therapeutic Radionuclides*. [Online] Available at: <https://www-nds.iaea.org/radionuclides>

IAEA, 2014. *Experimental Nuclear Reaction Data (EXFOR)*. [Online] Available at: <https://www-nds.iaea.org/exfor/exfor.htm>

IAEA, 2014. *Radiation protection and safety of radiation sources: International Basic Safety Standards. IAEA SAFETY STANDARDS SERIES No. GSR Part 3*, Vienna: International Atomic Energy Agency.

IBA Molecular, 2007. Cyclone 18/9, Standard & High Current model, Production description.

ICRP, 1990. *Recommendations of the International Commission on Radiological Protection*. Publication 60, Pergamon Press Oxford, 1990.

ICRP, 1996. *Conversion Coefficients for use in Radiological Protection against External Radiation*. ICRP Publication 74.. *Annals of the IRCP*, 26(3-4).

ICRP, 2007. *ICRP Publication 103. The 2007 recommendations of the International Commission on Radiological Protection*., s.l.: J. VALENTIN.

ICRP, 2010. *Conversion Coefficients for Radiological Protection Quantities for External Radiation Exposures*. ICRP Publication 116. *Ann. ICRP*, 40(2-5).

ICRU, 1977. *Neutron Dosimetry for Biology and Medicine*, ICRU Report 26 International Commission on Radiation Units and Measurements, Bethesda, Maryland

IEC, 1995. *IEC Standard 61452. Nuclear instrumentation – measurement of gamma-ray emission rates of radionuclides – calibration and use of germanium spectrometers*, Geneva: International Electrotechnical Commission.

Infantino, A. et al., 2014a. Comparison of several assessments of neutron dose measurements around a biomedical cyclotron. *Eur J Nucl Med Mol Imaging*, 41(Suppl 2), p. S307.

Infantino, A. et al., 2011. Prediction of ⁸⁹Zr production using the Monte Carlo code FLUKA. *Applied Radiations and Isotopes*, Volume 69, pp. 1134-1137.

Infantino, A. et al., 2015a. Accurate Monte Carlo modeling of cyclotrons for optimization of shielding and activation calculations in the biomedical field. *Radiation Physics and Chemistry*, doi:10.1016/j.radphyschem.2015.01.001(In Press).

Infantino, A. et al., 2014b. Monte-Carlo assessment of the saturation yield for liquid and solid targets at a medical cyclotron using FLUKA. *Eur J Nucl Med Mol Imaging*, 41(Suppl 2), p. S450.

Infantino, A. et al., 2015b. Assessment of the production of medical isotopes using the Monte Carlo code FLUKA: simulations against experimental measurements. *Nuclear instruments and methods in research B*, Volume Manuscript submitted for publication.

Infantino, A., 2015c. Advanced aspects of radiation protection in the use of particle accelerators in the medical field. PhD thesis. Dottorato di ricerca in Ingegneria Energetica, Nucleare e del Controllo Ambientale.

Infantino, A. et al., 2016. Assessment of the neutron dose field around a biomedical cyclotron: FLUKA simulation and experimental measurements. pp.1602-1608. *PHYSICA MEDICA* - ISSN:1120-1797 vol. 32 (12). DOI:10.1016/j.ejmp.2016.11.115.

ISO, 1998-2001. Reference neutron radiations. Parts 1-3. International Standard ISO 8529 (Geneva: ISO)

Kalos, M. H. and Whitlock, P. A., 2008. Monte Carlo Methods, 2nd edn.. Berlin: Wiley-VCH

Knoll, G. F., 2000. *Radiation detection and measurement. 3rd Edition*. s.l.:Jhon Wiley & Sons, Inc..

Koning, A. J., Hilaire, S. & Duijvestijn, M. C., 2007. *TALYS-1.0*. Nice, EDP Sciences.

La Torre, F., 2014. Study of induced radioactivity in proton accelerator facilities. Inauguraldissertation der Philosophisch-naturwissenschaftlichen Fakultät der Universität Bern.

Lux, I. and Koblinger, L., 1990. Monte Carlo Particle Transport Methods: Neutron and Photon Calculations (Boca Raton, FL: CRC Press).

Mairani, A. et al., 2013. A Monte Carlo-based treatment planning tool for proton therapy. *PHYSICS IN MEDICINE AND BIOLOGY*, Volume 58, pp. 2471-2490.

Marengo, M., 2002. La fisica in medicina nucleare. Patron, p.544. ISBN:8855525824

Matzke, M., 1994. Unfolding of pulse height spectra: the HEPRO program system. Report PTB-N-19. Physikalisch Technische Bundesanstalt. Braunschweig.

Moritz, L., 2001. Decommissioning of accelerators. Erice, October 2001.

- Mosegaard, K. & Sambridge, M., 2002. Monte Carlo analysis of inverse problems. *Inverse Problems*, Volume 18, pp. R29-R54.
- NCRP, 1976. *NCRP Report No. 51. Radiation protection design guidelines for 0.1-100 MeV particle accelerator facilities*, Bethesda: National Council on Radiation Protection and Measurements.
- NCRP, 2003. *NCRP Report No. 144. Radiation Protection for Particle Accelerator Facilities*, Bethesda: National Council on Radiation Protection and Measurements.
- NCRP, 2004. *NCRP Report No. 147. Structural Shielding Design for Medical X-Ray Imaging Facilities*, Bethesda: National Council on Radiation Protection and Measurements.
- NCRP, 2005. *NCRP Report No. 151. Structural Shielding Design and Evaluation for Megavoltage X- and Gamma-Ray Radiotherapy Facilities.*, Bethesda: National Council on Radiation Protection and Measurements.
- NIST, 2014. *National Institute of Standards and Technology*. [Online] Available at: <http://www.nist.gov>
- Nuclear Data Service, 2017a. "Experimental nuclear reaction data (EXFOR)". Available at: <http://www-nds.iaea.org/exfor/servlet/E4sMakeE4>.
- Opelka, J. H. et al., 1979. *ANL/ES-82. Particle-accelerator decommissioning.*, Argonne: Argonne National Laboratory.
- Parodi, K., Ferrari, A., Sommerer, F. & Paganetti, H., 2007a. Clinical CT-based calculations of dose and positron emitter distributions in proton therapy using the FLUKA Monte Carlo code. *PHYSICS IN MEDICINE AND BIOLOGY*, Volume 52, pp. 3369-3387.
- Parodi, K. et al., 2007b. PET/CT imaging for treatment verification after proton therapy: a study with plastic phantoms and metallic implants. *Med. Phys.*, 34(2), pp. 419-435.
- Pelliccioni, M., 2000. Overview of fluence-to-effective dose and fluence-to-ambient dose equivalent conversion coefficients for high energy radiation calculated using the FLUKA code. *Radiation Protection Dosimetry*, 88(4), pp. 279-297.
- Reginatto, M., Goldhagen, P., 1999. MAXED, a computer code for maximum entropy deconvolution of multisphere neutron spectrometer data. *Health Phys.* 77, 579-583.
- Routti, J.T., Sandberg, J.V., 1985. Unfolding activation and multisphere detector data. *Radiat. Prot. Dosim.* 10, 103-110.

Seghour, A., Seghour, F.Z., 2001. Unfolding neutron energy spectra from foil activation detector measurements with the Gold algorithm. *Nuclear Instruments and Methods in Physics Research A* 457 617-626.

Sommerer, F. et al., 2009. In-beam PET monitoring of mono-energetic ^{16}O and ^{12}C beams: experiments and FLUKA simulations for homogeneous targets. *PHYSICS IN MEDICINE AND BIOLOGY*, Volume 54, pp. 3979-3996.

Spanier, J. and Gelbard, E. M., 1969. Monte Carlo Principles and Neutron Transport Problems, Reading, MA: Addison-Wesley.

Stabin, M. G., 2007 *Radiation Protection and Dosimetry, an introduction to Health Physics*, Springer 2007.

Sweezy, J., Hertel, N., Veinot, K., 2002. BUMS - Bonner sphere unfolding made simple: an HTML based multisphere neutron spectrometer unfolding package. *Nucl. Instrum. Meth. Phys. Res. A* 467, 263-269.

Tavendale, A.J., and G.T. Ewan, 1963, *Nucl. Instrum. & Methods* 25, 185.

Thermo Scientific, 2013. The modular system for radioactivity measurements. Available at: <http://www.thermoscientific.com/en/home.html>

Thermo Scientific, 2013. *The Modular System for Radioactivity Measurements*. [Online] Available at: <http://www.thermoscientific.com/en/home.html>

Tomás, M., Fernández, F., Bakali, M., Muller, H., 2004. MITOM: a new unfolding code based on a spectra model method applied to neutron spectrometry. *Radiat. Prot. Dosim.* 110, 545-548.

Venkataraman, R. et al., 2005. Improved detector response characterization method in ISOCS and LabSOCS. *Journal of Radioanalytical and Nuclear Chemistry*, 264(1), pp. 213-219.

Vichi, S., Infantino, A., Cicoria, G., Pancaldi D., Mostacci, D., 2016. Efficiency calibration of a portable CZT detector for non-destructive activation assessment of a cyclotron bunker. *Radiation Effects and Defects in Solids*, 2016, 171:9-10, 705-713, DOI: 10.1080/10420150.2016.1244675.

Vlachoudis, V., 2009. *FLAIR: A Powerful But User Friendly Graphical Interface For FLUKA*. New York, Saratoga Springs.

Weisskopf, V., 1937. Statistics and Nuclear Reactions. *Phys. Rev.* 52, 295 - august 15 1937 volume 52. DOI: <https://doi.org/10.1103/PhysRev.52.295>

Wyckoff, J. M. & Chilton, A. B., 1973. *Dose due to practical neutron energy distributions incident on concrete shielding walls*. Springfield, Virginia, Snyder, W.S., Ed., pp. 694-699.

Zagni, F. et al., 2014. Monte Carlo modeling provides accurate calibration factors. *Applied Radiations and Isotopes*, Volume 94, pp. 158-165.

Ringraziamenti

Vorrei prima di tutto ringraziare il Prof. Domiziano Mostacci per avermi guidato, motivato e supportato dai primi anni universitari fino ad oggi. Nel mio percorso universitario e professionale è stato un punto di riferimento fondamentale e continuerà ad esserlo, senza di lui questo percorso non ci sarebbe stato. Lo ringrazio per tutte le esperienze formative che mi ha permesso di fare sia in ambito nazionale che internazionale e per la disponibilità, attenzione e dedizione con cui si dedica a tutti i suoi studenti.

Un ringraziamento speciale va al Dott. Mario Marengo perché è sicuramente una delle persone che più hanno segnato la mia crescita professionale, scientifica e personale. La passione, l'interesse, l'entusiasmo e la professionalità con cui cura ciascun aspetto del suo lavoro (compresi i QC) sono sicuramente un esempio che porterò sempre con me. Lo ringrazio per la disponibilità, per la pazienza, l'appoggio costante, i consigli, per avermi coinvolto, permesso di osservare e di collaborare con lui insegnandomi tanto. Lo ringrazio perché, qualsiasi percorso intraprenderò nel futuro, rappresenterà sempre il modello che cercherò di seguire quanto più possibile.

Ringrazio il Dott. Gianfranco Cicoria per il suo costante aiuto, sostegno e supporto. Sapere di poter contare su di lui e sulla sua innata capacità di risolvere o semplificare problemi di qualsiasi tipo è stato per me fondamentale in questi anni.

Ringrazio il Dott. Saverio Braccini per la grande opportunità che mi ha dato, lo ringrazio per avermi dato fiducia contribuendo in maniera sostanziale a questo lavoro e condividendo con me parte del suo, mostrandomi e insegnandomi in poco tempo così tante cose nuove. Insieme a lui ringrazio ovviamente tutto il gruppo dell'LHEP di Berna e quello di SWAN per avermi accolto fin da subito come parte del gruppo con grande disponibilità facendomi sentire a casa.

Vorrei poi ovviamente ringraziare tutto il gruppo del Sant'Orsola con il quale trascorro le mie giornate ormai da un bel po' di anni. Ringrazio in particolare Angelo, Federico, Giulia, Giorgia, Davide, Vittorio e Andrea perché sono stati quelli che, in momenti diversi, mi hanno accompagnato più da vicino in questo percorso. Ringrazio poi tutti i ragazzi del padiglione 30 come Alberto, Claudio, Erica, Fabrizio, Filippo, Igor, Luca, Remo, Nadir, Stefano Costa, Stefano Boschi, Simona ma anche tutti i medici, gli specializzandi, i tecnici, le signore delle pulizie e tutti quelli che sono passati di qui per brevi o lunghi periodi a fare una tesi o un tirocinio. Con ciascuno di loro ho condiviso

momenti fondamentali per questo percorso, sia a livello professionale che personale. Porterò sempre con me questi anni condivisi con voi. Non voglio dilungarmi troppo con le parole perché so bene che l'unico modo per dimostrarvi veramente gratitudine è la dispensazione perpetua di finocchiona del Tegoletto.

Ringrazio infine la mia famiglia e le mie amiche per la forza che mi danno, ciascuno in maniera diversa, ma soprattutto perché mi continuano a sopportare nonostante questo sia il terzo periodo pre-tesi al quale li sottopongo.

A tutte queste persone dedico il lavoro di questi anni.

Sara